Characterization and Modeling of Dry Etch Processes for Titanium Nitride and Titanium films in Cl_2/N_2 and BCl_3 Plasmas

by

N. Moorthy Muthukrishnan

Dissertation submitted to the Faculty of the
Virginia Polytechnic Institute and State University
in partial fulfillment of the requirements for the degree of

Doctor of Philosophy
in
Electrical Engineering

APPROVED:

Aicha Elshabini-Riad
Aicha Elshabini-Riad, Chair

Kostas Amberiadis

Diana Farkas

Anbo Wang

Wansheng Su
Wansheng Su

November 1996
Blacksburg, Virginia

Keywords: plasma etch, titanium, titanium nitride, response surface methodology, chlorine, boron trichloride

Characterization and Modeling of Dry Etch Processes for Titanium Nitride and Titanium films in Cl_2/N_2 and BCl_3 Plasmas

by

N. Moorthy Muthukrishnan

Aicha Elshabini-Riad, Chair

Kostas Amberiadis, main advisor at LSI

Abstract

In the past few years, the demands for high speed semiconductor integrated circuits have warranted new techniques in their fabrication process which will meet the ever-shrinking dimensions. The gaseous plasma assisted etching is one of these revolutionary processes. However, the plasma and the etch process are very complex in nature. It has been very difficult to understand various species present in the plasma and their role in the etch reaction. In addition, the submicron geometries also require interconnect materials which will satisfy the necessary properties such as thermal stability and low electrical resistance. Titanium (Ti) and titanium nitride (TiN) are widely used as barriers between aluminum (Al) and silicon (Si) to prevent the destructive intermixing of these two materials. The process of patterning of the interconnect containing Ti and TiN along with Al has been a challenge to the semiconductor process engineers. Therefore, complete characterization of the plasma etch process of Ti and TiN films and development of mathematical models to represent the responses such as the etch rate and uniformity is necessary for a good understanding of the etching process. A robust and well controlled

metal etch process usually results in good die yield per wafer and hence can translate into higher profits for the semiconductor manufacturer.

The objective of this dissertation is to characterize the plasma etch processes of Ti and TiN films in chlorine containing plasmas such as BCl_3 and Cl_2/N_2 and to develop mathematical models for the etch processes using statistical experimental design and analysis technique known as Response Surface Methodology (RSM). In this work, classical experiments are conducted on the plasma etch process of Ti and TiN films by varying the process parameters, such as gas flow, radio frequency (RF) power, reaction pressure, and temperature, one parameter at a time, while maintaining the other parameters constant. The variation in the etch rate with the change in the process parameter of the film is studied and the results were explained in terms of the concepts of plasma. These experiments, while providing very good understanding of the main effects of the parameters, yield little or no information on the higher order effects or interaction between the process parameters. Therefore, modern experimental design and analysis techniques using computerized statistical methods need to be employed for developing mathematical models for these complex plasma etch processes.

The second part of this dissertation concentrates on the Design and Analysis of Experiments using Response Surface Methodology (RSM) and development of models for the etch rate and the etch uniformity of the Ti and TiN films in chlorine-containing plasmas such as Cl_2/N_2 and $Cl_2/N_2/BCl_3$. A complete characterization of the plasma etch process of Ti and TiN films is achieved with the RSM technique and a well fitting and statistically significant models have been developed for the process responses, such as the etch rate and the etch uniformity. These models also provide a means for quantitative

comparison of main effects, which are also known as first order effects, second order effects and two factor interactions. The models, thus developed, can be effectively used for an etch process optimization, prediction of the responses without actually conducting the experiments, and the determination of process window.

This dissertation work has achieved a finite study of the plasma etch process of Ti and TiN films. There is tremendous potential and scope for further research in this area, limited only by the available resources for wafer processing. A few of the possibilities for further research is discussed in the next few sentences. The optimized process derived from the RSM technique needs to be implemented in the actual production process of the semiconductor ICs and its effects on the wafer topography, etch residue and the resulting die yield have to be studied. More research studies are needed to examine the effect of process parameters such as temperature, the size and shape of the etch chamber, the quality of the film being etched, among other parameters. It is worth emphasizing in this respect that this dissertation marks beginning of research work into the ever-increasing complexities of gas plasma.

Acknowledgments

I am very much thankful to Dr. Kostas Amberiadis and Prof. Aicha Elshabini-Riad for their support and guidance throughout this research work. Dr. Kostas Amberiadis was extremely helpful in getting the materials and the equipments available for this work. He was a great technical resource during the entire course of this work. I am very much indebted to Prof. Aicha Elshabini-Riad who was very helpful in reviewing the technical papers and this thesis and made valuable suggestions towards improving the quality of the thesis. Thanks are due to Prof. Diana Farkas, Prof. Anbo Wang, and Dr. Wansheng Su for their guidance by being a member of my advisory committee. I would like to thank Loretta Estes and Lori Hughes at the Electrical Engineering department for their help through e-mail with several pieces of information regarding admission and thesis related issues.

I am very grateful to the LSI Logic corporation for their support and encouragement of this research work . Thanks to David Heine for critical review of this work and informative discussions. My sincere thanks are due to Mike Bruner, Sharad Prasad, and Ashok Kapoor for reviewing my technical papers. Special thanks to Rich Schinella and Kevin McAndrews for their help in approval of the research papers for publication.

The motivation and support of my wife Eswari Muthukrishnan, who herself is a doctoral student, and the sacrifice by my parents, brother and sister, and encouragement from my friends in the Silicon Valley have brought me to this level today. I am extremely thankful to all of my family members and friends.

I dedicate this thesis to my parents, who made a lot of sacrifices to get me to this level and my wife Eswari, who had been very supportive and motivational during this work.

Table of Contents

List of Figures

List of Tables

Chapter 1
Introduction

In the semiconductor IC processing aluminum based alloys have been traditionally used for interconnection. The interconnection material has to keep the contact resistance low while maintaining the integrity of the metal/silicon interface. Aluminum based alloys have definite limitations as the device dimensions shrink to submicron levels. These interconnect schemes pose problems such as high contact resistance, thereby leading to reduced speed of operation due to high RC time constant, high IR voltage drop along the metal line, cross talk and high power consumption [13]. So it is necessary to use multilevel metal stack for interconnection to achieve the necessary performance levels in submicron ICs.

In the processes where aluminum is used as interconnection metal, it is essential to anneal wafers at 400-450 °C to dissolve native silicon dioxide at the interface between silicon and metal in the contacts, reduce the defects in the metal and gate oxide thereby reducing the interface charge density. During this process, silicon diffuses into aluminum to satisfy the solid solubility of silicon in aluminum. This process leads to aluminum spikes and silicon pits at the Al/Si interface. If the semiconductor junctions are shallow, which is the case in the submicron devices, this process of silicon diffusion in aluminum can lead to junction shorting. In order to avoid this problem, 1-2% of silicon is added to aluminum to saturate the aluminum alloy with silicon. But this results in silicon precipitation in the contacts when the wafers are cooled after annealing. Silicon precipitates thus formed lead to high contact resistance, and open contacts in the worst case.

One solution to this problem is formation of silicides by reacting a metal with the underlying silicon in the contact windows. Silicides form a stable interface between metal and silicon, and the surface defects and contaminants at the interface get absorbed in the silicide layer, leaving the interface free of defects. In addition to this, silicides have self-alignment feature. Two classes of materials - noble, near-noble metals such as Pt, Pd, Co, and Ni and refractory metals such as Ti, Mo, W, Ta - are used for the formation of silicides. The first group of metals - Pt, Pd, Co, Ni - are good for devices with junction depths over 0.5 mm. These metal silicides are formed relatively at low temperatures with less lateral silicide formation, and low probability of bridging between adjacent lines. The refractory metal silicides, on the other hand, are more difficult to form by thermal reaction. So ion bombardment is used for silicide formation. These refractory metal silicides are much more stable at temperatures over 700 °C. Above 700 °C, noble and near-noble metals tend to diffuse into silicon and polysilicon, leading to junction leakage and gate degradation.

One of the refractory metals, titanium is a very good candidate for titanium disilicide, $TiSi_2$, formation, because it can dissolve native oxide on silicon and polysilicon and thermally react with them to form silicides. $TiSi_2$ results in nonbridging silicide structures if formed in N_2 ambients, where N_2 acts as a barrier for diffusion. But the disadvantages of $TiSi_2$ include its high reactivity with silicon and lower thermal stability compared to WSi_2 and $MoSi_2$.

The silicides act as a stable interface between silicon and aluminum up to 400 °C, but fail at higher temperatures. So another stable barrier layer is needed for temperatures over 400 °C. The barrier layer is one that prevents destructive interaction of two materials

when interposed between them, at the same time having minimal interaction with the two materials it separates. The requirements for the barrier material are thermal stability, good thermal and electrical conductivity, low thermal stress, and ability to adhere well to the two materials it separates. There are three types of barriers: a stable or passive barrier, a sacrificial barrier, and a stuffed barrier. TiN is a very good passive barrier used in the present day silicon technology. In the following sections, the properties of Ti and TiN films are discussed in more detail.

1.1 Applications of TiN film

In this section the usage and properties of TiN film are discussed.

1. TiN forms an excellent passive barrier between aluminum and silicon [3, 6, 9].
2. TiN film reduces the contact resistance in submicron contacts by eliminating regrowth of silicon [21].
3. TiN film improves adhesion between silicon and tungsten if formed before tungsten deposition.
4. TiN film serves as a seed layer for aluminum deposition to improve reliability.
5. TiN is also used as an antireflection layer on Al metal films to reduce the reflection of light from the surface of the Al metal film during photolithographic process, thereby reducing the effects such as necking and notching of patterned photoresist and widen the exposure window in the photolithographic process.[21].
6. It is also used as a means of reducing hillock formation on the Al alloy metallization. [21].

1.2 Properties of TiN Film

The contact resistivity of TiN over low resistivity silicon is of the order of 10^{-5} of $\mu Ohm.cm^2$. The TiN is metallic with resistivities of 20 to 100 μOhm.cm. [7, 9]. In general, the resistivity of CVD TiN film is higher than that of bulk material. The resistivity of TiN film deposited decreases with decrease in pressure and increase in temperature of deposition. The resistivity of a CVD TiN film deposited at atmospheric pressure and 650 °C is 300 μOhm.cm and low pressure with a temperature of 500 °C resulted in a film with resistivity of 525 μOhm.cm. When the temperature is increased to 750 °C, the resistivity of the film is 47 μOhm.cm. The barrier height of TiN on high resistivity silicon is 0.49 eV.

The test wafers for the experiments were reactively sputtered in a commercially available MRC Eclipse RF sputtering system with Ti target with argon and nitrogen gas ambient. The bulk resistivity of the TiN film is calculated from the daily sheet resistivity monitor data. The bulk resistivity of the film is found to be 148.58 μOhm-cm.

1.3 Deposition Methods of TiN Film

In semiconductor industry, the TiN film is formed by one of the following techniques:

1. reactive sputtering of Ti in an Ar-N_2 ambient [15,77]
2. evaporation of Ti in an N_2 ambient and annealing at 700-900 °C [13].
3. chemical vapor deposition (CVD) of TiN film [9]
4. reaction of sputtered Ti film with nitrogen containing ambients [76]

Reactive sputtering of TiN involves sputtering of Ti target in a nitrogen containing ambient. Argon is typically used as a sputtering gas. Reactive sputtering of TiN is more complex than reactive evaporation because there are more parameters involved with sputtering [77]. On the other hand, this process provides more flexibility to tailor the properties of the film by changing the process parameters. Reactive evaporation of TiN film is normally done in a vacuum system. Pure Ti is evaporated using resistive heating or by means of electron gun in an ambient containing nitrogen. Nitrogen pressure and the substrate temperature are the most influential factors in this process. [77]. The chemical vapor deposition of TiN is typically carried out in a cold wall reactor. The wafer is heated to temperatures around 700 °C using a tungsten lamp. Reactive gases NH_3 and $TiCl_4$ are introduced through two separate lines into the chamber and mixed in a shower head. The gases NH_3 and $TiCl_4$ react close to the hot wafer and deposit TiN on the substrate. [9]. The fourth method of TiN film preparation involves sputtering of pure Ti in a sputtering chamber. Heating the Ti film to temperatures of 600 to 800 °C in an ambient containing nitrogen gas such as NH_3 causes Ti film to react with nitrogen to form TiN film.

The TiN film used in our experiments were reactively sputtered in a commercially available MRC Eclipse Sputtering system using a chamber containing Ti target in argon and nitrogen gas ambient.

1.4 Applications of Ti Film

Titanium is used to form silicides ($TiSi_2$) on silicon/polysilicon, a process commonly known as salicide process, which reduce the contact resistance and prevent metal spiking in Al-Si contacts. $TiSi_2$ is also used over polysilicon gate material to reduce the polysilicon

gate resistance, thereby helping to reduce the RC time constant of the interconnects. Of the four materials used form silicide - W, Ta, Mo, and Ti - titanium silicide has the lowest thin film resistivity [17]. Titanium is one of the few refractory materials that can form silicides consistently on silicon and polysilicon by thermal reaction, because it can dissolve native SiO_2 on silicon surfaces during annealing [13]. In addition to this, $TiSi_2$ can form nonbridging salicide structures when reacted in N_2 or other inert gas ambients. Nitrogen-stuffed or nitrogen-reacted Ti is used as a diffusion barrier to suppress lateral silicide formation.

$TiSi_2$ has a few disadvantages such as its reactivity to SiO_2 and lower thermal stability when compared to silicides formed with W and Mo. $TiSi_2$ readily dissolves in most mineral acids that also etch Si and SiO_2, thereby making it impossible to etch it using wet chemical etch process [17]. In addition to that, silicides are not stable in contact with Al. Therefore a stable diffusion barrier such as TiN is required between $TiSi_2$ and Al.

1.5 Properties of Ti Film

As discussed in section 1.4, Ti is deposited on the silicon wafer and converted to TiSi2 and/or TiN for the device application. The bulk resistivity of Ti used in our experiments is 65.07 μOhm.cm. Ti has the capability to react with nitrogen, oxygen and silicon at high temperatures and form compounds, such as TiN, TiO_2 and $TiSi_2$. TiN is used as a barrier material as described in section 1.1 and $TiSi_2$ is used to form a low-resistance interface between silicon and metal.

1.6 Deposition Methods of Ti Film

Titanium film, as discussed in section 1.4, is converted to its silicide for use in the semiconductor devices. Titanium film can be formed using one of the following techniques as discussed by S.P. Muraka [79]:

1. evaporation of Ti and formation of a film on a substrate under vacuum
2. sputtering of Ti target under vacuum to deposit Ti film on a substrate
3. electroplating of a thin film on a substrate.

All of the processes listed above are followed by sintering to form silicide. Silicide can also be formed by ion implantation followed by annealing.

The Ti film is deposited on the substrate through one of the first three techniques listed above. In the first method of vacuum evaporation, the Ti material is heated and evaporated by a filament or electron gun in a vacuum system and gets deposited on a cold substrate such as silicon wafer. In the second technique, Ti target is sputtered by dc or RF power in a vacuum chamber using an inert gas such as argon and made to deposit on a substrate. Ti film can also be deposited using conventional electroplating techniques in which the substrate to be coated with Ti film is connected as the cathode and a Ti film is connected as the anode. Both the electrodes are immersed in an electrolyte to provide path for ion movement and Ti film deposition.

Instead of forming Ti film followed by sintering for achieving $TiSi_2$, a few techniques involve direct formation of $TiSi_2$ film. Co-sputtering of Ti and Si from two independent targets, sputtering from a sintered pressed-powder $TiSi_2$ target, coevaporating Ti and Si

from thermal or e-beam sources followed by sintering, and chemical vapor deposition are the other techniques for forming $TiSi_2$ film [13].

1.7 Dry Etching Techniques of Ti and TiN Films

The dry etching of a thin film commonly involves generation of plasma of an etchant gas under vacuum. Chlorine or Fluorine containing gases are commonly used for etching Ti and TiN films. Cl_2 or F_2 gases react with Ti or TiN to form volatile $TiCl_4$ gas that can be pumped away along with other etch products [22]. Etching of Ti in CF_4+O_2 and SF_6 plasmas is reported [21]. With CF_4+O_2 plasma, the etch rate is low and the selectivity to the underlying SiO_2 is poor. Moreover, organic photoresist can not be used as an effective etch mask because O_2 has a tendency to etch photoresist. In SF_6 plasma, the etch rate is lower than the results obtained with CF_4+O_2 plasma, but the Ti/SiO_2 selectivity is found to be better at 2.3. CF_4+O_2 plasma has also been used to etch $TiSi_2$, which is the most commonly used form of Ti film in the VLSI devices [17]. Investigations of both plasma etch and reactive ion etch using this plasma has been reported in the same paper.

Chlorine containing gases such as BCl_3 and $CHCl_3$ are also used for etching metal films. In VLSI and ULSI applications, Ti and TiN are always used as one of the layers in the multilayer metal interconnect stack. Chlorine is capable of etching aluminum along with Ti and TiN, and hence widely used as the etchant gas. A combination of Cl_2, BCl_3 and $CHCl_3$ with inert gases He or N_2 is used for etching the metal stack. BCl_3 helps to etch the native oxide on the metal film and also scavenges moisture from the etch chamber. $CHCl_3$, in combination with photoresist, is used to form sidewall polymer to achieve

directional etching, thereby leading to vertical sidewalls for metal lines. Inert gases, He and N_2, act as carrier gases and also provide ions for isotropic etching.

In this dissertation work, the etch characteristics of Cl_2 and BCl_3 on Ti and TiN films are studied to get a better understanding of the effect of the individual process parameters on the etch characteristics of these films and the etch mechanisms involved in the etch processes. An experiment was designed to study the main effects and interaction between the factors in the etch process in the case of Ti and TiN films. From the results of the experiments, a model for Ti or TiN etch process in the plasma was developed. The following chapters describe the experiments done and discuss the results.

1.8 Motivation for Dissertation

The Ti and TiN films are widely used in the VLSI (very large scale integration) circuit interconnects. However, most of the published research work concentrate on the etch characterization of Al film, which forms the bulk of the interconnect. In the literature, there is very little information available on the etch characteristics of the Ti and TiN films and hence Ti and TiN etching is one of the least understood processes. In addition, the Ti/TiN etching process in Lam Rainbow 4600 is not well characterized. Therefore, the objective of this work is to characterize the plasma etching process of Ti and TiN films and develop mathematical models using statistical experimental design and analysis. The author hopes that the characterization of the etch processes done in this work would help one to better understand the Ti and TiN etch processes. The mathematical models for Ti and TiN etch processes developed in the course of this work would help one to optimize these etch processes without conducting a whole lot of experiments, thereby resulting in

robust etch processes. The optimized process, if implemented in the production line, would lead to robust, reliable and repeatable etching of Ti and TiN films and would increase the die yield per wafer thereby increasing the revenues for the semiconductor manufacturer.

1.9 Scope of Dissertation

This dissertation describes the characterization of Ti etching process in Cl_2/N_2 plasmas and TiN etching process in Cl_2/N_2 and BCl_3 plasmas. The effects of the process parameters are investigated by varying one parameter at a time and their effects on the etch are discussed using plasma fundamentals. This work also includes design of experiments, analysis, and modeling of Ti and TiN etch processes using statistical techniques, known as response surface methodology (RSM). These models provide a means for determining the relative significance of each of the parameters, second order effects and two factor interactions. A detailed description along with the definitions of statistical terms of the RSM technique is provided. A brief discussion on the process optimization is also presented. However, the implementation of the optimized process and further investigations into the constituents of the plasmas is not covered in this dissertation.

1.10 Organization of Dissertation

This dissertation is organized into three main parts. The first part, consisting of Chapter 2, briefly describes the process and equipments used for depositing the Ti and TiN films, plasma etch, and sheet resistance measurements. The second part, consisting of Chapters

3, 4, and 5, presents a discussion on the conventional characterization experiments for TiN and Ti etch processes. The fundamental concepts of plasma are used to explain the behavior of the etch characteristics.

The Chapter 6 constitutes the third major part of this dissertation. It discusses the statistical experimental design, analysis, and modeling of the Ti and TiN plasma etch processes using RSM technique. This chapter emphasizes the importance of the design of experiment in model development and process optimization. Chapter 7 summarizes the research work and lists the conclusions drawn from the experiments. It also presents a list of recommendations for further research, building up on the results obtained from this work.

Chapter 2

Equipments Used for Deposition, Etching, and Measurement

2.1 Introduction

The semiconductor processing involves several individual steps and appropriate processing equipments/systems and measurement tools are needed to perform the specialized functions. A reasonably good understanding of the system configuration, the modules constituting the equipments, their functions and their operation is needed in order to perform the process related work and to understand and interpret the results. This dissertation work involves characterization of plasma etch processes for Ti and TiN films. Therefore this dissertation report would not be complete without a background information on the equipments used for film deposition, plasma etching, and film measurement, which would make the reader understand the ideas and concepts discussed in the later parts of this dissertation. In this chapter, the configuration and operation of the equipments used in this dissertation work are presented. Several state of the art equipments/systems were used for Ti and TiN film deposition, plasma etching, and sheet resistance measurements. This chapter is organized into individual sections that describe the major equipments used for film deposition, plasma etch, and thickness measurement. Each section contains a description of the principle of operation, followed by a description of the modules constituting the system, the operating procedure, and the process. In addition, the important features of the equipments are also discussed..

2.2 Equipments for Ti, TiN Deposition

In this section, the equipments/systems used for depositing the Ti and TiN films are described. Two systems were used for deposition - ULVAC for Ti deposition and MRC Eclipse for TiN deposition. Both the systems use DC sputtering technique for physically removing the materials off a target and deposit them on a substrate, in this case, a silicon wafer. First, the fundamentals of metal sputtering process are presented followed by a description of each of these equipments is given with schematic diagrams in the following subsections.

2.2.1 Fundamentals of metal sputter deposition process

The terminals of the a semiconductor device in an IC, such as source, gate and drain of MOS device, and the terminals of devices on the same chip are connected using a conductive material to perform a designated function. At device levels, polysilicon can be used for interconnection. Long interconnections prohibit the use of polysilicon as the resistance becomes high. The high resistance would limit the speed of operation of the IC. Therefore, low resistance materials such as Al alloys are used for interconnections. As discussed in Chapter 1, the Ti and TiN are used as barriers between Al alloys and silicon substrates and to improve the contact resistance. Traditionally, the metal and metal alloys were deposited using vacuum evaporation techniques. In these techniques, there is very little or no control over the thickness of metal deposition. As a result, new metallization techniques are being introduced to the semiconductor fabrication. The most popular technique among them is sputtering or physical vapor deposition (abbreviated as PVD).

The sputtering or PVD process involves physically removing the material, atom by atom or layer by layer, from a source, which is known as target, and depositing it on a substrate. The entire process is carried out in an evacuated chamber. The operating pressure is in the order of 10 mTorr. A roughing pump such as a mechanical rotary vane pump is used to evacuate the system from atmosphere to about 150 mTorr. To achieve high vacuum levels needed for sputtering processes, the pumping system may consist of a liquid-nitrogen-cooled trap and a turbomolecular pump, or a trap and a closed cycle helium refrigerator cryopump [2]. An inert gas such as Ar is ionized in the chamber. The argon ions used as the missiles to hit the target and dislodge the target atoms/molecules and help deposit them on the substrate. A plasma is generated by providing power to the chamber through a DC or RF source connected between the electrodes holding the substrate and the target. The purity of the argon gas is also a factor. Therefore, the entire sputtering system along with its components has to be maintained clean and vacuum tight. All precautions are taken to maintain the partial pressures of other gases, such as water vapor and oxygen, below 10^{-2} mTorr. These gases may have detrimental effect on the quality of the deposited film. To achieve this, the throttle valve of the pumping system is placed between the trap and the vacuum pump. This enables the argon pressure to be adjusted by varying the pumping speed of the vacuum pump, while the full pumping speed of the trap for water vapor is utilized. Other gases, such as nitrogen, are added in order to deposit TiN film by reacting nitrogen with Ti sputtered off a target.

2.2.2. MRC Eclipse metal sputter deposition system

The MRC Eclipse PVD metal sputter deposition system was used to deposit TiN film for this work [133]. In this section, a description on this system is presented. Fig. 2.1

illustrates the schematic diagram of MRC Eclipse sputtering system. This system has a cassette-to-cassette wafer transfer for high wafer throughput for production environment. The MRC Eclipse system, like any other modern semiconductor process equipment, is controlled by a computer. The computer supervises the wafer transfer, program/recipe generation and execution, and real time monitoring of process parameters such as gas flow and RF power levels. A loadlock is provided in the system to act as a wafer holding area before and after processing. The loadlock also prevents the process chamber from getting exposed to atmosphere thereby preventing contamination and other gases from getting into the process chamber. The process chamber is maintained at the base pressure of the system (10^{-2} mTorr) while the wafer gets transferred from the loadlock into the process chamber. Since the process chamber does not open to the atmosphere, the pumping time required for achieving the process pressure of about 10 mTorr from the base pressure is greatly reduced, thereby increasing the wafer throughput. The MRC Eclipse sputtering system consists of four process stations. The first station is an RF sputter etch station. The RF sputtering process is used to etch native oxide on top of metals such as Al before depositing another metal layer. Removal of native oxide is very important to achieve good low resistance contact between metal layers. The second station is used for sputter deposition of Ti. A Ti target is used in this chamber. The sputtering process takes place in the presence of Ar ions generated in a DC plasma. The third station is used for reactive sputter deposition of TiN. Like the second station, this station also uses a Ti target, but nitrogen is added to argon in the plasma to provide nitrogen ions for reacting with Ti to form TiN. Ti and TiN are deposited in two different stations because reactive sputtering of TiN tends to convert the Ti target into TiN and hence using the same station for both Ti and TiN will lead to cross contamination between these two films. The fourth and final station is used for the Al alloy deposition. The sputtering target is an alloy of Al, Si, and

Cu, the composition being determined by the technology. The substrates, in this case wafers, are heated from the backside by a temperature controlled heater. The wafers are heated to temperatures between 200 and 400 °C to improve metal grain size control and step coverage.

A metal stack in a submicron device normally consists of a Ti/TiN barrier layer, Al-Cu bulk metal, and an TiN antireflective coating (ARC) . Ti and Al-Cu films are deposited in MRC Eclipse system by DC sputtering. TiN film is deposited by reactive sputtering of Ti in nitrogen/argon plasma. The Ti/TiN barrier and the Al-Cu metal layers are deposited in the first pass of the wafer through the system. The ARC TiN is deposited in the second pass since the wafers flow in a sequence and can not be backed up to get top ARC TiN layer.

2.2.3 ULVAC sputter deposition system

The Ti film used in this work was deposited using DC magnetron sputtering process in an ULVAC sputtering system. The ULVAC sputtering system uses the same operating principle as MRC Eclipse sputtering system and the schematic diagram of this sputtering system is also similar except for a few small differences such as the chamber dimensions, configuration, and the process conditions. Therefore no separate schematic diagram is given in this report. The line of discussion on the ULVAC system mostly follows that of MRC Eclipse system. Similar to MRC Eclipse system, ULVAC system is also controlled by a computer.

Like the MRC Eclipse system, ULVAC sputtering system is also a cassette-to-cassette wafer transfer machine with multiple sputtering chambers. It is used for high volume production. This system contains a loadlock to enable wafer transfer from the cassette into the process chambers. The function of loadlock was discussed in section 2.2.2. An RF etch station is provided as one of the process modules, just like most of the sputter deposition systems. This etch station uses an inert gas plasma, such as Ar or N_2, generated by an RF discharge in an evacuated chamber to etch the native oxide on top of metals like Al before depositing other conductive materials, such as second level of metal. The removal of the native oxide is necessary in order to ensure good contact between different levels of metals. The second chamber is a Ti deposition chamber, in which the Ti from a target is sputtered off by Ar ions in a plasma generated by DC power source and deposited on a substrate. Nitrogen gas can not be used in the Ti deposition process as it has a tendency to react with Ti to form TiN. This property of N_2 is desirable in TiN deposition in the third chamber. In the third chamber, which is known as TiN deposition chamber, a plasma containing Ar and N_2 gases is used to deposit TiN material on the wafer. As discussed before, nitrogen gas reacts with the Ti material sputtered off from the Ti target to form TiN on the silicon substrate. Recent developments in the target technology have enabled one to use TiN target to deposit TiN material instead of relying on the reaction between Ti and N_2 inside the sputtering chamber in the presence of plasma. The wafers are heated to 200 to 400 °C during deposition to control the step coverage and grain size of the deposited film. The CVD (chemical vapor deposition) processes are slowly replacing TiN sputter deposition processes as CVD films are more conformal over the steps and hence provide much better step coverage when compared to sputtering processes.

The ULVAC system may also contain an additional sputtering chamber for deposition of Al-Cu alloys. These chambers use an Al-Cu target in an inert gas plasma generated by DC power source. The ULVAC system can be used for deposition of the complete metal interconnect film stack of Ti/TiN/Al-Cu/TiN. To achieve this, the wafers have to be passed through the system more than once depending on the arrangement of the sputtering chambers in the system configuration and the process sequence.

2.3 Equipment for Metal Etching

The interconnect pattern between the device terminals and between devices on a chip are be defined by the functional design of the chip. In the fabrication process, the pattern is transferred from the mask onto the wafer by a photolithographic process. The photolithography process utilizes coating of a photosensitive resist, which is commonly known as photoresist, and exposure of the resist through a mask. The exposed resist is developed by an appropriate developer and rinsed off with deionized water, leaving the photoresist only on the required interconnects. This pattern is ultimately transferred on to the interconnect material, such as Al-Cu alloy or polysilicon, by an etch process. The function of the etch process is to remove material from unwanted areas of the chip. In the early days of semiconductor fabrication, the etching process was performed in sinks containing wet chemicals. Although the wet etching process is simple, pouring of fresh chemicals into the sinks and disposal of used chemicals is hazardous to both the operators and environment. In addition, the wet etch process is a batch process in which a whole cassette containing several wafers is loaded for process. The process monitoring and control in any batch process is difficult and the etch time becomes longer as the solution gets depleted of the etchant chemicals. Additionally, the wet etching processes are

isotropic, therefore line width control is almost impossible making them unsuitable for patterning submicron geometries. Because of these drawbacks of the wet processing, the dry etching processes using plasmas containing etchant gases are gaining popularity in VLSI processing. In the following subsection, the basics of the dry etching processes are discussed before getting into the description of the Lam 4600 metal etcher that uses this principle.

2.3.1 Basics of dry metal etching process

Dry etching means plasma assisted etching which includes several techniques that use plasmas in the form of low-pressure gaseous discharges. The plasma is generated by application of RF or DC power across the electrodes enclosing the gas mixtures. These processes are used in VLSI processing because of their high fidelity pattern transfer. The gases that constitute the plasma are so chosen that their radicals or ions generated in the plasma react with the material to be etched and form a volatile product that can be pumped away by a vacuum pumping system. For example, chlorine containing gases such as pure Cl_2, BCl_3 and CCl_4 are used for etching aluminum and its alloys. Fluorine containing gases, such as CF_4 and CHF_3, are used for etching silicon and silicon dioxide as the reaction product silicon tetrafluoride SiF_4 is more volatile than silicon tetrachloride $SiCl_4$. Inert gases such as nitrogen and argon are added to the gas mixture to dilute the reactant gas, to act as coolants, and to provide ions for bombardment for anisotropic etch. Anisotropic etch is necessary to minimize the loss of pattern dimensions due to etching and thus conserve valuable silicon area on a chip. In some applications, vertical profiles are required for patterns such as polysilicon gates, metal interconnect lines and contact/via holes. In these applications, anisotropic etch process is achieved by physical

material removal though highly directional inert ion bombardment of the wafer in addition to chemical reaction. During the etch process, a polymeric film is formed along the sidewall of the etched pattern. This polymeric film protects the sidewall of the pattern and thus leads to vertical profiles. The sidewall polymer and the remaining photoresist on top of the etched pattern have to be removed before the wafer is moved to the next process step.

Most of the metals are etched using anisotropic Reactive Ion Etching (RIE) process. The RIE process is a combination of physical sputtering with the chemical reaction of reactive species which enables material selective anisotropy. A basic RIE process involves the following steps [1]:

(i) Generation of active species, such as positive and negative ions, radicals, electrons, and neutrals from the feed gas by application of RF or DC power.

(ii) Formation of DC self bias at the wafer to enable acceleration of ions towards the wafer.

(iii) Transport of the active species towards the wafer surface by diffusion

(iv) Adsorption of reactive ions or radicals to the surface to be etched

(v) Reaction of the adsorbed species with the substrate material

(vi) Desorption of the reaction product

(vii) Pumping out of the volatile reaction product.

Several metal etch systems based on the plasma etch processing are available in the market. In this research work, Lam Rainbow 4600 metal etch system was used for conducting etching experiments. In the following section, a brief description of the Lam Rainbow 4600 metal etch system is provided in order to build a basic understanding of

the configuration and operation of the system before going into the discussion on the aspects of process during the experimental phase.

2.3.2 Lam Rainbow 4600 metal etch system

In the beginning stages of the use of plasma etching processes in the semiconductor device fabrication, almost all of the etchers were batch loading systems where several wafers had to be loaded in one pass. The operation of these systems involved extensive wafer handling and lacked precise process control. Moreover, batch etchers were hard to automate as the wafer loading procedure is rather complicated. When there are insufficient number of wafers, dummy silicon wafers have to be loaded in empty spots. In these situations, the loading effect, which is dependent on the total exposed area of the film being etched, plays an important role. The etch time could be affected by the loading effect, due to the pattern density and the number of wafers loaded in the system. In such cases, the etch time has to be calculated based on the available data and manually entered into the recipe. The etch time thus calculated may not be long enough to etch the film completely leading to across-the-wafer and wafer-to-wafer nonuniformity. To solve this problem, an endpoint monitor is used to detect the end of etching. The endpoint monitor usually looks at one spot on a wafer or plasma to determine the end point. When one wafer is being monitored for endpoint, the other wafers may not have been etched completely. Hence the wafer to wafer variation could run into several tens of percentage. In addition to that, almost all of the batch etchers are isotropic etchers, and hence may not be used for submicron device processing in which the control of feature dimension is critical. The new generation metal etchers are single wafer, high etch rate systems with RIE (reactive ion etching) capability. Most of the new etchers come with post etch

passivation capability, such as bake and rinse modules, to remove the residual chlorine in the photoresist that could lead to corrosion upon exposure to moisture in the atmosphere.

Lam Rainbow 4600 is a single wafer metal etcher that is specially designed for etching aluminum, its alloys, and multilevel metal stacks. Fig. 2.2 shows the schematic diagram of Lam Rainbow 4600 metal etch system. This system is fully automated system controlled by a 386/486 or compatible Personal Computer. The wafers are transferred one at a time from the input cassette, processed and unloaded into the output cassette. All the wafers must be oriented in the same direction before they are transported into the etch chamber to enable the wafer clamp inside the etch chamber to make a tight seal around the wafer. The wafer orientation system, which is also referred to as flat finder, is a noncontact system that finds the major flat of the wafer using a optical LED source and light detector. Loadlock chambers are provided before and after the etch chamber to prevent the etch chamber from being exposed to the atmosphere during wafer transfers form in and out of the etch chamber. The loadlock chambers also increase the system throughput because the etch chamber needs to be pumped down to process pressure from a slightly higher than base pressure of the loadlock hence reducing the pumpdown time. The loadlocks also reduce the particle contamination from the environment by pumping the contaminants away through the loadlock pumps.

The main etch chamber consists of two electrodes, a bottom electrode and a top electrode. The schematic diagram of the Lam 4600 parallel electrode etch chamber is shown in Fig. 2.3. These electrodes are made of anodized aluminum which is found to be the most suitable material that can withstand harsh etch conditions of chlorine based plasmas. The wafer to be etched is transferred in to the etch chamber by a pick-and-place robotic arm.

The wafer sits on the bottom electrode and a mechanical clamp made of high quality ceramic holds the wafer down on the bottom electrode. The bottom electrode contains grooves through which helium is flowed to cool the wafer during the etch process. The temperature of each electrode is controlled by a separate water cooled chiller. The process gases are flowed through the holes uniformly distributed in the top electrode. The amount of gas flow is controlled by mass flow controllers (MFCs) tied to the computer. The across-the-wafer uniformity can be improved by modifying the pattern of holes. The RF power can be applied to either the top electrode or bottom electrode providing the user the capability to operate the system in isotropic plasma chemical etch mode or anisotropic reactive ion etch mode. The gap between the electrodes is adjustable through the recipe. A focus confinement ring is provided around the top electrode to confine the plasma to the region between the electrodes. The etch chamber is evacuated by a vacuum port surrounding the bottom electrode that holds the wafer during the etch process. Unlike other vacuum processing systems, the vacuum port is not a single opening. It is an annular opening surrounding the bottom electrode. The annular construction of the vacuum port enables uniform gas transport from the center to the edge of the wafer in all directions. The vacuum pumping system consists of a dry pump backed by a mechanical roughing pump connected in tandem.

The exit loadlock can be configured as a post etch passivation module. In this module, the chlorine absorbed by the photoresist during etch process is replaced with less corrosive fluorine to assist in preventing corrosion. CF_4 and O_2 gas plasmas are used for this purpose. From the plasma loadlock, the wafer is transferred to a spin chuck in the wet station, where it is rinsed with deionized water and dried with nitrogen. This combination of dry and wet post etch treatment eliminates the possibility of corrosion.

The entire etch system is controlled by a 386 or 486 based personal computer. The function of this computer is to supervise the wafer transfer, interface with the operator in creation and execution of recipes, keep track of the configurations, and check and enforce the safety interlocks, among the others. The system is provided with a color monitor to display the recipes or the system configuration. The position of wafers in the system is also displayed on the screen during the process.

The system runs on a menu driven software. The process recipes are made using this software. A typical recipe consists of a gap movement step, gas flow stability step, etch one or more etch process steps, gas purge steps, and gap homing step. A typical recipe is shown in Fig. 2.4. Each step is optimized to get the most efficient etch process. After stabilization of gap, gas flows, and pressure, RF power is turned on and the plasma is ignited. First the native oxide is removed from the top of the metals such as Al. Then bulk metal is etched. The main etch step has to ensure vertical sidewalls by the etch anisotropy and polymer formation along the sidewall to minimize lateral etching. Gases such as CCl_4 and BCl_3 are added to Cl_2 to achieve sidewall formation. These gases also help in removing the native oxide layer on top of Al or Ti films. The main etch step is usually endpointed using an optical endpoint detector which continuously monitors the presence of certain species with a particular wavelength in the plasma. In most cases, the etch products in the plasma are monitored as a means of detecting the end of the etch process. A sudden drop in the intensity corresponding to the wavelength of the etch product such as $AlCl_3$ in the case of Al etching is detected as the end point and switches the recipe to overetch step. The main etch step is followed by overetch step to remove metal stringers along the sides of the steps on a substrate with topography and residues like silicon and

copper. Unlike the main etch step, the overetch step is a timed etch process. In most of the etch chemistries, the plasma used for etching the bulk metal such as Al-Cu can also be used to etch barrier metals such as Ti, TiN, and TiW, which also serve as antireflective coatings.

2.4. Equipment for Sheet Resistance Measurement

The thickness of a conductive film can be calculated from the sheet resistance measurements of the same film. The sheet resistance measurement is usually a nondestructive technique. The most popular method used for sheet resistance measurement is the four-point probe measurement technique. The four point probe technique was extensively used in this work in order to calculate thickness and hence the etch rate of the films. In this section, first the principle behind the measurement is described and then the details of the 4D four-point probe measurement tool are discussed.

2.4.1 Basics of four-point probe measurement

The sheet resistance of a conducting film can be measured by four-point probe technique. (Fig. 2.5). The four probes are arranged along a straight line. These probes are placed in contact with the conductive film under measurement. A current I is passed through the two outer probes and the resultant voltage drop V across the inner two probes is measured. The measured resistance is converted to resistivity by the following formula:

$$\text{Sheet resistance } \rho_s = CF\ (V/I) \qquad (2.1)$$

where CF is the correction factor depending on the geometry and the probe spacings [2]. A table containing the correction factors is given in ref [2]. The magnitude of the correction factor increases as the ratio of the diameter of the sample to the probe spacing increases. When this ratio is very large, approaching infinity, the correction factor reaches a value of 4.53. When measuring a diffused film such as a shallow film with low dopant concentration, noise must be avoided in order to get reliable measurements. The noise problem can be overcome by doing the voltage measurements with the current flowing in two opposite directions, then taking the average of the two readings. The average reading also removes some of the effect of the contact resistance of the probes. If the difference in voltage readings are large for the current flow in two directions, the probe tips and the cleanliness of the measured substrate surface have to be checked. The measurements must be repeated at several current levels to ensure the accuracy of the measurements. The measurement can be reproduced within $\pm$ 2% if the instrument, probe tip diameter, probe pressure, and current level are appropriately chosen. For example, to measure low resistance films, the current level is increased so that the measured voltage is between 2 and 20 mV. The ambient temperature could also affect the sheet resistance - about 1 %/°C at 23 °C for a 10 Ohm-cm material. Therefore, in order to avoid the temperature effects on resistance, some of the four-point probe systems are equipped with a temperature controlled chuck.

The four-point probe sheet resistance measurement technique is used wherever sheet resistance needs to be measured, such as dopant density measurement of a diffused film and thickness of a conductive film. The four-point probe technique was used throughout this research work to measure the sheet resistance of Ti or TiN metal film, since it was the simplest and most convenient technique available at the fabrication facility. The film

thickness can be calculated from the measured sheet resistance ρ_s by using equation (2.2) knowing the bulk resistivity of the material.

$$\text{Sheet resistance } \rho_s = \frac{\text{Bulk resistivity } \rho}{\text{film thickness } \quad d} \qquad (2.2)$$

The sheet resistance measurements were made before and after etch process and the film thickness was calculated. The difference in the thickness of the films before and after etch yields the etched thickness. The etch rate of the conductive film was obtained by dividing the etched thickness by the etch time in minutes.

$$\text{Etch rate} \quad = (d_1 - d_2)/t \qquad (2.3)$$

where d_1 is the film thickness before etch, d_2 is the film thickness after etch, and t is the etch time.

2.4.2. 4D four-point probe sheet resistance measurement system

The four-point probe instrument used in this work is Model 280S made by Four Dimensions, Inc [139]. A schematic diagram of this system is shown in Fig. 2.6. The heart of the system is a 486 compatible computer controlled probing station. The measurements are recipe driven. Up to 200 customized recipes can be created and stored in the hard disk of the computer. Each recipe consists of up to 30 test and information parameters, including test site geometry, test pattern, number of points, wafer size, test diameter, wafer type and control limits, in addition to the details such as operator identification, equipment/process name, date and time of measurement.

The substrate to be measured, wafer diameter ranging from 50 mm to 200 mm (2 inches to 8 inches), is held by vacuum on a chuck. The temperature of the chuck can be controlled by a feedback temperature control system. The movement of the chuck is controlled by software through a set of stepper motors. These stepper motors are used because they are more reliable than the conventional hydraulic pistons which are prone to jamming, need periodic lubrication and replacement. The four probes are radially situated in the quickly changeable probe-head. This system reduces the measurement error by employing dual configuration system in which two measurements are made by switching the current-driving and voltage sensing pairs of probes. This system is provided with auto-current adjustment which automatically checks the resistivity of each wafer at the beginning of the measurement and chooses the optimum probe current to achieve maximum measurement accuracy. The auto-compensation feature zeroes the amplifier drift in each wafer test, while the auto-gain feature chooses the low or high gain preamplifier at the beginning of each measurement to reduce the noise. The system also has internal calibration option which automatically calibrates the system at periodic intervals in order to ensure the measurement accuracy. The probe heads are chosen from three types with different probe tip radius appropriate for the film under measurement.

The 4D four-point probe system can be programmed to measure 1 to 650 points on each of the wafers (Fig. 2.7). These measurement sites can be chosen from standard polar or cartesian patterns. The powerful software running on 486 based computer has SPC (Statistical Process Control) data analysis and mapping capability. The recipes can be programmed to output the data in a user-defined format such as sheet resistance or thickness that can be calculated from sheet resistance. The measurement data can be

mapped in a histogram, a two dimensional contour map, or a three dimensional map. The specification and control limits can also be set for each recipe. The SPC charts can be used for monitoring and comparison of the processes or equipments. The process capability can be automatically checked against AT&T standard SQC (Statistical Quality Control, which is a synonym to Statistical Process Control) rules and warnings can be given if the process violates any of these rules.

2.5 Summary

The objective of this chapter was to provide the reader with sufficient background information on the equipments and processes used in the course of this research work. In this chapter, the basic principles behind the processes used in this research work, such as sputter deposition of materials, plasma etch, and sheet resistance measurements were discussed. This was followed by a brief description of the equipments used for this work. A discussion on the principle behind the sputter deposition process was presented in section 2.2, followed by a description of the various modules and their function in an MRC Eclipse sputter deposition system, aided by a schematic diagram. A similar description for ULVAC sputter deposition system was also provided. The section 2.3 presented the basic principles behind plasma assisted etch processes. A brief description of the Lam Rainbow 4600 metal etcher, which was the main equipment used in this study, was presented along with a schematic diagram. The Lam Rainbow 4600 etch chamber configuration was also described. Finally, the four-point probe sheet resistance measurement technique was discussed, along with a description of the 4D four point probe measurement system that was used for sheet resistance measurement from which the film thickness could be calculated.

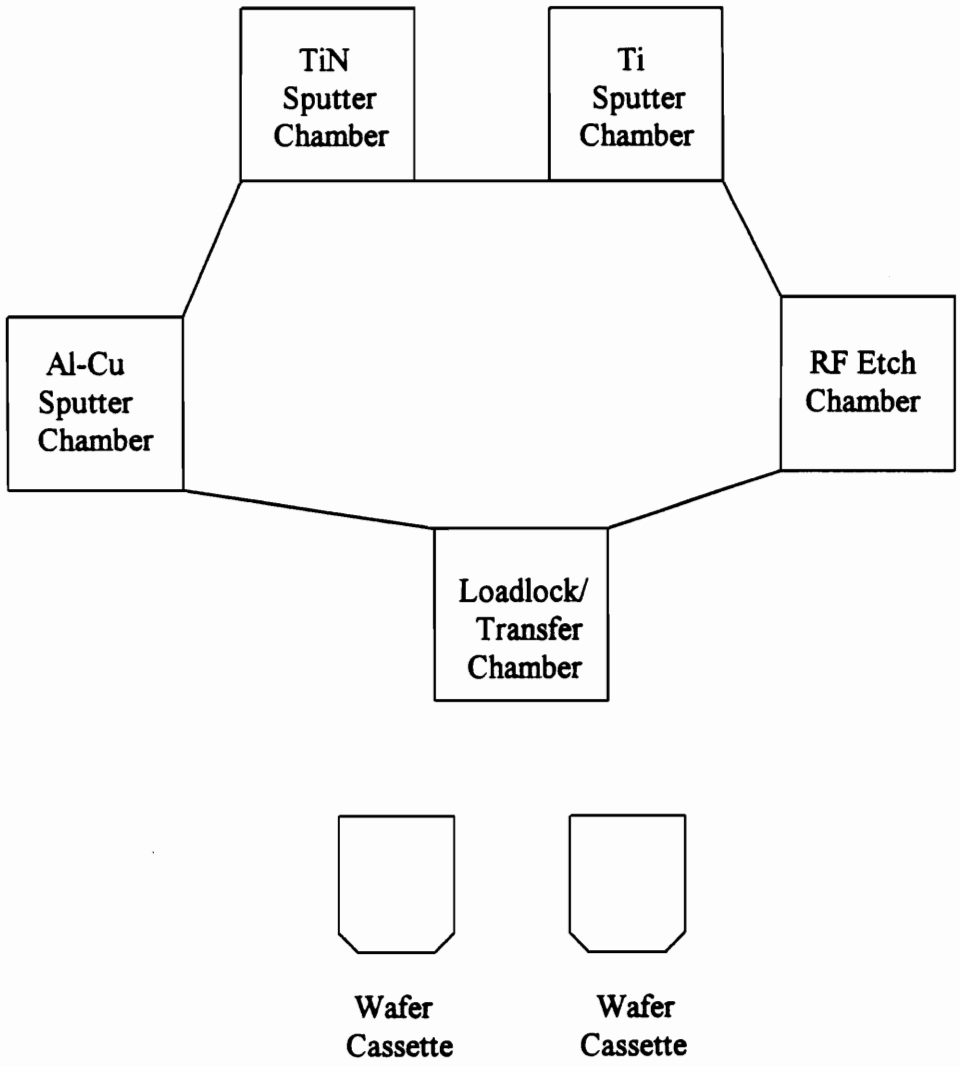

Fig. 2.1. Schematic diagram of MRC Eclipse sputter deposition system.

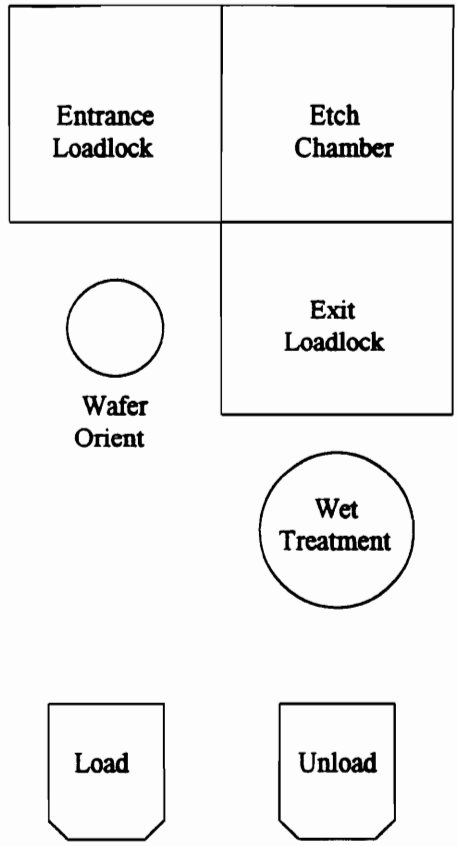

Fig. 2.2. Schematic diagram of Lam Rainbow 4600 metal etch system.

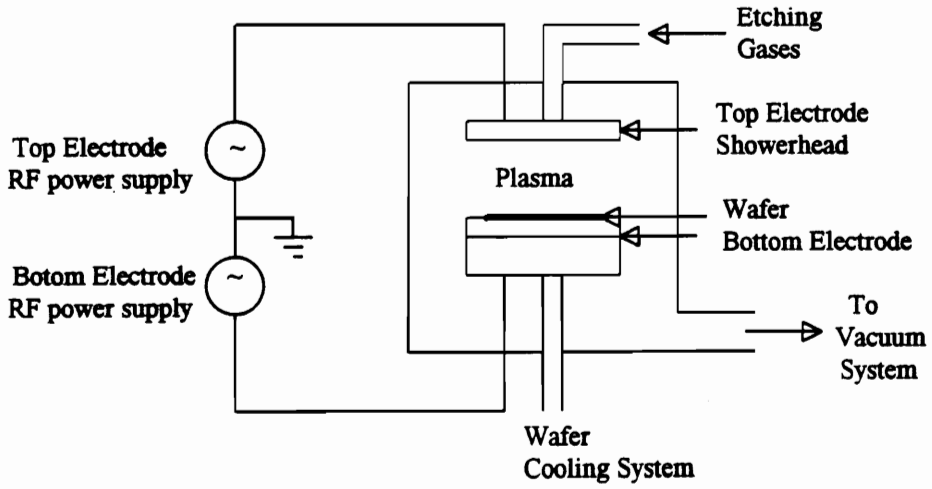

Fig. 2.3. Schematic diagram of Lam 4600 parallel electrode etch chamber.

	Step 1	Step 2	Step 3	Step 4	Step 5	Step 6	Step 7
Pressure (mT)	5	700	700	700	2000	2000	0
Power (W)	0	0	0	350	0	0	0
Gap (cm)	3	3	3	3	3.5	4.5	5.56
Cl2 (sccm)	0	25	25	25	0	0	0
BCl3 (sccm)	0	75	75	75	0	0	0
N2 (sccm)	0	50	50	50	100	100	0
He (sccm)	0	0	0	0	0	0	0
He Clamp (T)	0	0	12	12	0	0	0
Compl	[stability]	[stability]	[stability]	[time]	[time]	[time]	[end]
Time (seconds)	20	20	20	60	7	10	

Fig. 2.4. A typical TiN etch recipe for Lam Rainbow 4600 etcher

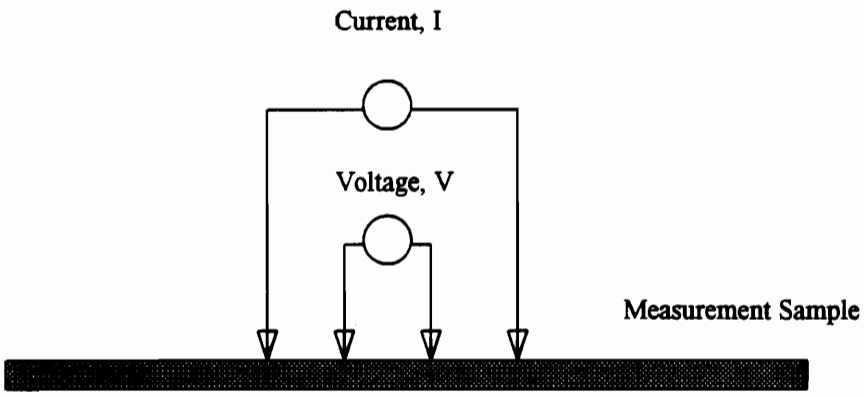

Fig. 2.5. Typical four-point probe arrangement.

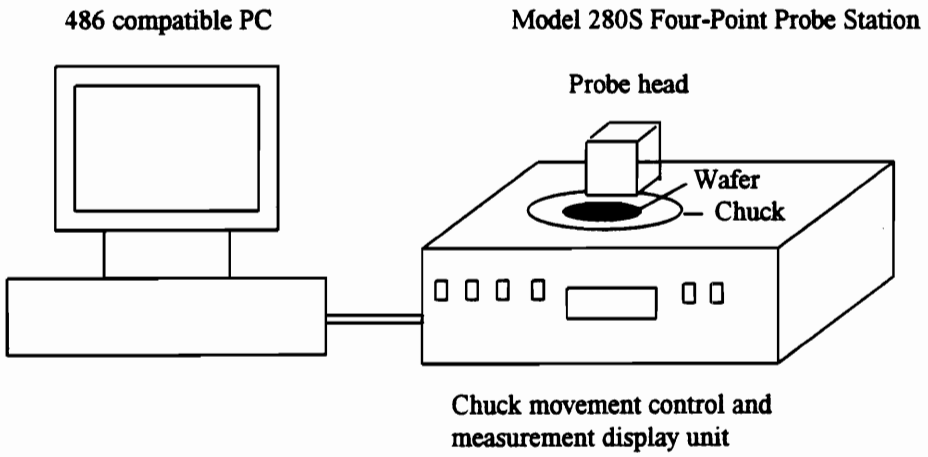

Fig. 2.6. Schematic diagram of 4D Model 280S Four-Point Probe measurement system.

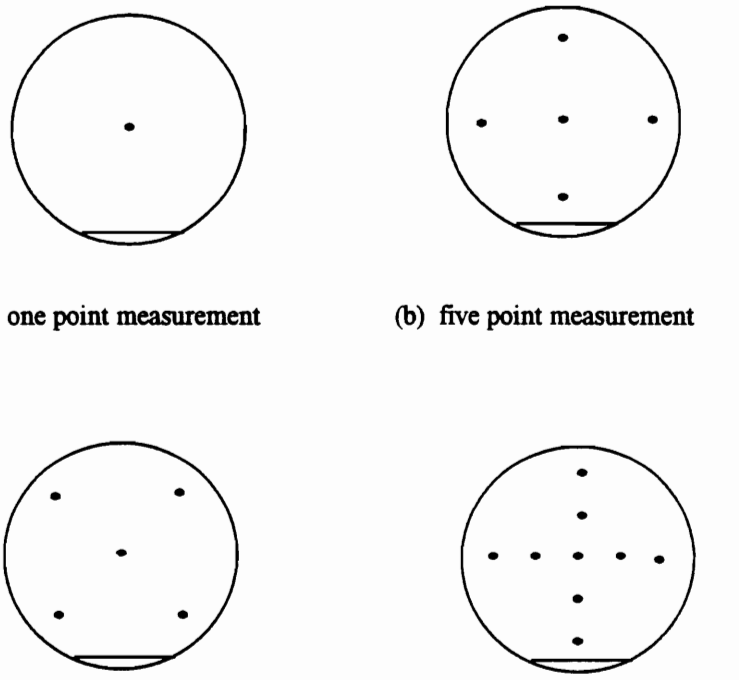

Fig. 2.7. Typical Four-point probe test patterns on a wafer.

Chapter 3

TiN etch in Cl_2/N_2 plasma

3.1 Introduction

It is well known that TiN can be etched in Cl_2 and Cl_2/N_2 plasmas, but detailed study of the characteristics of TiN etching in Cl_2/N_2 plasma is not available in the literature. The work done by C. Jerbic and K. Amberiadis [3] serves as the foundation for this study. The goal of this study is to characterize the etching process of TiN film in Cl_2/N_2 plasma when the process parameters are varied one at a time. The simplest and classical experimental technique for investigating the effect of the process parameters is to vary one parameter at a time while maintaining others at a constant level. This type of experiment is known as Manhattan grid experiment. In this chapter, the classical characterization experiments conducted to characterize TiN etch are described. The effect of the process parameters such as time, chlorine and nitrogen gas flow, power, and pressure is studied by varying one parameter at a time, and the etch rate is measured in this set of experiments. From these experiments, the main effect of that particular parameter can be studied. An attempt is made to explain the results in terms of the plasma physics and chemistry. However, these process parameters may have interactions and higher order effects on the etch rate, which are not obtainable from the above mentioned classical experiments. Therefore, an additional experimental technique, Response Surface Methodology, known as RSM, must be used. The RSM experiment is designed using JMP software and conducted to study the main effects and interactions between the input

parameters along with second order effects using statistical analysis techniques. An empirical model for the TiN etch rate is developed using the results obtained from this experiment. Details of this experiment will be discussed in Chapter 6.

The experiment was conducted on 4000 Å of reactively sputtered TiN film on an CVD deposited oxide film with thickness of 13000 Å on a bare silicon wafer with <100> orientation. The bulk resistivity of the film was assumed to be 148.58 μOhm-cm. This number was calculated from the previous measurements of thickness and sheet resistivity. In all the experiments, the etch rate is calculated by measuring the sheet resistivity before etch and after etch at 49 points using 4D four-point probe machine. 3-Sigma uniformity of TiN deposition thickness and sheet resistivity was better than ± 7%. The derivation of the calculation of etch rate from the sheet resistivity measurement is shown in Appendix A. Appendix B presents the Lotus 123 program for the calculation of the etch rate from the sheet resistivity value.

The wafers were etched in a commercially available Lam Rainbow 4600 single wafer metal etcher. The detailed description of the system was presented in Section 2.3. The etch rate was nonuniform along the radius of the wafer and center and the edge of the wafer had higher etch rate when compared to the middle. Therefore, the points of measured sheet resistivity were grouped into three regions - center, middle and edge are analyzed separately.

3.2 Etch Reaction

Plasma etching, which plays a major role in the current submicron semiconductor manufacturing process, is the interaction of gaseous species with solid films to form volatile compounds. Plasma etching is mainly used for transferring patterns onto the substrate, after a mask is applied on it by photolithographic techniques.

The etching of a solid material in a gas phase consists of the following steps [83]:

(1) nondissociative adsorption of gas species at the surface of the solid that is being etched

(2) dissociation of this adsorbed gas

(3) reaction between the adsorbed atoms and the solid surface to form an adsorbed product molecule

(4) desorption of the product molecule into the gas phase

(5) removal of nonreactive residue.

Any one of the steps listed above may be rate limiting and if any one of the steps does not occur, then the etching reaction will not proceed.

The etching of solid films in the gas plasma can be divided into two major categories. These categories are

(1) plasma etching

(2) ion etching

Plasma etching involves etching of a solid material exposed to a reactive gas plasma in which there is no ion bombardment on the sample. The plasma etching process is generally isotropic. In a parallel plate etcher, such as Lam 4600 used in this study, the RF power is applied to the top electrode to achieve plasma chemical etching and a reactive gas is used

in the plasma. On the other hand, the ion etching involves removal of atoms from the surface of the sample material by bombardment with energetic ions or atoms [34]. Ion etching process is also know as sputtering. In this process, the substrate material is removed by physical etching, not by chemical reaction. Ion etching process is generally anisotropic and the direction of etching depends on the angle of incidence of the ions. An inert gas, such as Ar or N_2, is used in a parallel plate etcher such as Lam 4600 in order to provide the ions/atoms for etching. The RF power is applied to the bottom electrode in order to create an electric field so as to accelerate the ions towards the electrode on which the sample is kept [34].

A combination of the two basic etch processes is called reactive ion etching (RIE). In this etching method, the reaction of the gas species in the plasma with the substrate is induced or assisted by ion bombardment. The reactive gas species is used to increase the etch rate, while the etching by ion bombardment maintains directionality and high resolution in the etching process. A balance between chemical (neutral) and physical (ionic) etching processes is to favor the sputter etching component in order to prevent the accumulation of silicon and copper-rich residues in the etched areas when an Al alloy contains silicon and copper [46]. The reactive ion etching involves a process known as chemical sputtering. This refers to those sputtering processes where the sputtering is influenced by chemical modification of the top layer of the substrate. Three examples of such processes can be provided:

(1) bombardment with reactive ions (such as Cl^+)

(2) simultaneous exposure to inert ions and a reactive neutral gas (such as Ar^+ and Cl_2)

(3) simultaneous exposure to reactive ions and a reactive neutral gas (such as Cl^+ and Cl_2) [22].

The reactive gas species is chosen on the basis of ease of volatility of the reaction products. For example, fluorine containing gases are used for silicon etching as the reaction product SiF4 is readily volatile at process pressures. Metals, such as Al and Ti, and metallic compounds, such as TiN, are etched in chlorine based chemistry because the reaction products are more volatile than those in fluorine plasma [89]. Therefore, in this work the characteristics of etching of Ti and TiN in chlorine based plasma is studied.

In order to etch TiN which is a solid material, it has to be broken down into its constituents titanium and nitrogen. Nitrogen is a gas and hence it can be pumped away from a reaction chamber by a vacuum system. Ti atoms have to be reacted with a reactant to form a volatile compound or a gas at process pressures so that it can be easily pumped away by the vacuum pumping system. The following reaction takes place while etching TiN with Cl_2.

$$2TiN + 4Cl_2 \rightarrow 2TiCl_4 + N_2 \qquad (3.1)$$

At atmospheric pressures, in order for this reaction to take place, temperature of TiN film has to be increased such that it can react with chlorine to form $TiCl_4$ in the form of a film on the wafer. The etching process, in order to be effective, has to have a means of carrying the reaction products away from the substrate so as to facilitate further etching of the TiN film. In a planar diode reactor such as the one used in this experiment, the chamber is pumped down to a low pressure of between 0.5 to 1 Torr, and an RF power is applied across the electrodes. Plasma is generated and sustained by the energy supplied from the RF source. This plasma consists of electrons, ions of the gases, and neutrals. The ions, such as Cl^+ generated in the plasma, are highly reactive. In addition to this, because

of their positive charge, they are attracted towards the cathode. These ions chemically react with the substrate material placed on the cathode or physically remove the substrate material by bombardment. Either of these two processes or their combination lead to removal of the substrate material by etching. It has been observed by Choe et al., [46], and Danner et al., [86] among several other workers that chlorine molecules also participate in the etching process of materials like Al even in the absence of plasma. Thus, it can be assumed that the etch reaction occurs due to Cl ions and Cl_2 molecules. The heavier ions in the plasma, such as Ar^+ and N^+ which are generally used as carrier gases, can also assist the material removal process due to their bombardment and thereby physically dislodging the atoms from their lattice structures [8]. The reaction products are gases in the range of process pressures and hence get pumped away by the pumping system.

In the following sections, the effects of process parameters, such as time, gas flow rate, RF power, and pressure are studied. The results are discussed using the concepts of plasma physics and chemical reactions.

3.3 Time versus Etch Rate

In this section, the etch rate variation due to etch time is studied. The substrates were exposed to 3:1 Cl_2/N_2 plasma (75:25 sccm actual gas flow) for time durations ranging from 5 seconds to 25 seconds. The process pressure was maintained at 700 mTorr. The bottom electrode was heated to 40 °C and the top electrode was maintained at 70 °C. The etch chamber was heated to 70 °C in order to prevent the reaction products from depositing on the chamber walls, causing a buildup which would affect the etch process.

The etch rate increases by about an order of magnitude when the etch time is increased from 5 seconds to 25 seconds. The etch rate is plotted against etch time. Fig. 3.1 shows the etch rate at center, middle and edge of the wafer on separate curves. Fig. 3.2 shows the plot of the average etch rate against etch time. There is a delay of about 3 seconds before the start of etching after plasma is turned on. This delay, known as induction time, is due to the time taken to etch through a thin layer of oxynitride (TiN_xO_y) on top of TiN film or for stabilization of plasma or etcher. The etch rate increases by about 1000 Å/min when the etch time is increased from 5 to 10 seconds and the increase in the etch rate is more substantial for the etch times between 10 and 20 seconds etch time. The etch rate steadily increases as the etch duration is increased because of wafer heating effects due to prolonged exposure to the plasma. The etch rate levels off at around 8000 Å/min for an etch time of 25 seconds. The etch rate variation for the etch times of over 25 seconds could not be obtained because all of the TiN film was etched away for etch time of 30 seconds and above since the TiN film thickness was only 4000 Å. Based on the results, the leveling off of etch rate for etch durations over 25 seconds can be explained due to the fact that the wafer reaches thermal steady state and the temperature remains constant.

From Fig. 3.1, it can be observed that the edge of the wafer etches faster than the center. In the metal etcher Lam 4600 used for the study, the gases flow through the shower head which also acts as the top electrode. The residual gases and reaction products are pumped away by the vacuum pumps through the opening surrounding the bottom electrode on which the wafer is placed during the etching process. So the edge of the wafer is closer to the pumping port than the center and hence the reaction products and other residual gases are transported from the edge much faster than from the center of the wafer. This

effect causes a localized increase in the etch rate near the edge of the wafer when compared to the center of the wafer.

3.4 Cl_2/N_2 Flow Rate versus Etch Rate

In this section, the dependence of the etch rate on chlorine and nitrogen flow is studied. The chlorine gas acts as the reactant in the chemical reaction. The nitrogen gas acts as a carrier gas and also provides ions for bombardment during the etch process. In the first set of experiments, the effect of chlorine flow is investigated. The nitrogen flow is kept constant at 25 sccm and the chlorine flow is varied from 25 sccm to 200 sccm. That is the Cl_2:N_2 ratio is varied from 1:1 to 8:1.

The TiN film is etched by reaction of atomic chlorine and molecular chlorine [86]. In the plasma, the atomic chlorine is generated by dissociation of chlorine molecule by electron attachment. The chlorine is not completely dissociated into chlorine atoms in the plasma. The chlorine molecules are still present in the plasma. As observed by Danner and Hess, both chlorine atoms and molecules contribute to the etch reaction in Al etching in chlorine plasmas [86]. Extending the same argument to TiN etching, it can be assumed that both atomic and molecular chlorine act as reactants. The atomic concentration of chlorine in the plasma can be increased by diluting the feed gas with pure chlorine because noble gases or nitrogen as these are less efficient than molecular chlorine as third bodies for atom recombination [86]. The equation 3.2 shows the dissociation of chlorine molecule in the plasma.

$$2Cl_2 + e^- \rightarrow Cl_2 + 2Cl + e^- \qquad (3.2)$$

Fig. 3.3 presents the etch rate variation at the center, middle and edge separately and Fig. 3.4 shows the average etch rate variation with the chlorine flow. It is easier to visualize the effects of Cl_2 using the average etch rate versus the chlorine flow than with the etch rate curves for center, middle and edge and then extend the discussion to the latter. As the chlorine flow is increased from 25 sccm to 75 sccm, the TiN etch rate increases by ~ 50% and then increases only by ~ 10% when the chlorine flow is increased to 150 sccm. The etch rate levels off at 4900 Å/min when the chlorine flow is increased beyond 150 sccm. In the simplest case, the etch rate increases with the flow rate and decreases with the area of the etched surface. This is the so called 'loading effect' which is simply a depletion of reactant gas from the gas phase [82]. In the low flow region of up to 75 sccm, the etch rate is limited by the availability of the reactant chlorine species and hence the TiN etch rate increases as the chlorine flow is increased. The concentration of chlorine atoms in the plasma increase with the addition of pure chlorine because dilution increases atom yield in the discharge [121]. In high flow region of 100 sccm and beyond, there is only a very little or no increase in the etch rate because the chlorine etchant species can be pumped away before they get a chance to react with the substrate TiN film due to increase in pumping speed to maintain constant pressure operation [12]. The overall etch rate is a function of product of supply rate limited and pumping rate limited phenomena.

Nitrogen is an inert gas, which is mainly used as a carrier gas in plasma etch processes [8, 33]. It also provides ions for sputter etching and for assisting or inducing etch processes by another etchant species such as chlorine. Nitrogen is also used for stabilization of plasma and as a cooling medium. It was also observed by Clyne and Stedman [122] that the noble gases and nitrogen are less efficient than molecular chlorine as third bodies for

atom recombination. This effect makes it possible to obtain the ratio of atomic to molecular chlorine in the etch gas greater than one. In addition, dilution with gases like N_2 permits the variation of the etchant concentration independent of pressure. For thin films, this offers a means of slowing down the etch rate by reducing the atomic and the molecular concentration in the etch gas so that better control of etch time can be achieved. Finally, dilution allows high flow rates, thereby reducing the transport limitations, without increasing the usage of the etchant gas [86]. The effect of nitrogen gas on TiN etch rate was determined by increasing the nitrogen flow from 0 to 100 sccm while maintaining chlorine flow at 75 sccm. That is the Cl_2:N_2 ratio was varied from very small ratio of 75:0 to less than 3:4. In this experiment, etching was done at a constant pressure of 700 mTorr with an RF power of 350 Watts applied to the bottom electrode.

Figs. 3.5 and 3.6 illustrate the etch rate variation due to variation in nitrogen flow. The etch rate is at the highest level (5050 Å/min) for 75 sccm chlorine flow and no nitrogen flow. The etch rate experiences a gradual decrease to ~ 50% of its initial value as the nitrogen flow is increased from 0 to 100 sccm. The effect of nitrogen flow on TiN etch rate can be explained as follows:

When there is no nitrogen flow, the TiN is etched only due to its chemical reaction with chlorine. As the nitrogen flow is increased, the etch rate decreases almost linearly, reaching a low of 2648 Å/min for the maximum nitrogen flow of 100 sccm. There are two etch mechanisms occurring when nitrogen is added to the etch gas. First, Nitrogen provides ions for bombardment of the substrate. Secondly, as the nitrogen flow is increased, the partial pressure of chlorine is decreased to maintain constant pressure due to the presence of nitrogen. This effect, which is called dilution effect, reduces the amount of chlorine etchant species available for etching in the chamber, leading to a

decrease in the etch rate. A decrease in the TiN etch rate is observed (Fig. 3.6) with the addition of N_2 and hence it can be concluded that the dilution effect due to nitrogen is predominant over the ion etching. The effect of N_2 flow over 100 sccm on etch rate could not be studied due to the maximum limit of the nitrogen mass flow controller (MFC). In both of the above cases, TiN film near the edge of the wafer etched faster than the center of the wafer as can be seen in Figs. 3.3 and 3.5 .

3.5 RF power versus Etch Rate

In this experiment, the effect of RF power on the TiN etch rate is studied. RF power is applied between the electrodes in order to generate a plasma and provide sufficient energy to sustain it. Frequency of RF source is so chosen that it equals or exceeds the ionization energy of the reactant gas species. The plasma contains Cl_2 and N_2 gas molecules, ions and radicals. The RF power can be applied to either of the electrodes. For the other experiments in this study, the RF power is applied to the bottom electrode. In this experiment, RF power is applied to either the top or the bottom electrode and its effect on etch rate is studied. Ideally speaking, the top electrode and the bottom electrode are symmetrical and hence the plasma generation should not be affected by the application of RF power to either of the two electrodes.

The effect of RF power is studied by varying the applied RF power either to the top electrode or bottom electrode, while maintaining the pressure at 700 mTorr, with Cl_2:N_2 ratio of 3:1 (with actual flow of 75:25 sccm). Figs. 3.7 and 3.8 show the etch rate as a function of RF power applied to bottom electrode. The etch rate increases linearly with the applied RF power between 100 and 300 watts and then the increase of etch rate is

steeper for RF power over 300 W. The maximum etch rate reaches 8250 Å/min for an applied RF power of 600 W. When the RF power is increased, the ionization is increased leading to increased density of radicals and ions in the plasma. An increase in the RF power also increases the mean electron energy and the ion energy incident on the substrate leading to an increase in the etch rate. Thus, the etch rate increases irrespective of the etching mechanism - chemical or ion etching or both. If the etching is ion assisted, the etch anisotropy is improved. When the RF power is applied to the bottom electrode, the self bias dc voltage, Vdc, appearing across the sheath region (sheath is the space charge region containing accumulated positive charges, created due to repulsion of negative charges by the positive potential of a floating substrate) near the substrate placed on the bottom electrode is negative [12]. This negative Vdc accelerates positive ions from the plasma and causes ion bombardment on the substrate placed on the bottom electrode. In addition to the already existing plasma chemical etching due to chlorine atoms, reactive ion etching due to chlorine and ion etching due to nitrogen ions [88] also contribute to the etching process. It was also observed that the magnitude of Vdc increased when the RF power applied to bottom electrode was increased, thereby causing increased etching due to more ions reaching the substrate. Choe et al [46] observed that the Al etch rate was insensitive to change in RF power and hence concluded that chlorine molecules are as reactive as any other chlorine bearing radicals in the plasma. The researcher's results appear to contradict this. The TiN etch rate increases with the RF power as can be seen from Figs. 3.7 and 3.8. It can be concluded that the dominant etching mechanism in Cl_2/N_2 plasmas is ion bombardment of chlorine and nitrogen ions on TiN film. Essentially, all the applied power is dissipated as heat in the etch chamber. The increase in RF power also leads to an increase in substrate temperature causing an increase in the etch rate due to elevated reaction rates of chlorine species with TiN. It is predicted that the etch rate

will level off at high power densities because of ionization of gases reaching its maximum limit and the wafer reaching a thermal steady state where there may not be any further increase in the wafer temperature. The excess heat is conducted away by the cooling system of the etcher. At very high power densities, the substrate require effective heat sinking as elevated substrate temperatures will lead to harmful effects such as photoresist flow and charring and loss of selectivity [88]. Therefore, an efficient wafer cooling system is necessary for achieving high etch rates in plasma etchers.

Figs. 3.9 and 3.10 illustrate the etch rate dependence on RF power applied to top electrode. In this case, the average etch rate is less when compared to the case where the power is applied to the bottom electrode. Similar to the previous case where the bottom electrode was powered, the etch rate increases almost linearly with the increase of RF power. The maximum etch rate is around 4560 Å/min for an RF power of 600 W. As discussed in the previous case, the density of ions and radicals increase due to the increase in RF power, leading to an increase in the etch rate. When the RF power is applied to the top electrode, a positive Vdc appears in the sheath region close to the substrate. This positive Vdc retards positive ions from the plasma and hence only the ions containing more energy to overcome this potential barrier can reach the substrate to contribute to etching. Hence it can be concluded that the etching mechanism is predominantly plasma chemical etching when the RF power is applied to the top electrode.

3.6 Pressure versus Etch Rate

The effect of variation the reaction chamber pressure on TiN etch rate is studied and reported in this section. The etch chamber pressure is increased from 500 to 1000 mTorr

in increments of 100 mTorr, while maintaining the RF power at 350 W, at a constant gas flow of 75 sccm chlorine and 25 sccm nitrogen (3:1 ratio). An increase in the chamber pressure has just the opposite effect of increasing the RF power as can be seen from Figs. 3.11 and 3.12. Fig. 3.11 shows the pressure dependence of the average etch rate and Fig. 3.12 shows the effect of pressure on center, middle, and edge etch rates. When the RF power is applied to the top electrode, the magnitude of initial etch rate is 12% lower because of the reasons described in section 3.5 on the effect RF power. The etch rate linearly decreases by 15% when the pressure is increased from 500 mTorr to 800 mTorr. For pressures beyond 800 mTorr, the etch rate remains leveled at around 4650 Å/min for the case in which top electrode is powered. The linear decrease in etch rate extends up to 800 mTorr, compared to the case where RF power is applied to the bottom electrode for which the etch rate bottoms out at 700 mTorr. When RF power is applied to the bottom electrode, the etch rate displays a similar dependence, except that the value of the etch rate is higher than that in the powered top electrode. The etch rate rapidly decreases by ~ 10% as the pressure is increased from 500 to 700 mTorr. The etch rate starts at 6590 Å/min for a pressure of 500 mTorr and decreases linearly and levels off at 5800 Å/min for pressures of 700 mTorr and above. No further decrease in the etch rate is observed for further increase in the pressure. Figs. 3.13 and 3.14 show the etch rate dependence on the pressure when the bottom electrode is powered.

The effect of reaction pressure on TiN etch rate can be explained as follows:

At low pressures, the mean electron energy and ion energy incident on the substrate is high because of low probability of loss of energy due to collision with other ions or molecules in the plasma. The mean free path of the ions is high and hence the ions generated in the plasma have higher probability of reaching the substrate to contribute

towards etching. As the pressure is increased, the number of ions and molecules in the plasma increase to maintain the pressure. The ions and electrons lose larger amount of energy due to increased probability of collision with the ions or molecules in the plasma [88]. This phenomenon causes a decrease in TiN etch rate. Another important factor affecting the etch rate is the residence time of the reactant species in the plasma, which is defined as

$$\text{Residence time } t = (P\ V)/Q \qquad (3.3)$$

where P is the pressure, V is the reactor volume, and Q is the process gas flow rate.

As pressure P increases, the concentration of reactive chlorine atoms may be reduced by recombination reactions which occur at reactor surfaces and also at gas phase of the plasma [61]. Such recombination reactions reduce number of reactant chlorine atoms available for etching and thereby leading to reduction in etch rate. Increased pressure also decreases the volatility of the reaction products from the TiN surface, slowing down the etch process. It is also observed that the decrease in Vdc is not significant to cause decrease in etch rate. The effect of pressure on TiN etching can be attributed to one or all three of the etch mechanisms described above.

The etch rate shows a similar characteristics when the RF power is applied to the top electrode, with the magnitude of etch rate being slightly lower than when RF power is applied to the bottom electrode. This difference in etch rate can be attributed to reduced ion bombardment as discussed in section 3.5 on the dependence of etch rate on RF power.

3.7 Summary and Conclusions

In the sections 3.3 to 3.6 of this chapter, the etch characterization of TiN film with the variation of process parameters such as etch time, chlorine and nitrogen gas flows, RF power, and chamber pressure were discussed. From this type of experiments, the individual effects of the process parameters on the etch rate were determined. Using the results obtained from these experiments, the following conclusions can be made:

(i) There is a 3 second induction time before TiN film starts etching. The TiN etch rate increases upon an increase in the etch time and reaches a maximum probably due to an increase in wafer temperature with the prolonged exposure to plasma.

(ii) The etch rate increases linearly with the increase in chlorine flow in the low flow region due to the increase in the availability of the reactant gas species. At high chlorine flow, the etch rate levels off due to saturation of ionization of reactant chlorine.

(iii) Increase in nitrogen gas flow can decrease the etch rate due to dilution of the plasma of chlorine which is the main reactant.

(iv) The etch rate increases almost linearly with the increase in RF power. The average TiN etch rate is higher when the RF power is applied to the bottom electrode due to ion-assisted etching in addition to the plasma chemical etching already present .

(v) The increase in chamber pressure from 500 to 800 mTorr decreases the etch rate in both bottom powered and top powered processes, and the etch rate remains constant beyond 800 mTorr. The increased residence time appears to reduce the TiN etch rate.

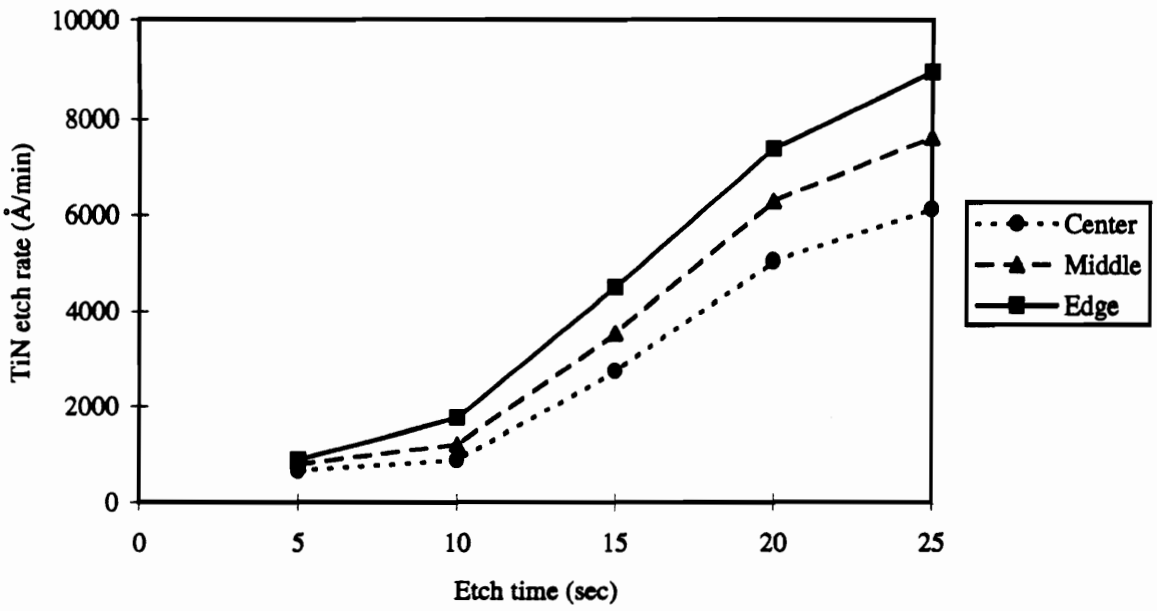

Fig. 3.1 Time Vs TiN etch rate in Cl2/N2 plasmas

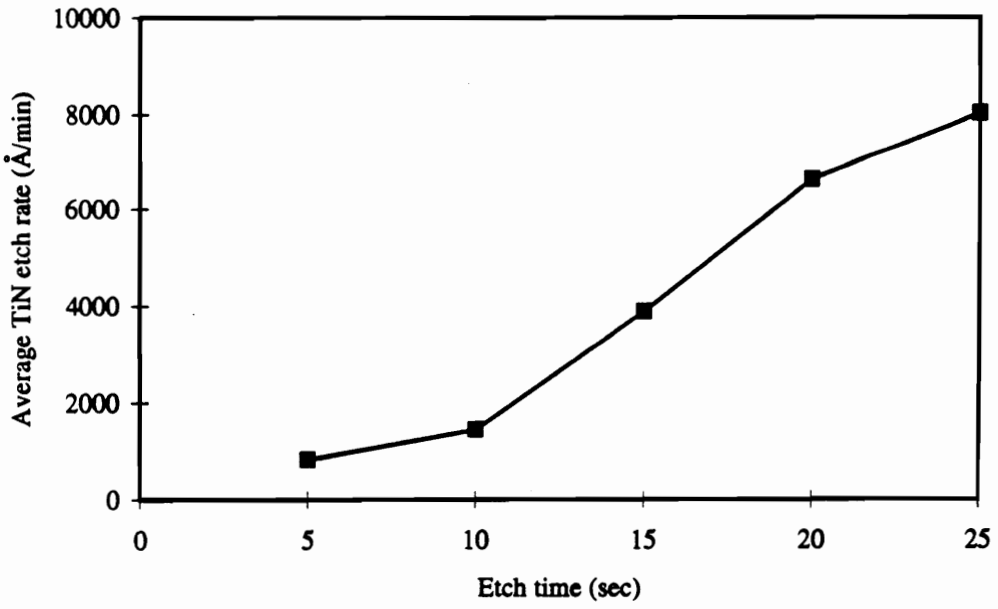

Fig. 3.2. Time vs average TiN etch rate in Cl2/N2 plasmas

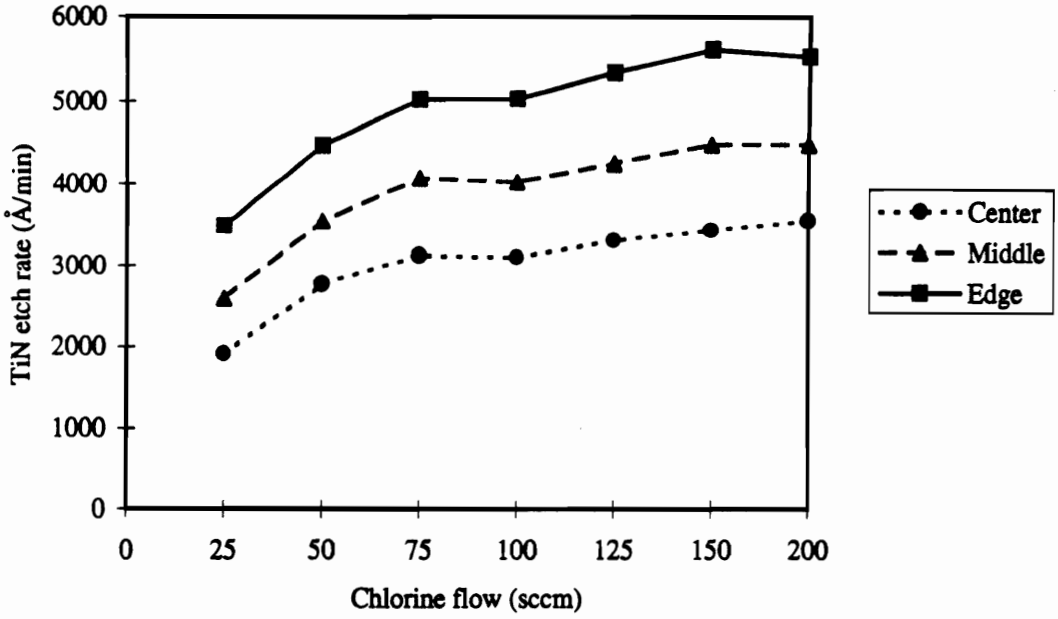

Fig. 3.3. Chlorine flow vs TiN etch rate in Cl2/N2 plasmas

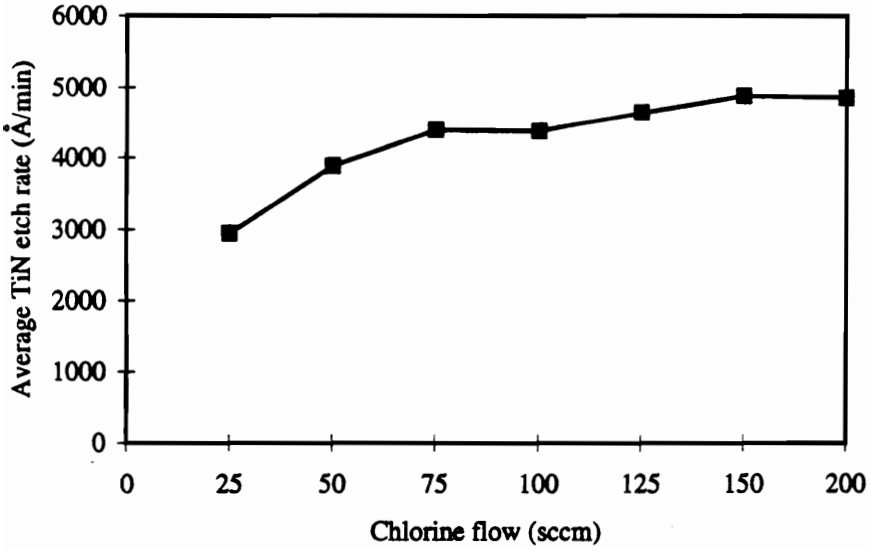

Fig. 3.4. Chlorine flow vs average TiN etch rate in Cl2/N2 plasmas

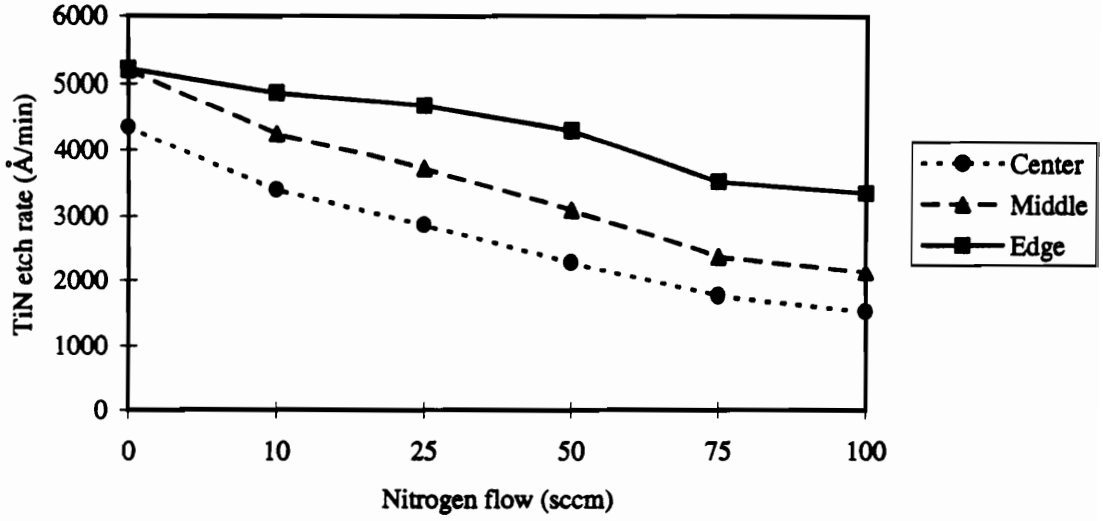

Fig. 3.5. Nitrogen flow vs TiN etch rate in Cl2/N2 plasma

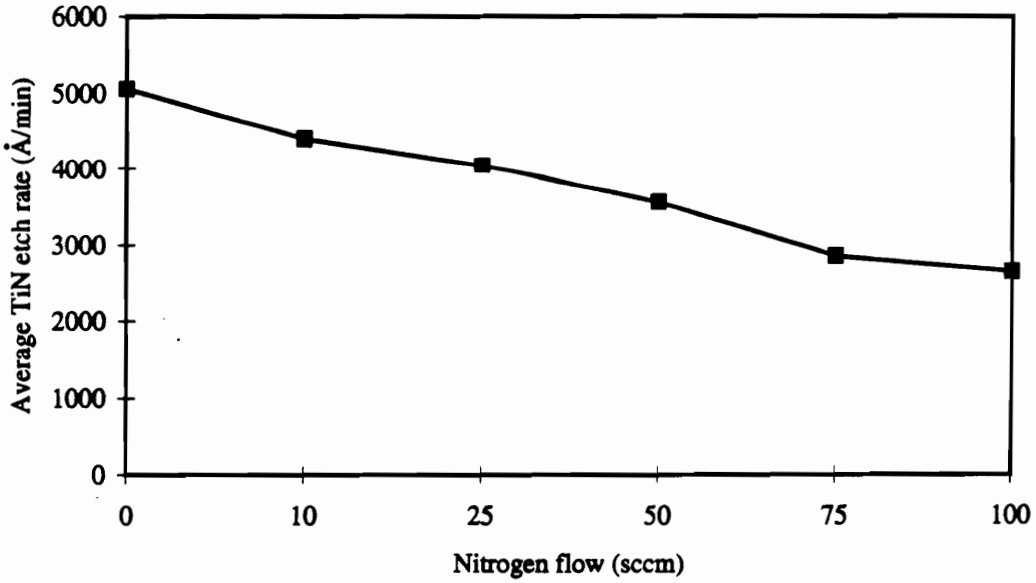

Fig. 3.6. Nitrogen flow vs average TiN etch rate in Cl2/N2 plasmas

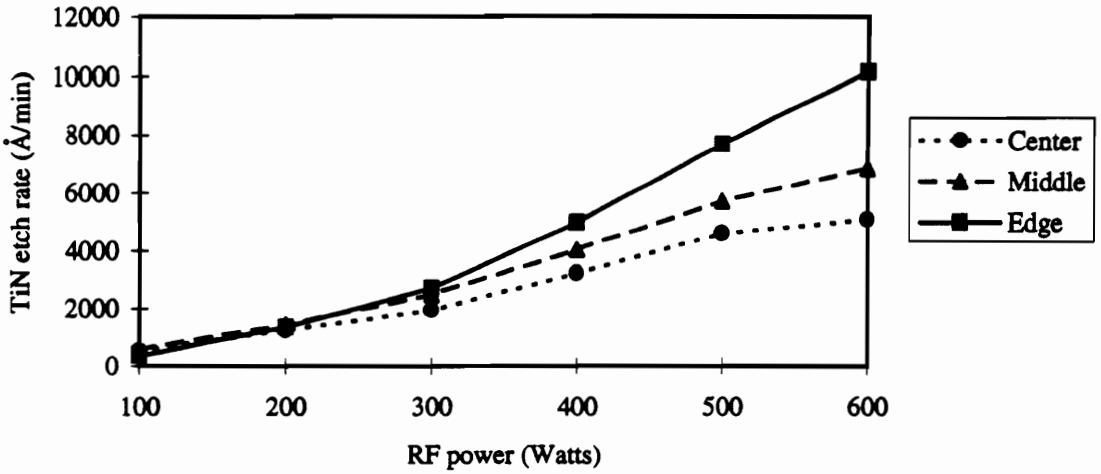

Fig. 3.7. Bottom electrode RF power vs TiN etch rate in Cl2/N2 plasmas

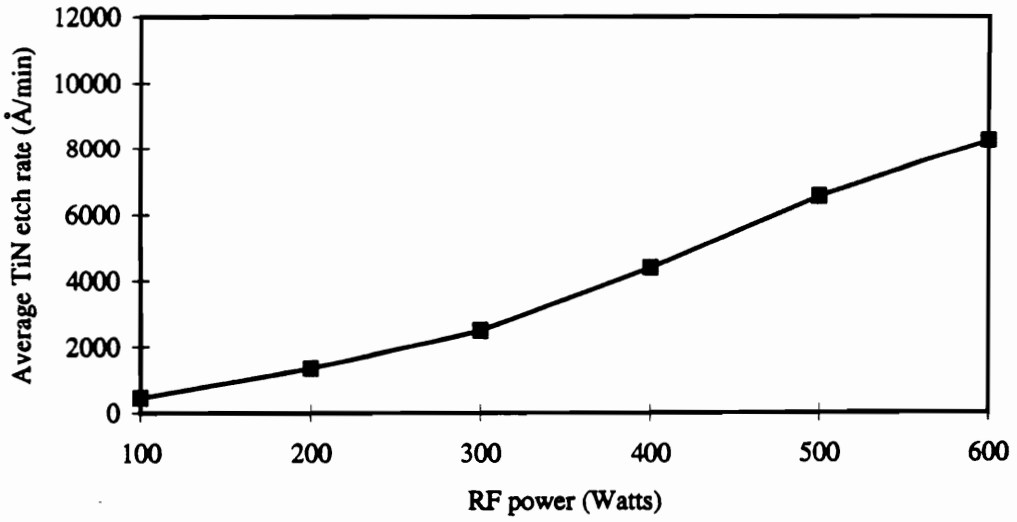

Fig. 3.8. Bottom electrode RF power vs average TiN etch rate in Cl2/N2 plasmas

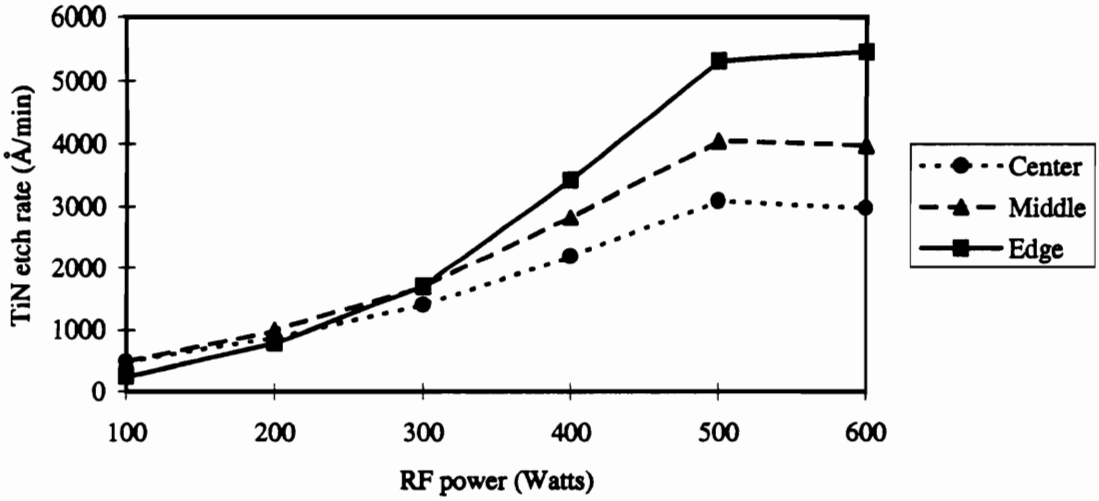

Fig. 3.9 Top electrode RF power vs TiN etch rate in Cl2/N2 plasmas

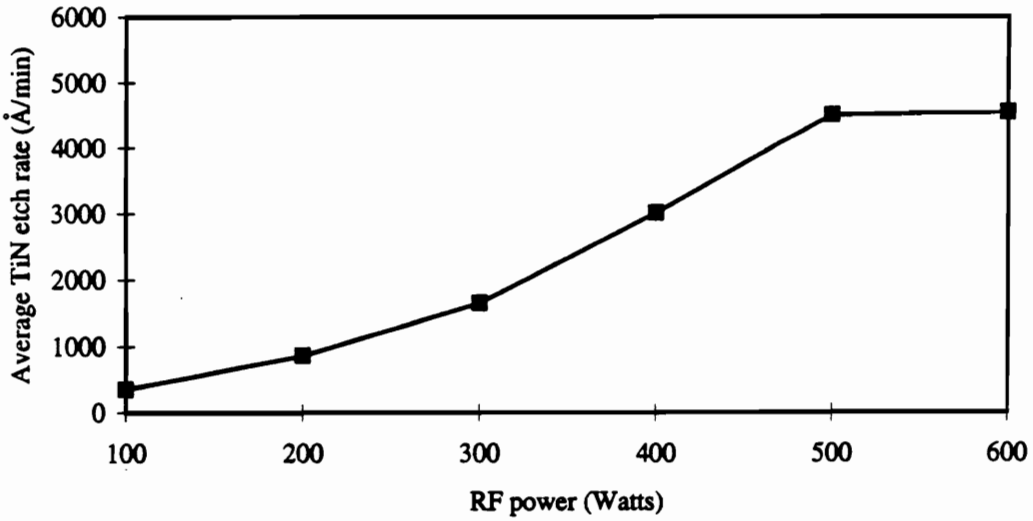

Fig. 3.10. Top electrode RF power vs average TiN etch rate in Cl2/N2 plasmas

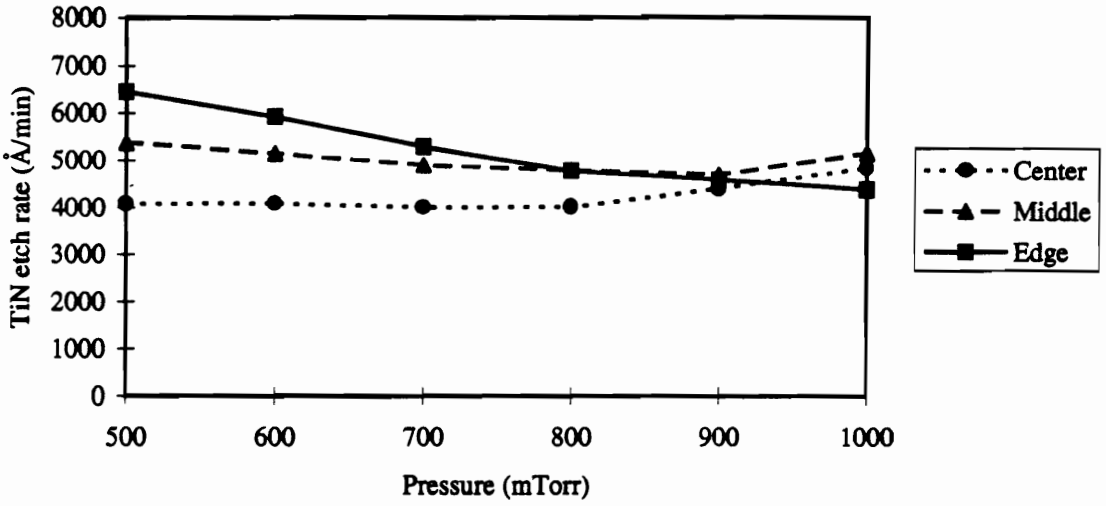

Fig. 3.11. Pressure vs TiN etch rate in Cl2/N2 plasmas (powered top electrode)

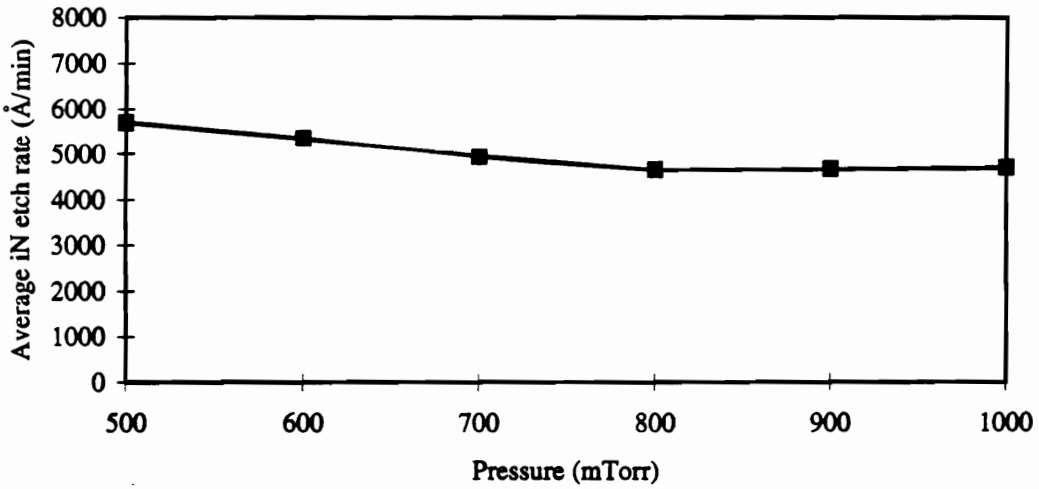

Fig. 3.12. Pressure vs average TiN etch rate in Cl2/N2 plasmas (powered top electrode)

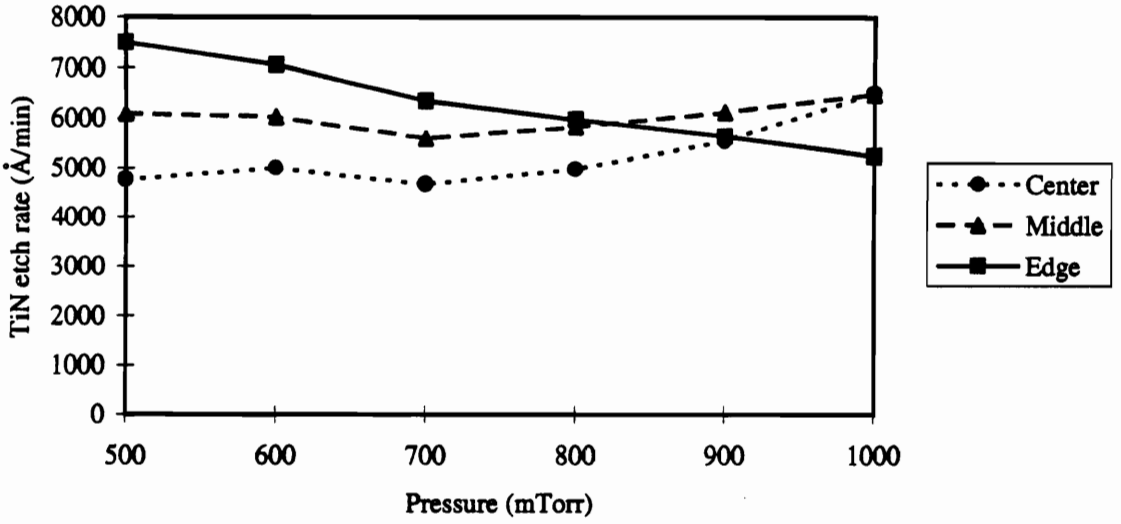

Fig. 3.13. Pressure vs TiN etch rate in Cl2/N2 plasmas (powered bottom electrode)

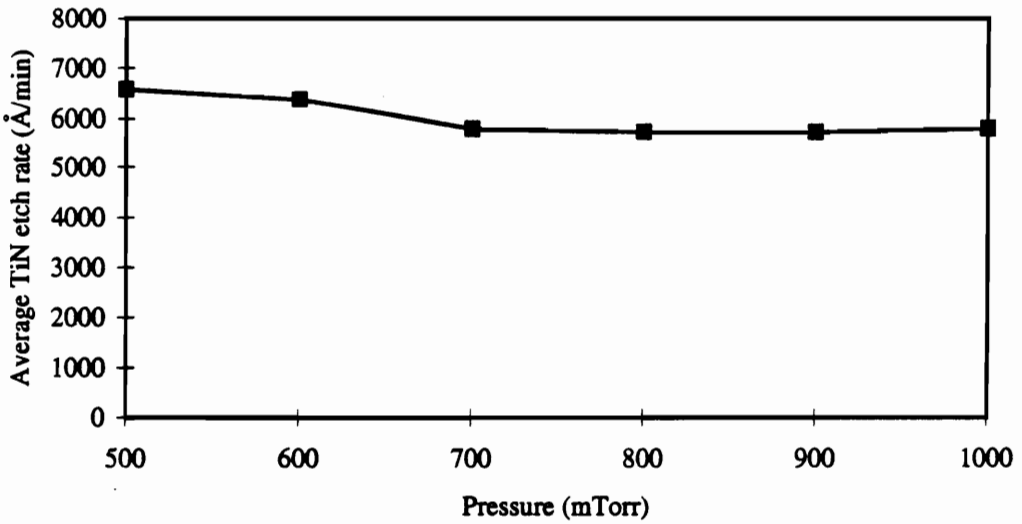

Fig. 3.14. Pressure vs average TiN etch rate in Cl2/N2 plasmas (powered bottom electrode)

Chapter 4
TiN etch in BCl_3 plasma

4.1 Introduction

In chapter 3, characterization of etching of TiN film in Cl_2/N_2 plasma was presented. In this chapter, etch characteristics of TiN film in BCl_3 plasma will presented. The TiN test wafers were prepared using the same procedure described in chapter 3. The test wafers were not patterned since the goal of the experiment was to study the effect of process parameters on the TiN etch rate and introduction of photoresist would further complicate the results [42]. The sheet resistance of the film before and after etch was measured on 49 points on each wafer using 4D four-point probe sheet resistance measurement tool and the corresponding thickness was calculated using the sheet resistance and the bulk resistivity. The difference between the thickness before and after etch when divided by the etch time in minutes gives the etch rate of the TiN film per minute. The derivation of calculation of the etch rate from the sheet resistivity measurement is presented in Appendix A. Appendix B presents the Lotus 123 program for the calculation of etch rate from the sheet resistivity. The etch rate thus calculated was analyzed by grouping the results of measurements in three annular regions of the wafer, namely, center, middle and edge, to study the radial variation of the etch rate across the wafer.

As discussed in chapter 3, the experiment was conducted in a commercially available Lam 4600 metal etcher, with adjustable gap between the electrodes. Lam 4600 has the capability to apply RF power at a frequency 13.56 MHz to either the top or bottom

electrodes. A detailed description and a diagram of the Lam 4600 system is presented in section 2.3. The self bias that appears between a substrate placed on the bottom electrode and ground is displayed by the system as Vdc. The temperature of each electrode is controlled by a chiller. The etch chamber is normally heated to temperatures above room temperature to minimize deposition of etch byproducts on chamber walls. The wafer is mechanically clamped to the lower electrode and cooled during etch by flowing helium along the groves in the bottom electrode. The plasma is confined within the area of the electrode by a confinement ring provided in the system.

4.2 Etch Reaction

The BCl_3 gas is used in the etching gas mixture to remove the top oxidized layer of aluminum. BCl_3 also removes oxygen and moisture, thus preventing further oxidation [8, 46]. The average etch rates of aluminum obtained with BCl_3 exclusively are comparatively low apparently due to insufficient supply of chlorine free radicals [46]. BCl_3 promotes the formation of a nonvolatile, unsaturated film of B_xCl_y on the sidewall of the patterned metal. As the BCl_3 flow is increased, the rate of formation of sidewall B_xCl_y film increases. As a result, the passivation becomes more effective in preventing trench formation [26]. The BCl_3 etch chemistry does not form the same type of polymer structures as does carbon. No polymer is observed on the chamber walls, but boron compounds (a combination of BCl_3 and boron oxychlorides) do condense or adsorb in the anodized aluminum or stainless steel reaction chamber walls. These compounds, when exposed to atmosphere during venting of the chamber, form white ($B(OH)_3$) deposits immediately [93].

The BCl_3 gas is dissociated into its radicals and chlorine due to electron impact in the plasma (see equations (4.1) and (4.2)).

$$BCl_3 + e^- \rightarrow BCl_2 + Cl + e^- \quad (4.1)$$

$$BCl_3 + e^- \rightarrow BCl + 2Cl + e^- \quad (4.2)$$

Oxygen scavenging occurs in the presence of BCl_3 through the reactions such as

$$2BCl_3 + 3H_2O \rightarrow B_2O_3 + 6HCl \quad (4.3)$$

$$2BCl_3 + O_2 \rightarrow B_2O_3 + 3Cl_2 \quad (4.4)$$

Conversion of B_2O_3 back to a volatile product can also occur through reaction with BCl_3 to form trichloroboroxines [50].

$$BCl_3 + B_2O_3 \rightarrow (BOCl)_3 \quad (4.5)$$

The chlorine atoms in the plasma get adsorbed by the TiN film and react with it to form volatile $TiCl_4$. K. Tokunaga et al. [93] discuss the reaction of BCl_3 with aluminum. Following the same line of argument, the possible sequence for etching TiN can be written as follows:

$$BCl_3 (gas) + e \rightarrow BCl_2 (gas) + Cl (gas) + e \quad (4.6)$$

$$Cl (gas) \rightarrow Cl (adsorbed) \quad (4.7)$$

$$Cl (ads) + TiN \rightarrow TiCl (ads) + N_2 (gas) \quad (4.8)$$

$$TiCl (ads) \rightarrow TiCl (gas) \quad (4.9)$$

A detailed discussion of the reaction process of chlorine with TiN was presented in Section 3.2, the only difference being the source of chlorine atoms and molecules. In chapter 3, pure chlorine was used in the etch chemistry, but in this chapter, the etchant chlorine is derived from dissociation of BCl_3 gas.

In the following sections, the effects of process parameters, such as etch time, BCl_3 gas flow rate, RF power, pressure and temperature are studied. The results of these experiments are discussed using the concepts of plasma physics and chemical reactions.

4.3 Time versus Etch Rate

In this experiment, the substrate was etched in BCl_3 plasma in the Lam 4600 metal etcher. The etch chamber was maintained at a pressure of 700 mTorr, with a BCl_3 gas flow of 110 sccm. An RF power of 350 watts was applied to the bottom electrode. Bottom electrode and top electrode temperatures were maintained at 40 °C and 70 °C, respectively. The etch chamber was also heated to 70 °C to prevent excessive condensation of reaction products and other compounds on the chamber walls. The etch time was varied from 15 seconds to 180 seconds and the variation in TiN etch rate is studied. Fig. 4.1 presents the etch rate at the center, middle and edge of the wafer and Fig. 4.2 presents the average etch rate against the etch time. From figure 4.2, it is observed that there is a delay of about 3 seconds between plasma turn-on and the beginning of the etch process. This delay is known as the induction time. This effect is mainly due to the time taken for etching through a thin layer of titanium oxynitride (TiO_xN_y) film formed on TiN due to exposure to atmosphere. The time taken for plasma and etcher stabilization also contributes towards the induction time. The TiN etch rate increases by ~ 60% when

the etch duration is increased from 15 seconds to 60 seconds, and then there is very little or no increase in TiN etch rate upon a further increase in the etch time. The initial increase in the etch rate can be attributed to the wafer heating effects due to exposure to plasma. The etch rate levels off after 60 seconds of etch time due to the fact that the wafer reaches a thermal steady state and the surface temperature of the wafer experiences no further increase.

From figure 4.1, it is observed that the edge of the wafer etches faster than the center. The TiN etch rate decreases from the edge to the center. This phenomenon has been discussed in section 3.3. The edge of the wafer is closer to the pumping port than the center. As a consequence, the reaction products and other residual gases are pumped away much faster from the edge than from the center of the wafer. This effect causes a localized increase in the etch rate near the edge of the wafer.

4.4 BCl_3 Flow Rate versus Etch Rate

In this section, the variation of the etch rate with BCl_3 flow is studied. The etch chamber was maintained at a pressure of 700 mTorr. An RF power of 350 Watts was applied to the bottom electrode. The temperatures of the electrodes and the chamber were maintained at the same levels specified in section 4.3 (with the top electrode at 70 °C, the bottom electrode at 40 °C, and the chamber at 70 °C). The BCl_3 flow was varied from 10 sccm to 120 sccm. All the test wafers were etched for 120 seconds. The etch time was so chosen to provide significant TiN etch rate. The etch rate was calculated from the sheet resistivity measurements before and after etch, as described in Appendix A. The etch reaction is discussed in detail in section 4.2. Fig. 4.3 presents the variation of the etch rate at the

center, middle and edge of the wafer with change in BCl_3 flow and Fig. 4.4 presents the average etch rate versus BCl_3 flow. From Fig. 4.4, it can be observed that the BCl_3 flow vs etch rate characteristics consists of two linear regions. The etch rate increases by approximately 200% for BCl_3 flow increase from 10 sccm to 20 sccm, and then the increase is less pronounced for further increase in BCl_3 flow. In the range of the BCl_3 flow used in this investigation, the TiN etch rate is limited by the supply of the BCl_3 gas, and hence the etchant chlorine species.

When the etch rates in three different regions of the wafer, namely edge, middle, and center, are plotted as shown in Fig. 4.3, it is observed that the edge of the wafer etches much faster than the center, with the etch rate of the middle of the wafer in between. The difference in the etch rate between the edge and the center of the wafer is more pronounced for BCl_3 gas flows below 20 sccm.

The average etch rates of TiN with BCl_3 exclusively, are low compared to those in Cl_2 plasma (section 3.4), due to insufficient supply of free chlorine radicals, that participate in the etch reaction. The same effect was observed by D. HG. Choe et al. [46] when etching Al in BCl_3 plasma. The degree of dissociation of a molecule is ultimately governed by the bond strength between chlorine and the particular parent molecule or fragment [33]. The following table 4.1 lists the bond dissociation energies.

Table 4.1 Bond dissociation energies

Bond	Dissociation energy (eV/molecule)
Cl-Cl	3.51
BCl_2-Cl	4.55
BCl-Cl	3.60
B-Cl	5.51

The etch rate of TiN increased linearly increased as BCl_3 flow was increased, contrary to the observations made by D.HG. Choe et al [46] and A.L. Keaton and D.W. Hess [107] on Al film, where there was little dependence of Al etch rate on the BCl_3 flow rate once the native oxide was removed. In the region of this investigation, between 10 and 120 sccm of BCl_3 flow, the etch rate is limited by the availability of reactant species. This phenomenon is known as generation-limited etch process.

4.5 RF Power versus Etch Rate

In this section, the etch characteristics of TiN with change in RF power is studied. The BCl_3 gas flow was maintained at 110 sccm. The effect of RF power applied to either top or bottom electrode is studied at three different pressure levels, 500 mTorr, 700 mTorr, and 1000 mTorr. RF power was varied from 200 W to 600 W in increments of 100 W. The test wafers were etched for 120 seconds to obtain significant etch rates. Similar to the

previous experiments, the etch rates for center, middle and edge of the wafer were plotted in a separate graph. For a pressure of 500 mTorr and the power is applied to the top electrode, the etch rate increases linearly when the RF power is increased from 200 W to 400 W, then levels off at around 150 Å/min upon further increase in the RF power. As the pressure is increased from 500 mTorr to 700 mTorr, the TiN etch rate increases linearly up to 500 W. For pressure of 1000 mTorr, a linear dependence of the etch rate on RF power is observed up to 600 W of applied RF power. (Fig. 4.5 and 4.6). The behavior of TiN etch characteristics in BCl_3 plasmas is similar to those in Cl_2/N_2 plasma discussed in section 3.4. Following the same line of argument, an increase in the RF power increases the ionization of the BCl_3 gas, leading to an increase in reactant chlorine species. The increased RF power also increases the mean electron energy and the ion energy incident on the substrate leading to an increase in the etch rate which is supported by the increase in the Vdc [88]. In the studies conducted by D.A. Danner et al. [33], it was observed that the ion accelerating voltage is established by system geometry and RF excitation frequency, while the ion flux varies with RF power. The heating effect of the substrate due to RF power also causes an increase in the substrate temperature as all of the applied RF power is essentially dissipated as heat. The etch rate levels off after a certain applied RF power due to the gases reaching its maximum ionization level and the substrate reaching its thermal steady state.

The experiment was repeated with the RF power applied to the bottom electrode (Figs 4.7 and 4.8). In general, the etch rate was higher than the previous case where the RF power was applied to the top electrode. For the chamber pressure of 500 mTorr, the average etch rate increases linearly with the RF power between 200 and 300 W. For further increase in RF power, the etch rate is found to level off at around 150 Å/min. When the tests were

repeated at a chamber pressure of 700 mTorr, the linear dependence of TiN etch rate on RF power exists up to 400 W. This linear increase of etch rate is extended up to 600 W applied RF power when the reaction pressure is further increased to 1000 mTorr. The average etch rate is found to increase when the pressure was increased from 500 mTorr to 700 mTorr, but decreases as the pressure is further increased to 1000 mTorr. The effect of pressure on the etch rate will be discussed in detail in section 4.6. The same discussion presented on the effect of RF power on the etch rate can be applied to describe the effect of bottom electrode power. In addition to this effect, when the RF power is applied to the bottom electrode, the etching mechanisms are ion assisted etching and plasma etching due to negative self bias Vdc appearing across the sheath near the substrate. So the magnitude of the etch rate is higher when the RF power is applied to the bottom electrode as the etching is due to plasma chemical etching, in addition to ion etching, as opposed to only plasma chemical etching when the RF power is applied to the top electrode.

Similar to the previous case, the edge of the wafer etches faster than the center of the wafer. The middle region of the wafer is etched at a rate in between the edge and the center. (Fig. 4.7). This effect, which is known as bull's eye effect, was discussed at the end of section 4.3.

4.6 Pressure versus Etch Rate

In this section, the etch characteristics with change in reaction pressure is studied. The pressure was varied from 500 mTorr to 1000 mTorr in increments of 100 mTorr. A constant BCl_3 gas flow of 110 sccm was maintained. The test wafers were etched for 120 seconds. The RF power can be applied to either the top electrode or the bottom

electrode. At first, an RF power of 350 Watts is applied to the top electrode. The electrodes and the chamber were maintained at the same temperatures as specified in section 4.3. Fig. 4.9 shows the etch rate dependence on the pressure at three annular regions of the wafer and Fig. 4.10 shows the average etch rate versus pressure with the RF power applied to the top electrode . When the pressure is increased from 500 mTorr to 600 mTorr, the average etch rate increases by 10%. This increase can be attributed to the increase in residence time of the reactant species in the chamber (see equation 4.10) leading to higher probability of the reactant species contributing to the etch process. As the pressure is further increased from 600 to 1000 mTorr, the etch rate gradually drops by 25%.

The effect of reaction chamber pressure on TiN etch rate was discussed in section 3.6. At low pressures, the mean electron energy and ion energy incident on the substrate is high because of low probability of loss of energy due to collision with other ions or molecules in the plasma. The mean free path of the ions is high and hence the ions generated in the plasma have higher probability of reaching the substrate to contribute towards etching. As the pressure is increased, the number of ions and molecules in the plasma increase to maintain the pressure. In the case of BCl_3 plasma, the TiN etch rate increases when the pressure is increased from 500 mTorr to 600 mTorr due to increased residence time of etchant chlorine species. An important factor affecting the etch rate is the residence time of the reactant species in the plasma, which is defined as

$$\text{Residence time } t = (P\ V)/Q \qquad (4.10)$$

where P is the pressure, V is the reactor volume, and Q is the process gas flow rate.

As the pressure is further increased beyond 600 mTorr, the ions and electrons lose larger amount of energy due to increased collision with other ions or molecules in the plasma [88]. This effect leads to a decrease in TiN etch rate. In addition to this effect, the concentration of reactive chlorine atoms may be reduced by recombination reactions which occur at reactor surfaces and also at gas phase of the plasma [61]. Such recombination reactions reduce the number of reactant chlorine atoms available for etching, thereby contributing to reduction in the etch rate. Increased pressure also decreases the volatility of the reaction products from the TiN surface, slowing down the etch process. It can be concluded that at pressures over 600 mTorr, one or all of the above mentioned factors override the effect of increased residence time, leading to a decrease in the etch rate. D.HG. Choe et al. observed the same effect on the etch rate of aluminum and arrived at the conclusion that the etch rates are flow rate limited, but not residence time limited [46]. It is worth noting in this respect that on a patterned wafer higher pressure leads to a tapered profile. According to the work done by J. Maa et al. [26] on silicon etching, at low pressures (175 mTorr), trenching appeared at the bottom of the opening. As the pressure was increased, this trenching disappeared. It is also observed that the decrease in Vdc with the increase in pressure is not significant to cause a decrease in the etch rate.

Within the wafer, the etch rate increases from the center to the edge. It is observed from the Fig. 4.9, where the etch rates in three annular regions, center, middle and edge are plotted as separate curves. This effect, called bull's eye effect, was discussed in section 4.3.

The experiment on the effect of RF power was repeated with the RF power applied to the bottom electrode. The gas flow, pressure, electrode and chamber temperatures and etch times were maintained at the same level as in the previous experiment. Figs. 4.11 and 4.12 show the etch rate characteristics with change in pressure when the RF power is applied to bottom electrode. The average etch rate increases from 177 Å/min to 193 Å/min as the pressure is increased from 500 to 600 mTorr. Beyond 600 mTorr pressure, the etch rate decreases, reaching a low of 140 Å/min at 1000 mTorr. Similar to the previous case where the RF power was applied to top electrode, the edge of the wafer etches faster than the center, with the middle of the wafer having an etch rate in between. It is observed that the etch rate characteristics shows a similar variation when the RF power is applied to the top electrode. When the RF power is applied to the bottom electrode, the etch rate is higher due to negative self bias, Vdc, appearing across the sheath region near the substrate. This phenomenon has been already discussed in detail in the section 3.5 on the effect of RF power in Cl_2/N_2 plasma.

4.7 Temperature versus Etch Rate

In this section, the TiN etch rate dependence on temperature in BCl_3 plasma is studied. The bottom electrode, the top electrode, and the chamber were maintained at the same temperature in order to avoid the complex effects of temperature gradients in the etch chamber on TiN etch rate. BCl_3 gas flow of 110 sccm was used. The etch chamber pressure was maintained at 700 mTorr. RF power of 350 Watts was applied to the bottom electrode. The temperature was varied from 55 °C to 80 °C in increments of 5 degrees. Fig. 4.13 and 4.14 present the etch rate characteristics with the variation in temperature.

The etch rate increases slightly from 144 Å/min at 55 °C to 162 Å/min at 65 °C and then came down to 154 Å/min at 80 °C.

Increase in temperature influences etch rate in plasma chemical etching mainly due to its effect of the etch rates of chemical reactions. If the activation energy of the material is small ($Q \leq 0.5$ eV/mole), the etch rate is found to have an Arrhenius dependence on the temperature (equation 4.11) [88].

$$\text{Etch rate} \sim \exp(-Q/kT) \qquad (4.11)$$

where Q is the activation energy, T is the absolute temperature of the substrate, and k is the Boltzmann's constant.

The etch rate decrease with increase in temperature may be attributed an increase in the rate of desorption of etchant species from the surface of the film being etched. For Al etching in Cl_2/BCl_3 plasma, it was observed by D.A. Danner et al. [33] that etch rate dropped off for temperatures below 50 °C due to limitation on product removal, at temperatures above 90 °C, the etch rates were high due to increased rate of reaction of etchant species with Al and rapid desorption of etch products. This work also indicated a transition region between etchant adsorption (> 90 °C) and product desorption (< 50 °C). Contrary to the Al etch, the change TiN etch rate with temperature is not significant. So none of the effects applicable to Al etching are present in TiN etching in BCl_3 plasma. Therefore, it can be concluded that TiN etch proceeds primarily due to ion etching, not by chemical reaction.

4.8 Summary and Conclusions

In sections 4.3 to 4.7 of this chapter, the etch rate characteristics of TiN film in BCl_3 plasma with the variation of the process parameters such as time, BCl_3 gas flow, RF power, reaction pressure, and temperature were discussed. The discussions on the effect of each of the parameters were presented in the corresponding section. The RF power seems to have the maximum effect on the TiN etch rate. The TiN etch rate is reactant supply limited as it is observed to increase with the increase in BCl_3 flow. The magnitude of etch rate in pure BCl3 plasma is approximately one hundredth of the etch rate in Cl_2/N_2 plasma due to the limited availability of the free chlorine atoms/radicals from BCl_3. A list of the conclusions are given below:

(i) The BCl_3 gas is used along with other gases such as chlorine to etch through the hard surface oxide on the metal films and to scavenge moisture from the etch chamber.

(ii) The TiN etch rates in BCl_3 plasma is about two to three orders of magnitude less than those in Cl_2 plasma. This is due to the decreased availability of the etchant chlorine species as the bond energy of BCl_3 and it is radicals is higher than that of Cl-Cl bond.

(iii) There is an induction time of 3 seconds before the etching of TiN started. The etch rate increased with etch time, but leveled off as the etch duration was increased to 50 seconds and beyond probably due to the wafer reaching a thermal steady state.

(iv) The etch rate increased with the increase in BCl_3 gas flow due to the increased supply of etchant species. The etch rate is observed to be flow-rate limited.

(v) A strong dependence of the etch rate on applied RF power was observed due to the fact that the ionization increases with increase in RF power. The etch rate is 10 % higher when the RF power is applied to the bottom electrode than when RF power is applied to the top electrode because of increased ion bombardment.

(vi) The pressure and the temperature do not have significant effect on the TiN etch rate. Therefore, it can be concluded that TiN etching in BCl_3 plasma is primarily flow rate limited.

In chapters 3 and 4, the characterization of TiN film was described in detail along with the discussion on the effects of process parameters on the etch rate. In the next chapter, chapter 5, similar characterization experiment done on Ti film, is discussed. The BCl_3 gas, which was used in the TiN etch process, was not used in Ti etch process as it was not found to have any effect on Ti etching.

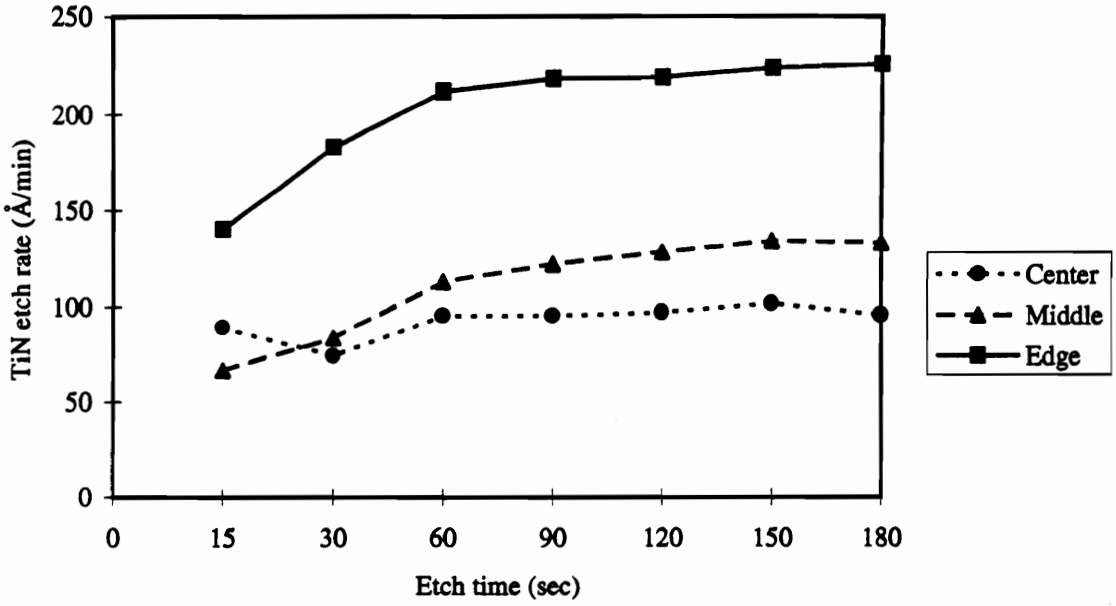

Fig. 4.1. Time vs TiN etch rate in BCl3 plasmas

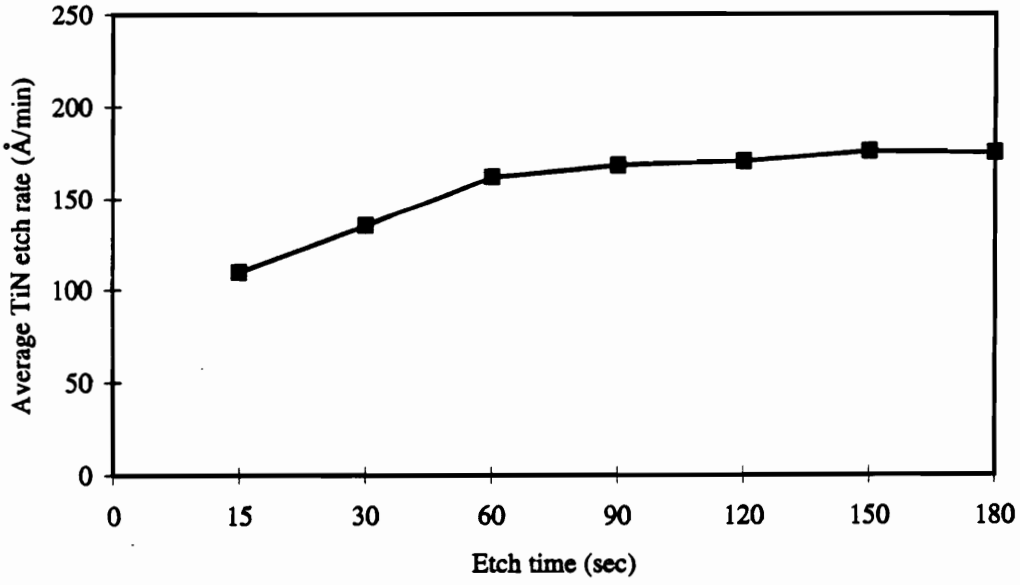

Fig. 4.2. Time vs average etch rate in BCl3 plasma

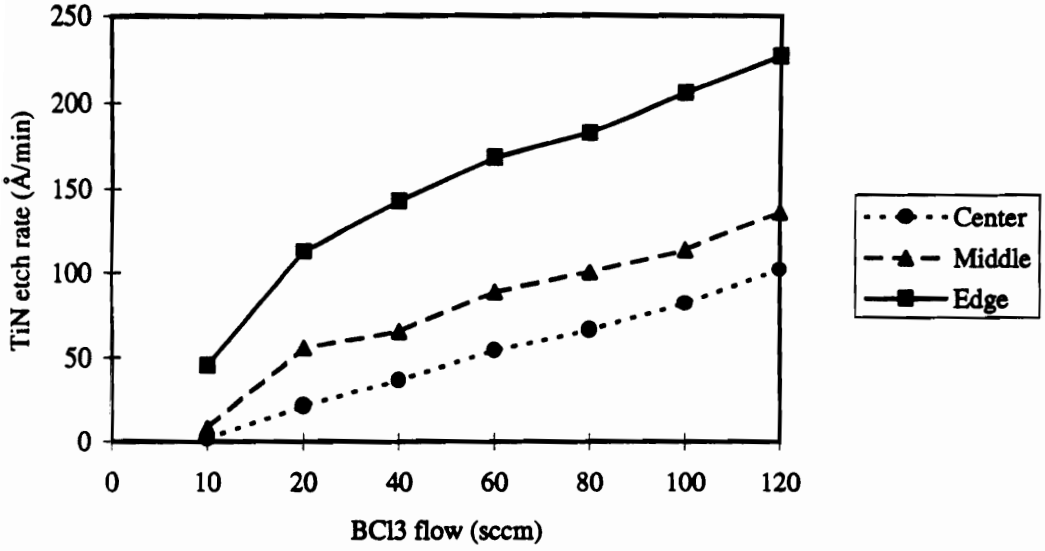

Fig. 4.3. BCl3 flow vs TiN etch rate in BCl3 plasmas

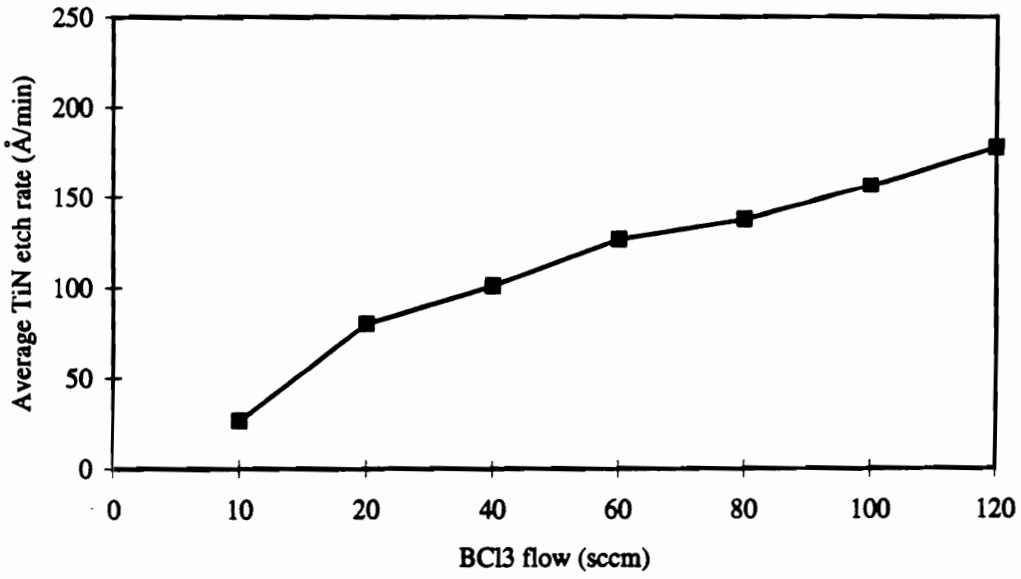

Fig. 4.4. BCl3 flow vs average TiN etch rate in BCl3 plasmas

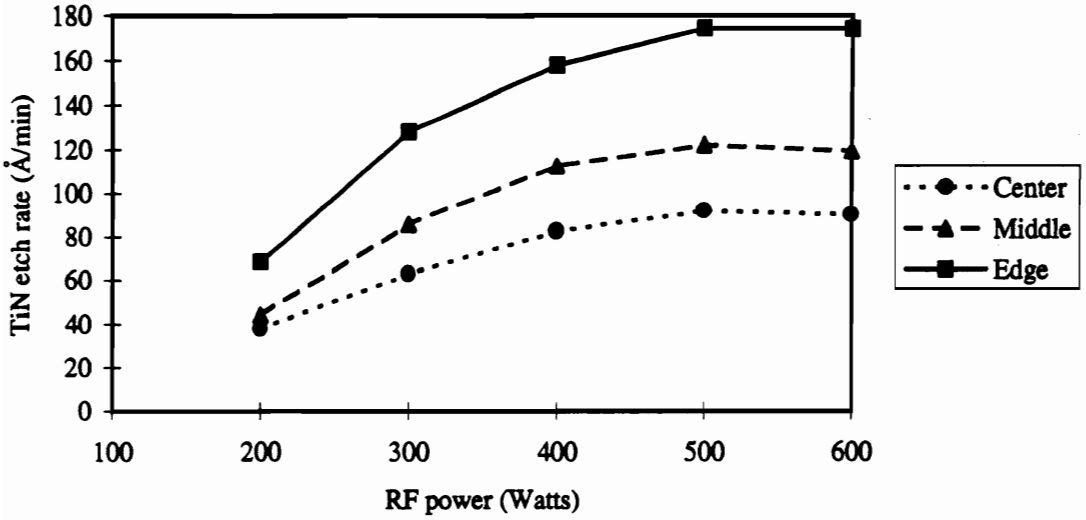

Fig. 4.5(a). Top electrode RF power vs TiN etch rate in BCl3 plasmas at 500 mTorr pressure

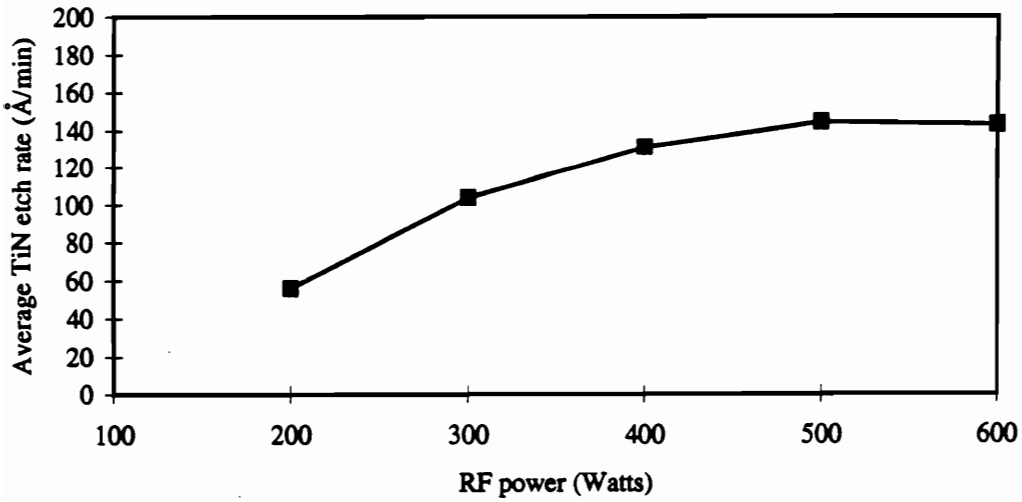

Fig. 4.6 (a) Top electrode RF power vs Average TiN etch rate in BCl3 plasmas at 500 mTorr pressure

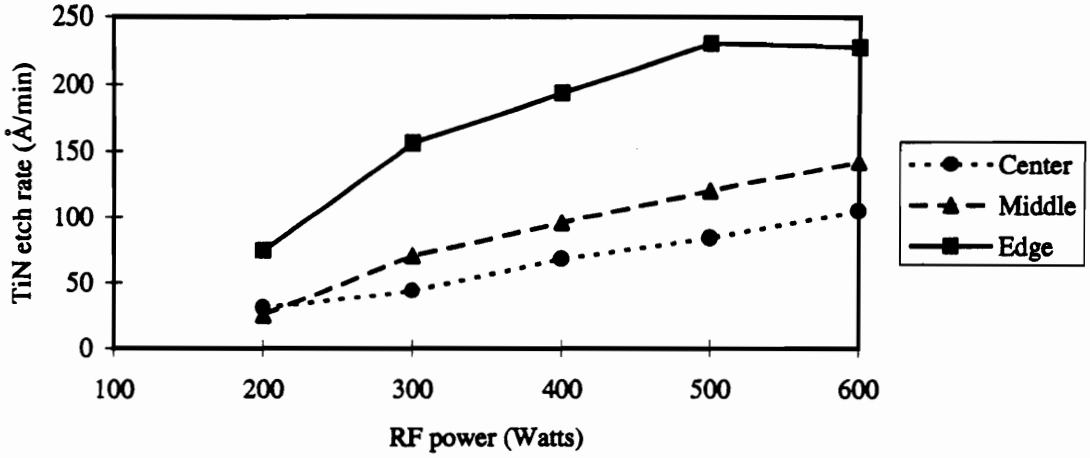

Fig. 4.5 (b) Top electrode RF power vs TiN etch rate in BCl3 plasmas at 700 mTorr pressure

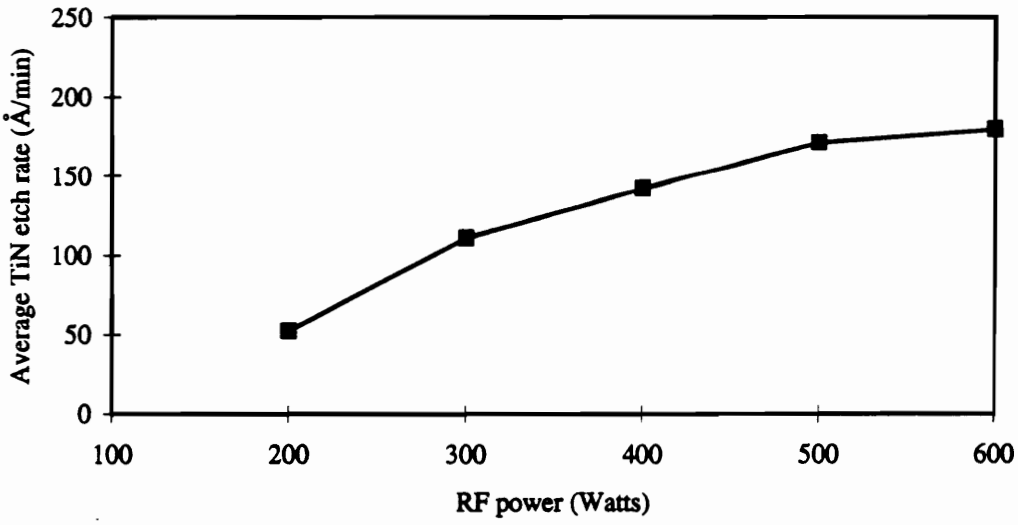

Fig. 4.6(b) Top electrode RF power vs average TiN etch rate in BCl3 plasmas at 700 mTorr pressure.

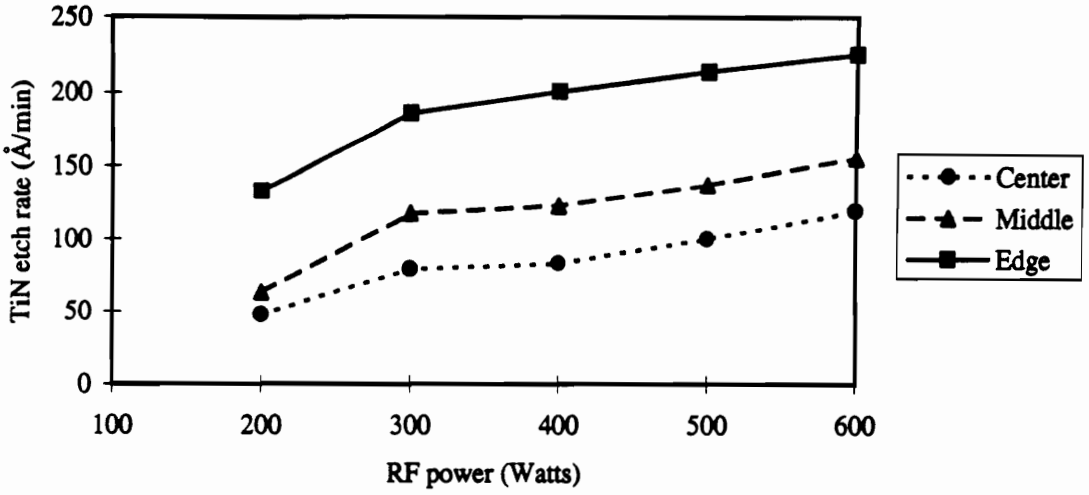

Fig. 4.7(a). Bottom electrode RF power vs TiN etch rate in BCl3 plasmas at 500 mTorr pressure.

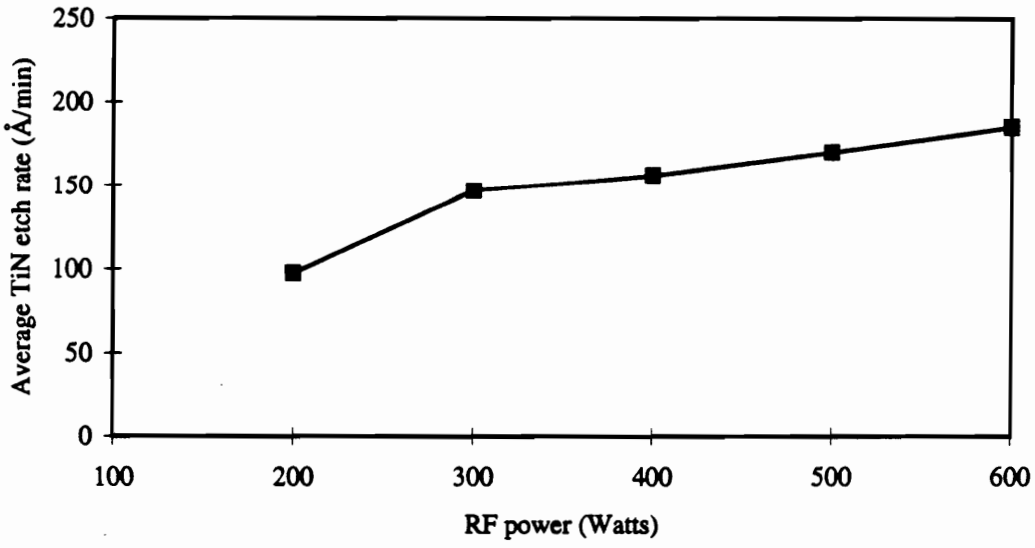

Fig. 4.8(a). Bottom electrode RF power vs average TiN etch rate in BCl3 plasmas at 500 mTorr pressure

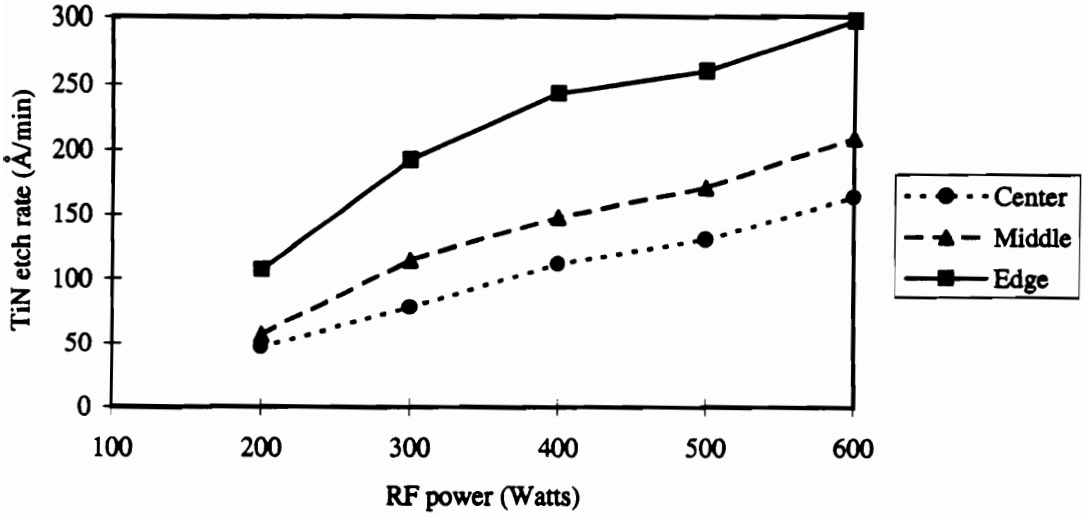

Fig. 4.7(b). Bottom electrode RF power vs TiN etch rate in BCl3 plasmas at 700 mTorr pressure.

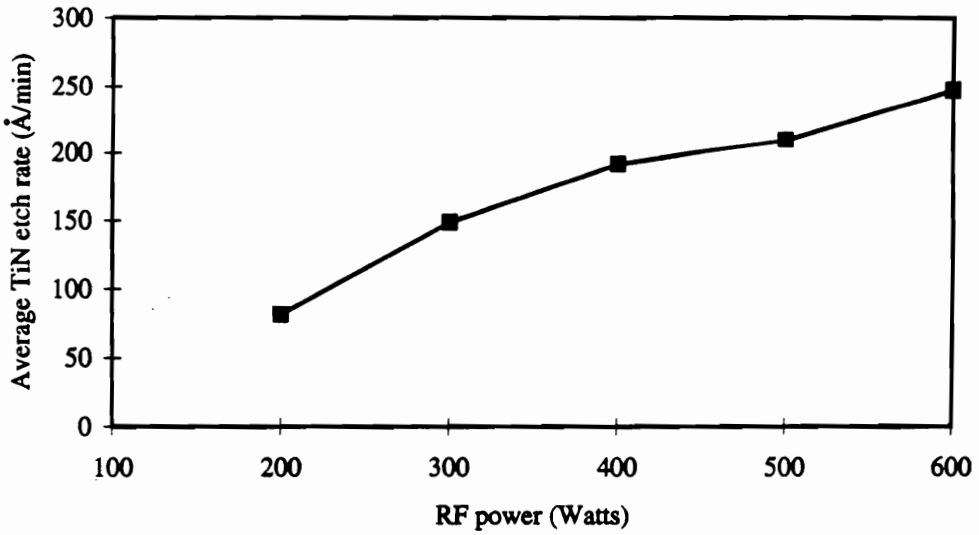

Fig. 4.8(b). Bottom electrode RF power vs average TiN etch rate in BCl3 plasmas at 700 mTorr pressure.

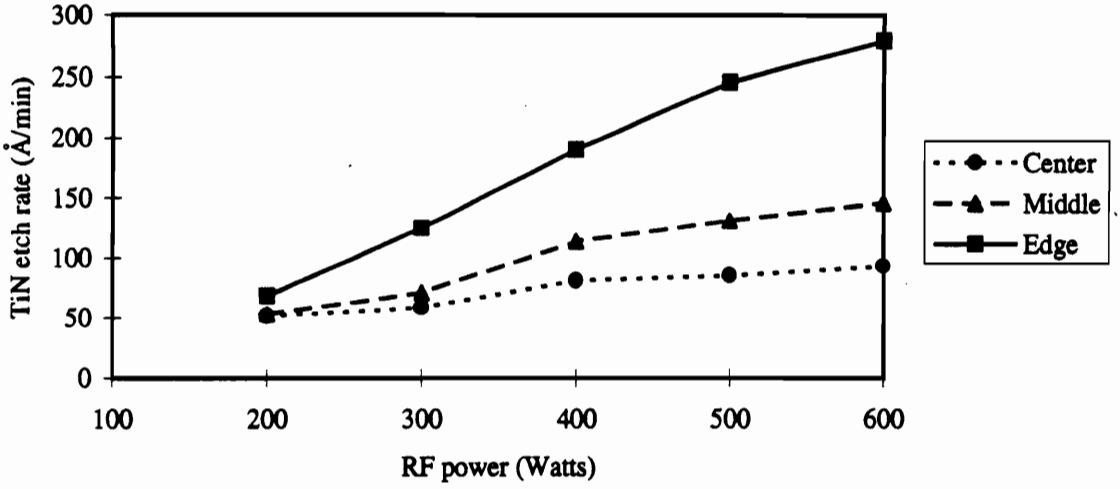

Fig. 4.7(c). Bottom electrode RF power vs TiN etch rate in BCl3 plasmas at 1000 mTorr pressure.

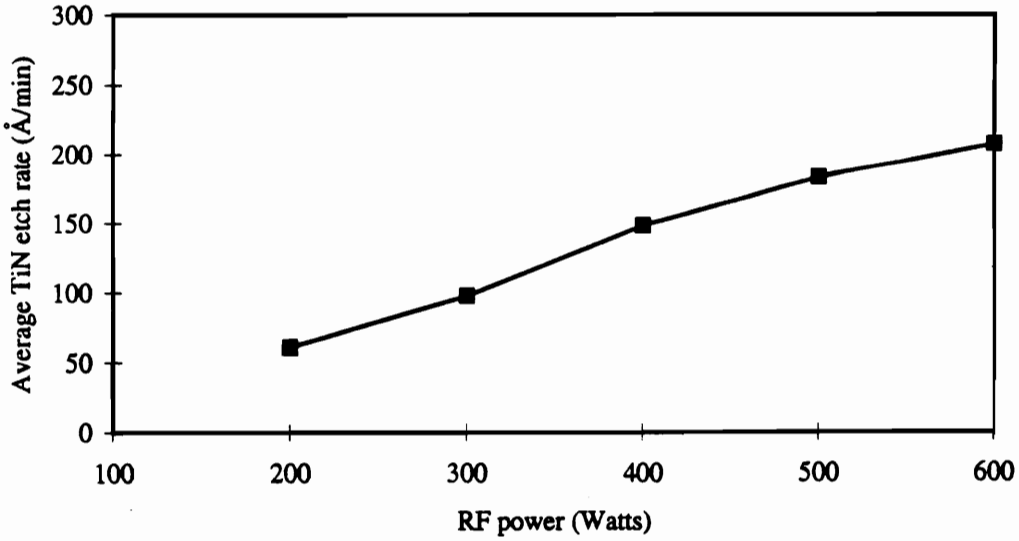

Fig. 4.8(c). Bottom electrode RF power vs average TiN etch rate in BCl3 plasmas at 1000 mTorr pressure.

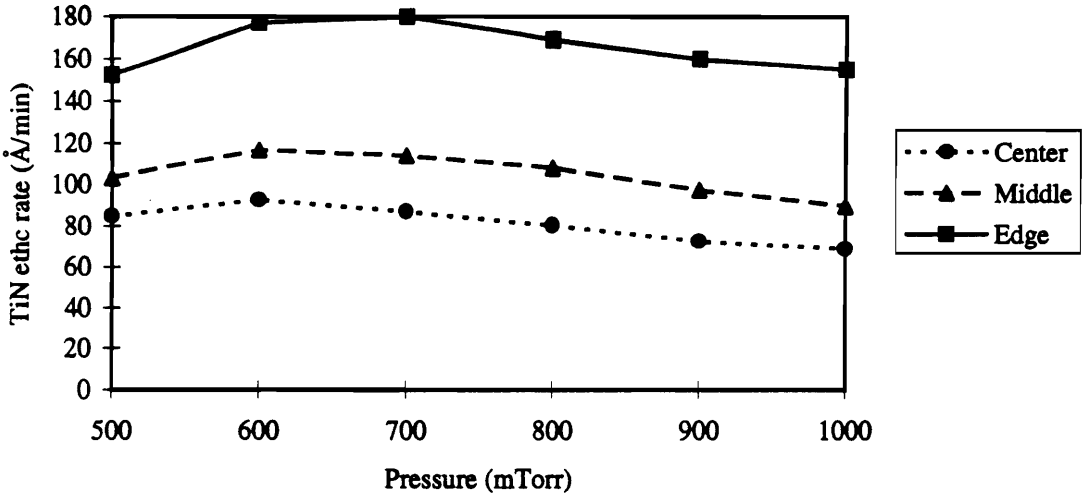

Fig. 4.9. Pressure vs TiN etch rate in BCl3 plasmas (powered top electrode).

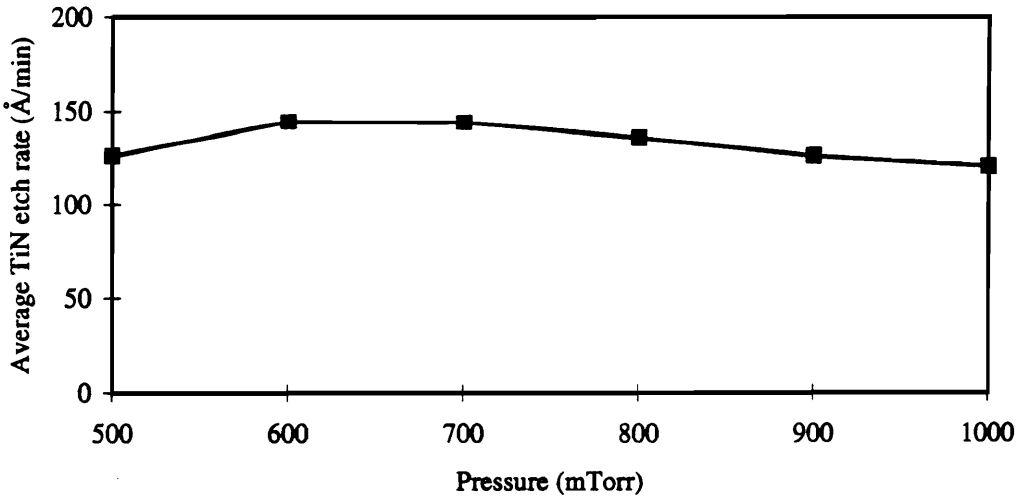

Fig. 10. Pressure vs average TiN etch rate in BCl3 plasmas (powered top electrode)

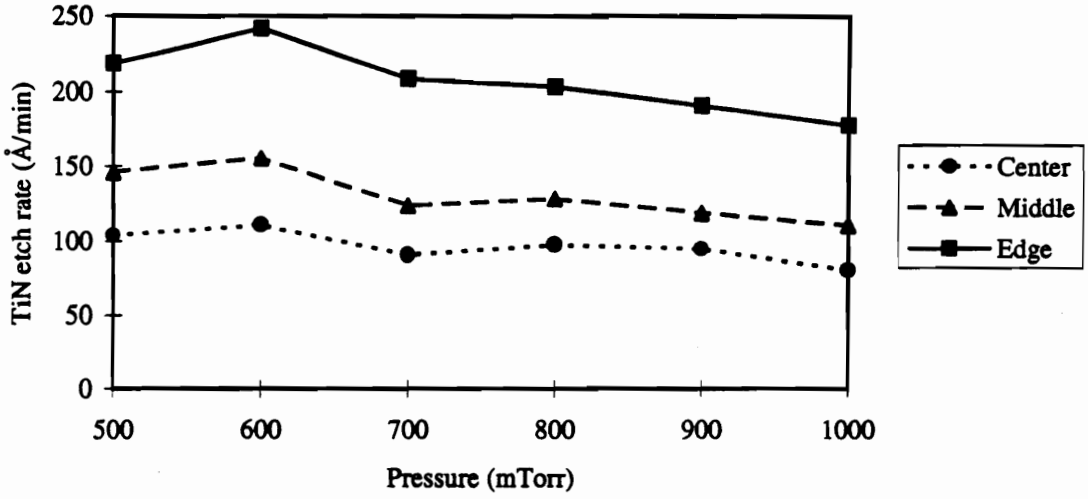

Fig. 4.11. Pressure vs TiN etch rate in BCl3 plasmas (powered bottom electrode)

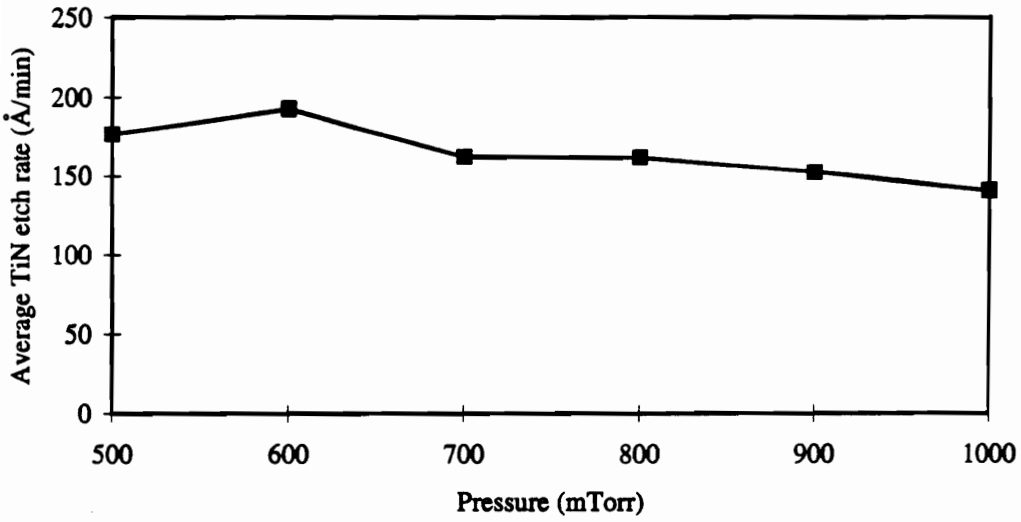

Fig. 4.12. Pressure vs average TiN etch rate in BCl3 plasmas (powered bottom electrode)

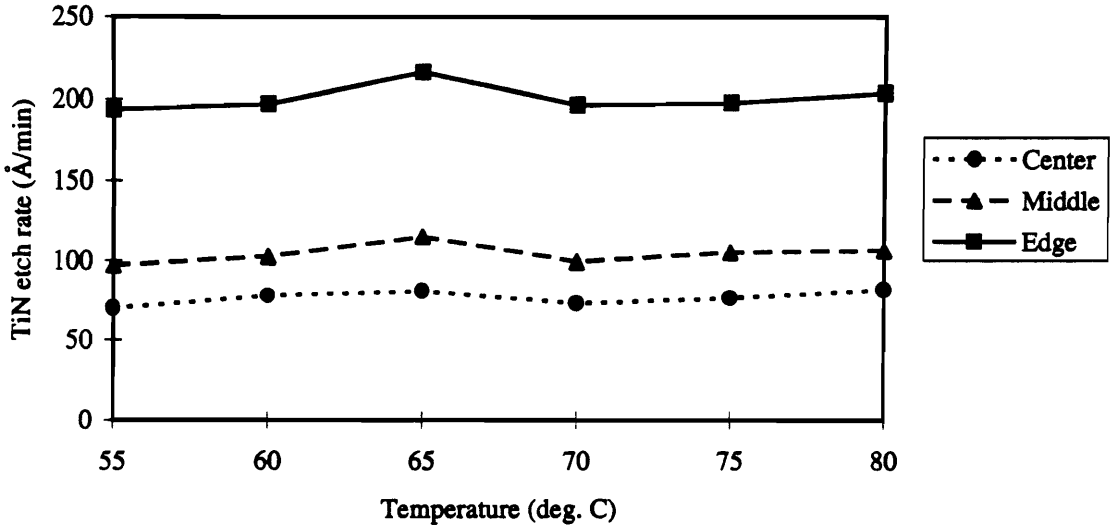

Fig. 4.13. Temperature vs TiN etch rate in BCl3 plasmas

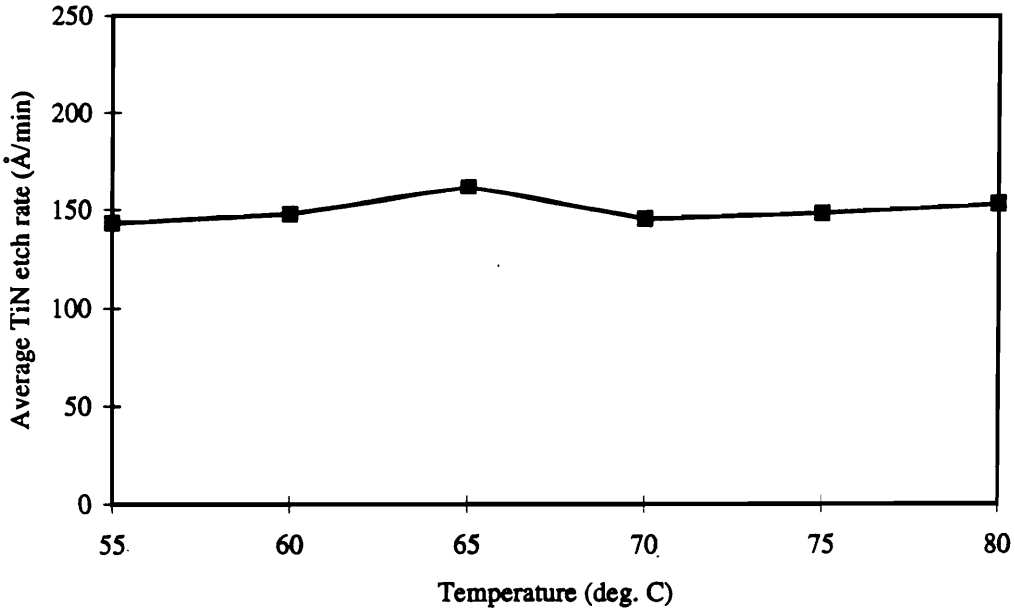

Fig. 4.14. Temperature vs average TiN etch rate in BCl3 plasmas.

Chapter 5
Ti etch in Cl_2/N_2 plasma

5.1 Introduction

Several materials, noble and near-noble metals, such as Pt, Pd, Co, and Ni, and refractory metals, such as Ti, Mo, W, and Ta, are used to form silicides at the aluminum-silicon interface in contacts. Silicides have several advantages including excellent electrical characteristics that help to reduce the contact resistance. Silicides are formed using self alignment feature, thereby eliminating one masking step [13]. Among the silicide forming materials listed above, Ti is more commonly used in the semiconductor industry. Metal interconnects, that use $TiSi_2$ at the silicon-aluminum interface are etched using plasma containing fluorine (F_2) or chlorine (Cl_2). In this chapter, characteristics of Ti etching in Cl_2/N_2 plasma is discussed. The effects of process parameters, such as etch time, Cl_2/N_2 gas flow, RF power, etch chamber pressure and temperature, are studied varying one parameter at a time. The etch rate is calculated from sheet resistivity obtained from four-point probe measurements. In order to study the effect of more than one variable and the interaction between variables, an experimental method, Response Surface Methodology, known as RSM, was used. An experiment was designed using JMP software and the runs according to the design were processed. A detailed discussion of the design, processing and analysis of the experiment is presented in chapter 6.

The experiment was conducted on 10000 Å of DC sputtered Ti film on a substrate with 13000 Å CVD deposited oxide on a bare silicon wafer of <100> orientation. The bulk

resistivity of the Ti film was assumed to be 70 μOhm.cm. This bulk resistivity value was calculated from the previous measurements of thickness and sheet resistivity. As discussed in the chapters 3 and 4 of this dissertation work, the etch rate was calculated by measuring the sheet resistivity before etch and after etch at 49 points using 4D four-point probe measurement system. 3-Sigma uniformity of Ti deposition thickness and sheet resistivity was better than ± 7%. The derivation of calculation of etch rate from the sheet resistivity measurement is presented in Appendix A. Appendix B presents the Lotus 123 program for the calculation of the etch rate from the sheet resistivity.

The wafers were etched in a commercially available Lam Rainbow 4600 single wafer metal etcher. The detailed description of the system is presented in section 2.3. The etch rate was nonuniform along the radius of the wafer. In order to analyze the etch rate variation across the wafer, the points of measured sheet resistivity was grouped into three regions - center, middle and edge and plotted and analyzed separately. In each of the study of the effect of process parameters, a graph of etch rate of three annular regions versus the process parameter is presented followed by a plot of the average etch rate. The average etch rate graph shows an overall picture of the effect of a particular parameter, whereas the plot containing the annular regions shows across-the-wafer variations.

5.2 Experiments on Gas Composition of Plasma

In normal etching process, a combination of two or more gases is used in the plasma etch chemistry. An etch chemistry normally consists of a main etchant gas such as Cl_2 or F_2 in addition to BCl_3, $SiCl_4$, CCl_4 and inert gases such as N_2, He, and Ar. Fluorine gas is not commonly used for Ti etching because the vapor pressure of TiF_4 is low as indicated by

sublimation temperature of 284 °C. This means that high temperatures are needed for achieving significant etch rates in F_2 containing plasma which would cause problems when photoresist masks are used for patterning. On the contrary, the vapor pressure of $TiCl_4$ is high enough to render Ti etching at room temperature, leading to the use of Cl_2 as the leading contender for Ti etch [116]. The presence of BCl_3 is necessary to etch the native oxide layer on top of aluminum, and to scavenge moisture and oxygen in the etch chamber. The BCl_3 gas is also used for forming a nonvolatile, unsaturated film of B_xCl_y on the sidewall of patterned metal [33]. $SiCl_4$ is mainly used as Al_2O_3 reducing gas in the aluminum etch chemistry. The $SiCl_4$ readily decomposes in the plasma and reacts with the native Al_2O_3 on the aluminum, thereby initiating the etch process [82]. CCl_4 gas is used to form a sidewall polymer along the patterned metal lines in order to achieve vertical metal line profiles [97, 116].

The objective of this part of the work is to study the effect of the process parameters in gas plasmas of BCl_3 or Cl_2/N_2. Preliminary etch rate tests were conducted using BCl_3 and Cl_2/N_2 plasmas separately to determine whether the gas or combination of gases in question can be effectively used for etching. It was observed that Ti film etch rate was negligibly small in BCl_3 plasmas and hence no significant results could be obtained that would lead to any useful conclusions. It was noted by D.HG. Choe et al. [46] that the metal etch rates obtained exclusively with BCl_3 are comparatively low due to insufficient supply of free chlorine radicals. On the other hand, the plasma containing Cl_2/N_2 gave significantly high etch rates. In an etch chemistry containing Cl_2, the plasma is not required to generate etchant species and the primary consideration in gas phase for etching is etchant diffusion (transport). It was also observed by several workers that both chlorine molecules and atoms contribute to metal etching [86]. On the other hand, BCl_3 has to be

dissociated in the plasma discharge to form the etchant chlorine ions or radicals. The degree of dissociation is dependent on the bond strength between chlorine atom and the particular parent molecule or fragment. The bond dissociation energy of BCl_2-Cl is 4.55 eV as compared to that of Cl-Cl which is 3.51 eV. The higher dissociation energy of BCl_3 leads to lower etchant species available in the plasma [33]. The significantly high Ti etch rates in Cl_2/N_2 plasma prompted this work to pursue the study using Cl_2/N_2 plasma only.

5.3 Etch Reaction

The fundamentals of plasma etching were discussed in section 3.2. In this section, additional details of plasma related to Ti etching is presented. Some of the earlier published work [20, 21] discusses Ti etching in fluorine containing plasmas such as CF_4/O_2 and SF_6 following the plasmas used for silicon and silicon dioxide etching. As discussed in section 5.2, the vapor pressure of the reaction product TiF_4 in fluorine containing plasmas is low as indicated by the sublimation temperature of 284 °C. This means that production-worthy etch rates can be achieved only if substrates are heated to high temperatures. The high temperatures, on the other hand, would lead to harmful effects on the photoresist which is generally used for masking. Bluemenstock and Stephani [116] studied the etch characteristics of chlorine containing plasmas such as CCl_4/O_2 and $CCl_4/CCl_2F_2/O_2$. Danner and Hess [86] observed that both atomic and molecular chlorine participate in etching of Al metal. Extending the same idea to Ti etching, it can be safely assumed that both atomic and molecular chlorine react with Ti thereby leading to removal of layers of Ti from the substrate. Nitrogen is added to the etch gas mixture as a carrier gas, a detailed discussion of which can be found in section 3.4. According to the work done by O'Brien et al. [114, 115], ion stimulation is necessary

to initiate Ti and Si etching by chlorine. However, this study used an Ar ion beam. In the present dissertation work, ionized nitrogen gas in the plasma provides ions for etching, although it is not a controlled beam of ions. So, N_2 in addition to acting as a diluent/carrier gas, provides ions for stimulation of etching.

When chlorine is used as the main etchant, the plasma is not required to generate the etchant species because undissociated molecular chlorine can also result in Ti etching. Equation (5.1) shows the dissociation of chlorine in the plasma due to electron attachment, the degree of dissociation being primarily governed by the Cl-Cl bond strength.

$$2Cl_2 + e^- \rightarrow Cl_2 + 2Cl + e^- \qquad (5.1)$$

From equation (5.1), it can be seen that undissociated chlorine molecules are still present in the plasma along with chlorine atoms and free electrons.

The chlorine molecules and radicals get adsorbed by Ti film, react with Ti to form volatile etch product $TiCl_4$ [116]. $TiCl_4$ is the only etch product that has sufficient vapor pressure at around 50 °C or lower temperatures to obtain etch rates shown in this work. O'Brien and Rhodin while investigating the substrate composition of Ti film etched in Cl_2 containing plasmas did not observe $TiCl_4$ and $TiCl_3$, leading to the conclusion that $TiCl_4$ is emitted into the gas phase soon after its formation during the etch reaction. The following equation describes the etch reaction.

$$Ti(solid) + 4Cl(gas) \rightarrow TiCl_4\ (gas) \qquad (5.2)$$

O'Brien et al. [114] proposed that the above mentioned reaction proceeds in four steps as shown below.

$$Ti + Cl \rightarrow TiCl \quad (5.3)$$

$$TiCl + Cl \rightarrow TiCl_2 \quad (5.4)$$

$$TiCl_2 + Cl \rightarrow TiCl_3 \quad (5.5)$$

$$TiCl_3 + Cl \rightarrow TiCl_4 \quad (5.6)$$

The reaction (5.3) is found to be an endothermic reaction, with heat of formation of 0.87 eV for TiCl. In order for this reaction to proceed, the heat of formation has to be supplied in the form of ion bombardment thereby validating the necessity of nitrogen ions.

5.4 Time versus Etch Rate

In this section, the Ti etch rate variation due to etch time is studied. Etch time was varied from 10 s to 80 s in increments of 10 s. The pressures was set at 700 mTorr and Cl_2/N_2 flow rate ratio was 3:1. The magnitude of Cl_2 flow rate was at 75 sccm and that of N_2 flow was maintained at 25 sccm. An RF power of 350 Watts was applied to the bottom electrode. The top electrode and the chamber were maintained at 70 °C and the bottom electrode was heated to 40 °C. The etch rate was plotted against etch time. Fig. 5.1 presents the etch rate at center, middle and edge, separately, and Fig. 5.2 shows the plot of the average Ti etch rate against etch time. From Fig. 5.2, it can be observed that the average etch rate increases slowly for the etch duration of 10 to 40 s. Beyond 40 s, the etch rate rises rapidly. The etch rate increases from 260 Å/min for an etch time of 10 s to 1560 Å/min for 40 s at a rate of about 300 Å/min for every 10 second increase in etch time. After 40 s, the increase in etch rate is very steep, showing an increase of 1300 Å/min for every 10 s increase in etch time. From the graph, it is found that the etch rate characteristics changes from one region to the other at an etch time of 40 s. It is observed from Fig. 5.1 that initially, for an etch time of 10 s the etch rate is high at the center of the

wafer and low at the edge of the wafer, with etch rate at middle of the wafer falling in between. As the etch time is increased from 20 to 40 s, the etch rates at the center, middle, and edge are almost the same, indicating that the etching is uniform across the wafer. When the etch time is increased beyond 50 s, the etch rate at the wafer edge is higher than at the center. So it is observed that the wafer clears from the edge towards the center as the Ti film is etched in Cl_2/N_2 plasma.

The variation of etch rate with etch time can be explained as discussed below:
The etch process has to proceed through three slightly different layers of Ti and its oxides. [20]
(i) The hard and nearly stoichiometric native titanium oxide (TiO_2) film, which is approximately 20 to 30 Å thick, formed when the Ti film is exposed to atmosphere.
(ii) A film of soft non-stoichiometric oxide which is 500-600 Å thick (TiO_x with $2>x>0$ where x progressively decreases with depth).
(iii) Pure titanium for the remainder of the film .

It is observed that there is a delay of about 4 s before the etch process begins. This time delay is know as induction time or initiation time which can be attributed to the time taken to break through the TiO_2 film on the surface of Ti film. After the initiation time, the etch rate increases linearly with increase in the etch time. The plasma in the reaction chamber takes a few seconds to stabilize and this leads to lower etch rate for the first 20 s of etch duration. In addition to that, the etching proceeds at a slower rate through the non-stoichiometric TiO_x. The test wafer, when exposed to plasma, is heated due to radiant heating effects of the plasma. As the duration of exposure of the wafer to the plasma increases due to increased etch time, the wafer temperature increases, causing an increase

in the reaction rate of the chlorine etchant species with Ti film, which manifests itself as an increase in the etch rate. The rapid increase in the etch rate after 30 s is also due to the fact that the etching of pure Ti proceeds at a much faster rate than the titanium oxide films. The linear relationship between the etch rate and etch time could not be examined beyond 80 s, because the Ti film was completely etched out in some areas of the wafer when the wafers were etched for durations longer than 80 s.

5.5 Cl_2/N_2 Flow versus Etch Rate

In this section, the etch rate dependence on chlorine and nitrogen flow is studied. Cl_2 gas acts as the reactant in the chemical reaction and N_2 gas acts as a carrier gas and also provides ions for bombardment during the etch process. The function of these gases in the etch reaction was discussed in detail in sections 3.3 and 5.2. In the first part of the experiment, nitrogen flow was kept constant at 25 sccm and the chlorine flow was varied from 25 sccm to 200 sccm. The chamber pressure was set at 700 mTorr and the top and bottom electrodes were heated to 70 and 40 °C, respectively, while the chamber was maintained at 70 °C. A constant RF power of 350 watts was applied to the bottom electrode. The Ti test wafers were etched for 30 s. Fig. 5.3 shows the etch rate variation at the center, middle, and edge, separately, and Fig. 5.4 shows the average etch rate variation with the chlorine flow. As in the previous sections, the graph of the average etch rate (Fig. 5.4) provides a very good tool for easy visualization and interpretation of the results. From this graph, it is observed that the etch rate increases linearly with chlorine gas flow for chlorine gas flows from 25 sccm to 100 sccm and then it levels off at 4880 Å/min for chlorine flows of 150 sccm and above. Further increase in the chlorine flow does not have any effect on the etch rate. The initial increase in the etch rate is attributed

to the increase in the reactant species in the plasma. Once the plasma is saturated with reactant species, any further increase in the amount of chlorine gas is not reflected as increase in the etch rate.

In Cl_2/N_2 plasma, chlorine is the main reactant species. At low pressures, it reacts with Ti to form a volatile $TiCl_4$ at low pressures that can be pumped away with the help of vacuum pumps. The flow rate of the gas determines the maximum possible supply of reactant. The actual supply of the reactant chlorine species depends on the balance between generation and loss of active species in the plasma. Chemical reaction of the chlorine species with the substrate Ti film and convective flow are the two major loss mechanisms for the reactant species. In general, the etch rate dependence on the reactant gas flow is a superposition of two different effects [12]. In the low flow region between 25 and 125 sccm, the etch rate increases linearly from 2600 Å/min to 5400 Å/min. In this region, the etch rate is limited by the availability of the chlorine reactant species and the loss of etchant chlorine species is mainly due to chemical reaction. This region is also know as supply rate limited etching. For further increase in chlorine flow beyond 125 sccm, the etchant species are lost due to convection rather than by chemical reaction. So no further increase in the etch rate is observed because the plasma is saturated with chlorine etchant species and any additional chlorine gas does not react with Ti. It is predicted that beyond 200 sccm, there will be a decrease in the etch rate as the Cl_2 flow is increased, because the pumping speed increases to maintain constant pressure, thereby pumping away the reactant species before they have a chance to react with Ti. The etch rate in this regime could not be obtained in this experiment because the etcher used in the experiment was equipped with a chlorine mass flow controller (MFC) having a maximum flow rate of 200 sccm.

In the second part of the experiment to determine the effect of gas flow, chlorine flow is fixed at a constant 75 sccm and the nitrogen flow is varied from 0 to 100 sccm. the reaction chamber pressure was set at 700 mTorr and an RF power of 350 W applied to the bottom electrode. As in the previous case, the chamber and top electrodes were heated to 70 °C while the bottom electrode was maintained at 40 °C. The wafers were etched for 60 s. Fig. 5.5 and 5.6 show the etch rate in the center, middle, and edge of the wafer and the average etch rate variation due to variation in nitrogen flow.

The Ti etch rate dependence on the N_2 flow is described as follows:

The Ti etch rate increases from 2300 Å/min to 3800 Å/min when the nitrogen flow is increased from 0 to 10 sccm, and decreases as nitrogen flow is further increased. When there is no nitrogen flow, only chlorine species are available for etching Ti and the etching is mainly due to chemical reaction of chlorine with Ti. When a small amount of nitrogen is introduced, nitrogen is ionized in the etch chamber and provides ions for bombarding the substrate. This effect assists the etch process due to chlorine, leading to an increase in etch rate of Ti film. This process is known as ion-assisted chemical etching [113, 114, 115]. As the nitrogen flow is further increased, the partial pressure of chlorine is decreased to maintain a constant pressure due to the presence of nitrogen. This effect, referred to as dilution effect, reduces the amount of chlorine etchant species available for etching in the chamber, leading to a decrease in the etch rate. It is worth to note in this regard as a special case that N_2 addition to gas mixtures containing CCl_4 initially causes an increase in the etch rate due to the formation of CN. This reaction reduces the polymer formation on the etched surface while it increases the amount of free chlorine radicals by tying up carbon [97]. In this case, the etch rate did not decrease up to 90% N_2

addition. Further addition of N_2 led to a decrease in the etch rate due to the etching mechanism becoming ion-assisted etching.

5.6 RF Power versus Etch Rate

In this experiment, the effect of RF power on the Ti etch rate is studied. In the previous experiments described in sections 5.2 to 5.4, the RF power was applied to the bottom electrode, but in this case the RF power was applied to either the top or bottom electrode. The etch rate was calculated through sheet resistivity measurements as described before. The top electrode and the bottom electrode are symmetrical and hence the plasma generation should not be affected by the application of RF power to either of the two electrodes.

The RF power was varied from 100 W to 600 W. The chlorine and nitrogen gas flows are maintained at 75 sccm and 25 sccm (3:1 ratio), respectively. The etch chamber was maintained at a pressure of 700 mTorr. Wafers were etched for 45 s. The etch time was picked low enough to obtain useful etch rate information throughout the range of this investigation without etching the Ti film completely. Fig. 5.7 and 5.8 illustrate the etch rate as a function of RF power applied to bottom electrode. From Fig. 5.8, it can be observed that the etch rate increases linearly with the RF power between 100 and 300 watts and then the increase of etch rate is sharper for RF power over 300 W. The increase in etch rate appears to be less after 500 W of applied RF power. The maximum etch rate reaches 8260 Å/min for an RF power of 600 W.

Fig. 5.9 and 5.10 present the etch rate dependence on RF power applied to top electrode. In this case, the average etch rate is less than that when the power is applied to the bottom electrode. Similar to the previous case where the bottom electrode was powered, the etch rate increases almost linearly with the increase of RF power. The maximum etch rate is around 4560 Å/min for an RF power of 600 W.

From the etch characteristics shown in Fig. 5.8, it is observed that the Ti etch rate increases slowly when the RF power is increased from 100 W to 300 W and then increases rapidly as the power is increased beyond 300 W. After 500 W of applied power, the rate of increase in the etch rate appears to decrease. When sufficiently high RF power is applied to the reactor electrodes, ionization of gas atoms and molecules occur [108]. In the region of 100 to 300 W of RF power, the etch rate increases from 130 to 1200 Å/min, but as the RF power is increased beyond 300 W, the etch rate increases to 9100 Å/min by about 5 times that of the original etch rate. This effect could be due to increased dissociation at higher power densities [107]. When the RF power is applied to the bottom electrode, a negative self-bias appears at the bottom electrode holding the wafer. This negative Vdc accelerates positive ions from the plasma and causes ion bombardment on the substrate placed on the bottom electrode. In this case, the etching mechanism is predominantly reactive ion etching or ion assisted etching. An increase in the RF power also leads to an increase in this negative self-bias voltage and hence leads to a substantial increase in the etch rate. Current enhancement of more fragmented ionic species compared to the less fragmented ionic species of Cl_2 with increasing power densities have been observed in Cl_2 plasma beam experiments [107]. When BCl_3 or BBr_3 gas is added to the Cl_2 plasma, the increase in power density primarily effect the removal of boron residues from the surface of the etched film. In this study, none of these two gases was used, and

hence it can be concluded that the etch rate increase is mainly due to an increase in ionization and the ion energy. Essentially, all the applied power is dissipated as heat in the etch chamber. The increase in the etch rate could also be an effect of increase in substrate temperature due to the heat dissipation from the plasma. The heating effect could also be caused by eddy currents in the metallic film [21].

When the RF power is applied to the top electrode, the magnitude of etch rate is ~ 20 % less that when RF power is applied to the bottom electrode. This could be due to a positive self-bias, Vdc, appearing at the substrate. This positive Vdc retards the positive ions such as N^+. So the etching has to proceed with the help of reactant chlorine species only without ion bombardment. So, the etching mechanism is considered to be predominantly plasma chemical etching. The edge of the wafer etched faster than the middle and the center of the wafer. This effect, which is known as bull's eye effect, may be due to faster reaction rate near the edge of the wafer. The residence time of the gases near the edge of the wafer could be shorter due to the fact that pumping is done through an opening near the edge of the wafer, and hence the reactant gases and etch products could be cleared from the surface of the wafer faster than at the center of the wafer.

5.7 Pressure versus Etch Rate

In this section, the effect of pressure on Ti etch rate is discussed. The etch mechanism depends on the reaction chamber pressure. C.B. Zarowin [108] observed that at low pressures (below 100 mTorr), the etching mainly due to reactive ion etching (RIE), and for pressures above 100 mTorr, plasma etching dominates . But this observation could be

dependent on the reactor volume. However, this concept could be used to explain the pressure dependence of etch rate in this study.

In this experiment, the pressure was increased from 500 to 1000 mTorr, with chlorine and nitrogen flows kept constant at 75 and 25 sccm, respectively. The RF power is applied to the top or bottom electrode. All the wafers were etched for 45 s. As described in the previous sections in this chapter, Ti etch rate is calculated using the sheet resistance measured using a four point probe instrument. Fig. 5.11 and 5.12 show the pressure dependence of center, middle, and edge etch rates and average etch rate , respectively. It can be observed that the etch rate is high at low pressure and decreases as the pressure is increased. Beyond 800 mTorr, the increase in pressure does not affect the etch rate very much and the etch rate remains constant at around 1600 Å/min . The experiment was repeated with the RF power applied to the bottom electrode. Fig. 5.13 and 5.14 show the etch rate dependence on the pressure when the bottom electrode is powered. The etch rate is higher than in the previous case where the RF power was applied to the top electrode, but the magnitude of the etch rate is higher because of the RIE mode of etching as discussed in section 5.6 displays characteristics similar to similar dependence, except that the value of etch rate is higher than that in the powered top electrode. The etch rate starts at 5700 Å/min for a pressure of 400 mTorr and decreases linearly and levels off at 1800 Å/min for pressures of 700 mTorr and above.

At low pressures, the ions from the plasma traverse the sheath without any collisions leading to loss of energy and reach the substrate to contribute to etching reaction. It could also be noted in this respect that the mean free path of the ions is long due to little or no collisions. As the pressure is increased, during the motion toward the substrate, the ions

collide primarily with neutral species because the ratio of ions to neutral species is very small [108]. As the pressure P increases, the concentration of reactive chlorine atoms may be reduced by recombination reactions which occur at reactor surfaces and also at gas phase of the plasma [33]. Such recombination reactions reduce the number of reactant chlorine atoms available for etching and thereby contribute to reduction in the etch rate. These phenomena could lead to a decrease in Ti etch rate.

Another important factor affecting the etch rate is the residence time of the reactant species in the plasma, which is defined as

$$\text{Residence time} \quad t = (P\,V)/Q \qquad (5.7)$$

where P is the pressure, V is the reactor volume, and Q is the process gas flow rate.

From the above equation, it can be observed that the residence time increases with the increase in pressure, as the reactor volume and the gas flow rate are constant in this experiment. The increase in residence time seems to adversely affect the etch rate. So it can be stated that the etch rate is not residence time limited. The increased residence time could lead to slow removal of the reaction products thereby slowing down the etch rate. It is also observed that the decrease in Vdc is not significant to cause decrease in etch rate.

The etch rate characteristics when RF power is applied to the bottom electrode can be explained using the same principles presented above. But the etch rate is slightly higher than that of the top powered electrode because of the negative Vdc appearing at the substrate which was discussed in detail in section 5.6.

5.8 Temperature versus Etch Rate

The effect of temperature on the Ti etch rate in Cl_2/N_2 plasma is discussed in this section. Like in the previous experiments, the Cl_2/N_2 flow is kept constant at a ratio of 3:1, with the gas flows 75:25 sccm, RF power is also kept constant at 350 Watts, applied to the bottom electrode. The process pressure was maintained at 700 mTorr. All the test wafers were etched for 30 s to provide significant etch rate throughout the range of temperatures, 55 to 80 °C, used in this experiment. The etch rate was calculated from the sheet resistivity measurements using four point probe method.

In Lam 4600 etcher, temperature of the top and bottom electrodes as well as the chamber can be individually controlled. In this experiment, temperature of the electrodes and the chamber were maintained at the same level in order to simplify the experiment and the analysis. Temperature of the chamber and both the electrodes was increased from 55 °C to 80 °C in increments of 5 °C. and the Ti etch rate was calculated. The etch rate, as described in the previous sections, was calculated in three regions of the wafer and plotted in Fig. 5.15. It is worth to note in this respect that in almost all of the previous sections, the edge of the wafer etched faster than the center, with the etch rate in the middle in between. In this case, the etch pattern across the wafer is similar up to a temperature of 60 °C, and for further increase in temperature, the center etches faster than the edge, and the middle etch rate being the lowest of the three. The average etch rate was also calculated and plotted as shown in Fig. 5.16. From these graphs, it is observed that the average Ti etch rate is 5630 Å/min at 55 °C and decreases by 390 Å/min to 5240 Å/min when the temperature is raised to 60 °C. When the temperature is increased further, the Ti etch rate

shows a steady, but small linear increase. It could be observed that the temperature dependence of the etch rate is weaker than RF power and flow rate.

Danner et al. [33] observed that at low temperatures below 50 °C, the Al etch rate falls off and terminates primarily due to a limitation in product removal from the etched surface. Due to the lower temperatures, the water vapor can condense on the substrate surface and form oxides that would inhibit etching. At temperatures above 90 °C, the etch rate was independent of temperature or flow rate. Such results indicated that the etch reaction and product desorption are rapid, but the etch rate is limited by the rate of arrival of etchant species at the Al substrate. The results obtained for Al etch in Cl_2/BCl_3 can be extended to Ti etching in Cl_2 plasma as the main etchant in both the plasmas is Cl_2. The temperature range (55 to 80 °C) of the experiment described in this section falls in the region of transition between etchant adsorption (> 90 °C) and product desorption (< 50 °C). In this region, it could be assumed that as the temperature is increased both the etchant adsorption and product desorption increase slightly. This leads to a slight increase in the etch rate.

As observed from the graph Fig. 5.15, the edge etch rate is higher than the center and the middle of the wafer. This effect, which is often known as Bull's eye effect, can be explained in terms of gradient in etchant concentration across the wafer. But, as the temperature is increased 65 °C and beyond, the center etch rate becomes higher than that at the edge, and the middle etch rate below that at the edge. This effect could be due to the temperature gradient across the wafer, probably the center being at a higher temperature than the edge.

5.9 Summary and Conclusions

In this chapter, the etch characteristics of Ti in Cl_2/N_2 plasmas with the variation of etch time, N_2 and Cl_2 flow, RF power, etch chamber pressure, and temperature are examined. In general, these experiments yield information on the individual effect of these process parameters on Ti etching. The Ti etch rate is found to be reactant supply rate limited in low Cl_2 flow region. Similar to TiN etch process, the RF power is observed to have the maximum effect on the Ti etch rate. The increase in N_2 flow appears to decrease the Ti etch rate due to dilution. From the experiments conducted, the following conclusions were made:

(i) There is about 4 seconds induction time before Ti etching starts. Then, the etch rate increases to ~ 5500 Å/min for 80 s etch time due to settling of plasma parameters and the heating effects of the plasma on the wafer.

(ii) The Ti etch rate is supply rate limited up to a chlorine flow of 125 sccm, and levels off due to saturation in ionization and/or reaction rate limiting.

(iii) An increase in N_2 flow up to 10 sccm, increased the etch rate due to increase in ion-assisted etching of Ti due to availability of nitrogen ions for bombardment. However, higher N_2 flows beyond 10 sccm, reduced the etch rate probably due to dilution.

(iv) RF power has the maximum effect on the etch rate causing a six fold increase as the RF power is increased from 200 W to 600 W. The etch rate increase with RF power can be attributed to increased ionization of gases in the plasma, heating effects of the plasma on the substrate due to high power density, and high negative Vdc in the case of bottom powered electrode. The Vdc is positive for top powered electrode.

(v) An increase in pressure leads to a decrease in the etch rate due to an increase in collisions between etchant species bound for the substrate and the atoms/molecules present in the plasma.

(vi) The temperature dependence of the Ti etch rate is weak when compared to other parameters such as RF power and Cl_2 flow rate in the region of this work. This region of temperature is believed to be in a transition between etchant adsorption and product desorption. This experiment has to be repeated in order to confirm the result that the etch rate actually decreases as the temperature is increased from 55 to 60 °C. In addition, an experiment has to be conducted with a wider temperature range, starting from 30 °C to 80 °C. The data has to be acquired at smaller intervals so as to determine the effect of temperature on the etch rate.

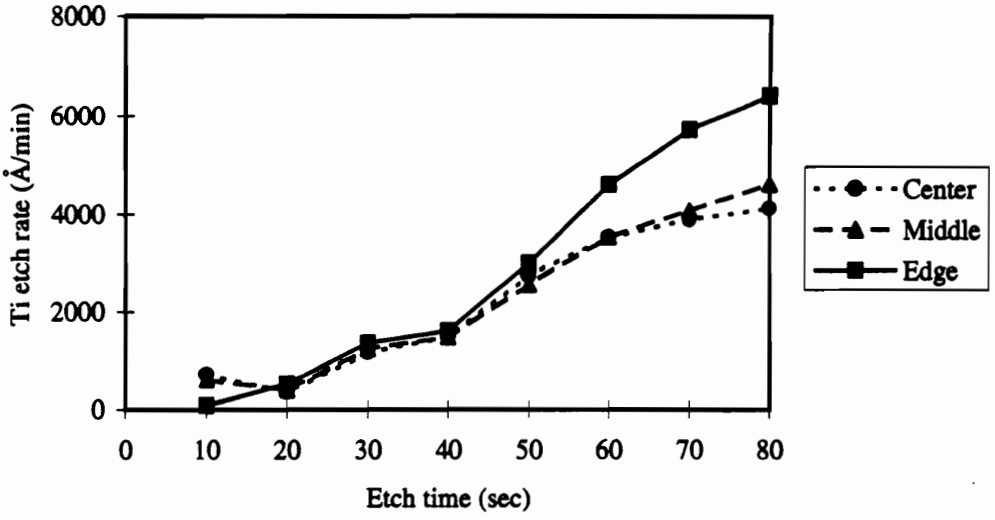

Fig. 5.1. Time vs Ti etch rate in Cl2/N2 plasmas

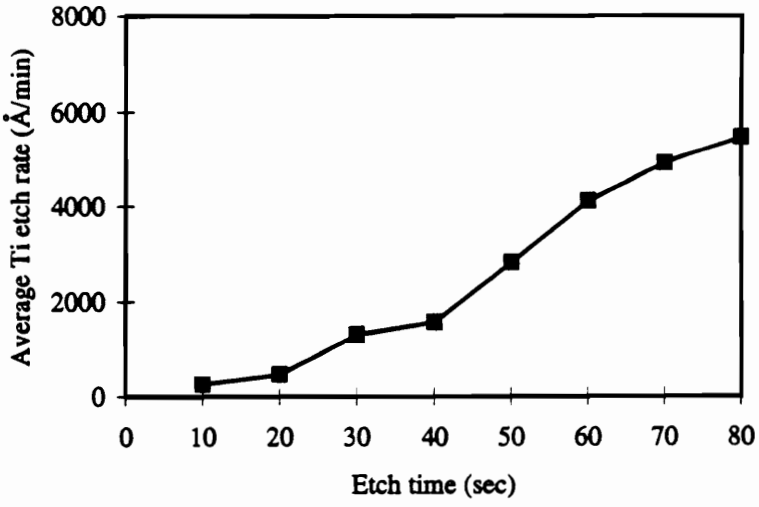

Fig. 5.2. Time vs average Ti etch rate in Cl2/N2 plasmas

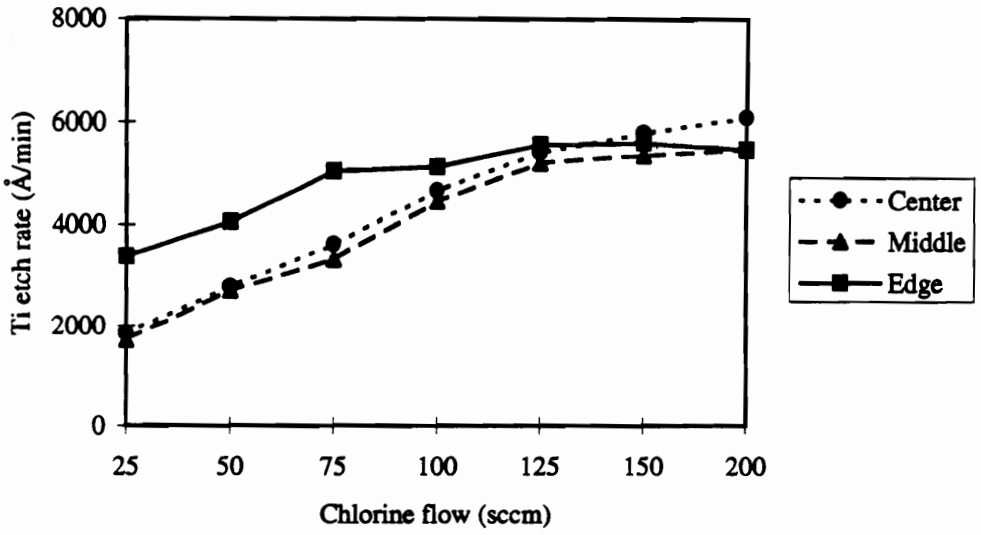

Fig. 5.3. Chlorine flow vs Ti etch rate in Cl2/N2 plasmas

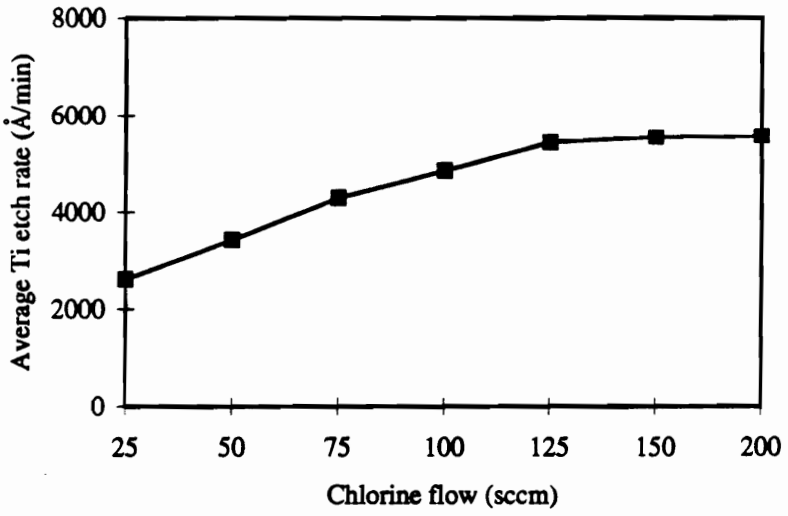

Fig. 5.4. Chlorine flow vs average Ti etch rate in Cl2/N2 plasmas

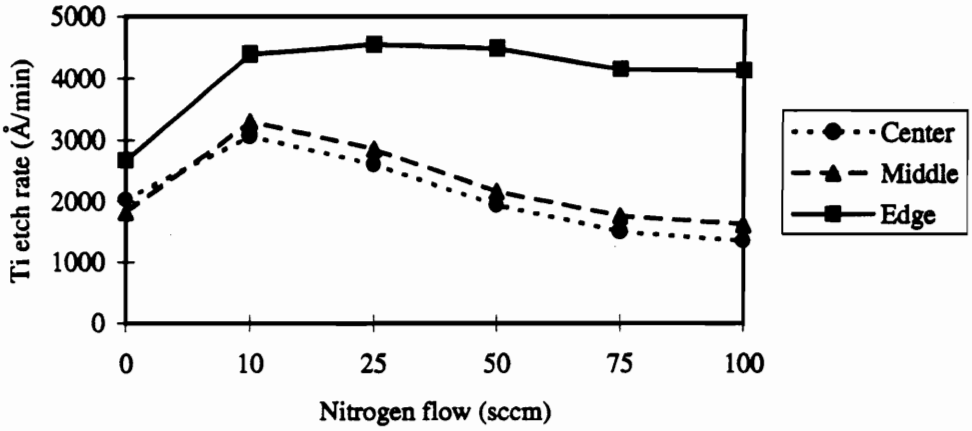

Fig. 5.5. Nitrogen flow vs Ti etch rate in Cl2/N2 plasmas

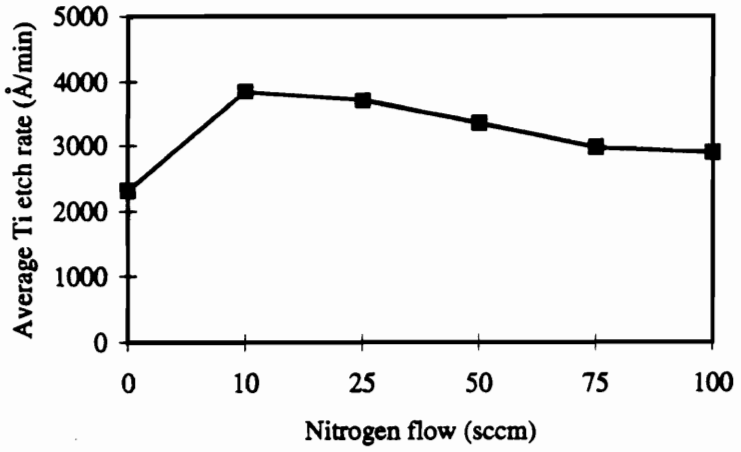

Fig. 5.6. Nitrogen flow vs average Ti etch rate in Cl2/N2 plasmas

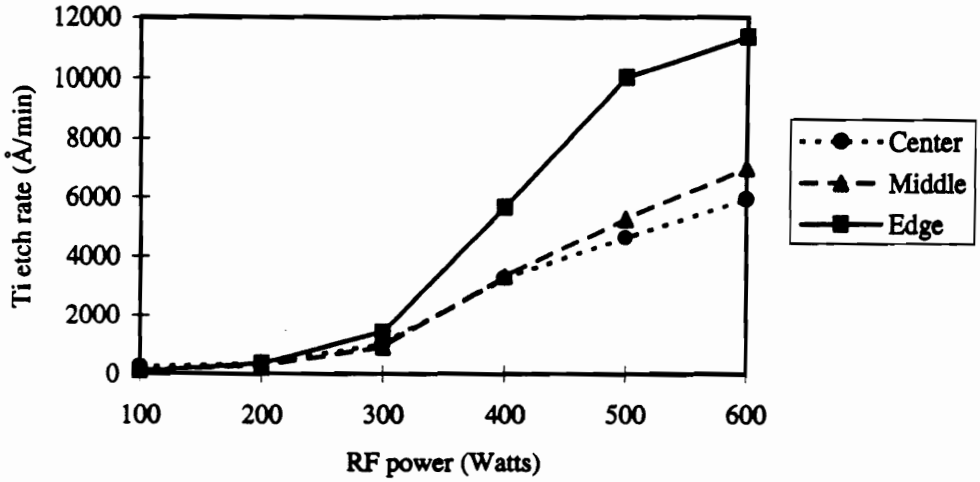

Fig. 5.7. Bottom electrode RF power vs Ti etch rate in Cl2/N2 plasmas

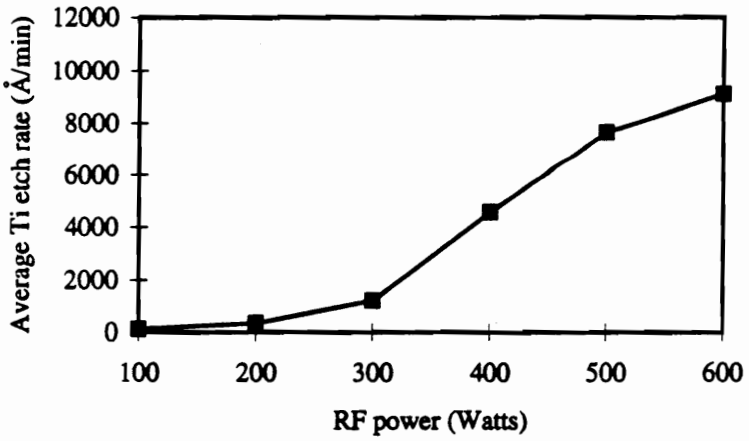

Fig. 5.8. Bottom electrode RF power vs Average Ti etch rate in Cl2/N2 plasmas

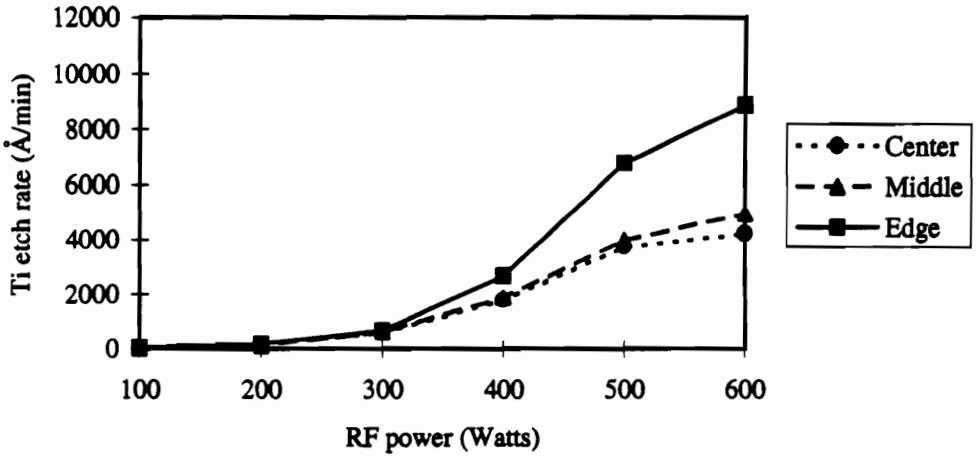

Fig. 5.9. Top electrode RF power vs Ti etch rate in Cl2/N2 plasmas

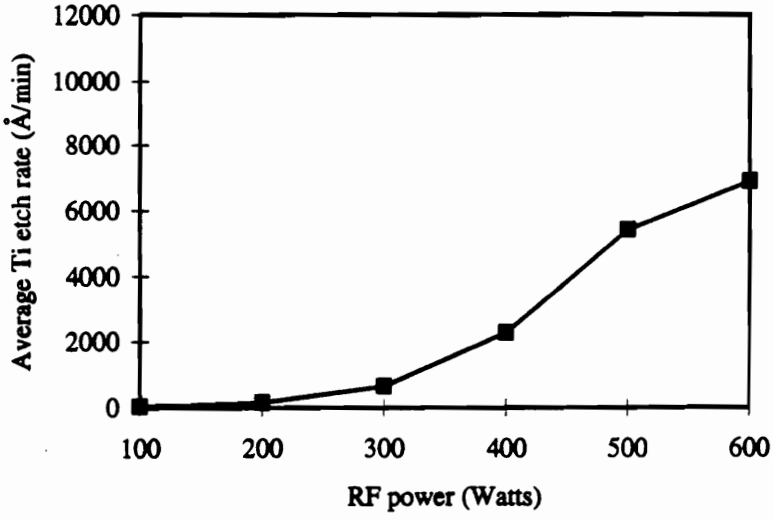

Fig. 5.10. Top electrode RF power vs average Ti etch rate in Cl2/N2 plasmas

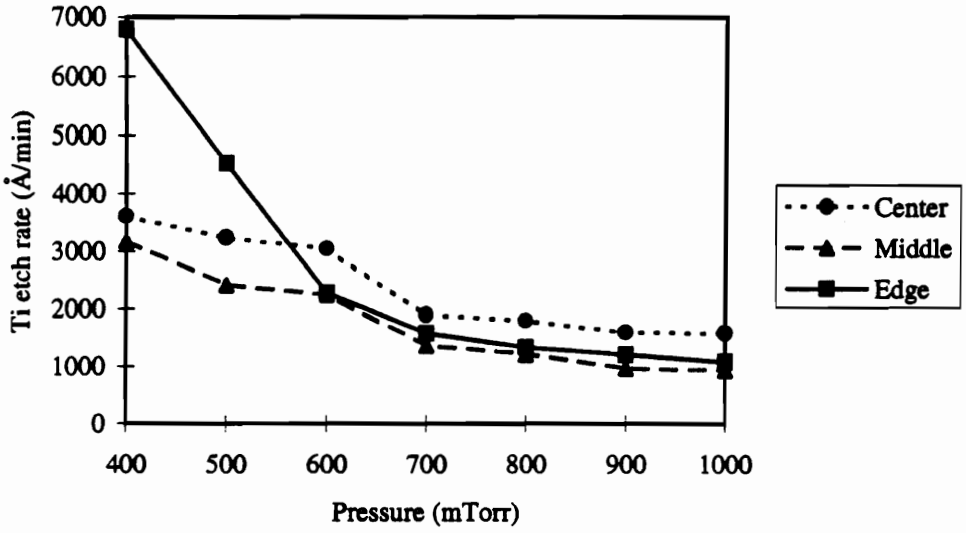

Fig. 5.11. Pressure vs Ti etch rate in Cl2/N2 plasmas (Powered top electrode)

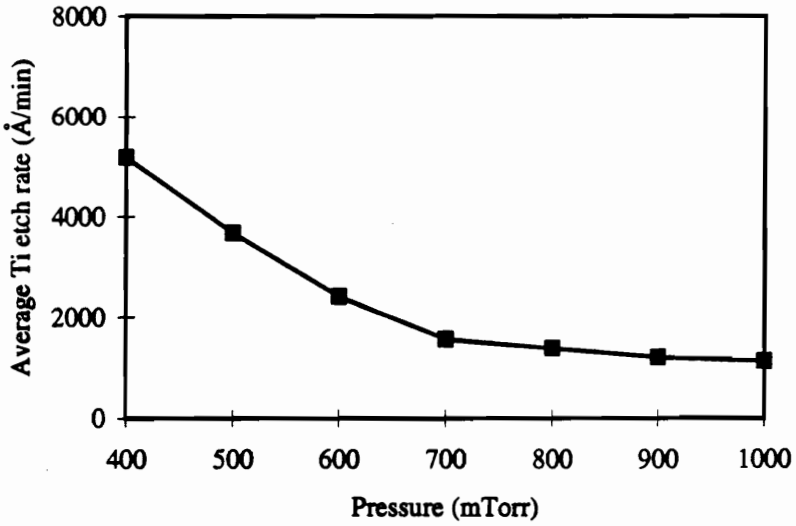

Fig. 5.12. Pressure vs average Ti etch rate in Cl2/N2 plasmas (Powered top electrode)

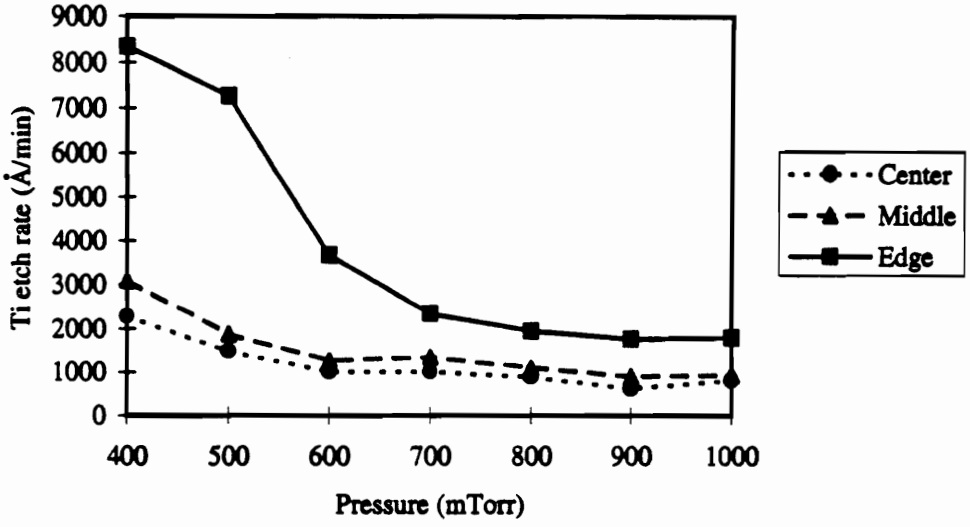

Fig. 5.13. Pressure vs Ti etch rate in Cl2/N2 plasmas (Powered bottom electrode)

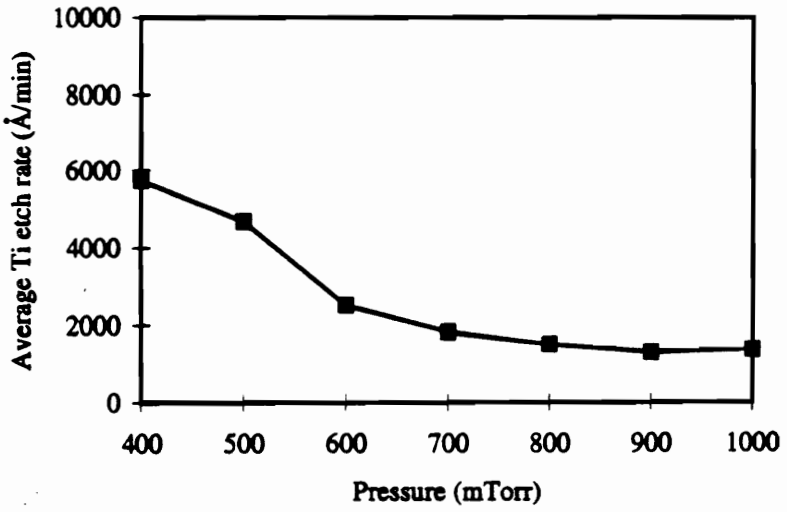

Fig. 5.14. Pressure vs Average Ti etch rate in Cl2/N2 plasmas (Powered bottom electrode)

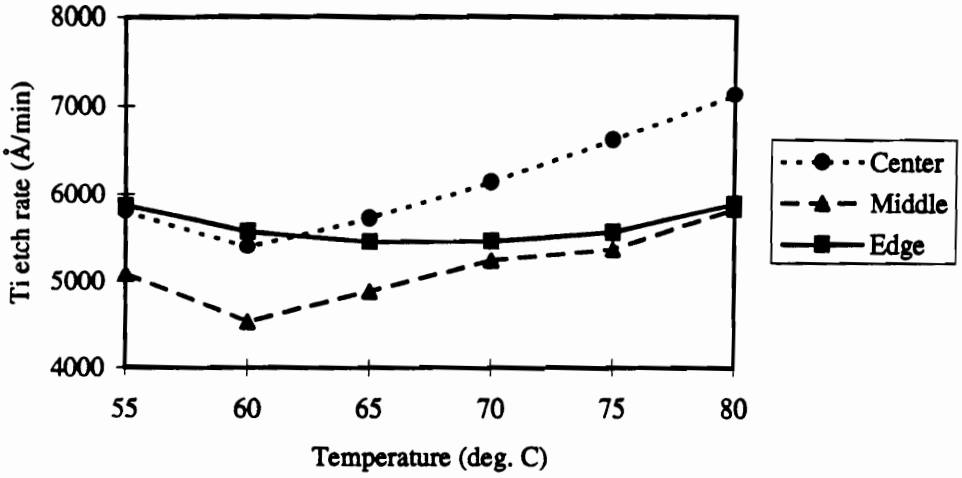

Fig. 5.15. Temperature vs Ti etch rate in Cl2/N2 plasmas

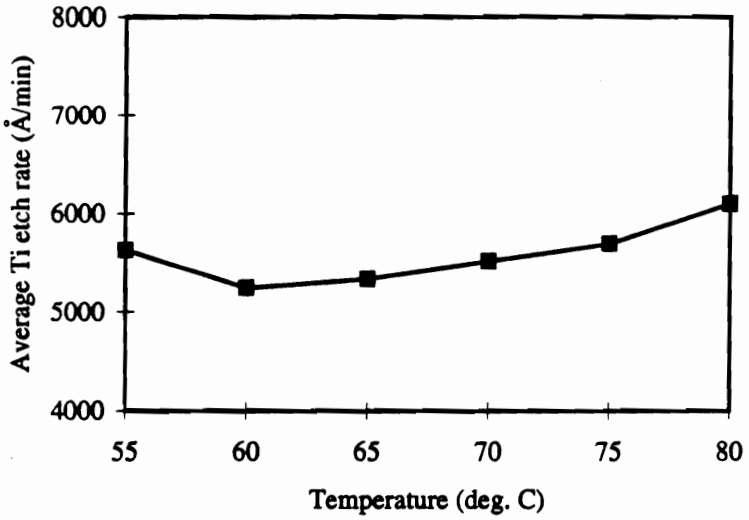

Fig. 5.16. Temperature vs average Ti etch rate in Cl2/N2 plasmas

Chapter 6

Design of Experiment and Modeling for Ti, TiN Plasma Etch Processes

6.1 Introduction

In the previous chapters of this dissertation, the effects of each of the process parameters, such as the etch time, the gas flow, the RF power, and the temperature, on the etch rate of the Ti and TiN films were studied by varying one parameter at a time while keeping other parameters constant. This technique is both expensive and time consuming, and usually requires several experiments before a process is satisfactorily characterized. Moreover, this technique gives only the main effects of independent variables (also referred to as process parameters or factors) and gives no quantitative information on the interaction among the process variables. A good mathematical model representing the process can not be developed from the responses obtained from this technique since the information available from the experiment is insufficient. The plasma processes that are used in the semiconductor IC fabrication are very complex and usually involve several simultaneous chemical reactions, such as electron-impact, gas-gas, and gas-surface interactions, in addition to the physical etching by ion bombardment [123]. Therefore, a more sophisticated technique for designing and conducting an experiment and deriving a model for a plasma process is required. In this chapter, the Response Surface Methodology (RSM) technique for designing and conducting experiments for TiN and Ti plasma etch processes is described. The Taguchi technique was not used in this work since the number of input factors were less than six and hence the required number of runs for an RSM

experiment is below 32. The RSM technique also provides information on the two factor interactions and second order effects for all the factors. An empirical model for the TiN and Ti etch processes is developed. An attempt is made to explain the model and the relative significance of the factors through plasma physics and chemistry. A statistical analysis software package, JMP [137], is used for designing and analyzing the experiments.

6.2 Fundamentals of Design of Experiments, Analysis, and Modeling

In the development of any plasma process, the effect of several process variables (also known as factors in the design of experiments) need to be considered. As discussed in Chapters 3, 4, and 5, the individual effects of these factors can be analyzed by varying one variable at a time while keeping the other parameters at a fixed level. While this approach is simple, it is expensive and can yield incomplete and misleading results. This type of experiments requires several runs at many factor levels, and does not account for experimental errors. In addition, it completely ignores the interactions (that is, setting of one variable affecting the response to another variable) among the variables. The plasma processes involve many variables and are too complex to be studied using this technique. Understanding of a particular process may help in determining the significance of the variables. However, plasma processes are very complex and make decision on the significance of the factors difficult [123]. Therefore, some kind of structured experiment has to be designed and run to obtain quantitative information on the main effects and interaction of the variables on the response and possibly higher order effects.

A typical plasma etch process consists of a large number of variables (also referred to as factors). Table 6.1 shows a list of factors in a typical plasma etch process. The measurable output quantities obtained from the experiments are called responses. Table 6.2 shows a list of typical responses in a plasma etch process. The setting of factor X_1 can affect the response Y differently based on the setting of factor X_2. This is called interaction between factors X_1 and X_2. Therefore, the effect of settings of all the factors X_1, X_2, ..., X_n, on the response Y has to be considered simultaneously in order to obtain a realistic model and reliable process optimization. A mathematical model developed from the experimental results can quantitatively represent the responses as a function of process variables. This model makes the relative significance of the effect of factors on the responses more visible. The model can also be used for identification of best settings for a given process and thus the optimization of the process. The mathematical models also help in determining the process window, in which the response can be maintained within the tolerance limits when the parameters are changed by a certain amount. Several of the plasma processes such as generation, transport, and loss of species can be represented by mathematical models developed from fundamental principles using techniques such as continuum approach and/or Monte Carlo simulation [123]. However, the rate coefficients and cross sections for most reactions are unknown. Hence, the empirical modeling technique is widely accepted as the most suitable and economical alternative in the semiconductor fabrication for process characterization and optimization. The Table 6.1 lists the typical process parameters or factors used to design in an experiment and Table 6.2 shows the typical responses obtained from the experiment.

Table 6.1. Process parameters (factors)

1. RF power
2. Gas flow
3. Gas mixture ratio
4. Pressure
5. Wafer temperature or electrode temperature
6. Electrode spacing or gap between the electrodes
7. Wafer area that needs to be processed

Table 6.2 Responses

1. Etch rate
2. Etch uniformity
3. Selectivity
4. Profile of the etched pattern
5. Critical dimension (CD)

Response Surface Methodology (RSM) is a statistical technique by which the experimental strategy and data analysis are combined efficiently to generate a mathematical model that represents a process response [123]. The RSM technique can be used only if the responses are continuous. For example, the etch rate and the uniformity in a plasma etch process are continuous. Some the responses are discrete quantities. For example, the number of good dice on a wafer is a discrete quantity. Therefore, it cannot be included as a response in the RSM technique. But such discrete responses can be transformed into continuous quantity, such as percentage yield (ratio of good dice to total number of dice on a wafer, expressed as a percentage). Normally, unstable process conditions that lead to abrupt and discontinuous change in the response are avoided while designing an experiment. Therefore, only the smooth and continuous regions of interest are selected for analysis using this technique. The RSM techniques are typically used for modeling and analyzing the parameter space within the limits of the parameter/factor settings, and the models are not valid for the regions beyond these factor settings. The RSM technique consists of the following steps:

(i) experimental design with uniform sampling in a multiparameter space,

(ii) data collection at the points specified by the design,

(iii) development of an empirical model for the response surfaces (such as etch rate and uniformity) by fitting the observations to an equation that relates the responses to the independent variables, and

(iv) process optimization with response surfaces (such as contour plots) or models (mathematical equations) [121].

6.2.1 Experimental Design

In order to completely determine the effect of n factors on a response, an experiment has to be conducted at all the levels of all factors. If there are k levels used for each of the factors, then k^n runs are required. This design is called full-factorial design. For example, a full-factorial experimental design with 3 factors at 2 levels would require $2^3 = 8$ runs. As the number of factors and the levels increase, the number of runs required becomes very large. To reduce the number of runs, a fractional factorial design, which is a subset of the runs in full-factorial design, is used.

The RSM designs are fractional factorial designs requiring 3 or more levels for each process variable (factor). It is a common practice to normalize the factors about its center point as shown in (6.3).

$$x_t = [(x_i - x_{av})/\sigma_x] \qquad (6.1)$$

where x_t is the scaled value, x_i is the unscaled value of the factor, x_{av} is the mean, and σ_x is the standard deviation of factor x. The actual values of the factors such as power, pressure and gas flow, have various ranges, but when they are scaled as shown in (6.1), the range is reduced to -1 to +1 for all the factors. This technique makes the comparison of the

magnitude of the coefficients of the model thus making it simple to visualize the relative importance of the model terms. The number of runs required for an RSM design must be higher than the number of coefficients in the model. If the number of coefficients and runs are the same, then the solution will have no degrees of freedom for error estimation, and a perfect, but erroneous fit will be obtained. Collecting additional data points from the additional runs and replicating the runs enable one to separate the lack-of-model-fit and experimental errors.

In RSM designs, a quadratic relationship between the factors and the response is assumed. Therefore, the chosen design will support linear, two-factor interaction, and quadratic terms for curvature. The general form of a quadratic model is shown below:

$$Y = C_0 + \sum_{i=1}^{n} C_i X_i + \sum_{i=1}^{n-1} \sum_{j=2}^{n} C_{ij} X_i X_j + \sum_{i=1}^{n} C_{ii} X_i^2 \qquad (6.2)$$

For a design consisting of n factors, the quadratic model as shown above contains one constant term, n linear terms, n(n-1)/2 two factor interaction terms, and n second order terms. Thus the model for a three-factor RSM design can be represented by (6.3).

$$Y = C_0 + C_1X_1 + C_2X_2 + C_3X_3 + C_{12}X_1X_2 + C_{23}X_2X_3 + C_{31}X_3X_1 \\ C_{11}X_1^2 + C_{22}X_2^2 + C_{33}X_3^2 \qquad (6.3)$$

This model shown above contains 10 terms. As in the case of simultaneous equations, to solve for these ten coefficients, at least 10 equations are needed. Extending this concept to experimental design, at least 10 runs are required to develop the model with no degrees of freedom. In order to estimate the experimental error, a minimum of 5 replicates should be added. The number of factor levels should be sufficient to support the model. For example, a quadratic model requires at least three factor levels and a cubic model requires

at least four. Additional data points obtained from additional runs provide more degrees of freedom for error calculation and model fitting.

Common RSM designs consist of Box-Behnken design and Central Composite designs. Box-Behnken design involves runs at the middle of the edge of the parameter space and a replicated run at the center. Fig. 6.1 illustrates a Box-Behnken design for three-factor experiment. Face Centered Cubic (FCC) designs, as shown in Fig. 6.2, consists of runs at the corner points, at the center of the faces, and a replicated run at the center of the parameter space. The third type of design is known as Central Composite design. In this design, each factor varies over five levels. These designs are built upon two level fractional factorial design and used for fitting second order response surface models. The central composite designs require smaller number of runs than the Box-Behnken designs. These designs are rotatable. Two types of central composite designs, namely circumscribed and inscribed designs, are normally used. Fig. 6.3 illustrates these designs. In the circumscribed design as shown in Fig. 6.3(a), the experimental space includes all of the parameter space and additional space. The runs at the centers of the face are pushed outwards by a distance of $2^{n/4}$, n being the number of factors, thereby sampling at positions equally spaced from the center. The circumscribed designs are employed when the space outside the parameter space needs to be explored. The other type of design, inscribed design as shown in Fig. 6.3(b), when the factor value cannot exceed a particular level. The design is inscribed in a circular area with the maximum factor level as the radius. The runs at the corner are pushed inward to a distance of $1/(2^{n/4})$, n being the number of factors. This design has a disadvantage of not covering the entire region of interest (-1 to +1).

6.2.2 Experiment and Data Collection

An experiment is designed using one of the techniques described in section 6.2.1. The experiment can be a full-factorial design, fractional factorial design, or RSM design as appropriate to the process under development. If there are more than six factors involved, a screening design, such as Taguchi design (Robust Design) or fractional-factorial design, is first used to determine the factors that have the most significant effect on the response [65]. Then, a second experiment is designed with only the most significant factors, fixing less important factors at particular convenient levels. The second experiment involves a fewer factors, and is designed such that all the main effects, first order interactions, and higher order effects are characterized. This experiment can be an RSM design such as FCC or Box-Behnken designs. RSM designs can only model the response within the factor range of the experiment. A narrow range may not give the true effects of the factors and the nonlinearity of the response. Therefore, a wider range for the factors that is greater than experimental error must be selected for statistical significance. Table 6.3 shows a typical full-factorial experimental design involving three factors at two levels.

Table 6.3. Full factorial design - 3 factors, 2 levels.

Run No.	Factor X_1	Factor X_2	Factor X_3
1	-	-	-
2	-	-	+
3	-	+	-
4	-	+	+
5	+	-	-
6	+	-	+
7	+	+	-
8	+	+	+

Each line in the experimental design above corresponds to one run. Replicate runs are processed at the center point of the parameter space in order to calculate the experimental error. The experiment is conducted by processing one sample, in this case, one wafer, at the factor settings corresponding to one line in the design. In some cases, the order of the experiment is randomized to remove any memory effects of the factors (the present experimental run being affected by previous run or runs). The replicate runs at the center points are distributed throughout the design to remove any temporal effects of the factors on the response. The response data is collected using the appropriate measurement tool. For example, the etch rates are obtained by measuring the difference in the film thickness before and after the etch process. The response data is analyzed using statistical methods offered by powerful computer programs such as RS1 [136], JMP [137], or XSTAT. The fundamentals of the data analysis are described in the following section.

6.2.3 Statistical Analysis and Modeling

In this section, the analysis of experimental data using statistical methods, related statistical terms, and modeling techniques are described. A more detailed description of these terms can be found in Box, Hunter and Hunter [135]. Earlier workers in this field had to rely on hand calculations to obtain the results. With the advent of computers, numerous powerful computer programs, such as RS1 [136], JMP [137] are available for performing the statistical analysis. However, an insight into the analysis is necessary for better understanding of the technique and hence good model development and process characterization.

A quadratic model, as represented by equation (6.2), is fitted to the experimental data. The quadratic model is chosen because it requires only three levels for each factor and adequately represents the experimental responses while limiting the number of required runs to economical numbers. Several established experimental designs such as Box-Behnken and FCC designs are readily available in the commercial software, making the design and analysis easier. The data obtained from the experiment can be analyzed by least squares regression (LSR) technique. This LSR technique takes the best fitting model that has the minimum quantity

$$S = \sum_{i=1}^{n} (y_i - y_m)^2 \qquad (6.4)$$

which is the sum of squared differences between the observed values y_i and the values given by the model y_m. The model coefficients are obtained by minimizing the residual [135].

An indication of agreement between the model and the data is determined by R^2 index, as shown in Figs. 6.4(c) and 6.5(c). The R^2 index is thus a measure of the proportion of the total variation accounted for by the model. A detailed derivation of the following equations can be seen in ref. [138].

$$R^2 = \frac{\text{Sum of squares for the model}}{\text{Sum of squares for C total}} \qquad (6.5)$$

where sum of squares for C total is the sum of squared distances of each response form the overall sample mean.

$$\text{Also, } R^2 = 1 - [\, SSE/S_{YY}] \qquad (6.6)$$

where SSE is the sum of squared errors, and S_{YY} is the sum of squares of the difference between actual response and the average of all the responses. The equation (6.7) mathematically represents R^2.

$$R^2 = 1 - [\Sigma (y_i - y_{ex})^2 / \Sigma (y_i - y_{av})^2] \quad (6.7)$$

where y_i is the actual value of response

y_{ex} is the expected value of response, and

y_{av} is the average value of response.

In general, the value of R^2 is high, the value being 1.0 for ideal fit of model to data. In addition to this, another term, R^2_{adj} is also used to determine the model fit. The R^2_{adj} adjusts R^2 to make it more comparable over models with different number of parameters by using the degrees of freedom in its computation. It is the ratio of mean squares instead of sums of squares. R^2_{adj} is represented by the equations (6.8) and (6.9) shown below.

$$R^2_{adj} = 1 - \frac{\text{Mean square for error}}{\text{Mean square for C total}} \quad (6.8)$$

where mean square for error and mean square for C total can be calculated from sum of squares divided by their respective degrees of freedom.

$$R^2_{adj} = 1 - \frac{SSE/(n-p-1)}{S_{YY}/(n-1)} \quad (6.9)$$

where n is the number of factors and p is the number of terms in the model. R^2_{adj} can also be represented in terms of R^2 as shown in (6.10).

$$R^2_{adj} = 1 - \frac{(n-1)}{(n-p-1)} (1 - R^2) \quad (6.10)$$

Since R^2_{adj} involves the number of terms in the model, it serves as a good indication when the model is optimized by removing the statistically less significant terms. The R^2_{adj}

increases as the lease significant terms are removed from the model. The optimum model is obtained when R^2 and R^2_{adj} are the closest.

C_p is another parameter that is used to measure the performance of the variables in terms of the standardized total mean square error of prediction for the observed data points irrespective of the unknown true model. The mathematical representation of C_p is given in (6.11).

$$C_p = [(SSE)_p / \sigma^2] + (2p-n) \quad (6.11)$$

$$\text{where } (SSE)_p = (y_i - y_{ex})^2 \text{ for p factors, and} \quad (6.12)$$

$$\sigma^2 = (SSE)_q / (n-q-1) \quad (6.13)$$

where q is the number of terms in the second model. The expected value of C_p is equal to p.

$$E[C_p] = p \quad (6.14)$$

The summary of fit table also contains root mean square error and mean of response. The root mean square error is the square root of the mean square for the error found in the Analysis of Variance table. It estimates the standard deviation of the random error. The mean of the response is the arithmetic average of the response variable.

The output of analysis includes an Analysis of Variance (ANOVA) and lack of fit tables. These tables show the quality of fit and the sources of error, respectively. The Analysis of Variance (ANOVA) table (Figs. 6.4(c) and 6.5(c)) partitions the total variation into its components - error SS and model SS (SS stands for sum of squares). The total (C-Total) is the sum of squared distances of each response from the overall sample mean. This is the sum of squares for the base model (or simple mean model) used for comparison with other

models. The error is the sum of squared distances from each point to its respective group mean. This is the remaining unexplained error SS after fitting the analysis of variance model. The difference between total SS and the error SS gives the sum of squares attributed to the model. The F-ratio is the ratio of mean square regression to the residual mean square. If the probability associated with the F ratio is small, then the model is considered a better statistical fit for the data than the response mean alone.

When replicate runs are included in the experimental design, a lack-of-fit table is displayed in the output (Figs. 6.4(c) and 6.5(c)). The experimental error, which is also known as pure error, can be estimated from the replicate the experimental runs at center points and calculating the sum of squares of the replicate differences. This portion of the error can not be explained or predicted. The difference between the error from the model and the experimental error is known as lack-of-fit error. The F-ratio in lack-of-fit table is the ratio of lack-of-fit mean square to the replicate error. A large F-ratio in this case indicates that the residual or error is mainly caused by lack-of-fit rather than experimental error. If the lack-of-fit error is significant when compared to the experimental error, then more terms, such as interaction terms have to be added to the model. This means that additional number of experimental runs are required to calculate the lack-of-fit [137].

The output table containing parameter estimates (Figs. 6.4(d) and 6.5(d)) typically includes the estimates and standard errors for each parameter in the model. The t-ratio and the observed probability are given to compare each parameter to zero. The estimates are the coefficients of the model and are determined by least squares. The t-ratio is test statistics for the hypotheses that each parameter is zero. The coefficients that have an

absolute t-value of greater than 2 are considered to be significant because it approximates 5 % significance level.

The effect tests table shown in Figs. 6.4(e), 6.4(f), 6.5(e), and 6.5(f) are joint tests that all the parameters making up an individual effect are zero. The response surface tables lists shown in Figs. 6.4(g), 6.4(h), 6.5(g), and 6.5(h) list the coefficients of the quadratic model. The solution table lists the critical values for each variable in the model and states whether the solution is maximum, minimum, or a saddle point.

Contour plots are very powerful tools to represent the response variation with respect to two or more factors. The contour plots are generated for models that fit well and often used for optimizing the process variables in order to obtain a specific response [123]. Several contour plots can be overlaid in order to combine the effects of several factors on the response [135]. This approach of contour plot overlay has the following advantages:

(i) clearly shows how and whether the requirements for a process can be met,

(ii) helps to determine the new factor settings if the requirement for response value changes, and

(iii) helps to determine the direction in which the process changes are to be made if the response falls out of specifications.

Contour plots are generated for the etch rate and the uniformity responses in terms of two factors taken at a time are shown in Figs. 6.4(p), 6.4(q), 6.5(p) and 6.5(q) for analysis of TiN and Ti etching experiments.

6.3. TiN Etch Process in $Cl_2/N_2/BCl_3$ Plasmas

This section is devoted to the discussion on the design of experiments, analysis and modeling for TiN etch process in $Cl_2/N_2/BCl_3$ plasmas. In chapters 3 and 4, the effect of the process parameters such as etch time, gas flow, RF power, pressure, and temperature on TiN etch were explored. The process parameters were varied one at a time while keeping other parameters at a constant level. This type of classical experiment is good for examining the effect of one variable, but it does not provide any information on the interaction between the parameters. Therefore, in order to determine the interaction effects and to develop an empirical model, it is necessary to design an RSM experiment and perform and analyze it using statistical methods. The subsections 6.3.1 to 6.3.3 are devoted to design of experiment, data acquisition, and analysis, and modeling. Section 6.3.4 contains discussion on results of the TiN etch experiment.

6.3.1. Design of Experiment

An RSM-FCC experiment was designed using JMP software with the factors RF power, pressure, chlorine flow, nitrogen flow, and boron trichloride (BCl_3) flow. The etch time was not included as one of the factors. Instead, the etch time was fixed at a convenient 15 seconds. The etch time was so chosen that significant etch rates were observed for the entire range of factor settings without clearing the film from any part of the wafer at the extreme factor settings. The temperature and the electrode spacing were not included in this experimental design following many other researchers [119] owing to the reasons stated below: The wafer temperature does not have significant effect in ion etching processes. In addition, varying the electrode temperature between runs is very time

consuming and hence it would take several hours to finish one experiment. In most of the etch processes, the electrode gap is fixed. An adjustable gap system almost always develops mechanical problems. The gap setting is not reproducible and requires frequent calibration. In addition, mechanical movement of the components in the vacuum chamber generate particles which may ultimately lead to low die yields. Therefore, the trend is leaning towards fixed electrode systems and hence leaving the electrode gap as one of the factors in the experiment can be justified. Table 6.4 shows the factors used in this experiment and their settings. The TiN etch rate and etch uniformity were measured as the responses. The factors were standardized as shown in equation 6.1. The advantages of standardization were discussed in Section 6.2.1. A total of 32 runs were required in the RSM design. Out of these 32 runs, 16 runs were located at the face of the parameter space, 10 runs were located at the corner points and 6 replicate runs at the center point. As discussed before, the six replicate runs were included in the experiment to determine the experimental error. These replicate runs were distributed throughout the experiment to include the temporal effects of the factors and the etching system.

Table 6.4 Factors and Responses in RSM experimental design for TiN etch:

Factors	Range
RF Power	200 - 500 W
Pressure	500 - 1000 mTorr
Chlorine Flow	25 - 150 sccm
Nitrogen	0 - 100 sccm
BCl_3	0 - 120 sccm

Responses:	
TiN etch rate	in Å/minute
Percentage etch uniformity	in %

6.3.2. Experiment and Data Acquisition

The experiment was carried out in the Lam 4600 metal etcher, detailed description of which is provided in Section 2.3. Wafers containing 4000 Å TiN film on 13,000 Å CVD oxide deposited wafers were used for these experiments. The sheet resistance of these wafers were measured at 49 points per wafer before the etch using the 4D four point probe system. The temperature of the bottom and top electrodes were maintained at 40 and 70 °C, respectively. The etch chamber was heated to 70 °C to prevent the etch products from depositing on the chamber walls. All the test wafers were etched for 15 seconds. One wafer was etched at the factor settings for each run in the design. The sheet resistance of the wafers was measured again using the 4D four-point probe system. The etch rate was calculated from the sheet resistance measurements and the etch time as described in Chapter 3. The percentage etch uniformity was also determined from the sheet resistance measurements. The percentage etch uniformity is defined as follows:

$$\% \text{ Etch uniformity} = \frac{\text{(Maximum etched thickness - Minimum etched thickness)}}{\text{2 x Average etched thickness}} \times 100 \qquad (6.15)$$

6.3.3 Data Analysis and Modeling

The etch rate and percentage uniformity data obtained from the experiment were entered in the response columns of the RSM experimental design. The data was analyzed by least square regression (LSR) technique using JMP software. The output of the analysis is shown in Fig. 6.4. The adjusted R^2 is high, 97.6% and 91.5% for etch rate and uniformity, respectively. The high adjusted R^2 indicates that the data is represented well in

the quadratic empirical model for both these responses. In the case of TiN etch rate, a high ANOVA F-ratio of 64.32, which is the ratio of mean square regression to mean square error, indicates that the model is very significant. The high lack-of-fit F-ratio 82.19 for lack-of-fit to pure error indicates that the error is primarily caused by the lack-of-fit (the difference between the residual error from the model and the pure error is called lack of fit error) rather than the experimental error. This also suggests that the model fit can be improved by including additional terms such as third order terms. For the response of etch uniformity, the ANOVA F-ratio is 17.79. It suggests that the model represents the data very well. The lack-of-fit F-ratio is 15.16. This means that the pure error is ~ 6.2 % of the total error. Therefore, the lack of fit is mainly due to inadequacy of the model. A quadratic model for each of the responses is developed from the experimental data. The model coefficients are shown in the parameter estimates column of the output. Equations (6.16) and (6.17) demonstrate these mathematical models. The models derived from the experimental data are acceptable as the error is less than < 10% for both the models (1.6 % for etch rate and 5.6 % for uniformity), and thus they are acceptable.

$$\begin{aligned}\text{Etch rate} = {} & 5590.02 + 2672.55 \times (\text{Power}) - 61.52 \times (\text{Pressure}) + 1941.82 \times (Cl_2) \\ & - 690.73 \times (N_2) + 186.71 \times (BCl_3) - 107.31 \times (\text{Power} \times \text{Pressure}) \\ & + 1499.03 \times (\text{Power} \times Cl_2) - 407.98 \times (\text{Power} \times N_2) \\ & - 351.12 \times (\text{Power} \times BCl_3) + 133.80 \times (\text{Pressure} \times Cl_2) \\ & + 241.37 \times (\text{Pressure} \times N_2) - 271.30 \times (\text{Pressure} \times BCl_3) \\ & - 148.45 \times (Cl_2 \times N_2) + 480.47 \times (Cl_2 \times BCl_3) + 279.83\ (N_2 \times BCl_3) \\ & + 151.09 \times (\text{Power})^2 + 306.99 \times (\text{Pressure})^2 - 975.11\ (Cl_2)^2 \\ & + 325.01 \times (N_2)^2 - 1254.52 \times (BCl_3)^2 \end{aligned} \quad (6.16)$$

% Uniformity

$$= 24.81 - 0.17 \times (\text{Power}) - 6.24 \times (\text{Pressure}) - 8.99 \times (Cl_2)$$
$$- 3.33 \times (N_2) - 5.96 \times (BCl_3) + 1.55 \times (\text{Power} \times \text{Pressure})$$
$$+ 0.17 \times (\text{Power} \times Cl_2) + 0.05 \times (\text{Power} \times N_2)$$
$$+ 0.73 \times (\text{Power} \times BCl_3) + 0.90 \times (\text{Pressure} \times Cl_2)$$
$$- 2.35 \times (\text{Pressure} \times N_2) + 0.86 \times (\text{Pressure} \times BCl_3)$$
$$+ 0.90 \times (Cl_2 \times N_2) + 4.39 \times (Cl_2 \times BCl_3) - 0.07\ (N_2 \times BCl_3)$$
$$- 1.18 \times (\text{Power})^2 + 1.12 \times (\text{Pressure})^2 + 9.26\ (Cl_2)^2$$
$$- 3.76 \times (N_2)^2 + 5.52 \times (BCl_3)^2 \qquad (6.17)$$

In equations (6.16) and (6.17), scaled factors are used. Therefore, in order to determine the etch rate and uniformity for a given set of factors, the actual values of the factors have to be scaled to a range between -1 and +1 using the equation (6.1). The coefficients in the model shown in this respect are rounded to two decimal places in equations (6.16) and (6.17) for clarity. The actual values of the coefficients can be obtained from the corresponding parameter estimate columns of Fig. 6.4 (d).

6.3.4 Discussion of Results

A good comparison of the main effects and interaction of the factors can be made from the magnitude of the coefficient. For example in the etch rate model, the first order term of RF power has the maximum effect (2672.55), followed by first order term of Cl_2 (1941.82). First order pressure terms seems to have the least effect (61.52). The terms containing small coefficients can be considered less significant and can be removed from the model without significantly affecting the validity of the model. The first order terms should be

retained in the model however small the coefficient may be, so as include the main effects of those factors in the model. An attempt was made to reduce the model by removing the least significant terms during the optimization of the model in JMP software. The second order terms of power, pressure, and N_2, and pressure-power, Cl_2-pressure, and N_2-Cl_2 interaction terms were found to be the least significant and hence removed from the etch rate model. The R^2_{adj} slightly decreased from 97.61 % to 97.26 %, but it became closer to R^2 of 98.5 %. The response model was described in terms of the statistical terms in this paragraph of the section. An attempt is made to explain the results in terms of plasma concepts in the following paragraph.

As discussed before, the normalization of factors makes it easier to visualize relative significance of the effects and interactions of factors. The main effect of RF power appears to have the maximum influence on the etch rate with a model coefficient of 2673, followed by the main effect of chlorine with a coefficient of 1942. The effect of RF power on the TiN etch rate is three fold. The increase in RF power increases the ionization of the etchant chlorine gas, thereby increasing the density of the ions and radicals in the plasma. In addition, an increase in RF power applied to the bottom electrode increases the magnitude of negative Vdc leading to accelerated ion bombardment towards the wafer. The high influence of chlorine on the etch rate can be attributed to the increased availability of the etchant chlorine. Therefore, it can be observed that the etch process under investigation is in supply rate limited region. The chlorine-RF power interaction term is also high due to the fact that the increased RF power leads to increased ionization, and hence increasing the availability of chlorine species. Contribution of BCl_3 to etching process is less than one tenth of that of chlorine because the supply of free chlorine radicals available from BCl_3 is low. This effect is due to higher B-Cl bond

strength as compared to Cl-Cl bond strength, making it difficult to dissociate [33]. Thus, the experimental design is successful in identifying the low influence of BCl_3 on etch rate. This effect was also discussed in detail in Chapter 4 of this dissertation while examining the effect of BCl_3 alone. The nitrogen flow term has a negative coefficient, indicating that an increase in nitrogen causes a decrease in the etch rate, which can be attributed to the dilution effects. The pressure is found to have a slightly adverse effect on the etch rate as can be seen from a coefficient of -61.52. This effect can be due to loss of etchant chlorine species due to recombination reactions and decreased volatility of the reaction products [61]. The presence of second order terms in the model indicates that the relationship between the factor and the response is nonlinear. The relative amount of nonlinearity is indicated by the magnitude of the coefficient of the second order term. As the plasma processes are more complex, it is difficult to explain all of the nonlinear behaviors of the model. The presence of the second order terms in the model indicates the curvature of the response surface. Therefore, the good-fitting empirical model for a process is generally accepted within the regime of investigation.

In the uniformity model, the R^2_{adj} was 91.55 % when all the terms were included. The second order Cl_2 (Cl_2*Cl_2) term seems to have the maximum effect on the uniformity with a coefficient of +9.26, which means that the second order effect of chlorine increases the percentage uniformity. The first order Cl_2 term with a coefficient of -8.99, indicates that the uniformity is decreased with the main effect of Cl_2. The power-N_2 interaction has the lowest effect on the uniformity with a coefficient of 0.045. Like in the etch rate model, an attempt was made to remove the less significant terms. In the first attempt, ten terms including first order effect of power were removed by the JMP program. The R^2_{adj} improved to 92.98 %. As it was discussed earlier, the first order terms should be retained

in the model and hence power has to be put back in the model. The optimization of the model was repeated in steps, this time R^2_{adj} was closely monitored after each term was removed. The R^2_{adj} went up until the BCl_3*pressure term was removed when it decreased. Therefore, the BCl_3-pressure interaction term was put back in the model and the R^2_{adj} reached its peak of 93.96 %. The coefficients of the optimized model are shown in the column containing stepwise regression control of Fig. 6.4(o).

It can be seen from the TiN etch uniformity model in equation (6.17) and Fig. 6.4(m) that increase in chlorine, pressure, and BCl_3 decreases the percentage uniformity. This effect can be due to the availability of more etchant species throughout the area of the wafer due to the increase in Cl_2 and BCl_3 flow, and longer resident time due to the increase in pressure. The increase in N_2 flow on the contrary has an adverse effect on the etch uniformity, leading to an increase in percentage uniformity. The second order terms of chlorine and BCl_3 have large positive coefficients of 9.26 and 5.52, respectively, indicating a strong nonlinear relationship between the flow rate of these gases and the uniformity response. Nitrogen flow also appears to have a non-linear effect on the uniformity as the second order term is significant. The interaction terms, except nitrogen-pressure and BCl_3-chlorine, do not appear to have much influence on the uniformity as indicated by their coefficients. Examining the etch rate and uniformity models simultaneously, it can be observed that high RF power leads to high etch rate, but results in poor uniformity, however increased chlorine flow leads to higher etch rate and lower uniformity. Therefore, an optimum settings for the factors must be chosen depending on the goal of the experiment. For example, if high etch rate is needed without requirement for low uniformity, then high RF power and high chlorine flow must be used. If the uniformity has

to be low in the etch process, then the RF power has to be reduced, while keeping the chlorine flow high.

The contour plots are drawn for etch rate and uniformity as shown in Fig. 6.4(p) and 6.4(q), respectively. These contour plots are obtained from the JMP software output. There are ten contour plots for each of the responses, etch rate and uniformity as one contour map is drawn taking two factors at a time. The actual values, instead of the standardized values, of the factors are used to draw the contour maps in order to enable direct optimization of the process. For example, in the power-chlorine contour plot of Fig. 6.4(p), in order to obtain an etch rate between 4000 and 6000 Å/min, the RF power and chlorine flow corresponding to the band between these two etch rate curves must be used. This means that a chlorine flow of over 25 sccm and RF power over 250 Watts must be chosen as process parameters. In order to optimize the process with respect to all the factors in the designed experiment, the contour plots plotted with other factors in the experiment such as pressure, nitrogen, and BCl_3, must be overlaid. A process window must be selected and the factors corresponding to the process window can be used as parameters for the optimized process.

6.4 Ti Etch Process in Cl_2/N_2 Plasmas

This section describes the design of RSM experiment, analysis and development of an empirical quadratic model for Ti etch process in Cl_2/N_2 plasmas. In Chapter 5, the effect of the process variables such as RF power, pressure, gas flow were studied by varying one parameter at a time while fixing the others at a constant level. As discussed in Section 6.1, this type of classical experiments does not yield any information on the interaction among

the variables. Therefore, in order to develop a model for the Ti etch process that includes interaction and the second order effects, it is necessary to utilize the RSM design technique. The following subsections 6.4.1 to 6.4.3 discuss about the RSM design, experimentation, data acquisition, data analysis and modeling for Ti etch process in Cl_2/N_2 plasmas. A discussion on the results is provided in Section 6.4.4.

6.4.1. Design of Experiment

An RSM-FCC design was used for the Ti etch process experiment like in the TiN etch process. The JMP software package was used for experimental design and analysis. RF power, pressure, chlorine gas flow, and nitrogen gas flow were used as the factors of the experiment. BCl_3 was not included as the factor in this experiment since it did not have any effect on the Ti etching as observed through the preliminary experiments described in Chapter 5. Also, the electrode gap and the temperature were not included as factors as discussed in the Section 6.3.1. Similar to the TiN etch process, the etch rate and the etch uniformity were measured as responses. Table 6.5 shows the factors and their range of settings along with the response. The same range of factor settings that were used for TiN etch process were used for Ti etch experiment.

Table 6.5 Factors and Responses in RSM experimental design for Ti etch:

Factors	Range
RF Power	200 - 500 W
Pressure	500 - 1000 mTorr
Chlorine Flow	25 - 150 sccm
Nitrogen	0 - 100 sccm

Responses:	
Ti etch rate	in Å/minute
Percentage etch uniformity	in %

The factors were standardized as shown equation (6.1) for the reasons discussed before. A total of 31 runs were required for the design. Sixteen runs were located at the face-center of the parameter face, 8 runs were located at the corner points, and 7 replicate runs at the center of the parametric space. Similar to the TiN etch experiment, these replicate runs were distributed throughout the experiment to remove temporal effects of the factors and the etching system.

6.4.2. Experiment and Data Acquisition

The experiment was performed in a Lam 4600 metal etcher. The test wafers were built of approximately 10 kÅ of sputtered Ti film on top of 13 kÅ CVD deposited oxide on a single-crystal silicon wafer. The temperature of the bottom and top electrodes were maintained at 40 °C and 70 °C, while the etch chamber was heated to 70 °C to prevent deposition of etch products on the chamber walls. One wafer per run of the design was etched at the factor settings specified in the design. All the wafers were etched for 35 seconds. The etch time was so chosen that significant etch rates were obtained for the entire factor range of the experiment. The sheet resistance of each wafer was measured at 49 points per wafer before and after etch using 4D four-point probe tool. From the difference in sheet resistance, the etched thickness, and hence the etch rate was calculated. The percentage etch uniformity, as shown in equation (6.15), was also calculated.

6.4.3 Data Analysis and Modeling

The etch rate and uniformity data obtained from the experiments were entered as the responses in the Ti etch experimental design. The data was analyzed using LSR technique

in JMP software. The R^2_{adj} is high for etch rate response (88.51%), which indicates that the data is represented well for etch rate. But the R^2_{adj} is low for uniformity response (74.39%), which is an indication that the data is not represented as well as that of the etch rate. For the Ti etch rate model, an ANOVA F-ratio of 17.51 indicates the model is significant and the error is only 5.7 % of the etch rate response. The lack-of-fit F-ratio of 246.26 indicates that the experimental error is approximately 0.4 %, which is well within the acceptable limits of less than 10 %. Most of the error is caused by the inadequacy of the model.

For the Ti etch uniformity response, the ANOVA and lack-of-fit ratios are 7.22 and 6.69, respectively. The magnitude of these ratios are small when compared to those of Ti etch rate model. The pure error is approximately 13 % of the total error, and the total error is about is 12 % of the total response in the model. However, the quadratic model is more suitable than a simple arithmetic expression. Similar to the TiN etch process, a quadratic model is developed for the Ti etch rate and percentage uniformity using the coefficients in the parameter estimates column of the output. The following equations (6.18) and (6.19) represent the models for Ti etch rate and percentage uniformity, respectively. All the factors are scaled to a range between -1 and +1 by using the relationship (6.1). The coefficients are rounded to 2 decimal places to improve the clarity of the equations. For more accurate coefficients, the reader is referred to the parameter estimates part of the output in Fig. 6.5(d).

$$\text{Etch rate} = 1915.79 + 3579.45 \times (\text{Power}) - 895.56 \times (\text{Pressure}) + 1874.80 \times (Cl_2)$$
$$- 430.91 \times (N_2) - 865.48 \times (\text{Power} \times \text{Pressure})$$
$$+ 2009.05 \times (\text{Power} \times Cl_2) - 535.05 \times (\text{Power} \times N_2)$$
$$- 1034.87 \times (\text{Pressure} \times Cl_2) + 337.83 \times (\text{Pressure} \times N_2)$$
$$+ 82.01 \times (Cl_2 \times N_2) + 1658.78 \times (\text{Power})^2 + 674.07 \times (\text{Pressure})^2$$
$$- 102.21 \times (Cl_2)^2 - 377.59 \times (N_2)^2 \qquad (6.18)$$

% Uniformity

$$= 48.15 - 26.00 \times (\text{Power}) - 6.88 \times (\text{Pressure}) - 2.98 \times (Cl_2)$$
$$+ 4.27 \times (N_2) + 12.10 \times (\text{Power} \times \text{Pressure})$$
$$+ 0.47 \times (\text{Power} \times Cl_2) - 2.00 \times (\text{Power} \times N_2)$$
$$- 0.03 \times (\text{Pressure} \times Cl_2) - 2.65 \times (\text{Pressure} \times N_2)$$
$$- 8.38 \times (Cl_2 \times N_2) + 24.31 \times (\text{Power})^2 - 5.62 \times (\text{Pressure})^2$$
$$- 13.09 (Cl_2)^2 + 3.15 \times (N_2)^2 \qquad (6.19)$$

These models contain one constant term, four first order terms, six two factor interaction terms, and four second order terms.

6.4.4 Discussion of Results

As discussed in Section 6.3.4, the coefficients offer a very good means of comparing the different terms in the model. The relative influence of each of the factors and interactions can be determined from these model coefficients. From the Ti etch rate model shown in (6.18), it can be observed that RF power has the maximum effect with a coefficient of 3579.45, followed by power-chlorine interaction (coefficient of 2009.05). The main effect of chlorine comes next with a coefficient of 1874.80 and second order effect of RF power

has a coefficient of 1658.78. On the other hand, nitrogen-chlorine interaction has the smallest coefficient (82.01). The analysis of Ti etch rate yielded an R^2_{adj} of 88.51 % when all the terms in the model were included. But when the least significant terms such as second order effects of nitrogen, chlorine and pressure and nitrogen-pressure and nitrogen-chlorine interactions were removed from the model, the R^2_{adj} improved to 90.27 %.

As can be seen from the model for Ti etch rate in equation (6.18) and Fig. 6.5(d), the RF power has the maximum effect on the etch rate. As discussed in Chapter 5, and in section 6.3.4, the RF power has three-fold influence on the etch process. The increase in RF power increases the number of etchant species ions and radicals in the plasma due to ionization [107]. The RF power when applied to the bottom electrode induces a negative self bias voltage near the substrate thereby leading to acceleration of ions towards the substrate. The increased RF power can also lead to heating of the wafer, thus increasing the rate of chemical reactions on the surface of the wafer [21]. The chlorine gas flow appears to have the next most significant influence on the Ti etch rate after RF power. As discussed in Chapter 5, chlorine is the main etchant species in Ti etch process. As the chlorine flow is increased, the amount of etchant species available is increased, thereby leading to higher etch rate. Therefore, the etching process in the region under investigation can be considered as supply-rate limited [12]. The etch chamber pressure has a negative coefficient of -895 in the model, indicating that the increase in pressure causes a decrease in the Ti etch rate. This can be due to the decrease in the amount of ions due to gas-phase recombination reactions in the plasma and reduced ion and electron energies due to increased collisions within the plasma. The increase in pressure can also lead to decreased volatility of the reaction products, such as $TiCl_4$, which in turn can reduce the rate of

chemical reaction at the surface of Ti film. Nitrogen flow is also found to have a negative influence on the etch rate. This negative effect can be solely attributed to the dilution effect as discussed in chapter 5. The chlorine has strong interaction with RF power and pressure as can be seen from the model coefficients. The second order effects of RF power and pressure have significant coefficients in the model, indicating a strong nonlinear relationship of these factors with the etch rate.

Following the same line of discussion for the etch uniformity response in equation (6.19) , it can be seen that RF power (coefficient of 26.0) and second order effects of power (24.31) and Chlorine (13.09) are the most significant terms. On the other hand, chlorine-pressure and chlorine-power interactions are the least significant terms with coefficients of 0.031 and 0.465, respectively. The least significant terms in the model can be removed without affecting the validity of the model significantly. The R^2_{adj} is 74.39 % when all the terms are included in the model for etch uniformity. After the least significant terms, such as power-chlorine, pressure-chlorine, power-nitrogen, pressure-nitrogen interactions and second order effects of pressure and nitrogen, are removed from the model, the R^2_{adj} goes up to 79.73 %.

The increase in RF power, pressure, and chlorine flow appear to improve the uniformity, with RF power having the maximum influence with a coefficient of -26. The increase in RF power leads to a better uniformity probably due to better distribution of etchant species across the wafer. This effect may be also due to the temperature increase due to high RF power. The pressure increase leads to a decrease in percentage uniformity. This can be attributed to the increased residence time of the etchant species on the surface of the etched Ti film thereby allowing more time for the reaction of etchant species with Ti

film. The reduction in percentage uniformity with increase in chlorine can be due to the increased availability etchant species across the wafer. The nitrogen gas flow has an adverse effect on uniformity. The percentage uniformity appears to increase as the nitrogen flow is increased. This effect is not clear at this time, but this may be probably due to dilution of the plasma of the etchant chlorine species. As in the case of main effects, the second order terms of RF power, chlorine and pressure have significantly high coefficients indicating that the relationship of these factors with percentage uniformity is nonlinear. The pressure-RF power, and nitrogen-chlorine interactions are also significant. From the empirical models, it is clear that the interactions and the second order effects of the factors are also important.

As discussed in section, 6.3.4, contour plots are drawn for the Ti etch process, taking two factors at a time. There are six contour plots available for each of the responses, etch rate and uniformity. The contour plots, obtained from the analysis of Ti etch experiment using JMP software, are shown in Figs. 6.5(p) and 6.5(q). As in the case of TiN etch process, the contour plots can be overlaid and the process parameters corresponding to a required process window can be obtained. With the contour plots, the entire regime covering the range of factors in the experiment can be analyzed and an operating point can be picked depending on the process response specifications.

6.5 Summary and Conclusions

In this chapter, the concept of design of experiments and analysis was discussed in great detail. The terms used in the analysis of the experiments were defined. An RSM experiment was designed using JMP software for each of TiN and Ti plasma etch

processes. The experiment was performed according to the design and the results were analyzed using JMP software. Empirical quadratic models were developed for etch rate and uniformity in both TiN and Ti etch processes. These models enable an experimenter to observe the significance of the factors (process parameters) on each of the responses. The models, when combined with the knowledge of the process, could be used for optimization. From the RSM design and analysis of experiments, the following major conclusions can be drawn:

(i) The models for etch rate and uniformity developed using the observations from RSM experiments bring out the two factor interactions and second order effects in TiN and Ti plasma etch processes.

(ii) In both TiN and Ti etch processes, RF power and chlorine flow appear to be the most dominant factors in determining the etch rates. The observations obtained from these models are consistent with the theory developed in the Chapters 3, 4, and 5 based on the experiments done varying one parameter at a time.

(iii) Nitrogen addition dilutes the plasma of the etchant species and hence leads to reduction in etch rate.

(iv) The reactor pressure has an adverse effect on the etch rate. It affects Ti etch process much more than the TiN etch process as can be seen from the magnitude of these coefficients.

(v) Increase of all the factors except nitrogen lead to better uniformity. Chlorine is the most significant contributor to the uniformity in TiN etching whereas RF power is found to be the dominant contributor to Ti etching.

(vi) Increase of nitrogen flow leads to increase in percentage uniformity probably due to depletion of etchant species.

(vii) There is a high amount of interaction between chlorine and RF power in both TiN and Ti etch processes.

(viii) The presence of second order terms indicate the relationship between the factors and responses are not simply linear, but highly nonlinear for factors such as RF power.

(ix) Contour plots are drawn for etch rate and uniformity responses for both Ti and TiN processes taking two factors at a time. These contour plots are used as a powerful tool for determining operating point for a process according to the specifications and optimizing an existing process.

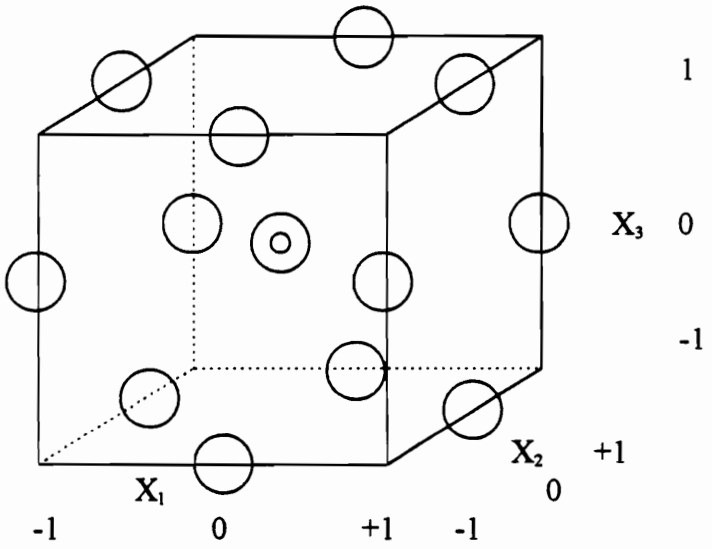

Fig. 6.1 Box-Behnken design of experiment with center point replication.

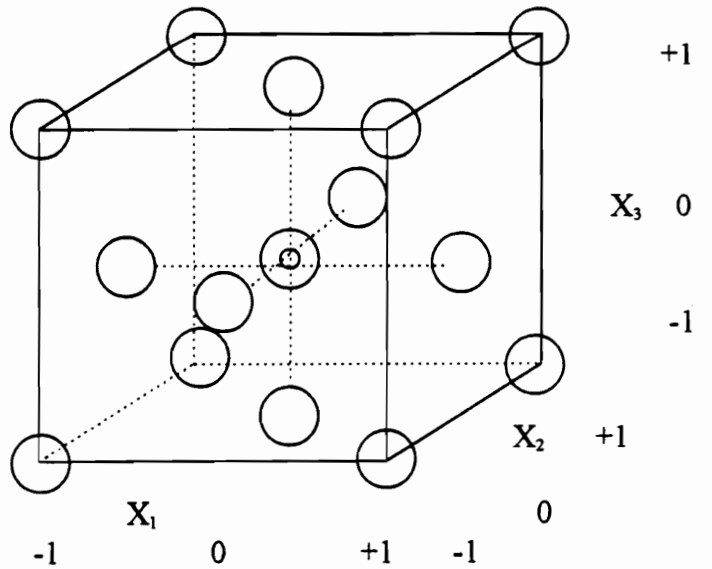

Fig. 6.2. Face Centered Cubic (FCC) design of experiment with center point replication.

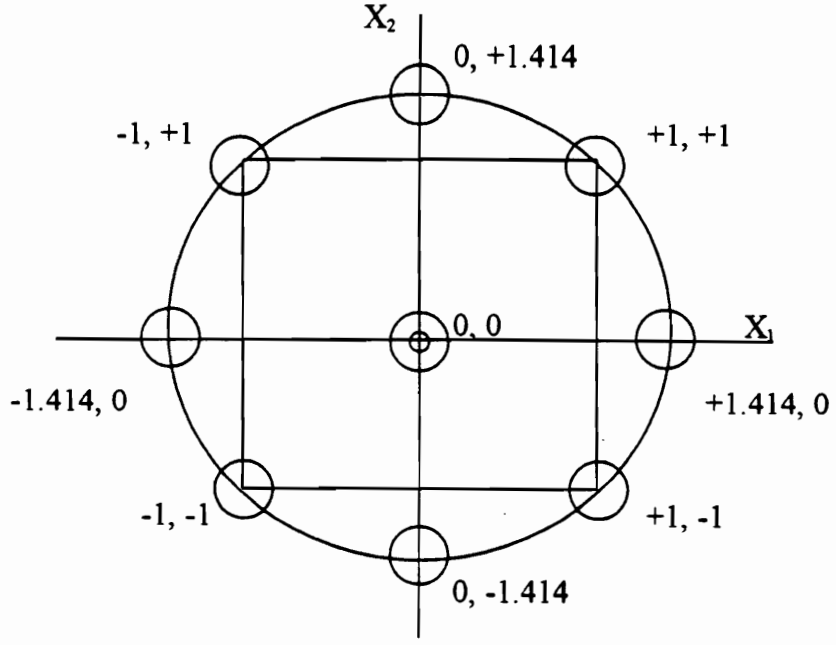

Fig. 6.3(a) Central composite design for two factors (Circumscribed) - CCC design

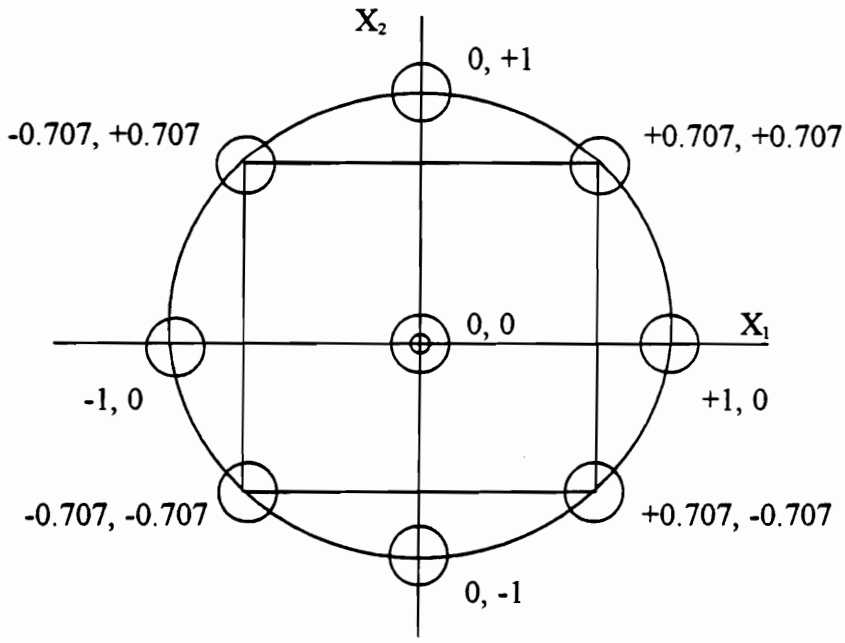

Fig. 6.3(b) Central composite design for two factors (Inscribed) - CCI design

TINDESN1.JMP

Rows	T.POWER	T.PRESSURE	T.CHLORINE	T.NITROGEN	T.BCL3	ETCH RATE	UNIFORMITY
1	1	-1	-1	1	1	2182.29	45.93
2	1	-1	1	-1	1	11942.46	23.89
3	1	-1	-1	-1	-1	5464.93	55.92
4	1	-1	1	1	-1	7990.57	39.87
5	1	0	0	0	0	9068.41	18.8
6	1	1	-1	1	-1	2981.82	47.39
7	1	1	1	1	1	9434.88	25.73
8	1	1	-1	-1	1	2367.38	30.3
9	1	1	1	-1	-1	11509.18	20.52
10	0	-1	0	0	0	6072.32	28.11
11	0	0	-1	0	0	3077.15	44.18
12	0	0	0	0	0	5579.36	23.75
13	0	0	0	0	0	5456.33	23.92
14	0	0	0	0	0	5431.43	23.92
15	0	0	0	1	0	5179.18	23.1
16	0	0	0	0	0	5512.4	24.6
17	0	0	0	0	1	5276.55	20.43
18	0	0	1	0	0	6252.95	24.07
19	0	0	0	0	0	5559.87	26.79
20	0	0	0	0	0	5599.57	25.53
21	0	0	0	0	-1	3494.73	40.34
22	0	0	0	-1	0	6751.16	19.1
23	0	1	0	0	0	5821.99	23.85
24	-1	-1	-1	-1	1	1457.82	37.32
25	-1	-1	-1	1	-1	249.06	70
26	-1	-1	1	-1	-1	1578.64	29.63
27	-1	-1	1	1	1	2660.47	37.69
28	-1	0	0	0	0	2514.11	28.57
29	-1	1	1	-1	1	2771.88	16.05
30	-1	1	-1	1	1	1070	25.58
31	-1	1	1	1	-1	1098.08	21.94
32	-1	1	-1	-1	-1	1435.95	44.65

Fig. 6.4(a) Design of Experiment for TiN etch in $Cl_2/N_2/BCl_3$ plasmas.

TINDESN1 JMP

Rows	Pattern	Block	POWER	PRESSURE	CHLORINE	NITROGEN	BCL3	Comment
1	+–++	1	500	500	25	100	120	FF
2	+-+-+	1	500	500	150	0	120	FF
3	+—	1	500	500	25	0	0	FF
4	+-++-	1	500	500	150	100	0	FF
5	+0000	1	500	750	87 5	50	60	Axial
6	++-+-	1	500	1000	25	100	0	FF
7	+++++	1	500	1000	150	100	120	FF
8	++–+	1	500	1000	25	0	120	FF
9	+++–	1	500	1000	150	0	0	FF
10	0-000	1	350	500	87 5	50	60	Axial
11	00-00	1	350	750	25	50	60	Axial
12	00000	1	350	750	87.5	50	60	Center-Ax
13	00000	1	350	750	87 5	50	60	Center-Ax
14	00000	1	350	750	87.5	50	60	Center-Ax
15	000+0	1	350	750	87.5	100	60	Axial
16	00000	1	350	750	87.5	50	60	Center-Ax
17	0000+	1	350	750	87 5	50	120	Axial
18	00+00	1	350	750	150	50	60	Axial
19	00000	1	350	750	87.5	50	60	Center-Ax
20	00000	1	350	750	87.5	50	60	Center-Ax
21	0000-	1	350	750	87.5	50	0	Axial
22	000-0	1	350	750	87.5	0	60	Axial
23	0+000	1	350	1000	87 5	50	60	Axial
24	—+	1	200	500	25	0	120	FF
25	—+-	1	200	500	25	100	0	FF
26	–+–	1	200	500	150	0	0	FF
27	–+++	1	200	500	150	100	120	FF
28	-0000	1	200	750	87.5	50	60	Axial
29	-++-+	1	200	1000	150	0	120	FF
30	-+-++	1	200	1000	25	100	120	FF
31	-+++-	1	200	1000	150	100	0	FF
32	-+—	1	200	1000	25	0	0	FF

Fig. 6.4(a) Contd. Design of Experiment for TiN etch in $Cl_2/N_2/BCl_3$ plasmas.

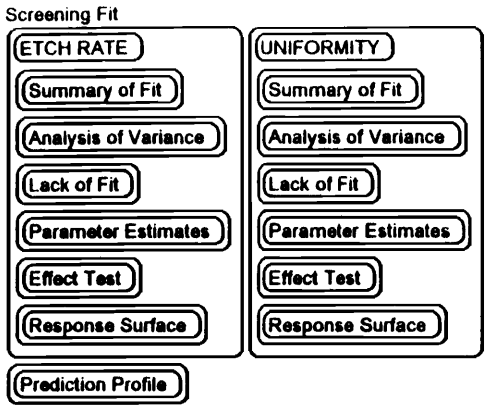

Fig. 6.4(b) List of outputs available from JMP software for TiN etch DOE.

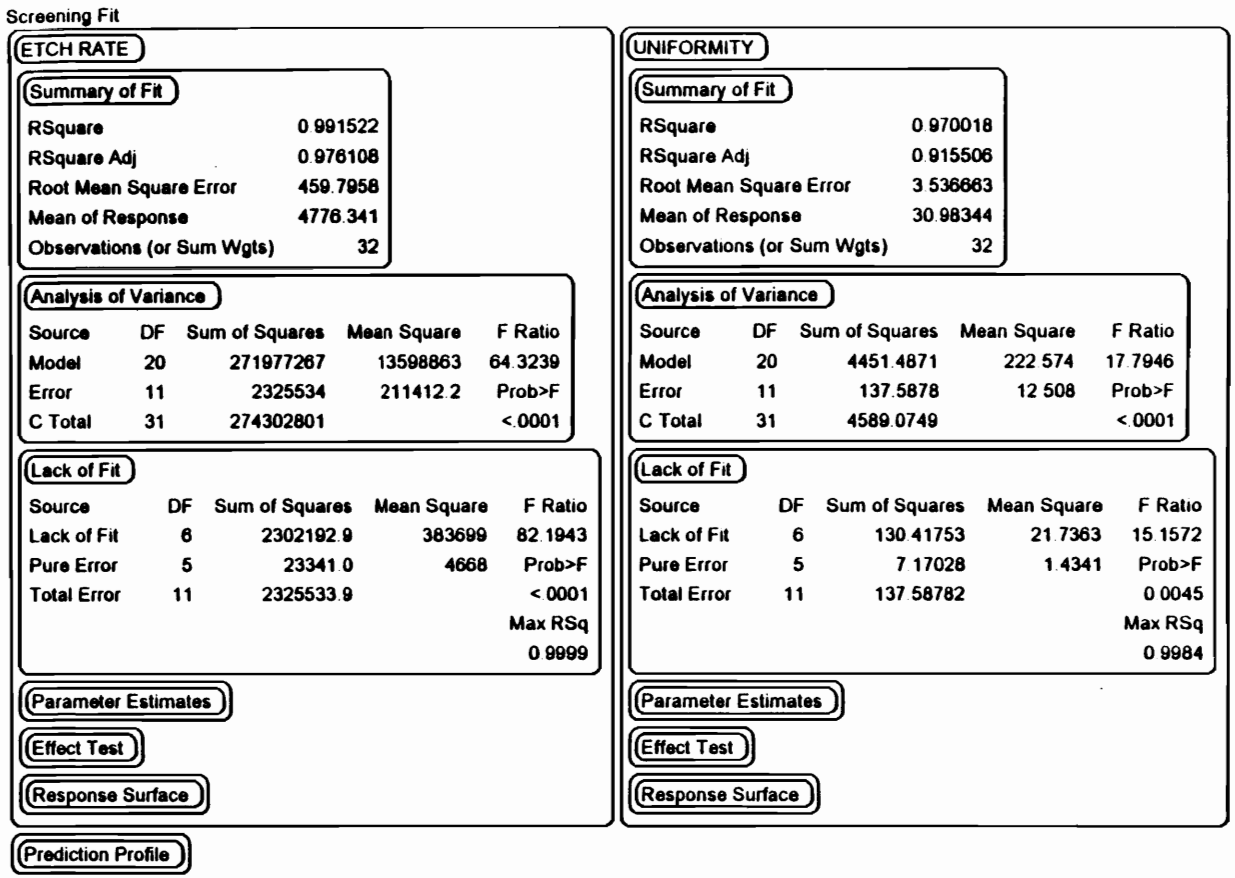

Fig. 6.4(c) Summary of fit, Analysis of Variance, Lack of Fit tables for TiN etch DOE.

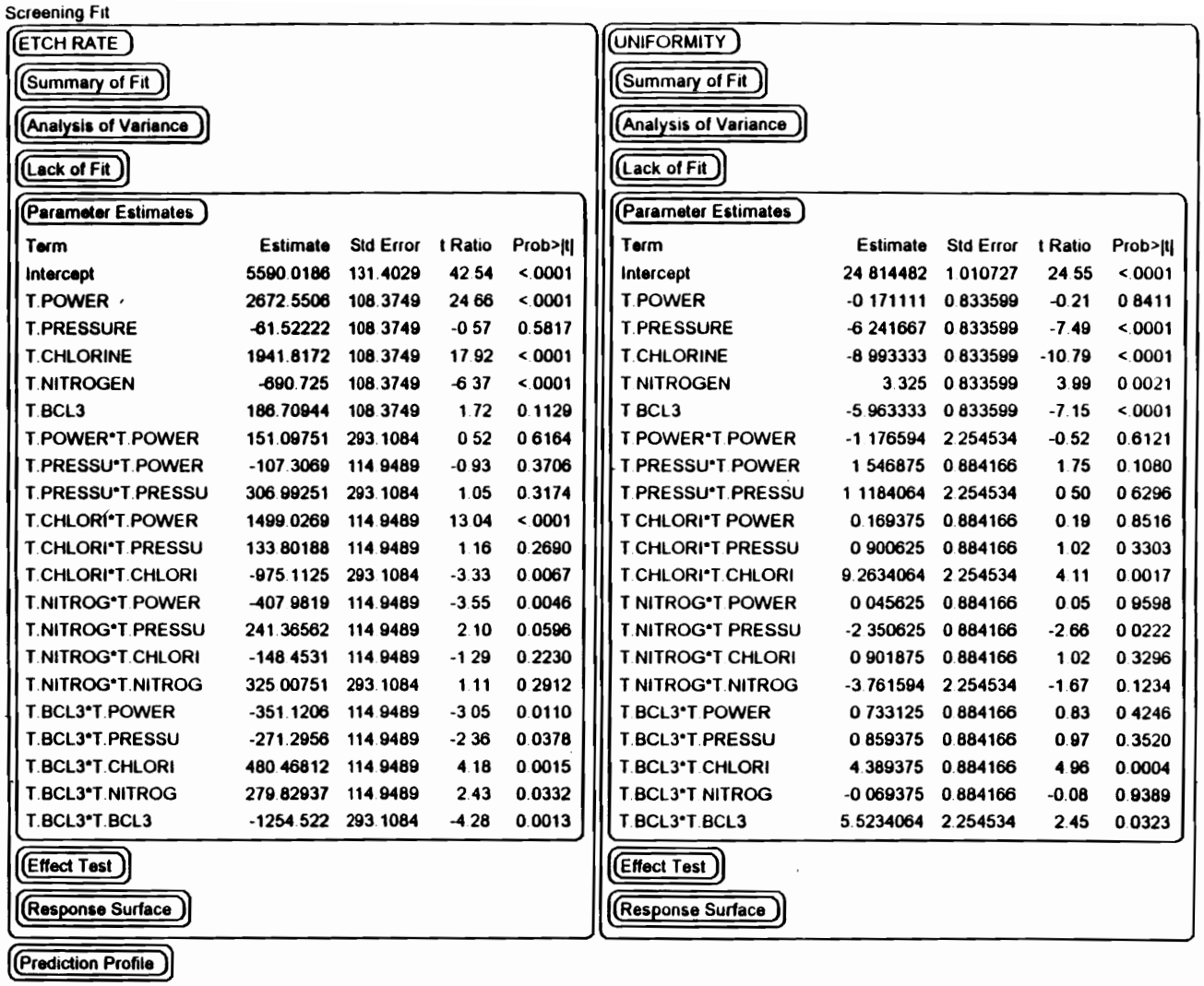

Term	Estimate	Std Error	t Ratio	Prob>|t|
Intercept	5590.0186	131.4029	42.54	<.0001
T.POWER	2672.5506	108.3749	24.66	<.0001
T.PRESSURE	-61.52222	108.3749	-0.57	0.5817
T.CHLORINE	1941.8172	108.3749	17.92	<.0001
T.NITROGEN	-690.725	108.3749	-6.37	<.0001
T.BCL3	186.70944	108.3749	1.72	0.1129
T.POWER*T.POWER	151.09751	293.1084	0.52	0.6164
T.PRESSU*T.POWER	-107.3069	114.9489	-0.93	0.3706
T.PRESSU*T.PRESSU	306.99251	293.1084	1.05	0.3174
T.CHLORI*T.POWER	1499.0269	114.9489	13.04	<.0001
T.CHLORI*T.PRESSU	133.80188	114.9489	1.16	0.2690
T.CHLORI*T.CHLORI	-975.1125	293.1084	-3.33	0.0067
T.NITROG*T.POWER	-407.9819	114.9489	-3.55	0.0046
T.NITROG*T.PRESSU	241.36562	114.9489	2.10	0.0596
T.NITROG*T.CHLORI	-148.4531	114.9489	-1.29	0.2230
T.NITROG*T.NITROG	325.00751	293.1084	1.11	0.2912
T.BCL3*T.POWER	-351.1206	114.9489	-3.05	0.0110
T.BCL3*T.PRESSU	-271.2956	114.9489	-2.36	0.0378
T.BCL3*T.CHLORI	480.46812	114.9489	4.18	0.0015
T.BCL3*T.NITROG	279.82937	114.9489	2.43	0.0332
T.BCL3*T.BCL3	-1254.522	293.1084	-4.28	0.0013

Term	Estimate	Std Error	t Ratio	Prob>|t|
Intercept	24.814482	1.010727	24.55	<.0001
T.POWER	-0.171111	0.833599	-0.21	0.8411
T.PRESSURE	-6.241667	0.833599	-7.49	<.0001
T.CHLORINE	-8.993333	0.833599	-10.79	<.0001
T.NITROGEN	3.325	0.833599	3.99	0.0021
T.BCL3	-5.963333	0.833599	-7.15	<.0001
T.POWER*T.POWER	-1.176594	2.254534	-0.52	0.6121
T.PRESSU*T.POWER	1.546875	0.884166	1.75	0.1080
T.PRESSU*T.PRESSU	1.1184064	2.254534	0.50	0.6296
T.CHLORI*T.POWER	0.169375	0.884166	0.19	0.8516
T.CHLORI*T.PRESSU	0.900625	0.884166	1.02	0.3303
T.CHLORI*T.CHLORI	9.2634064	2.254534	4.11	0.0017
T.NITROG*T.POWER	0.045625	0.884166	0.05	0.9598
T.NITROG*T.PRESSU	-2.350625	0.884166	-2.66	0.0222
T.NITROG*T.CHLORI	0.901875	0.884166	1.02	0.3296
T.NITROG*T.NITROG	-3.761594	2.254534	-1.67	0.1234
T.BCL3*T.POWER	0.733125	0.884166	0.83	0.4246
T.BCL3*T.PRESSU	0.859375	0.884166	0.97	0.3520
T.BCL3*T.CHLORI	4.389375	0.884166	4.96	0.0004
T.BCL3*T.NITROG	-0.069375	0.884166	-0.08	0.9389
T.BCL3*T.BCL3	5.5234064	2.254534	2.45	0.0323

Fig. 6.4(d) Parameter estimates table for TiN etch DOE

Screening Fit

ETCH RATE

Summary of Fit

Analysis of Variance

Lack of Fit

Parameter Estimates

Effect Test

Source	Nparm	DF	Sum of Squares	F Ratio	Prob>F
T.POWER	1	1	128565476	608.1271	<.0001
T.PRESSURE	1	1	68130	0.3223	0.5817
T.CHLORINE	1	1	67871774	321.0400	<.0001
T.NITROGEN	1	1	8587818	40.6212	<.0001
T.BCL3	1	1	627487	2.9681	0.1129
T.POWER*T.POWER	1	1	56181	0.2657	0.6164
T.PRESSURE*T.POWER	1	1	184236	0.8715	0.3706
T.PRESSURE*T.PRESSURE	1	1	231915	1.0970	0.3174
T.CHLORINE*T.POWER	1	1	35953305	170.0626	<.0001
T.CHLORINE*T.PRESSURE	1	1	286447	1.3549	0.2690
T.CHLORINE*T.CHLORINE	1	1	2339823	11.0676	0.0067
T.NITROGEN*T.POWER	1	1	2663187	12.5971	0.0046
T.NITROGEN*T.PRESSURE	1	1	932118	4.4090	0.0596
T.NITROGEN*T.CHLORINE	1	1	352613	1.6679	0.2230
T.NITROGEN*T.NITROGEN	1	1	259932	1.2295	0.2912
T.BCL3*T.POWER	1	1	1972571	9.3305	0.0110
T.BCL3*T.PRESSURE	1	1	1177621	5.5703	0.0378
T.BCL3*T.CHLORINE	1	1	3693594	17.4711	0.0015
T.BCL3*T.NITROGEN	1	1	1252872	5.9262	0.0332
T.BCL3*T.BCL3	1	1	3872848	18.3189	0.0013

Response Surface

Fig. 6.4(e) Effect test table for etch rate in TiN etch DOE

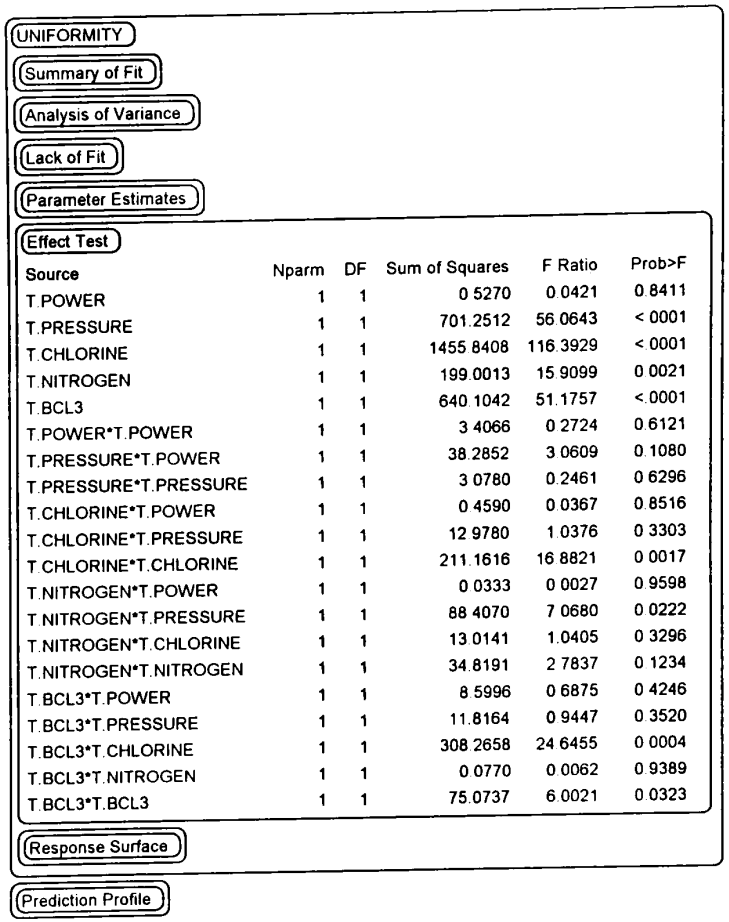

Source	Nparm	DF	Sum of Squares	F Ratio	Prob>F
T.POWER	1	1	0.5270	0.0421	0.8411
T.PRESSURE	1	1	701.2512	56.0643	< 0001
T.CHLORINE	1	1	1455.8408	116.3929	< 0001
T.NITROGEN	1	1	199.0013	15.9099	0.0021
T.BCL3	1	1	640.1042	51.1757	<.0001
T.POWER*T.POWER	1	1	3.4066	0.2724	0.6121
T.PRESSURE*T.POWER	1	1	38.2852	3.0609	0.1080
T.PRESSURE*T.PRESSURE	1	1	3.0780	0.2461	0.6296
T.CHLORINE*T.POWER	1	1	0.4590	0.0367	0.8516
T.CHLORINE*T.PRESSURE	1	1	12.9780	1.0376	0.3303
T.CHLORINE*T.CHLORINE	1	1	211.1616	16.8821	0.0017
T.NITROGEN*T.POWER	1	1	0.0333	0.0027	0.9598
T.NITROGEN*T.PRESSURE	1	1	88.4070	7.0680	0.0222
T.NITROGEN*T.CHLORINE	1	1	13.0141	1.0405	0.3296
T.NITROGEN*T.NITROGEN	1	1	34.8191	2.7837	0.1234
T.BCL3*T.POWER	1	1	8.5996	0.6875	0.4246
T.BCL3*T.PRESSURE	1	1	11.8164	0.9447	0.3520
T.BCL3*T.CHLORINE	1	1	308.2658	24.6455	0.0004
T.BCL3*T.NITROGEN	1	1	0.0770	0.0062	0.9389
T.BCL3*T.BCL3	1	1	75.0737	6.0021	0.0323

Fig. 6.4(f) Effect test table for uniformity in TiN etch DOE

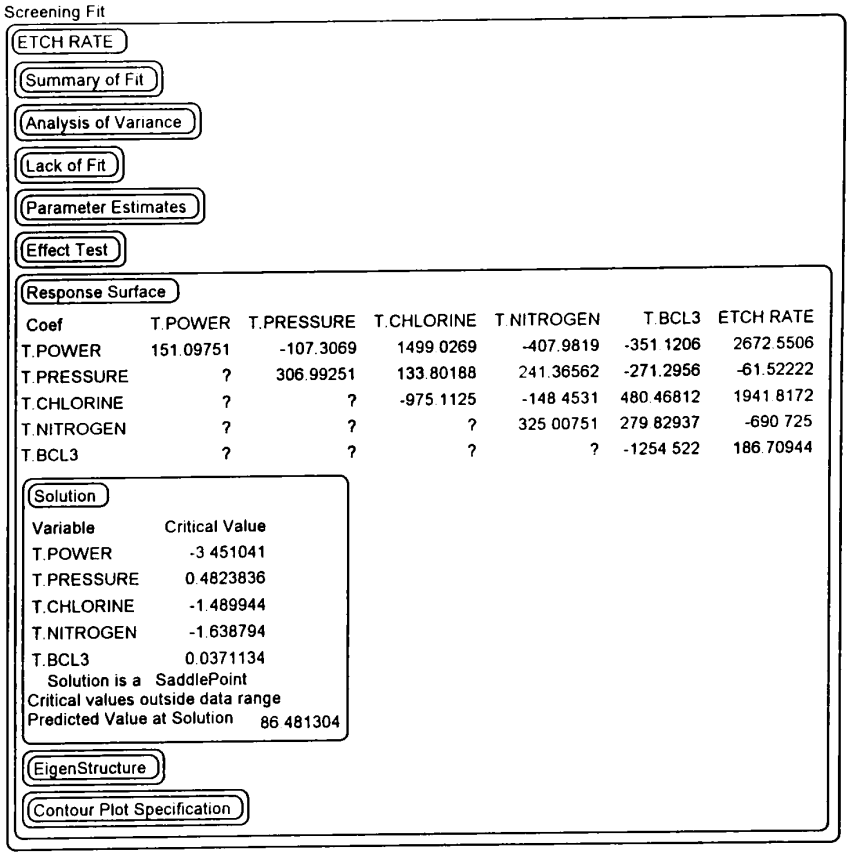

Fig. 6.4(g) Response surface table for etch rate in TiN etch DOE

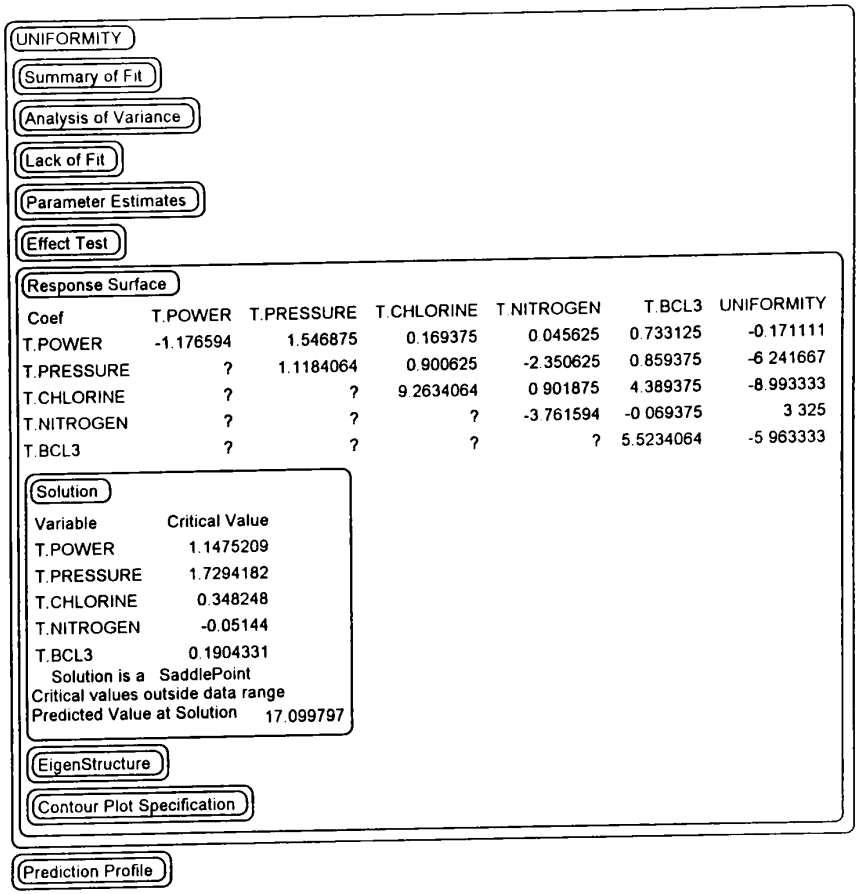

Fig. 6.4(h) Response surface table for uniformity in TiN etch DOE

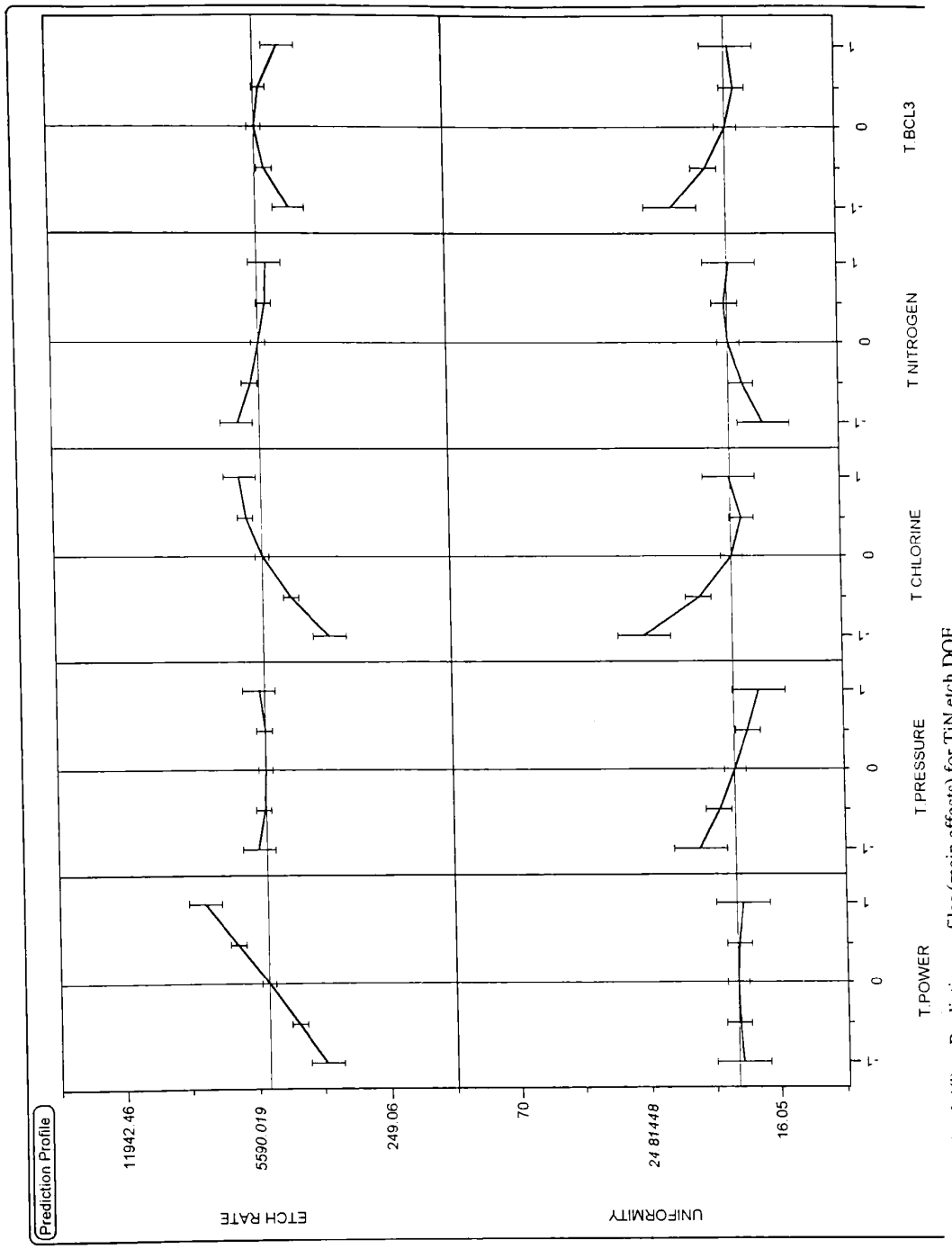

Fig. 6.4(i) Prediction profiles (main effects) for TiN etch DOE

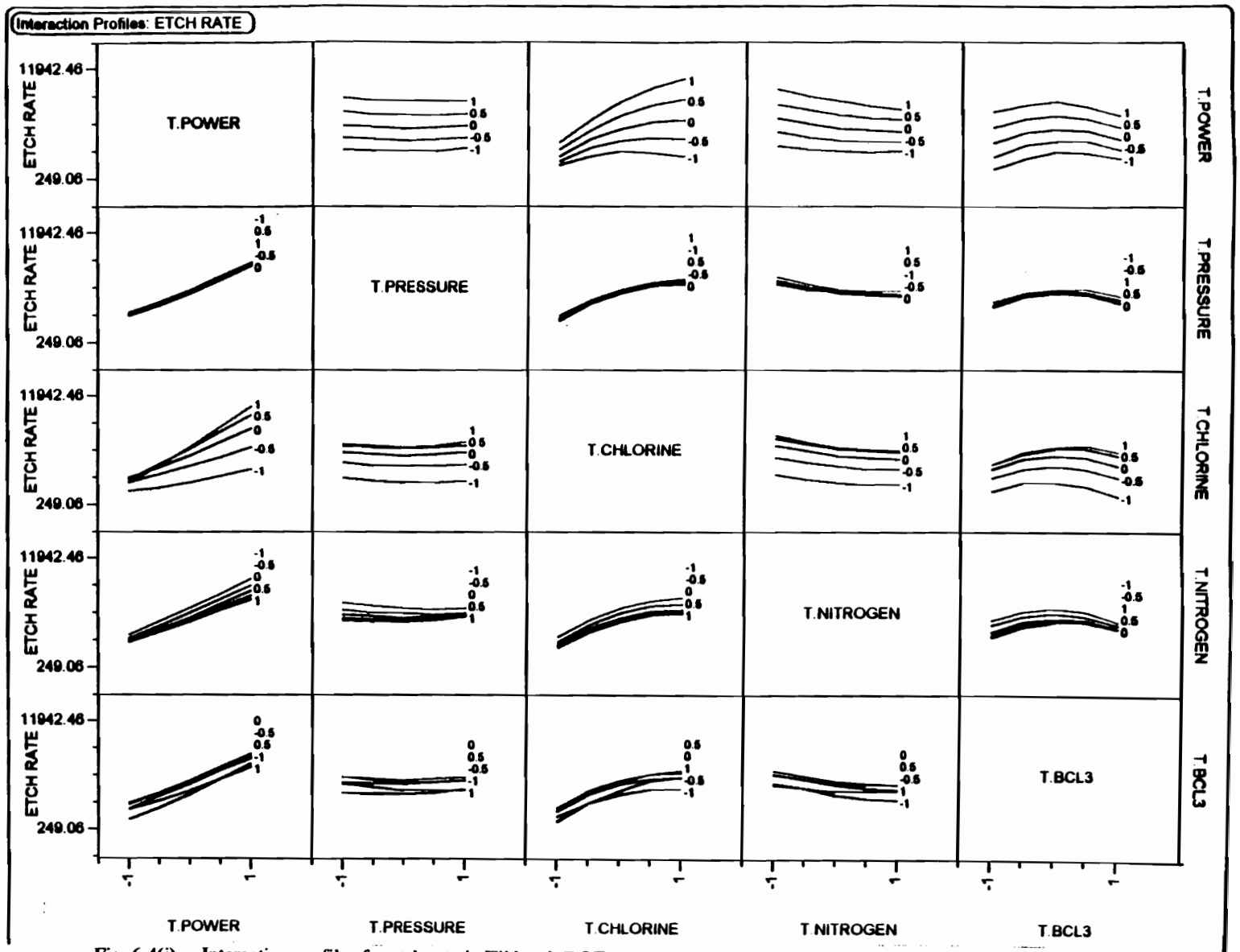

Fig. 6.4(j) Interaction profiles for etch rate in TiN etch DOE

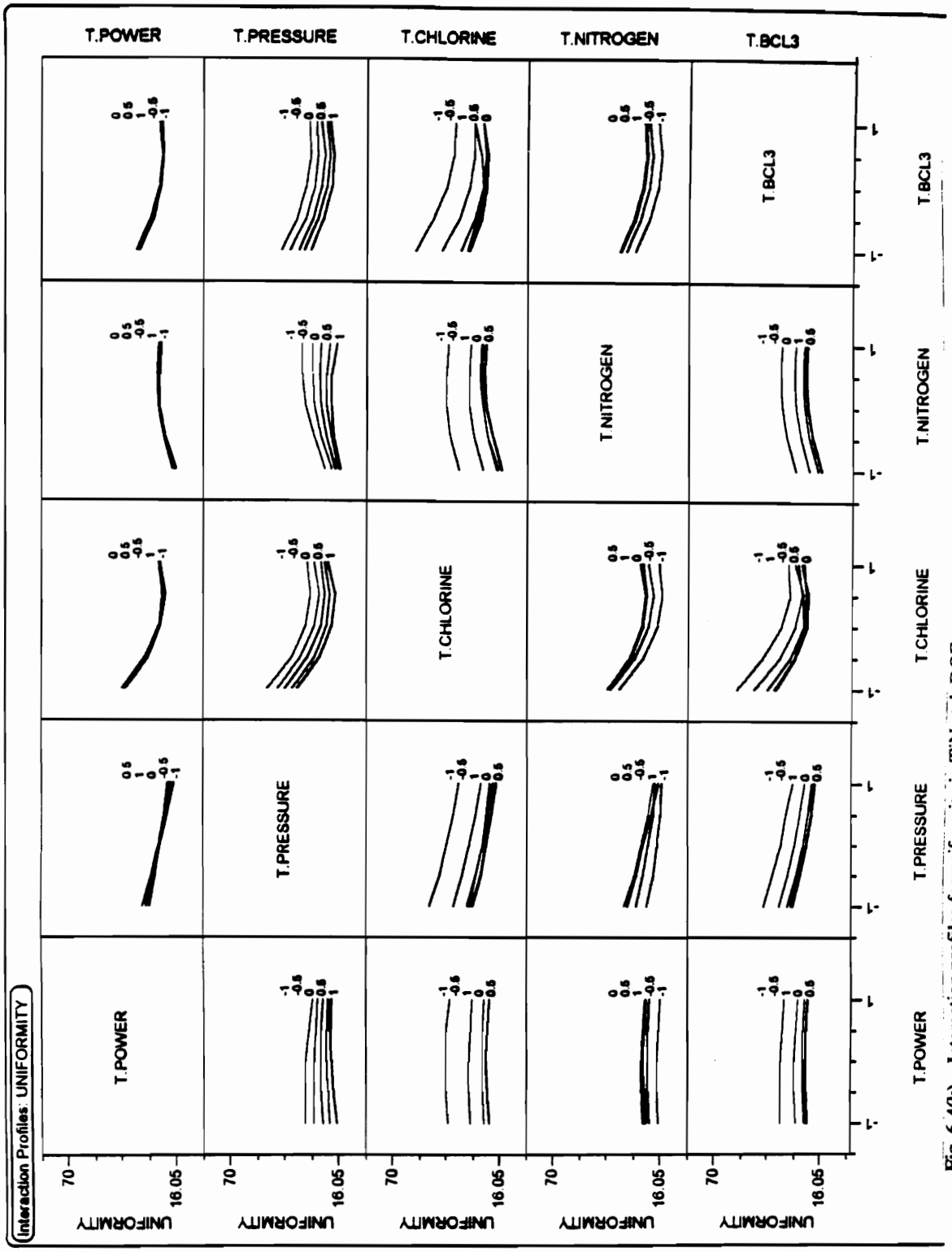

Fig. 6.4(k) Interaction profiles for uniformity in TiN etch DOE

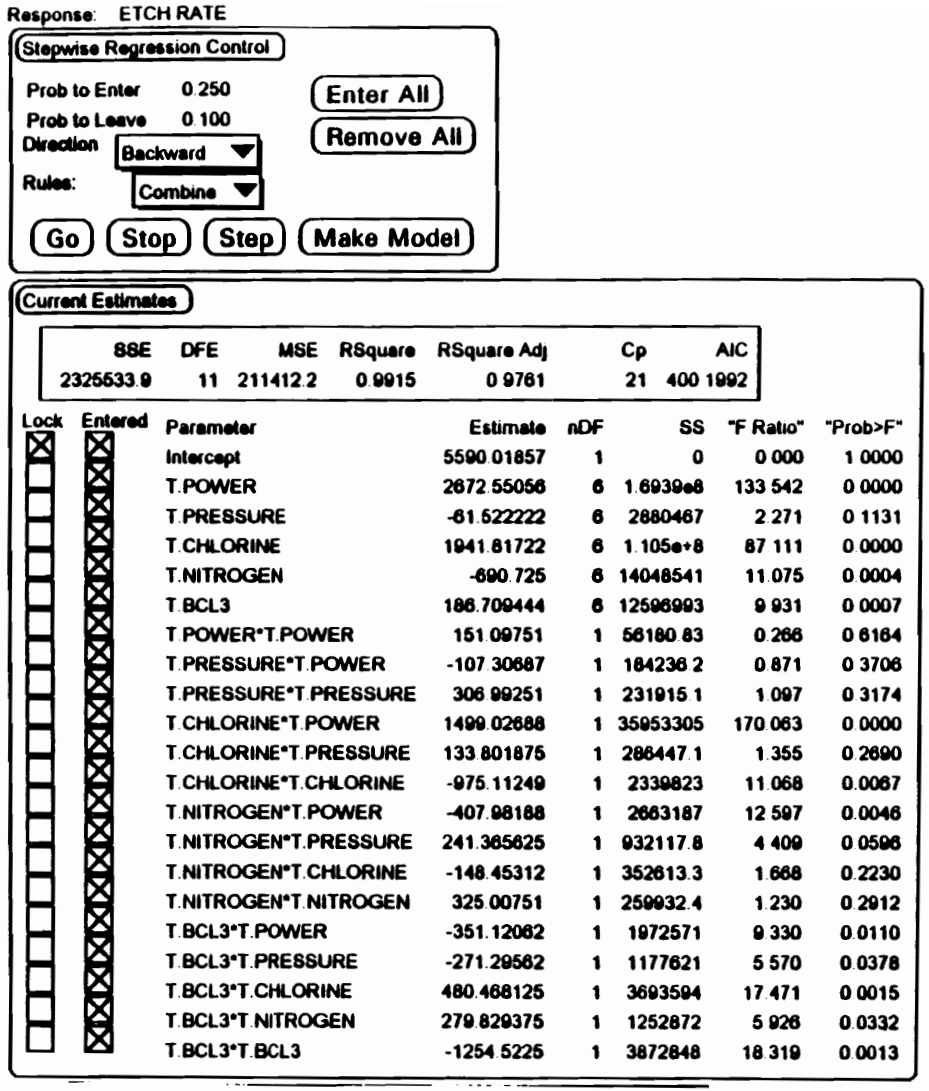

Fig. 6.4(l) Stepwise regression model optimization for etch rate in TiN etch DOE (all factors included)

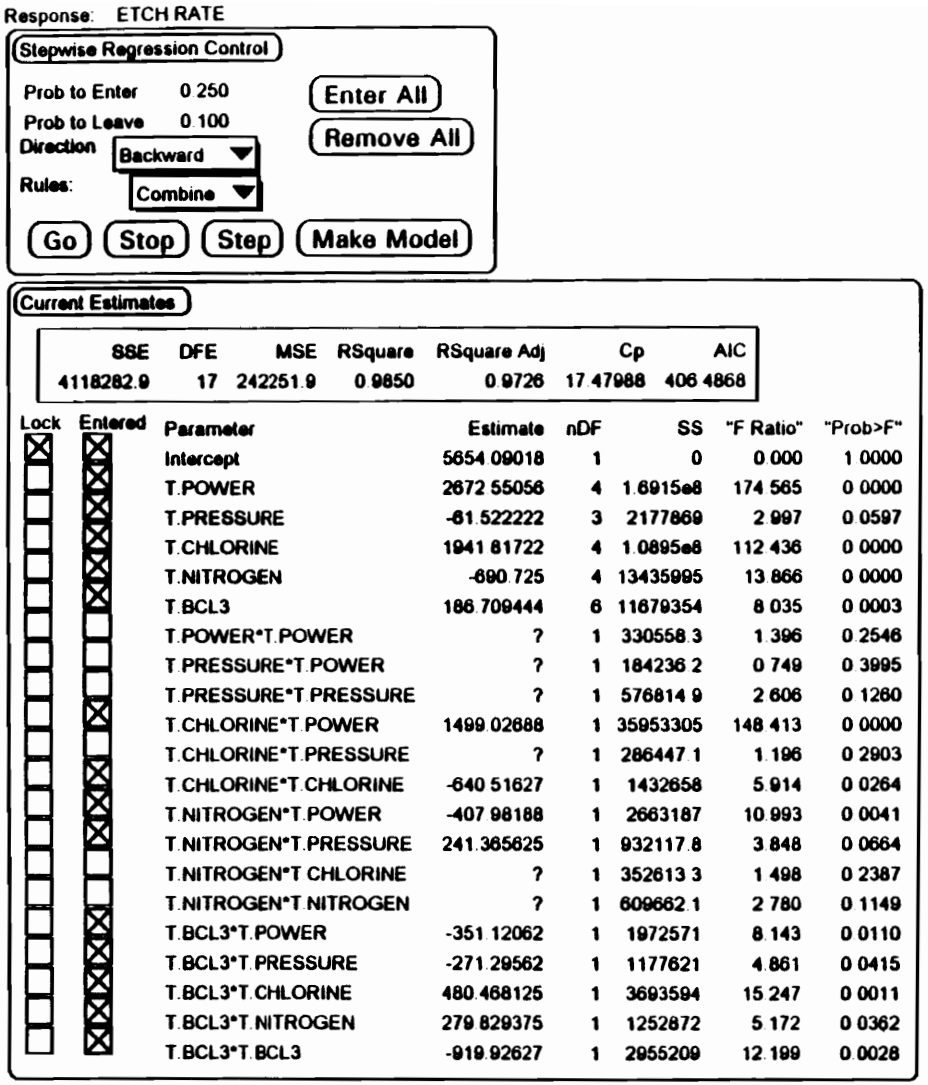

Fig. 6.4(m) Stepwise regression - optimized model parameters for etch rate in TiN etch DOE

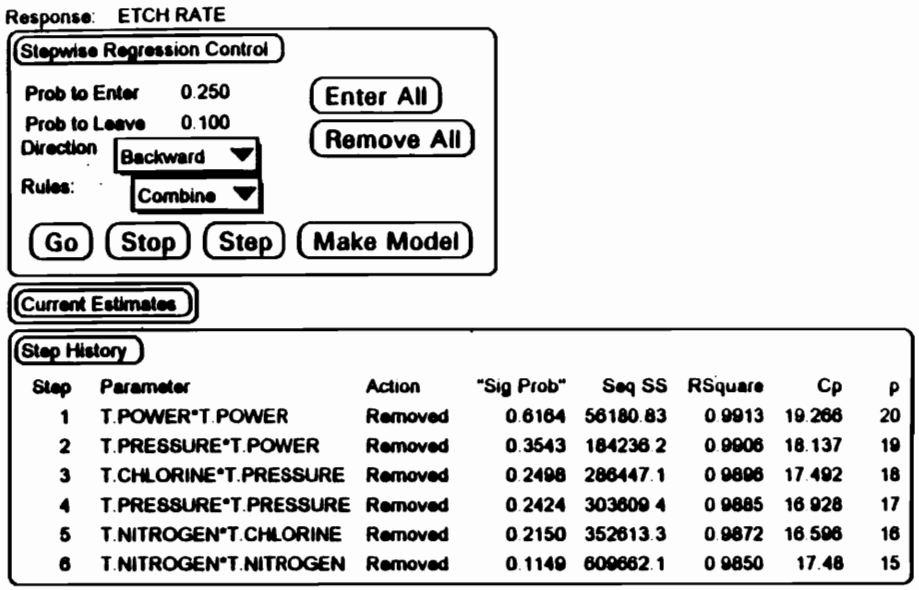

Step	Parameter	Action	"Sig Prob"	Seq SS	RSquare	Cp	p
1	T.POWER*T.POWER	Removed	0.6164	56180.83	0.9913	19.266	20
2	T.PRESSURE*T.POWER	Removed	0.3543	184236.2	0.9906	18.137	19
3	T.CHLORINE*T.PRESSURE	Removed	0.2498	286447.1	0.9896	17.492	18
4	T.PRESSURE*T.PRESSURE	Removed	0.2424	303609.4	0.9885	16.928	17
5	T.NITROGEN*T.CHLORINE	Removed	0.2150	352613.3	0.9872	16.596	16
6	T.NITROGEN*T.NITROGEN	Removed	0.1149	609662.1	0.9850	17.48	15

Fig. 6.4(m) Contd. Stepwise regression - optimized model parameters for etch rate in TiN etch DOE

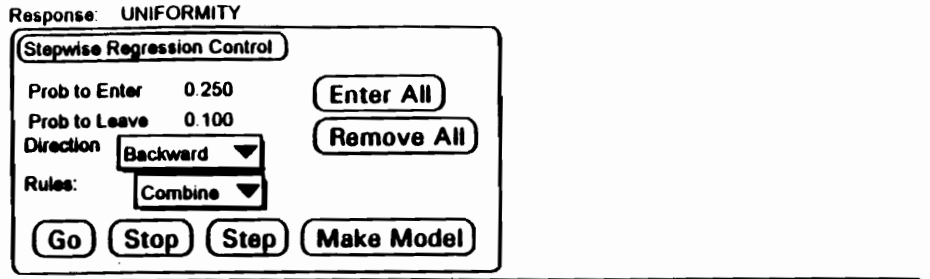

Current Estimates

SSE	DFE	MSE	RSquare	RSquare Adj	Cp	AIC
137.58782	11	12.50798	0.9700	0.9155	21	88.67285

Lock	Entered	Parameter	Estimate	nDF	SS	"F Ratio"	"Prob>F"
☒	☒	Intercept	24.8144821	1	0	0.000	1.0000
☐	☒	T.POWER	-0.1711111	6	51.31069	0.684	0.6671
☐	☒	T.PRESSURE	-6.2416667	6	855.8159	11.404	0.0004
☐	☒	T.CHLORINE	-8.9933333	6	2001.719	26.673	0.0000
☐	☒	T.NITROGEN	3.325	6	335.3517	4.469	0.0156
☐	☒	T.BCL3	-5.9633333	6	1043.937	13.910	0.0001
☐	☒	T.POWER*T.POWER	-1.1765936	1	3.406642	0.272	0.6121
☐	☒	T.PRESSURE*T.POWER	1.546875	1	38.28516	3.061	0.1080
☐	☒	T.PRESSURE*T.PRESSURE	1.11840637	1	3.07803	0.246	0.6296
☐	☒	T.CHLORINE*T.POWER	0.169375	1	0.459006	0.037	0.8516
☐	☒	T.CHLORINE*T.PRESSURE	0.900625	1	12.97801	1.038	0.3303
☐	☒	T.CHLORINE*T.CHLORINE	9.26340637	1	211.1616	16.882	0.0017
☐	☒	T.NITROGEN*T.POWER	0.045625	1	0.033306	0.003	0.9598
☐	☒	T.NITROGEN*T.PRESSURE	-2.350625	1	88.40701	7.068	0.0222
☐	☒	T.NITROGEN*T.CHLORINE	0.901875	1	13.01406	1.040	0.3296
☐	☒	T.NITROGEN*T.NITROGEN	-3.7615936	1	34.81908	2.784	0.1234
☐	☒	T.BCL3*T.POWER	0.733125	1	8.599556	0.688	0.4246
☐	☒	T.BCL3*T.PRESSURE	0.859375	1	11.81641	0.945	0.3520
☐	☒	T.BCL3*T.CHLORINE	4.389375	1	308.2658	24.646	0.0004
☐	☒	T.BCL3*T.NITROGEN	-0.069375	1	0.077006	0.006	0.9389
☐	☒	T.BCL3*T.BCL3	5.52340637	1	75.07365	6.002	0.0323

Fig. 6.4(n) Stepwise regression model optimization for uniformity in TiN etch DOE (All factors included)

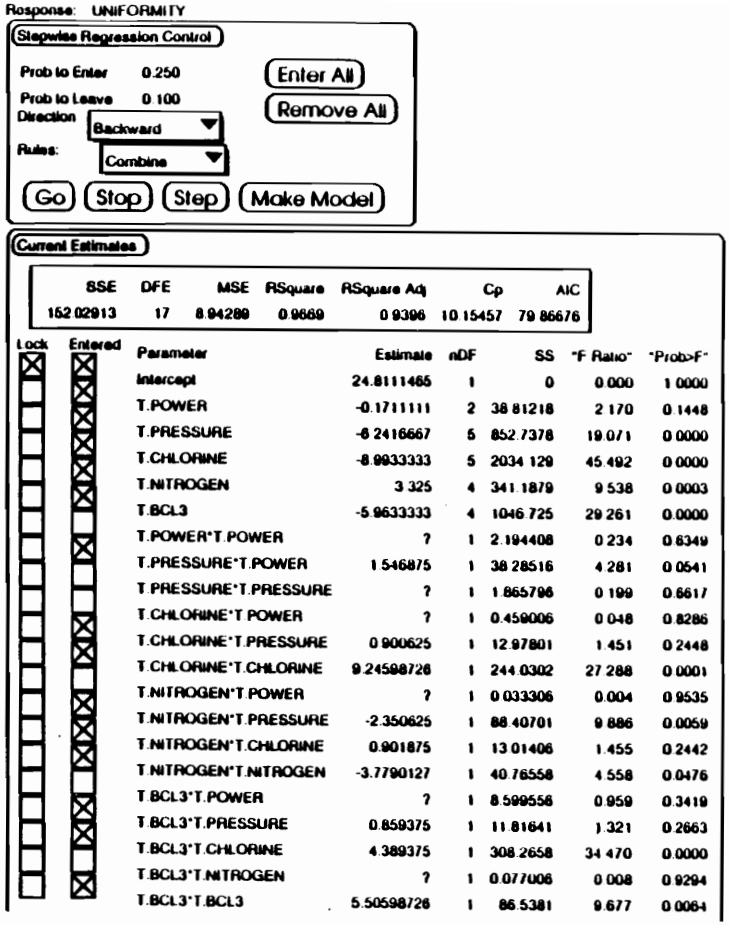

Fig. 6.4(o) Stepwise regression - optimized model parameters for uniformity in TiN etch DOE.

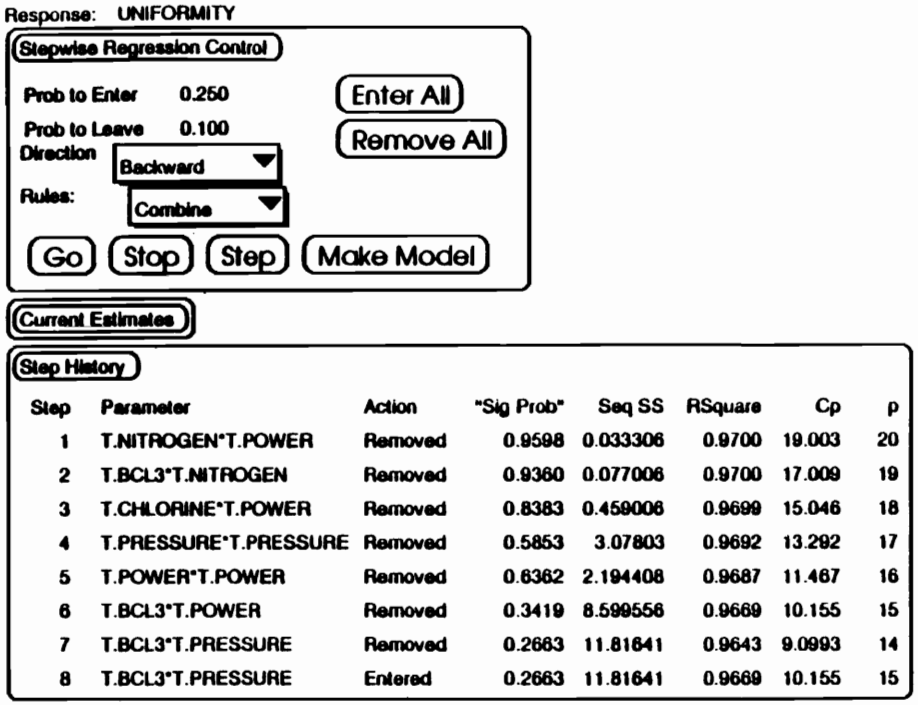

Step	Parameter	Action	"Sig Prob"	Seq SS	RSquare	Cp	p
1	T.NITROGEN*T.POWER	Removed	0.9598	0.033306	0.9700	19.003	20
2	T.BCL3*T.NITROGEN	Removed	0.9360	0.077006	0.9700	17.009	19
3	T.CHLORINE*T.POWER	Removed	0.8383	0.459006	0.9699	15.046	18
4	T.PRESSURE*T.PRESSURE	Removed	0.5853	3.07803	0.9692	13.292	17
5	T.POWER*T.POWER	Removed	0.6362	2.194408	0.9687	11.467	16
6	T.BCL3*T.POWER	Removed	0.3419	8.599556	0.9669	10.155	15
7	T.BCL3*T.PRESSURE	Removed	0.2663	11.81641	0.9643	9.0993	14
8	T.BCL3*T.PRESSURE	Entered	0.2663	11.81641	0.9669	10.155	15

Fig. 6.4(o) Contd. Stepwise regression - optimized model parameters for uniformity in TiN etch DOE.

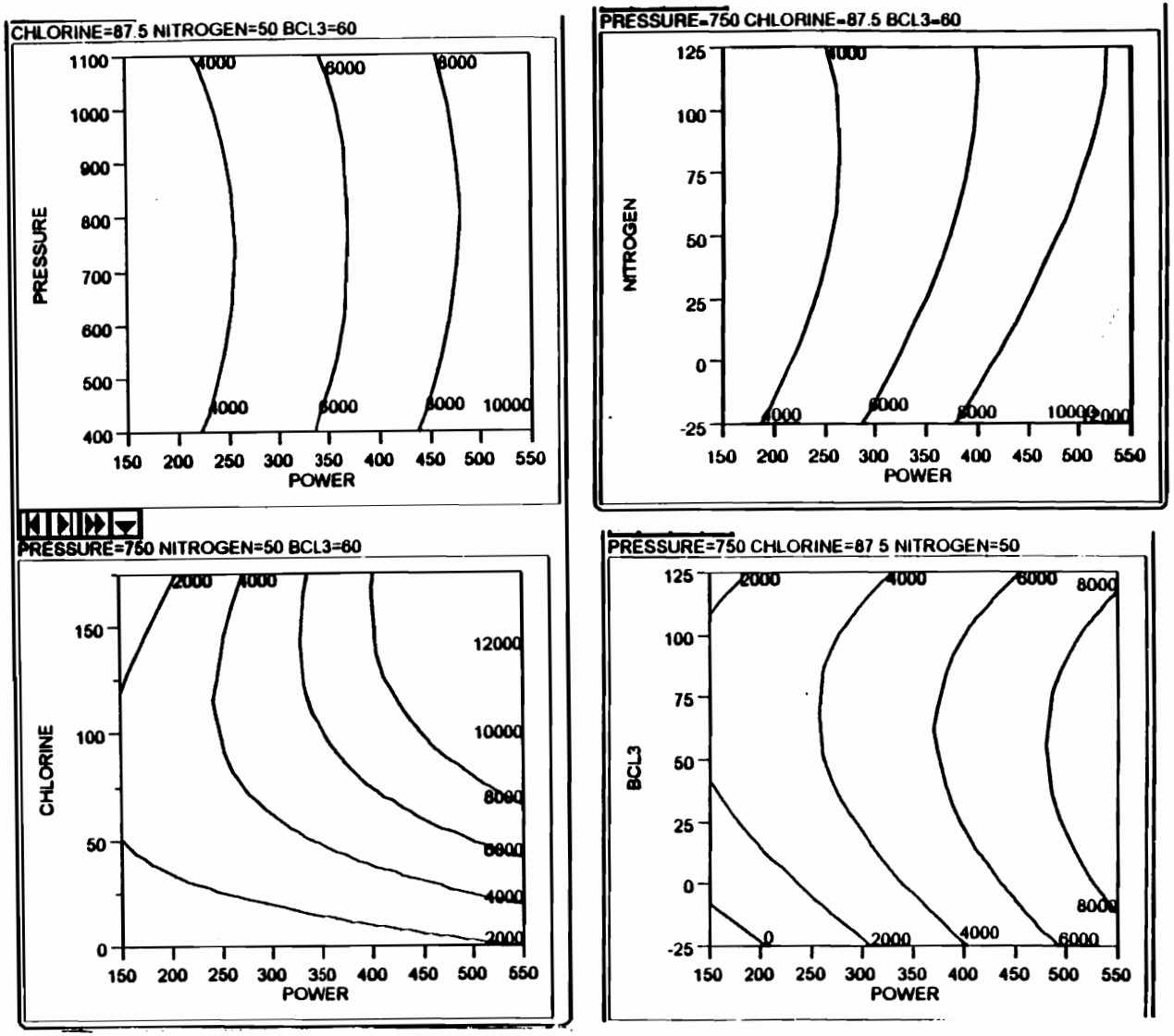

Fig. 6.4(p) Contour plots for etch rate in TiN etch DOE.

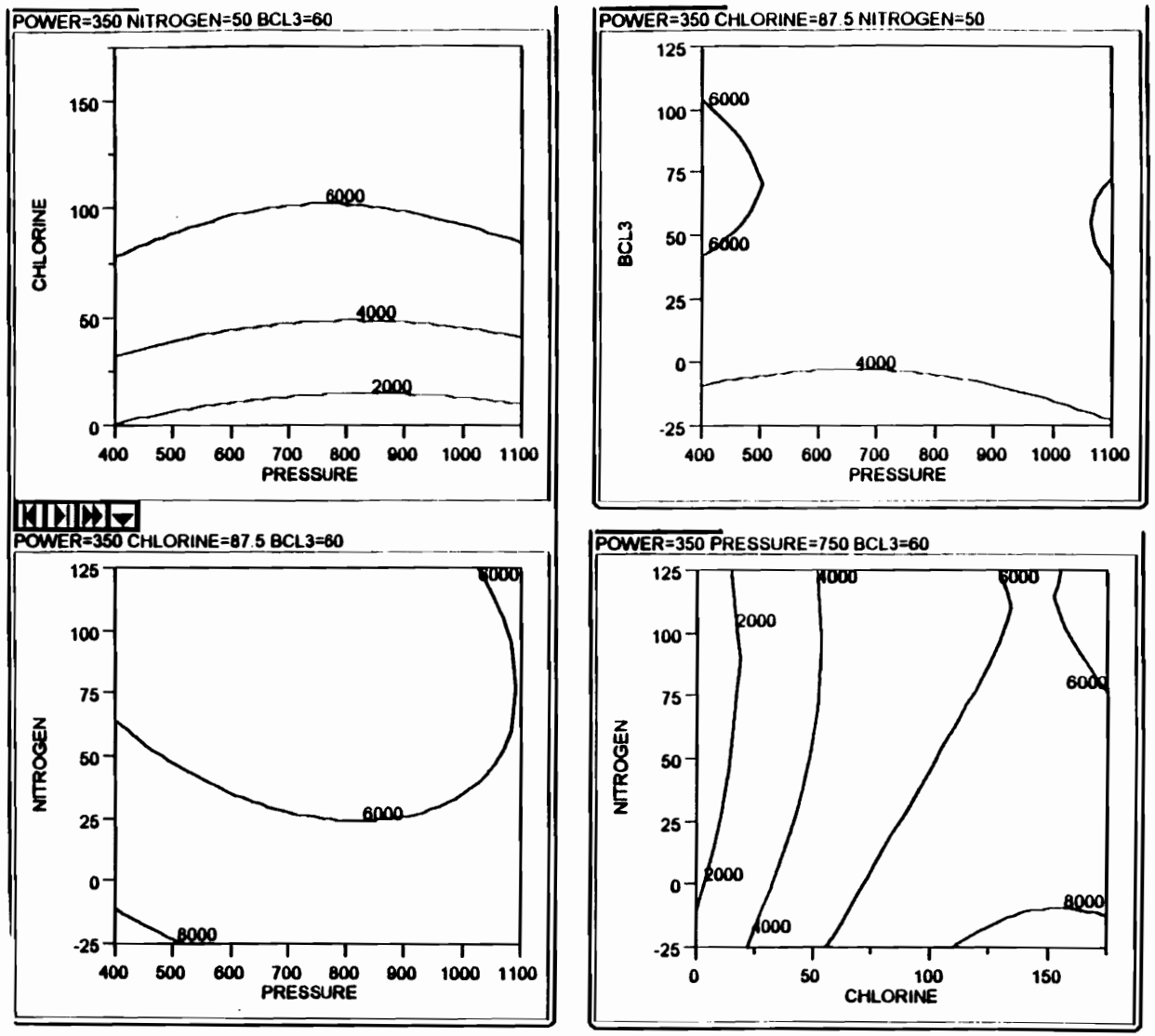

Fig. 6.4(p) Contd. Contour plots for etch rate in TiN etch DOE.

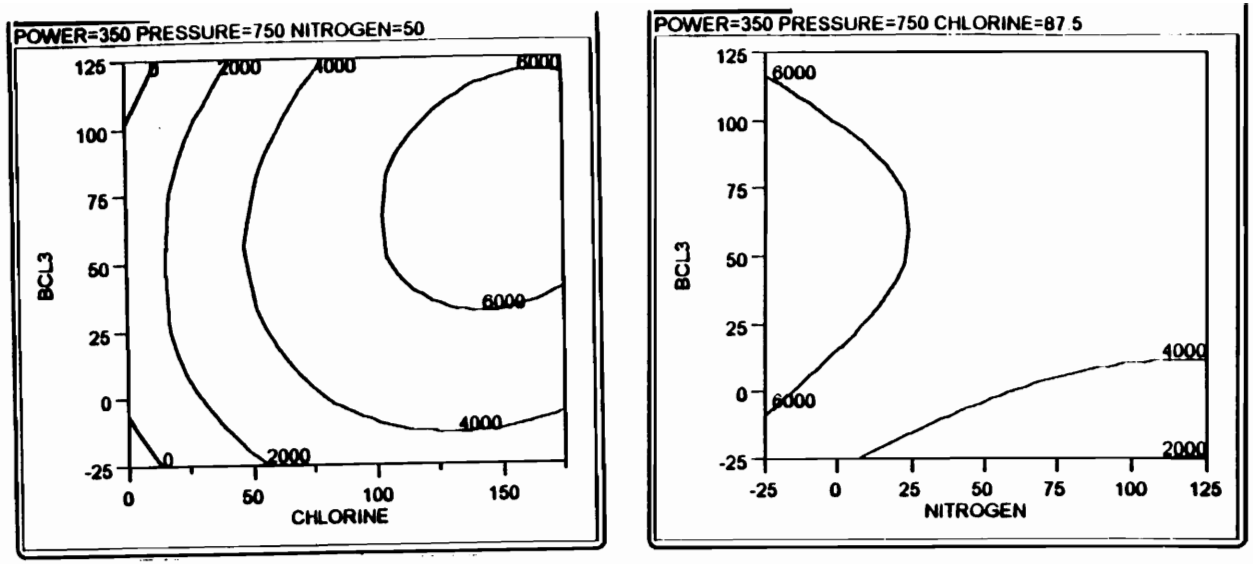

Fig. 6.4(p) Contd. Contour plots for etch rate in TiN etch DOE.

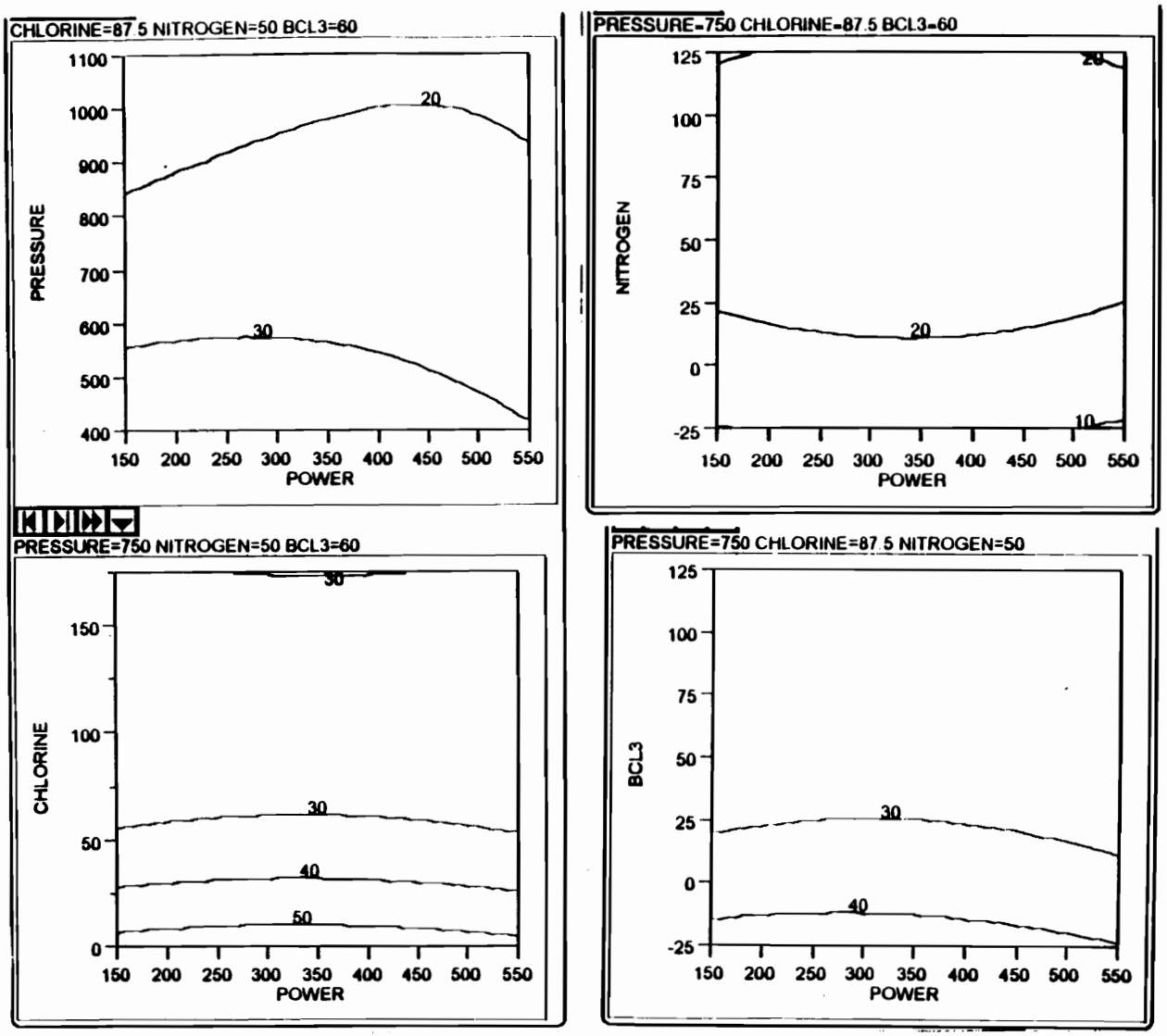

Fig. 6.4(q) Contour plots for uniformity in TiN etch DOE.

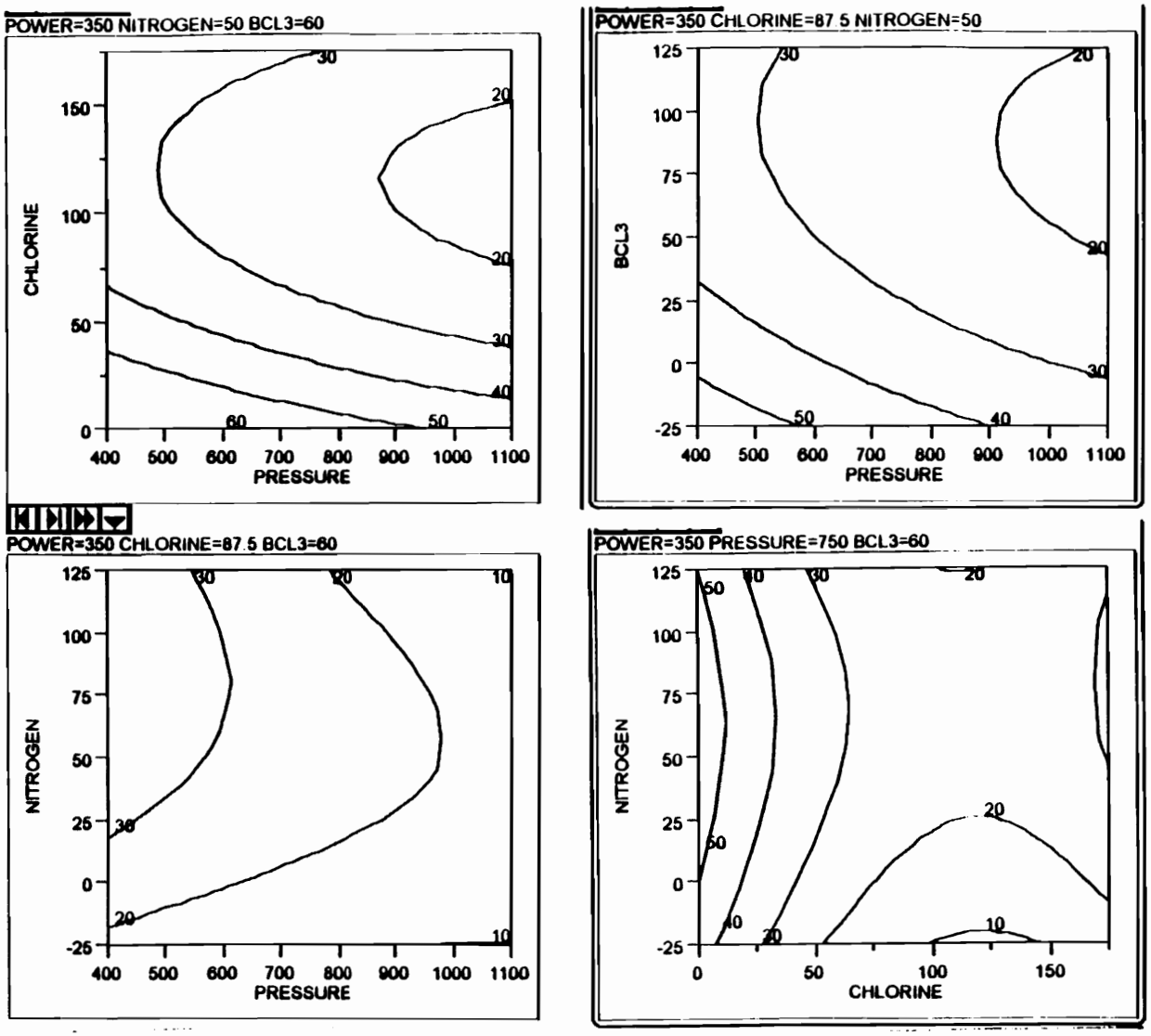

Fig. 6.4(q) Contd. Contour plots for uniformity in TiN etch DOE.

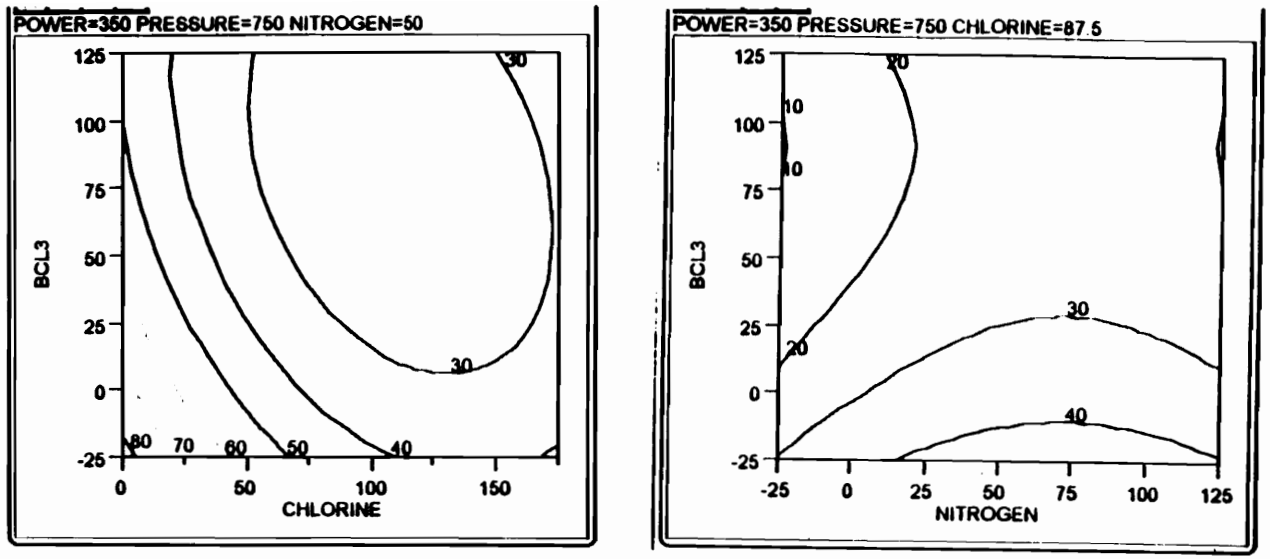

Fig. 6.4(q) Contd. Contour plots for uniformity in TiN etch DOE.

TIDESGN1.JMP

Rows	T.POWER	T.PRESSURE	T.CHLORINE	T.NITROGEN	ETCH RATE	UNIFORMITY
1	1	-1	1	-1	17474.27	25.78
2	1	-1	1	1	12930.38	30.32
3	1	-1	-1	-1	4135.32	15.14
4	1	-1	-1	1	1737.78	46.57
5	1	0	0	0	7167.44	29.81
6	1	1	-1	-1	4665.74	41.68
7	1	1	-1	1	2522.59	42.15
8	1	1	1	1	8090.83	23.79
9	1	1	1	-1	7216.02	38.44
10	0	-1	0	0	3828.82	35.6
11	0	0	0	0	1978.63	47.45
12	0	0	-1	0	1555.7	30.58
13	0	0	0	0	1750.76	60.95
14	0	0	0	0	1892.83	51.3
15	0	0	0	-1	1524.7	50.37
16	0	0	0	0	1772.33	47.89
17	0	0	0	0	1983.68	47.32
18	0	0	0	0	1804.35	42.83
19	0	0	1	0	2146.82	38.88
20	0	0	0	0	2001.84	41.29
21	0	0	0	1	1627.06	51.57
22	0	1	0	0	1426.25	48.81
23	-1	-1	1	1	453.48	77.38
24	-1	-1	-1	-1	136.23	78.39
25	-1	-1	-1	1	48.26	137.29
26	-1	-1	1	-1	56.09	113.23
27	-1	0	0	0	57.05	114.45
28	-1	1	-1	1	166.34	69.66
29	-1	1	1	-1	235.62	49.48
30	-1	1	-1	-1	123.12	55.6
31	-1	1	1	1	234.03	66.2

Fig. 6.5(a) Design of Experiment for Ti etch in Cl_2/N_2 plasmas.

TIDESGN1.JMP

Rows	Pattern	Block	POWER	PRESSURE	CHLORINE	NITROGEN	Comment
1	+-+-	1	500	500	150	0	FF
2	+-++	1	500	500	150	100	FF
3	+—	1	500	500	25	0	FF
4	+—+	1	500	500	25	100	FF
5	+000	1	500	750	87.5	50	Axial
6	++—	1	500	1000	25	0	FF
7	++-+	1	500	1000	25	100	FF
8	++++	1	500	1000	150	100	FF
9	+++-	1	500	1000	150	0	FF
10	0-00	1	350	500	87.5	50	Axial
11	0000	1	350	750	87.5	50	Center-Ax
12	00-0	1	350	750	25	50	Axial
13	0000	1	350	750	87.5	50	Center-Ax
14	0000	1	350	750	87.5	50	Center-Ax
15	000-	1	350	750	87.5	0	Axial
16	0000	1	350	750	87.5	50	Center-Ax
17	0000	1	350	750	87.5	50	Center-Ax
18	0000	1	350	750	87.5	50	Center-Ax
19	00+0	1	350	750	150	50	Axial
20	0000	1	350	750	87.5	50	Center-Ax
21	000+	1	350	750	87.5	100	Axial
22	0+00	1	350	1000	87.5	50	Axial
23	—++	1	200	500	150	100	FF
24	—	1	200	500	25	0	FF
25	—+	1	200	500	25	100	FF
26	—+-	1	200	500	150	0	FF
27	-000	1	200	750	87.5	50	Axial
28	-+-+	1	200	1000	25	100	FF
29	-++-	1	200	1000	150	0	FF
30	-+—	1	200	1000	25	0	FF
31	-+++	1	200	1000	150	100	FF

Fig. 6.5(a) Contd. Design of Experiment for Ti etch in Cl_2/N_2 plasmas.

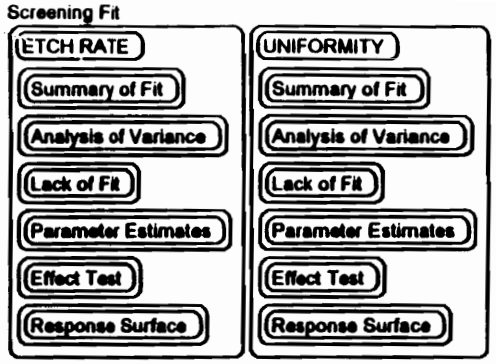

Fig. 6.5(b) List of outputs available from JMP software for Ti etch DOE.

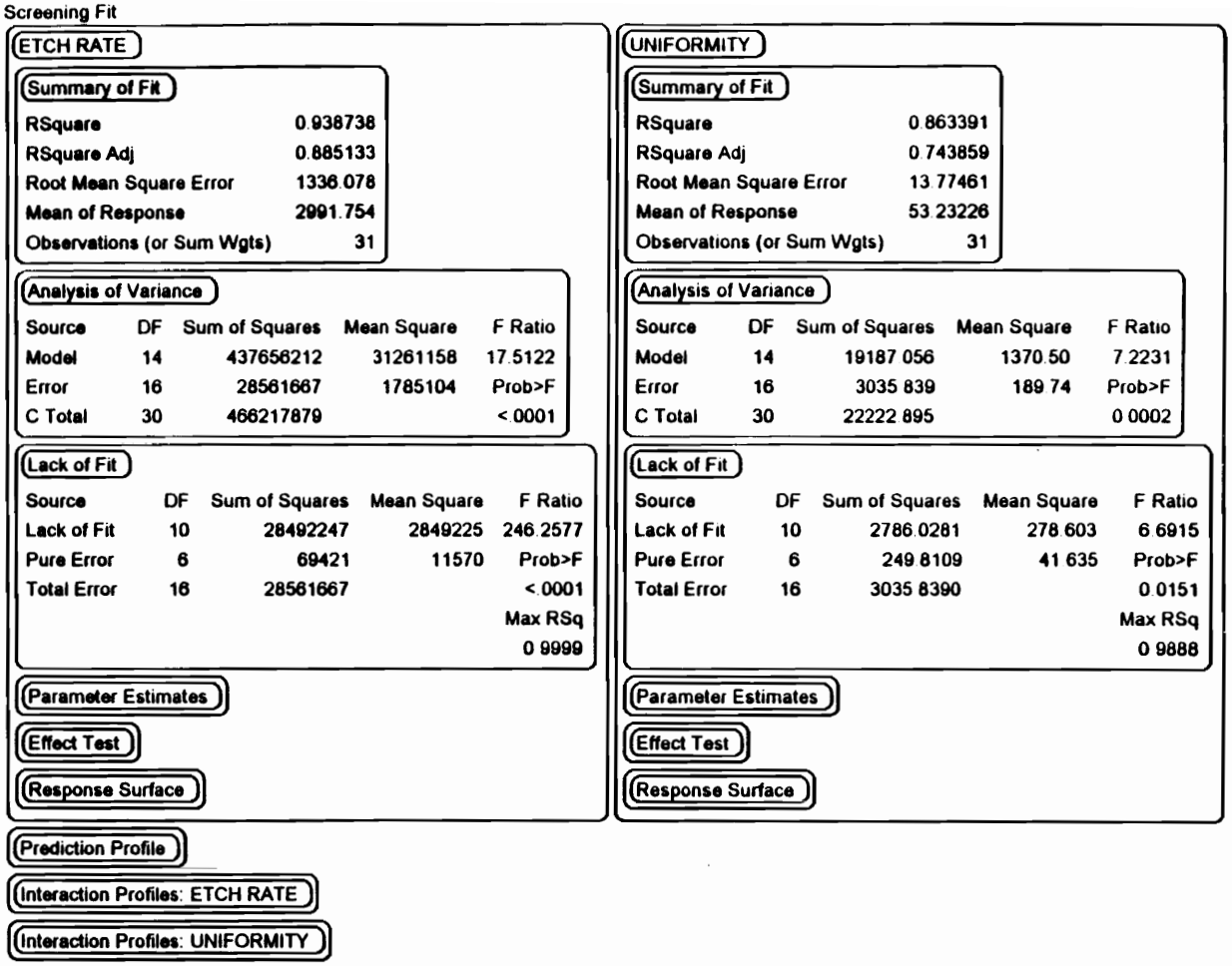

Fig. 6.5(c) Summary of fit, Analysis of Variance, Lack of Fit tables for Ti etch DOE.

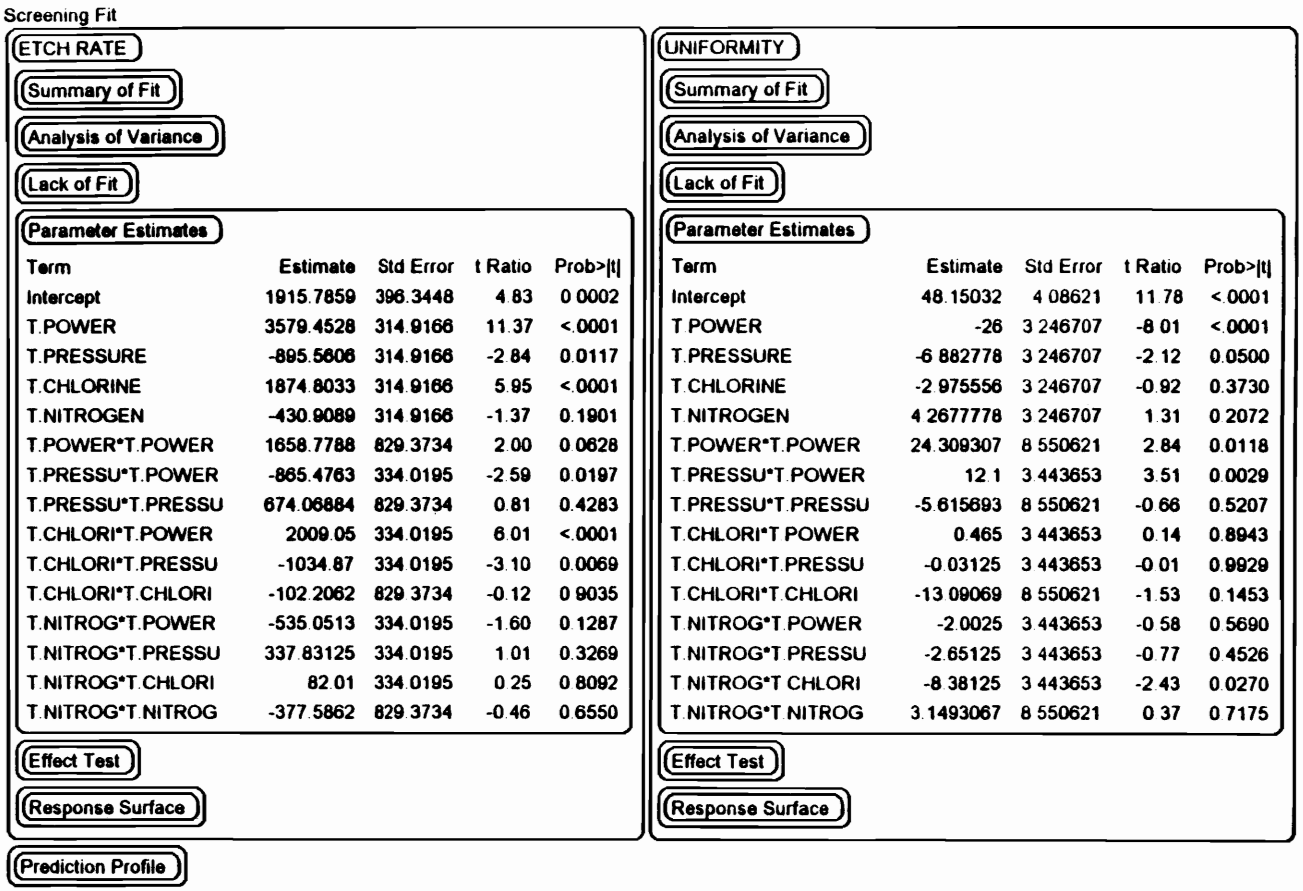

Fig. 6.5(d) Parameter estimates table for Ti etch DOE

Screening Fit

ETCH RATE

Summary of Fit

Analysis of Variance

Lack of Fit

Parameter Estimates

Effect Test

Source	Nparm	DF	Sum of Squares	F Ratio	Prob>F
T.POWER	1	1	230624679	129.1940	<.0001
T.PRESSURE	1	1	14436517	8.0872	0.0117
T.CHLORINE	1	1	63267976	35.4422	<.0001
T.NITROGEN	1	1	3342284	1.8723	0.1901
T.POWER*T.POWER	1	1	7140694	4.0002	0.0628
T.PRESSURE*T.POWER	1	1	11984786	6.7138	0.0197
T.PRESSURE*T.PRESSURE	1	1	1179158	0.6606	0.4283
T.CHLORINE*T.POWER	1	1	64580510	36.1774	<.0001
T.CHLORINE*T.PRESSURE	1	1	17135295	9.5990	0.0069
T.CHLORINE*T.CHLORINE	1	1	27109	0.0152	0.9035
T.NITROGEN*T.POWER	1	1	4580477	2.5659	0.1287
T.NITROGEN*T.PRESSURE	1	1	1826079	1.0230	0.3269
T.NITROGEN*T.CHLORINE	1	1	107610	0.0603	0.8092
T.NITROGEN*T.NITROGEN	1	1	369995	0.2073	0.6550

Response Surface

Fig. 6.5(e) Effect test table for etch rate in Ti etch DOE

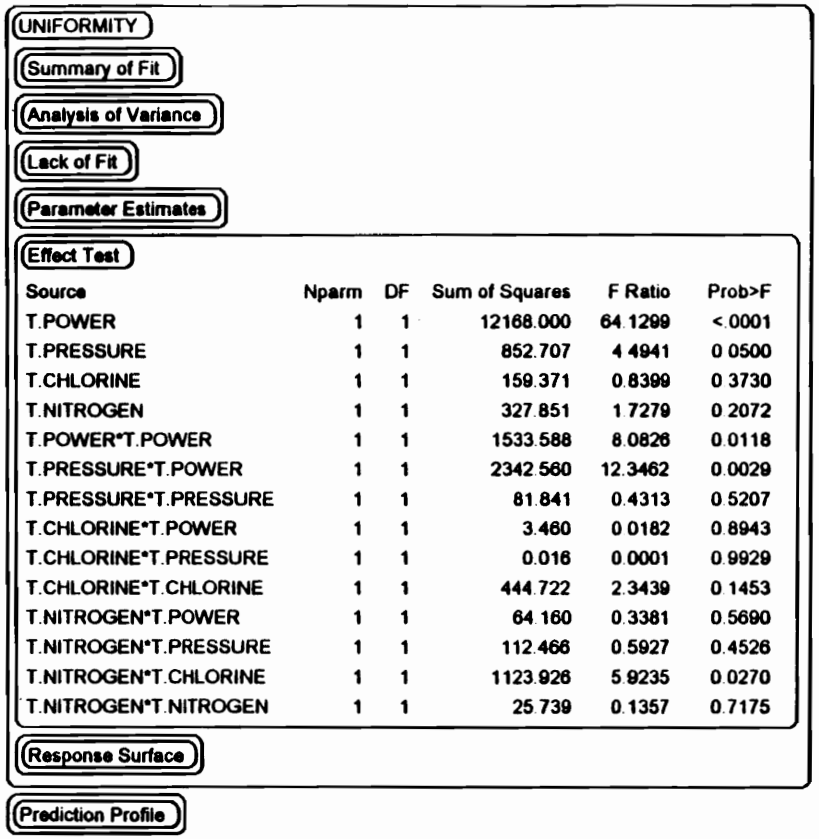

Source	Nparm	DF	Sum of Squares	F Ratio	Prob>F
T.POWER	1	1	12168.000	64.1299	<.0001
T.PRESSURE	1	1	852.707	4.4941	0.0500
T.CHLORINE	1	1	159.371	0.8399	0.3730
T.NITROGEN	1	1	327.851	1.7279	0.2072
T.POWER*T.POWER	1	1	1533.588	8.0826	0.0118
T.PRESSURE*T.POWER	1	1	2342.560	12.3462	0.0029
T.PRESSURE*T.PRESSURE	1	1	81.841	0.4313	0.5207
T.CHLORINE*T.POWER	1	1	3.460	0.0182	0.8943
T.CHLORINE*T.PRESSURE	1	1	0.016	0.0001	0.9929
T.CHLORINE*T.CHLORINE	1	1	444.722	2.3439	0.1453
T.NITROGEN*T.POWER	1	1	64.160	0.3381	0.5690
T.NITROGEN*T.PRESSURE	1	1	112.466	0.5927	0.4526
T.NITROGEN*T.CHLORINE	1	1	1123.926	5.9235	0.0270
T.NITROGEN*T.NITROGEN	1	1	25.739	0.1357	0.7175

Fig. 6.5(f) Effect test table for uniformity in Ti etch DOE

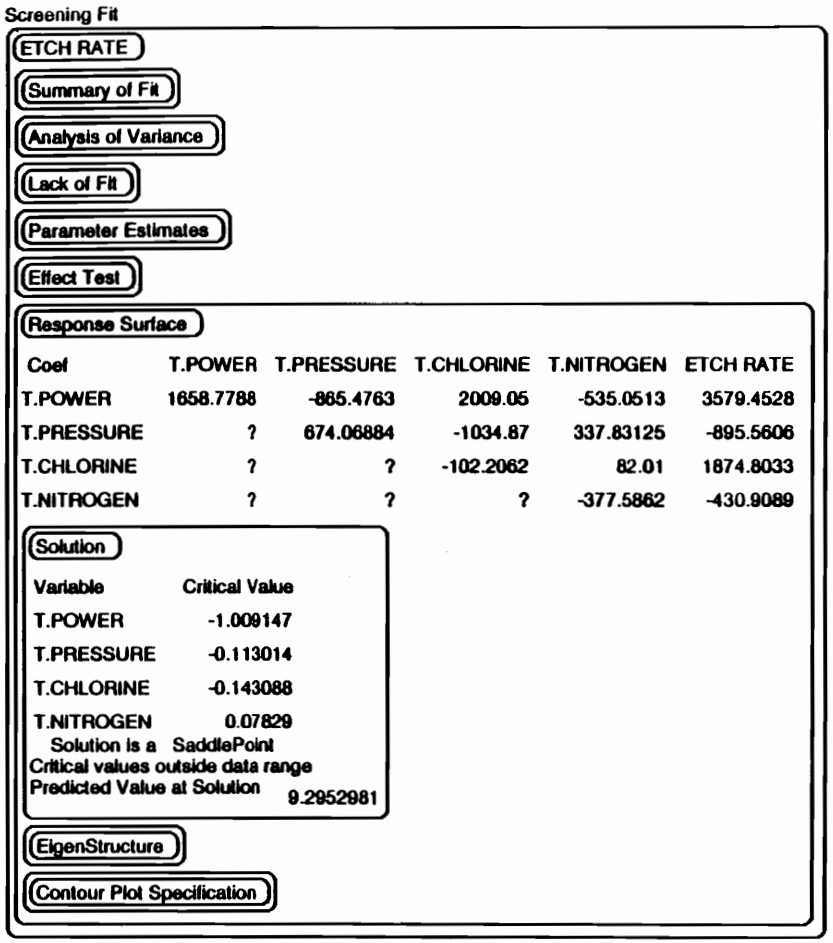

Fig. 6.5(g) Response surface table for etch rate in Ti etch DOE

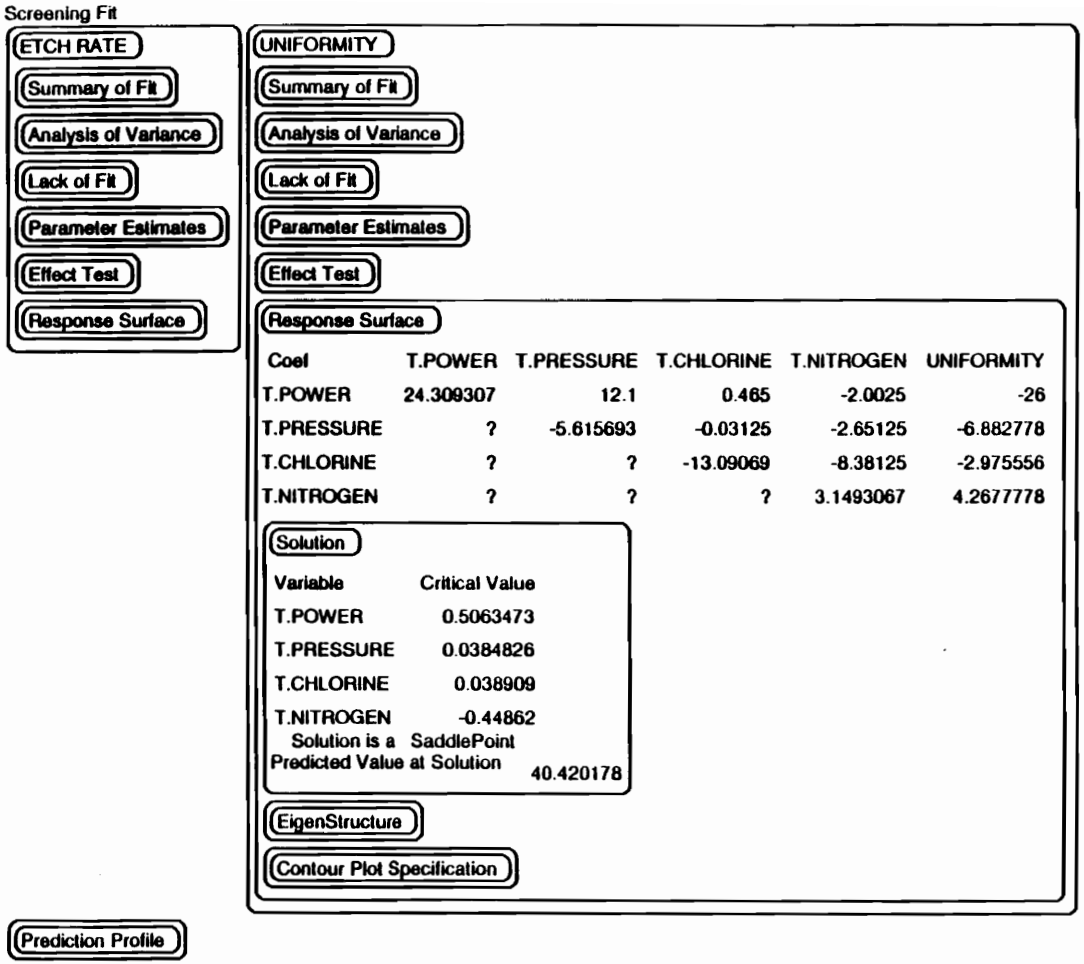

Fig. 6.5(h) Response surface table for uniformity in Ti etch DOE

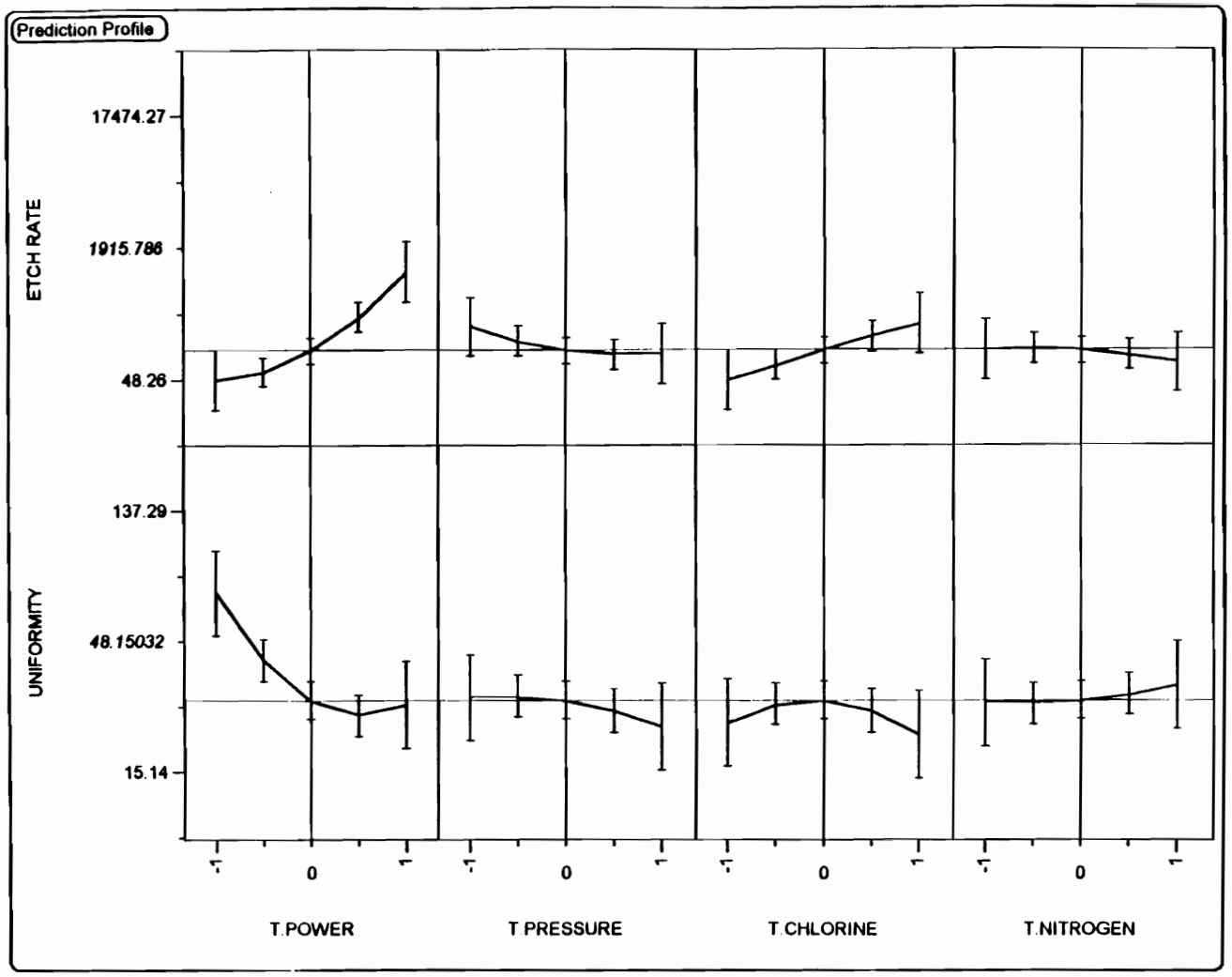

Fig. 6.5(i) Prediction profiles (main effects) for Ti etch DOE

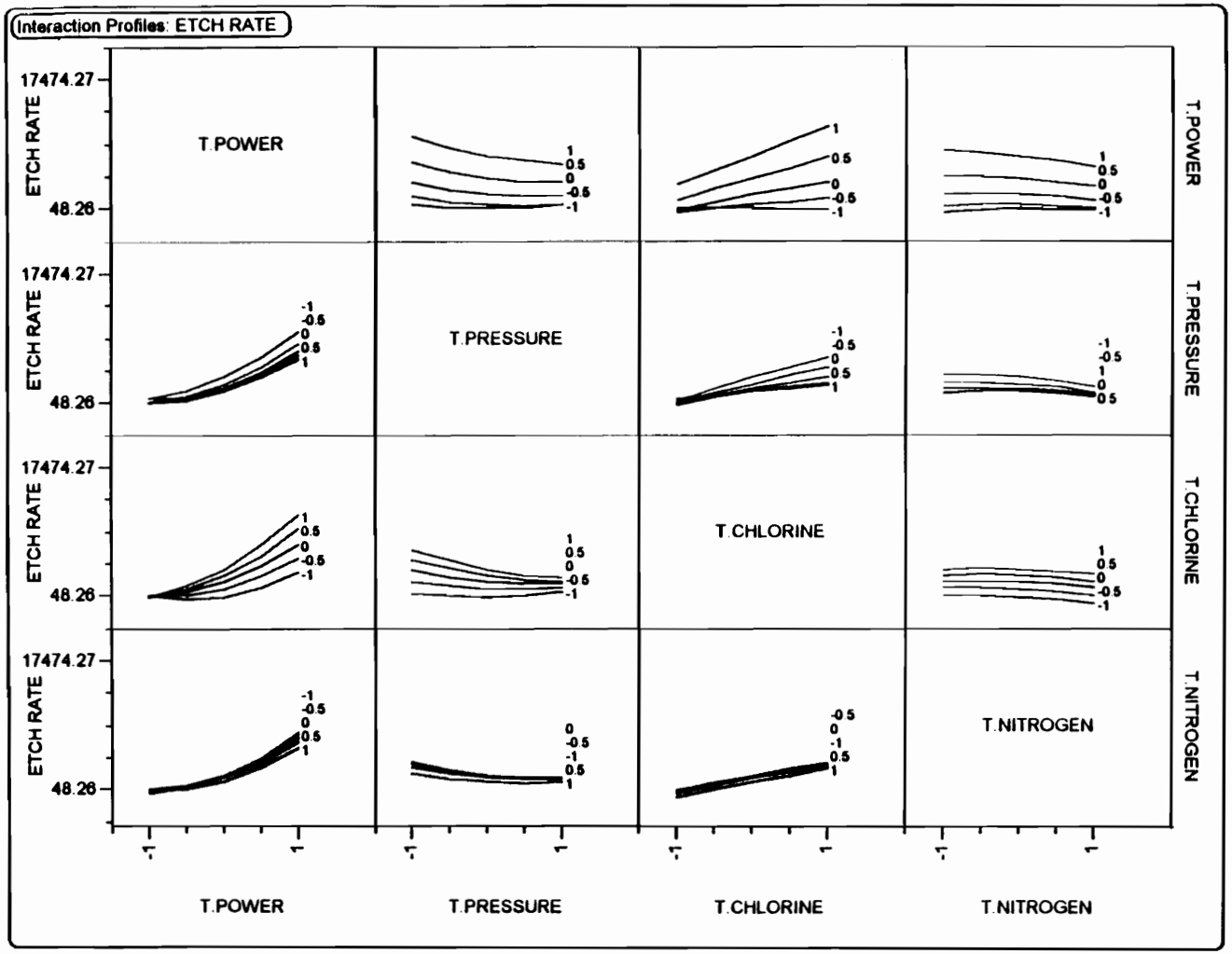

Fig. 6.5(j) Interaction profiles for etch rate in Ti etch DOE

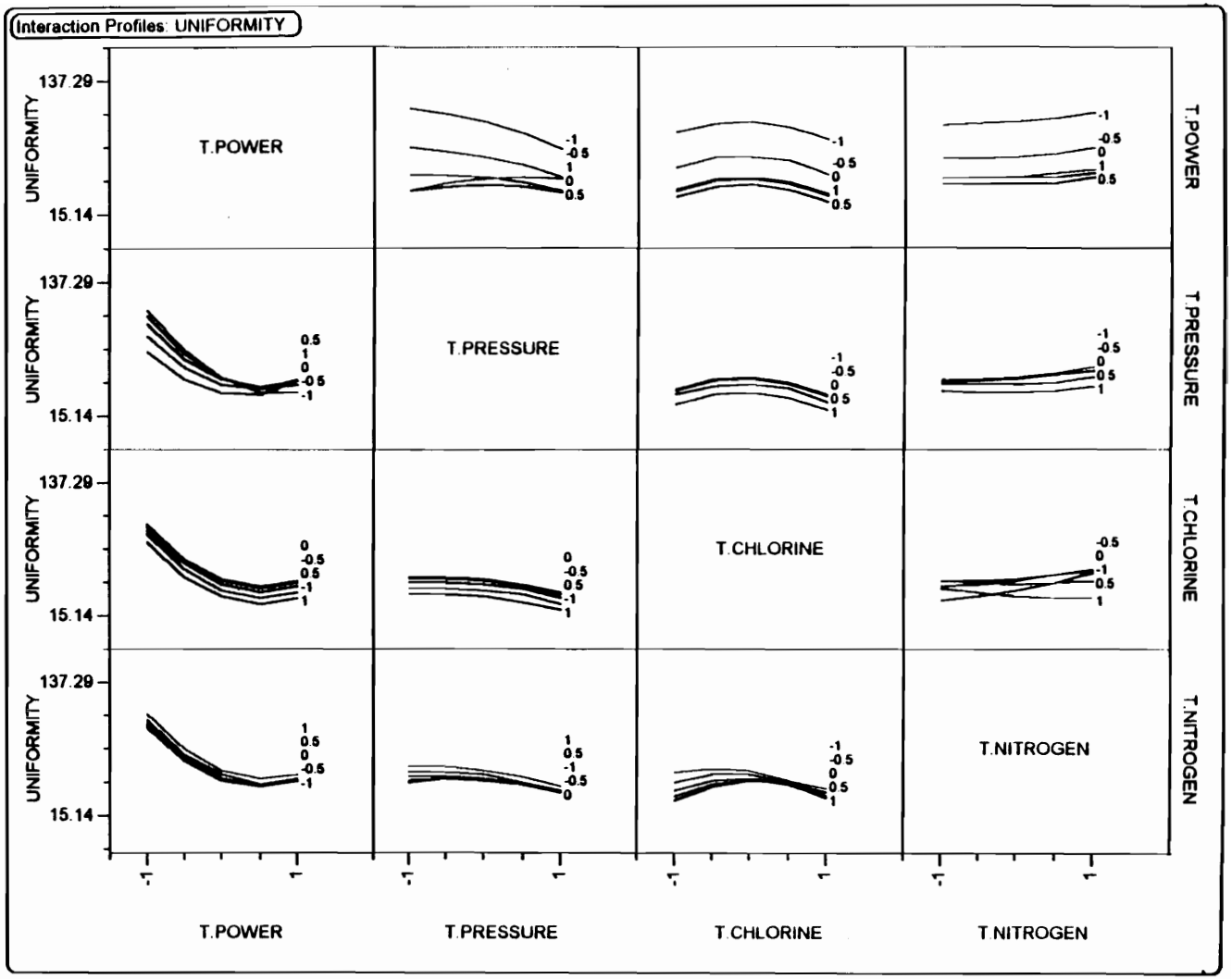

Fig. 6.5(k) Interaction profiles for uniformity in Ti etch DOE

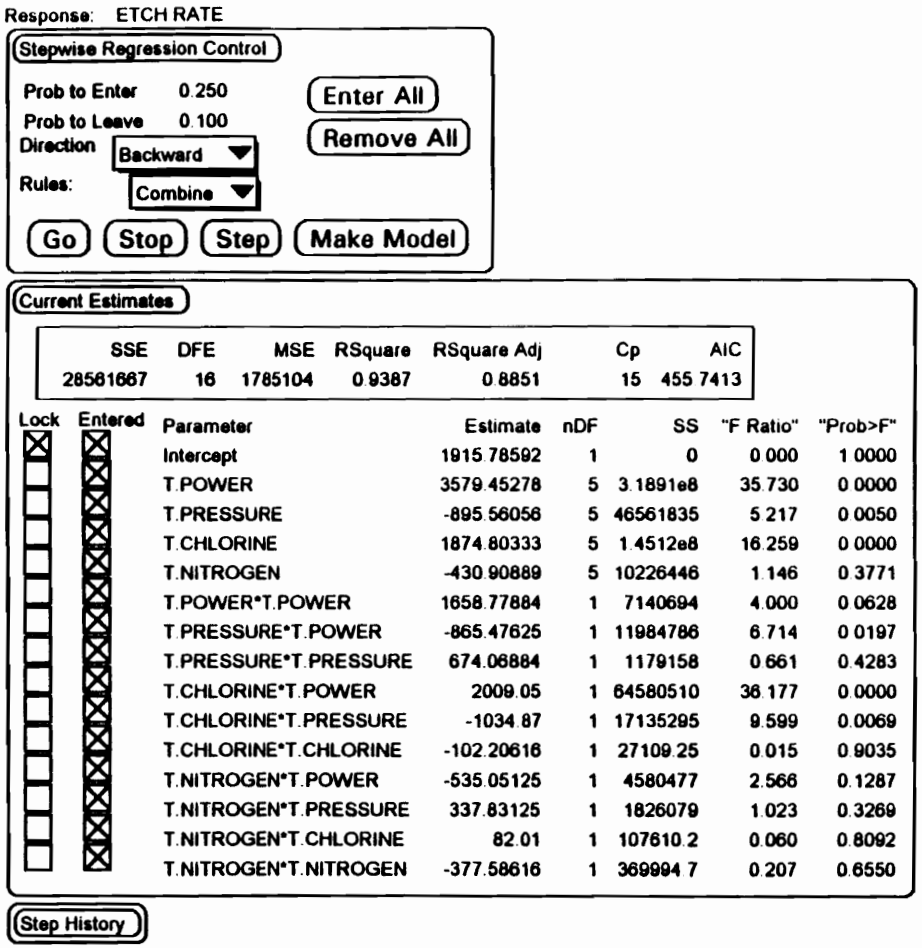

Fig. 6.5(l) Stepwise regression model optimization for etch rate in Ti etch DOE (all factors included)

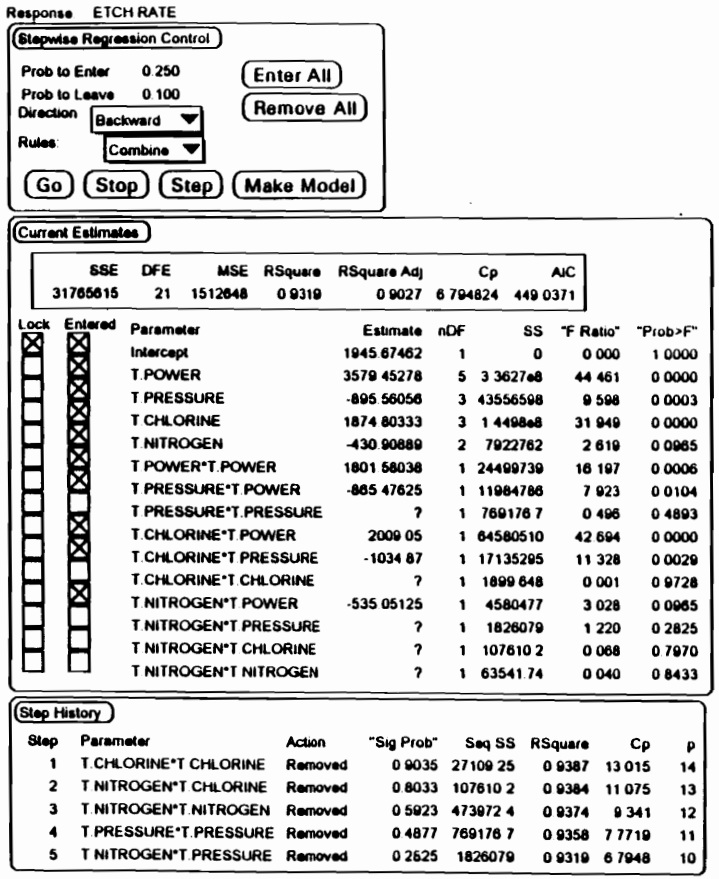

Response ETCH RATE

Stepwise Regression Control

Prob to Enter 0.250
Prob to Leave 0.100
Direction Backward
Rules Combine

Enter All
Remove All
Go
Stop
Step
Make Model

Current Estimates

SSE	DFE	MSE	RSquare	RSquare Adj	Cp	AIC
31765615	21	1512648	0.9319	0.9027	6.794824	449.0371

Lock	Entered	Parameter	Estimate	nDF	SS	"F Ratio"	"Prob>F"
☒	☒	Intercept	1945.67462	1	0	0.000	1.0000
☐	☒	T.POWER	3579.45278	5	3.3627e8	44.461	0.0000
☐	☒	T.PRESSURE	-895.56056	3	43556598	9.598	0.0003
☐	☒	T.CHLORINE	1874.80333	3	1.4498e8	31.949	0.0000
☐	☒	T.NITROGEN	-430.90889	2	7922762	2.619	0.0965
☐	☒	T.POWER*T.POWER	1801.58038	1	24499739	16.197	0.0006
☐	☒	T.PRESSURE*T.POWER	-865.47625	1	11984786	7.923	0.0104
☐	☐	T.PRESSURE*T.PRESSURE	?	1	769176.7	0.496	0.4893
☐	☒	T.CHLORINE*T.POWER	2009.05	1	64580510	42.694	0.0000
☐	☒	T.CHLORINE*T.PRESSURE	-1034.87	1	17135295	11.328	0.0029
☐	☐	T.CHLORINE*T.CHLORINE	?	1	1899.648	0.001	0.9728
☐	☒	T.NITROGEN*T.POWER	-535.05125	1	4580477	3.028	0.0965
☐	☐	T.NITROGEN*T.PRESSURE	?	1	1826079	1.220	0.2825
☐	☐	T.NITROGEN*T.CHLORINE	?	1	107610.2	0.068	0.7970
☐	☐	T.NITROGEN*T.NITROGEN	?	1	63541.74	0.040	0.8433

Step History

Step	Parameter	Action	"Sig Prob"	Seq SS	RSquare	Cp	p
1	T.CHLORINE*T.CHLORINE	Removed	0.9035	27109.25	0.9387	13.015	14
2	T.NITROGEN*T.CHLORINE	Removed	0.8033	107610.2	0.9384	11.075	13
3	T.NITROGEN*T.NITROGEN	Removed	0.5923	473972.4	0.9374	9.341	12
4	T.PRESSURE*T.PRESSURE	Removed	0.4877	769176.7	0.9358	7.7719	11
5	T.NITROGEN*T.PRESSURE	Removed	0.2525	1826079	0.9319	6.7948	10

Fig. 6.5(m) Stepwise regression - optimized model parameters for etch rate in Ti etch DOE

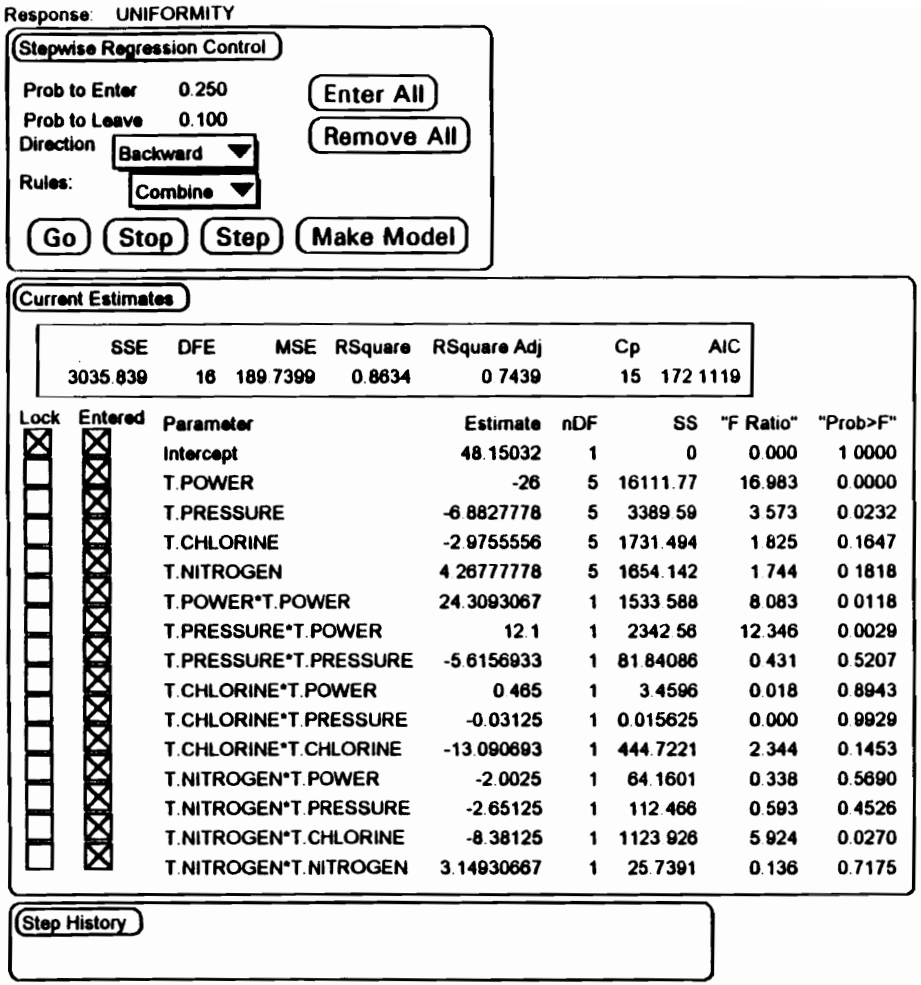

Fig. 6.5(n) Stepwise regression model optimization for uniformity in Ti etch DOE (All factors included)

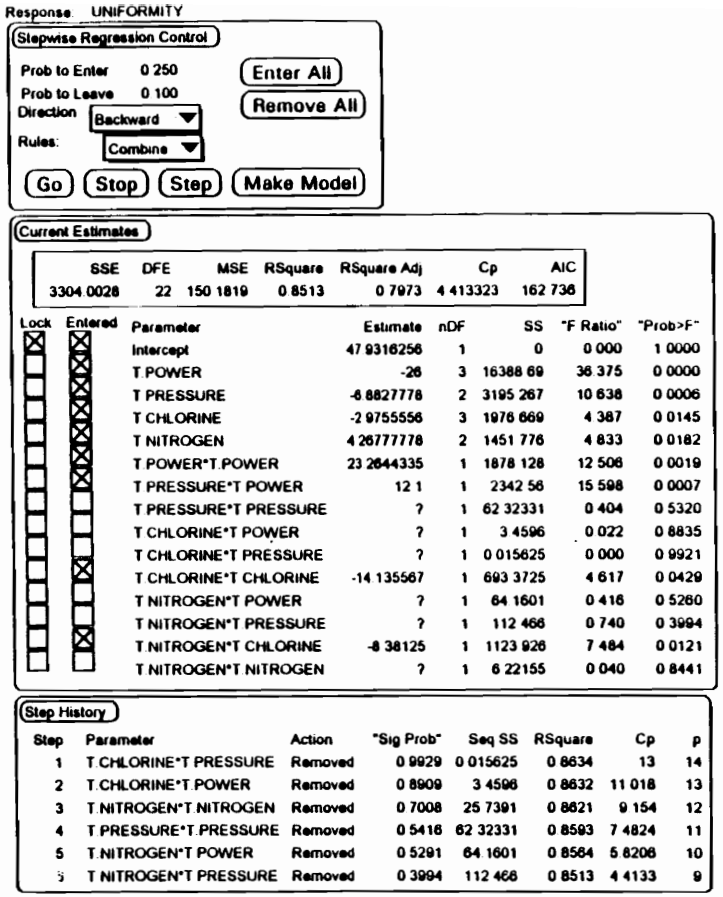

Response: UNIFORMITY

Stepwise Regression Control

Prob to Enter 0.250 | Prob to Leave 0.100 | Direction: Backward | Rules: Combine

Enter All | Remove All | Go | Stop | Step | Make Model

Current Estimates

SSE	DFE	MSE	RSquare	RSquare Adj	Cp	AIC
3304.0028	22	150.1819	0.8513	0.7973	4.413323	162.736

Lock	Entered	Parameter	Estimate	nDF	SS	"F Ratio"	"Prob>F"
☒	☒	Intercept	47.9316256	1	0	0.000	1.0000
☐	☒	T.POWER	-26	3	16388.69	36.375	0.0000
☐	☒	T.PRESSURE	-6.8827778	2	3195.267	10.638	0.0006
☐	☒	T.CHLORINE	-2.9755556	3	1976.669	4.387	0.0145
☐	☒	T.NITROGEN	4.26777778	2	1451.776	4.833	0.0182
☐	☒	T.POWER*T.POWER	23.2644335	1	1878.128	12.506	0.0019
☐	☒	T.PRESSURE*T.POWER	12.1	1	2342.56	15.598	0.0007
☐	☐	T.PRESSURE*T.PRESSURE	?	1	62.32331	0.404	0.5320
☐	☐	T.CHLORINE*T.POWER	?	1	3.4596	0.022	0.8835
☐	☐	T.CHLORINE*T.PRESSURE	?	1	0.015625	0.000	0.9921
☐	☒	T.CHLORINE*T.CHLORINE	-14.135567	1	693.3725	4.617	0.0429
☐	☐	T.NITROGEN*T.POWER	?	1	64.1601	0.416	0.5260
☐	☐	T.NITROGEN*T.PRESSURE	?	1	112.466	0.740	0.3994
☐	☒	T.NITROGEN*T.CHLORINE	-8.38125	1	1123.926	7.484	0.0121
☐	☐	T.NITROGEN*T.NITROGEN	?	1	6.22155	0.040	0.8441

Step History

Step	Parameter	Action	"Sig Prob"	Seq SS	RSquare	Cp	p
1	T.CHLORINE*T.PRESSURE	Removed	0.9929	0.015625	0.8634	13	14
2	T.CHLORINE*T.POWER	Removed	0.8909	3.4596	0.8632	11.018	13
3	T.NITROGEN*T.NITROGEN	Removed	0.7008	25.7391	0.8621	9.154	12
4	T.PRESSURE*T.PRESSURE	Removed	0.5416	62.32331	0.8593	7.4824	11
5	T.NITROGEN*T.POWER	Removed	0.5291	64.1601	0.8564	5.8208	10
6	T.NITROGEN*T.PRESSURE	Removed	0.3994	112.466	0.8513	4.4133	9

Fig. 6.5(o) Stepwise regression - optimized model parameters for uniformity in Ti etch DOE.

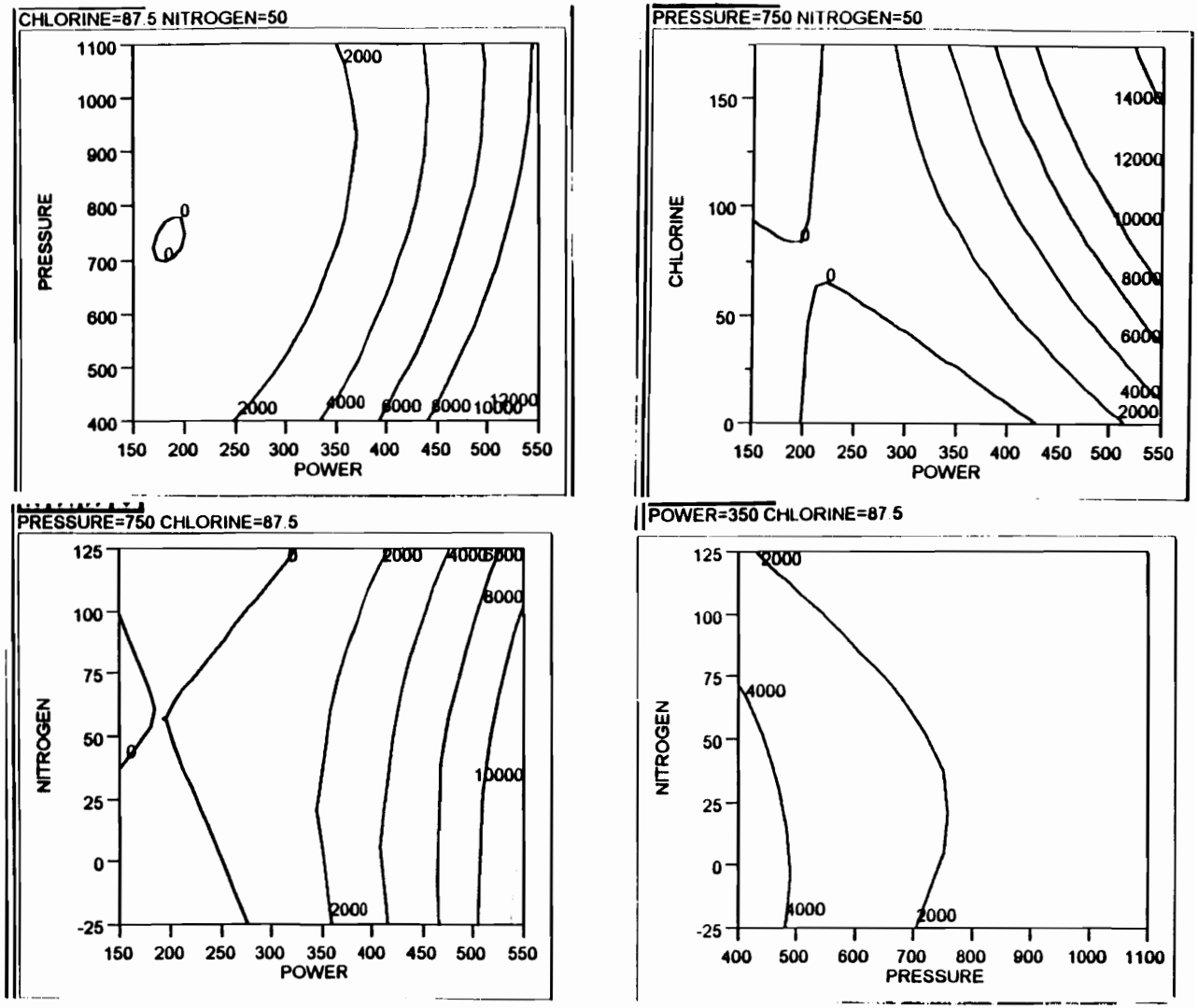

Fig. 6.5(p) Contour plots for etch rate in Ti etch DOE.

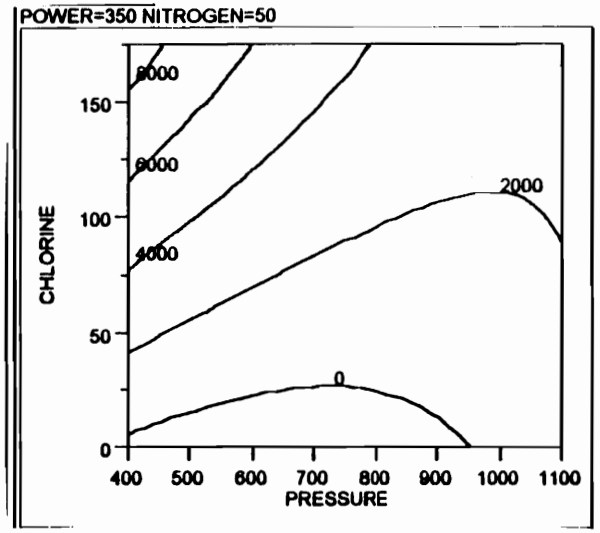

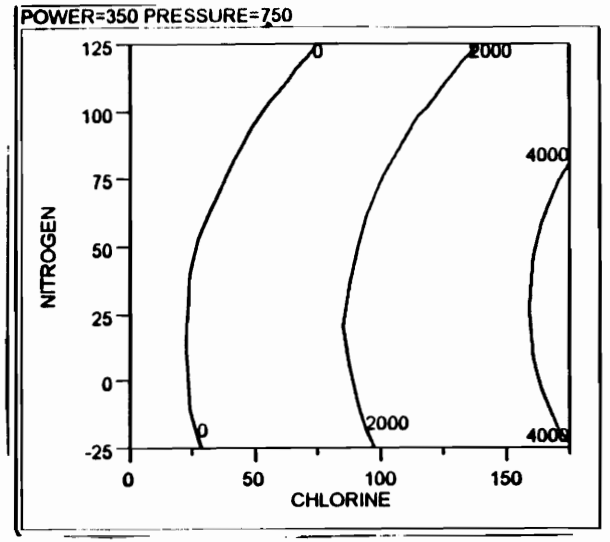

Fig. 6.5(p) Contd. Contour plots for etch rate in Ti etch DOE.

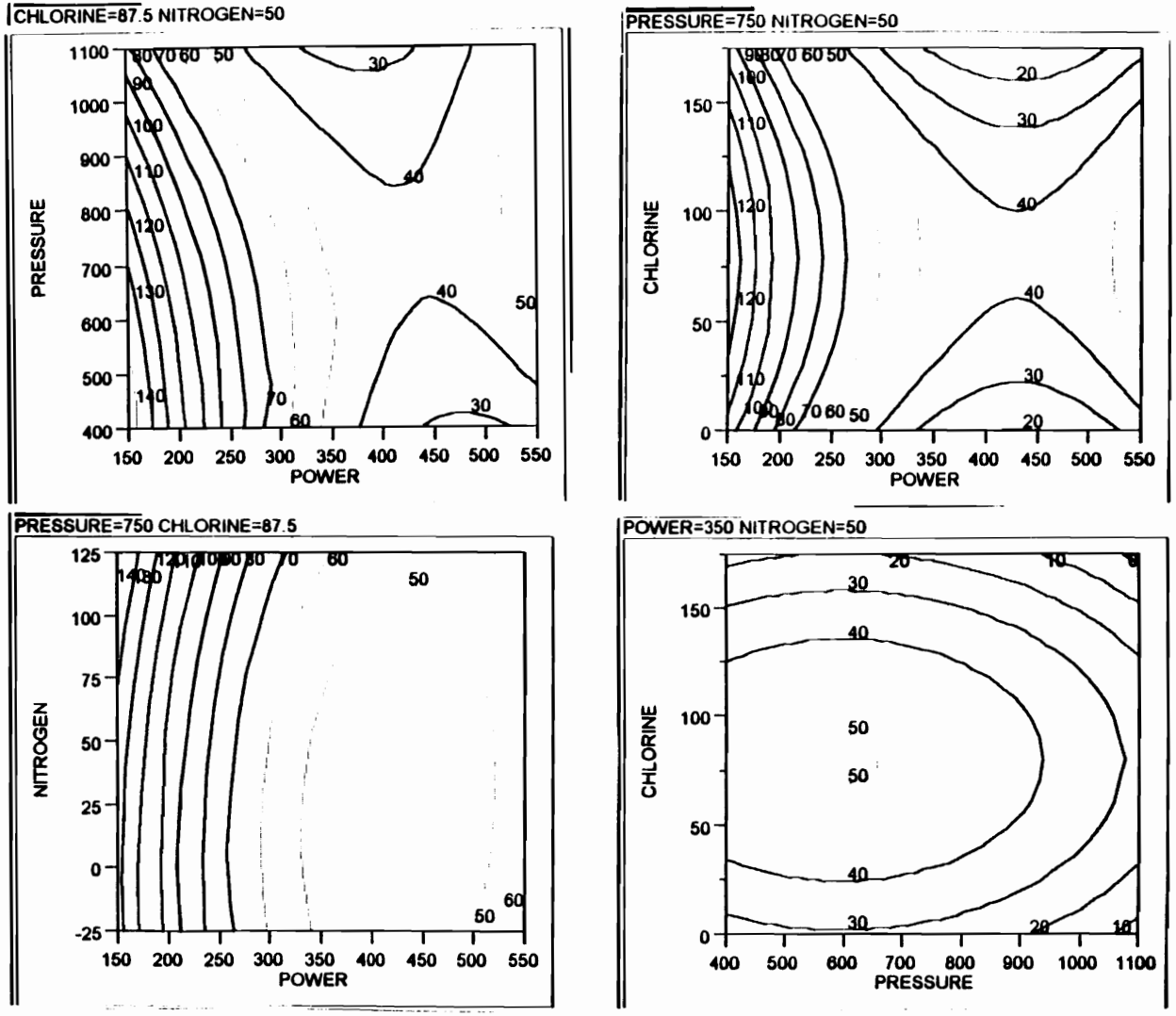

Fig. 6.5(q) Contour plots for uniformity in Ti etch DOE.

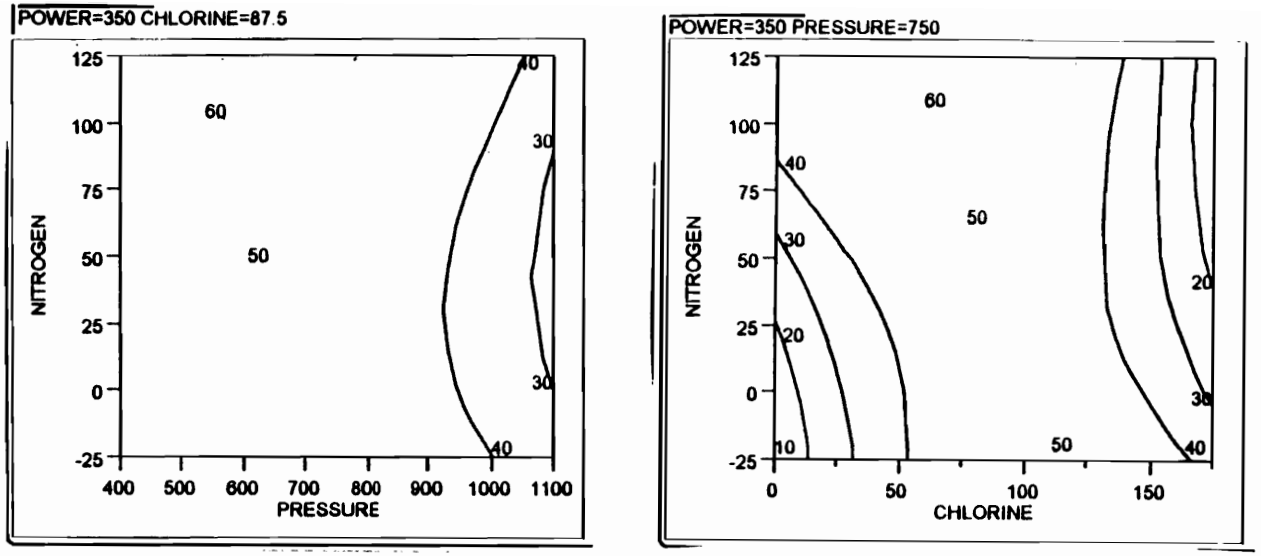

Fig. 6.5(q) Contd. Contour plots for uniformity in Ti etch DOE.

Chapter 7

Summary, Conclusions and Further Research

In the previous chapters, the Ti and TiN etch characterization experiments performed in Lam Rainbow 4600 were discussed. The effect of the process parameters on the Ti and TiN etch rates were discussed in detail and an attempt was made to explain the behavior of the etch process based on the plasma principles. In this concluding chapter, the contents of the previous chapters are summarized. The conclusions that were drawn from this work are also listed. Recommendations for further research to throw more light into the unanswered questions are discussed at the end of this chapter.

7.1 Summary

The research work was aimed at studying the complex characteristics of Ti and TiN etch processes in Cl_2/N_2 and $Cl_2/BCl_3/N_2$ plasmas, respectively. The etch rates and uniformity were studied as a function of the process parameters such as etch time, gas flow, RF power, pressure, and temperature in a classical type of experiment. Initially, the parameters were varied one at a time while maintaining other parameters at a fixed level. These experiments yielded an insight into the individual effect of the parameter on the etch rate and etch uniformity. However, the higher order effects and the interaction between the variables play a significant role in determining the outcome of the etch process. The classical experiments do not yield any quantitative information on higher order effects and the interactions. Therefore, statistical methods were used to design experiments and analyze them in order to develop response surface models to mathematically represent the

etch processes. These empirical models, in addition to main effects, include second order effects and two factor interactions. These models are found to be good representations of most of the processes. The availability of models enable one to predict the responses anywhere within the experimental space without actually running the experiment.

In chapter 1, the applications of Ti and TiN films were presented in order to emphasize the extent of use of these films in semiconductor devices. The important properties of these films were also discussed in this chapter. Major techniques used for deposition and etching of Ti and TiN films were also discussed, in order to provide the reader with necessary background information.

The chapter 2 discussed about the equipments used in this work. First, the fundamentals of sputter deposition process were discussed, followed by a description of the equipments, MRC Eclipse and ULVAC, which were used for TiN deposition and Ti deposition, respectively The basics of dry metal etch process was also discussed using plasmas, followed by a description of the Lam Rainbow 4600 metal etch system, in which all of the etch studies were conducted. This chapter also covered the four point probe technique used for sheet resistance measurements and the 4D four probe instrument.

In chapters 3, 4, and 5, a description on the characterization experiments was presented. These experiments were conducted to study the effect of individual process parameters on the etching of TiN or Ti film. In chapter 3, the etch characterization of TiN film in Cl_2/N_2 plasmas was presented. The effects of etch time, Cl_2, N_2 gas flow rate, RF power, pressure, and temperature were investigated based on the experiments performed. The results were explained based on the plasma fundamentals and the factors having major

impact on the etch process were identified. In chapter 4, the details of TiN etch characterization in BCl_3 plasmas were discussed. The effects of process parameters including BCl_3 gas flow were studied. In chapter 5, the same studies were conducted on Ti film in a Cl_2/N_2 plasmas. BCl_3 did not have any effect on the Ti etch process and hence it was not included in this study.

The plasma processes are very complex in nature and hence one needs to investigate the second and higher order effects of the process variables and interaction between the variables. The classical experimental techniques described in chapters 3, 4, and 5 yield only first order effects of the process variables. The statistical methods are available for design and analysis of experiments to obtain information on higher order effects and interaction between variables. In chapter 6, the design and analysis of experiments using RSM (response surface methodology) was discussed. Separate experiments were designed and conducted to study the etch characteristics of Ti and TiN films. Mathematical models were developed based on the results obtained from these experiments. Contour maps were drawn to visualize the responses in terms of process variables.

7.2 Conclusions

In this section, the conclusions drawn from the Ti and TiN etch characterization experiments are presented. A separate subsection is devoted to each of films in different plasmas. The last subsection summarizes the conclusions drawn from the RSM design of experiment and analysis.

7.2.1 TiN etch in Cl_2/N_2 plasmas

In chapter 3, the etch characterization of TiN film in Cl_2/N_2 plasmas with the variation of process parameters such as etch time, chlorine and nitrogen gas flows, RF power, and chamber pressure was discussed. From the results of these experiments, the following conclusions were derived:

(i) There is a 3 second induction time before TiN film starts etching. The TiN etch rate increases with increase in the etch time probably due to an increase in wafer temperature with the prolonged exposure to plasma and reaches a maximum as the wafer temperature reaches a steady state.

(ii) The etch rate increases linearly with the increase in chlorine flow in the low flow region due to increase in the availability of the reactant gas species. At high chlorine flow, the etch rate levels off due to saturation of ionization of reactant chlorine.

(iii) Increase in nitrogen gas flow can decrease the etch rate due to dilution of the plasma of chlorine which is the main reactant.

(iv) The etch rate increases almost linearly with the increase in RF power. The average TiN etch rate is higher when the RF power is applied to the bottom electrode due to ion-assisted etching in addition to the plasma chemical etching already present .

(v) The increase in chamber pressure from 500 to 800 mTorr decreases the etch rate both bottom powered and top powered processes, and remain constant beyond 800 mTorr. The increased residence time appears to reduce the TiN etch rate.

7.2.2 TiN etch in BCl_3 plasmas

In chapter 4, the etch rate characteristics of TiN film in BCl_3 plasmas with the variation of the process parameters such as time, BCl_3 gas flow, RF power, reaction pressure, and temperature were discussed. A summary of the results are given in this section.

(i) The BCl_3 gas is used along with other gases such as chlorine to etch through the hard surface oxide on the metal films and to scavenge moisture from the etch chamber.

(ii) The TiN etch rate in BCl_3 plasma is about two to three orders of magnitude less than the etch rate in Cl_2 plasma. This is due to the decreased availability of the etchant chlorine species as the bond energy of BCl_3 and it is radicals is higher than that of Cl-Cl bond.

(iii) There is an induction time of 3 seconds before the etching of TiN started. The etch rate increases with etch time, but levels off as the etch duration is increased to 50 seconds and beyond probably due to the wafer reaching a thermal steady state.

(iv) The etch rate increases with the increase in BCl_3 gas flow due to the increased supply of etchant species. The etch rate is observed to be in the flow-rate limited regime.

(v) A strong dependence of the etch rate on applied RF power is observed due to the fact that the ionization increases with increase in RF power. The etch rate is 10 % higher when the RF power is applied to the bottom electrode than when RF power is applied to the top electrode because of increased ion bombardment as a result of negative voltage, Vdc, induced at the surface of the wafer.

(vi) The pressure and temperature do not have significant effect on the TiN etch rate. So it can be concluded that TiN etching in BCl_3 plasma is primarily flow rate limited.

7.2.3 Ti etch in Cl_2/N_2 plasmas

In chapter 5, the etch characteristics of Ti in Cl_2/N_2 plasmas with the variation of etch time, N_2 and Cl_2 flow, RF power, etch chamber pressure, and temperature were examined. Examining the data obtained from the experiments, the following conclusions can be drawn:

(i) There is about 4 seconds induction time before Ti etching starts. Then, the etch rate increases to ~ 5500 Å/min for 80 s etch time due to settling of plasma parameters and the heating effects of the plasma on the wafer.

(ii) The Ti etch rate is supply rate limited up to a chlorine flow of 125 sccm, and levels off beyond 125 sccm of chlorine flow due to saturation in ionization and/or reaction rate limiting.

(iii) An increase in N_2 flow up to 10 sccm, increased the etch rate due to an increase in ion-assisted etching of Ti because of the availability of nitrogen ions for bombardment. However, higher N_2 flows beyond 10 sccm, reduced the etch rate due to dilution.

(iv) RF power has the maximum effect on the etch rate causing a six fold increase as the RF power is increased from 200 W to 600 W. The etch rate increase with RF power can be attributed to increased ionization of gases in the plasma, heating effects of the plasma on the substrate due to high power density, and high negative Vdc in the case of bottom powered electrode. The Vdc is positive for top powered electrode and does not contribute to ion-assisted etching.

(v) An increase in pressure leads to a decrease in the etch rate due to an increase in collisions between etchant species traveling towards the substrate and the atoms/molecules present in the plasma.

(vi) The temperature dependence of the Ti etch rate is weak when compared to other parameters such as RF power and Cl_2 flow rate in the region of this work. This region of temperature is believed to be in a transition between etchant adsorption and product desorption. Investigations need to be done to explain the decrease in the etch rate between 55 and 60 °C by performing etch rate experiments at temperatures below 60 °C.

7.2.4. RSM design of experiment and modeling

In chapter 6, the concept of design of experiments and analysis were discussed. The terms used in the analysis of the experiments were defined. An RSM experiment was designed using JMP software for each of TiN and Ti plasma etch processes. The experiment was performed according to the design and the results were analyzed using JMP software. Empirical quadratic models were developed for etch rate and etch uniformity in both TiN and Ti etch processes. These models enable an experimenter to observe the significance of the factors (process parameters) on each of the responses. The models, when combined with the knowledge of the process, could be used for optimization. From the RSM design and analysis of experiments, the following major conclusions can be drawn:

(i) The models for etch rate and uniformity developed using the observations from RSM experiments bring out the significance of two factor interactions and second order effects in TiN and Ti plasma etch processes.

(ii) In both TiN and Ti etch processes, RF power and chlorine flow appear to be the most dominant factors in determining the etch rates. The observations obtained from these models are consistent with the theory developed in the Chapters 3, 4, and 5 based on the experiments done varying one parameter at a time.

(iii) Nitrogen addition dilutes the plasma of the etchant species and hence leads to reduction in etch rate.

(iv) The reactor pressure has an adverse effect on the etch rate. It affects Ti etch process much more than the TiN etch process as can be seen from the magnitude of these coefficients.

(v) Increase of all the factors except nitrogen lead to better uniformity. Chlorine is the most significant contributor to the uniformity in TiN etching whereas RF power is found to be the dominant contributor to Ti etching.

(vi) Increase of nitrogen flow leads to increase in percentage uniformity probably due to depletion of etchant species.

(vii) There is a high amount of interaction between chlorine and RF power in both TiN and Ti etch processes.

(viii) The presence of second order terms indicate the relationship between the factors and responses are not simply linear, but highly nonlinear for factors such as RF power.

(ix) Contour plots are drawn for etch rate and uniformity responses for both Ti and TiN processes taking two factors at a time. These contour plots are used as a powerful tool for determining operating point for a process according to the specifications and optimizing an existing process.

7.3. Recommendations for Further Research

(i) More in depth studies are needed to determine the effect of temperature on the Ti and TiN etch rate. The etch rate experiments must be conducted at temperatures starting from 30 °C to 90 °C to determine whether there is an Arrhenius relationship.

(ii) The scope of the experiments need to be increased and experiments need to be performed outside the regime investigated in this work.

(iii) For the RSM design, confirmation runs have to processed at the optimized process conditions obtained from the model and the responses need to be compared against those obtained through the mathematical model to evaluate its validity.

(iv) Design of experiment has to be done to include wider parameter range. The experiments have to be repeated in order to confirm the models.

(v) Similar experiments need to be conducted on Ti and TiN films deposited in other sputter deposition equipments.

(vi) Characterization needs to be done on CVD TiN film, which are currently being used in semiconductor manufacturing.

(vii) Optimized processes for Ti and TiN etch need to be developed and implemented on a product wafer with topography. The results of these optimized processes on the product wafer need to be studied through CD (critical dimension) loss, etch residue, effect on the photoresist, extent of sidewall protection during etch, profile of the etched metal lines, the composition of sidewall polymer after etch (such as solubility in certain common solvents), selectivity to underlying silicon or silicon dioxide layers, step coverage, undercut/lateral etch, the effectiveness to etch Al-Cu, and W layers, and loading effect. SEM (Scanning Electron Microscope) pictures of the etched patterns could be done to determine its dimensions and profile.

(viii) Electrical measurements of the etched structures could be done in order to assess the minimum dimension and the statistical distribution across the wafer and wafer-to-wafer.

(ix) Analysis of species in the plasma needs to be done during the etch process using mass spectrometry of IR (Infrared) absorption and the results could interpreted based on the

variation of the amount of these species. Direct measurement of ion energies could be done to determine the extent and nature of ion bombardment.

(x) The effect of the etch processes on the surface composition of the Ti and TiN films could be investigated using X-Ray photospectroscopy and/or Auger electron spectroscopy.

(xi) Study of the damage to the MOS devices due to exposure to plasma could be done using antenna structures with various dimensions and new processes and equipment modifications could be developed to reduce the damage.

(xii) The photoemission from the plasma need to be analyzed using an optical spectrum analyzer and the variation of the signals at several wavelengths could be monitored. The etch endpoint detection could be done by identifying the signal wavelength that shows the maximum correlation to the end of etching of a particular film. This endpoint detection can be used to most suitable process recipe for etching a given film by switching the recipe after the previous film is etched.

There are endless possibilities for research in this topic and one is limited by only the time and availability of the processing and analysis facilities. The field of plasma processing is interesting and intriguing. The author hopes that his research work threw some light on the etching process of Ti and TiN films.

References

[1] G.S. Oehrlein, "Reactive ion etching", in Handbook of plasma processing technology, S.M. Rossnagel, J.J. Cuomo, and W.D. Westwood, Ed., Noyes Publications, New Jersey, pp. 195-232, 1990.

[2] C.J. Mogab, "Dry etching", in VLSI Technology, S.M. Sze, Ed., McGraw-Hill, pp. 303-345, 1983.

[3] C. Jerbic and K. Amberiadis, "Characteristics of TiN etching in Cl_2/N_2 plasmas", Proceedings of the Symposium on Interconnects, Contact Metallization, and Multilevel Metallization, The Electrochemical Society, Vol 93-25, pp 299-307, 1993.

[4] D. Heine, "Etch characteristics of reactively sputtered TiN", Project report, LSI Logic Corp., Milpitas, CA.

[5] D. Heine, "Pressure and power experiment on TiN and photoresist", Project report, LSI Logic Corp., Milpitas, CA.

[6] A. Kohlhase, M. Mandl, and W. Pamler, "Performance and failure mechanisms of TiN diffusion barrier layers in submicron devices", Journal of Applied Physics, Vol. 65. No. 6, pp. 2462-2469, 15 March 1989.

[7] M. Wittmer, "Self-aligned diffusion barrier by nitridation of $TiSi_2$", Journal of Applied Physics, Vol. 52, No. 19, pp. 1573-1575, 9 May 1988.

[8] C.K. Hu, N. Mazzeo, S. Basavaiah, and M.B. Small, "Dry etching of TiN/Al(Cu)/Si for very large scale integrated local interconnections", Journal of Vacuum Science and Technology, Vol. 8, No. 3, pp. 1498-1502, May/June 1990.

[9] A. Sherman, "Growth and properties of LPCVD titanium nitride as a diffusion barrier for silicon device technology", Journal of Electrochemical Society, Vol. 137, No. 6, pp. 1892-1897, June 1990.

[10] Y.H. Hu, S.K. Lee, D.K. Shih, and D.L. Kwong, "Suppression of lateral silicide growth by ion beam mixing and rapid thermal annealing", Applied Physics Letters, Vol. 52, No. 11, pp. 877-879, 14 March 1988.

[11] M. Rocke and M. Schneegans, "Titanium nitride for antireflection control and hillock suppression on aluminum silicon metallization", Journal of Vacuum Science and Technology B, Vol. 6, No. 4, pp. 1113-1115, July/August 1988.

[12] B. Chapman, "Glow Discharge Processes", pp 297-347, Wiley-Interscience, New York, 1980.

[13] S. Gupta, J-S. Song, and V. Ramachandran, "Materials for contacts, barriers and interconnects", Semiconductor International, pp. 80-87, October 1989.

[14] M.K. Khan and L. Schmidt, "Understanding electromigration: A simple new life profile technique", Semiconductor International, pp. 102-106, November 1989.

[15] D.J. Harra, "Improve reactive sputter deposition of titanium nitride films", Semiconductor International, pp. 96-99, December 1989.

[16] W.L. Smith, C.G. Wells, and A. Bivas, "Evaluating voids and microcracks in Al metallization", Semiconductor International, pp. 92-95, January 1990.

[17] K.C. Cadien, S. Sivaram, and C.D. Reintsema, "Dry etching of $TiSi_2$", Journal of Vacuum Science and Technology A, Vol. 4, No. 3, pp. 739-743, May/June 1986.

[18] K. Hashimoto and H. Onoda, "Bias-induced structure transition in reactively sputtered TiN films", Applied Physics Letters, Vol. 54, No. 2, pp. 120-122, 9 January 1989.

[19] C.S. Wang, "Plasma etch method for TiO2", United States Patent Number 4,574,177, March 4, 1986.

[20] R. d'Agostino, F. Fracassi, C. Pacifico, and P. Capezzuto, "Plasma etching of Ti in fluorine containing feeds", Journal of Applied Physics, Vol. 71. No. 1, pp. 462-471, 1 January 1991.

[21] M. Ranta, "Dry etching of titanium", ISPC-7 Eindhoven, pp. 966-970, July 1985.

[22] A. Manenschjin, E. van der Drift, G.C.A.M. Janssen, and S. Radelaar, "Cl_2 reactive ion etching mechanisms studied by in situ determination of ion energy and ion flux", Journal of Applied Physics, Vol. 69. No. 12, pp. 7996-8004, 15 June 1991.

[23] I. Miller, R. Frazier, and M. Su, "On Submicron devices", Microelectronics, January 1992.

[24] H. Aoki, E. Ikawa, T. Kikkawa, Y. Teraoka, and I. Nishiyama, "After-corrosion suppression using low-temperature Al-Si-Cu etching", Japanese Journal of Applied Physics, Vol. 30. No. 7, pp. 1567-1570, July 1991.

[25] M.C. Peignon, Ch. Cardinaud, and G. Turban, "Etching processes of tungsten in SF_6-O_2 radio-frequency plasmas", Journal of Applied Physics, Vol. 70. No. 6, pp. 3314-3322, 15 September 1991.

[26] J-S Maa, H. Gossenberger, and L. Hammer, " Effects on sidewall profile of Si etched in BCl_3/Cl_2 chemistry", Journal of Vacuum Science and Technology B, Vol. 8, No. 4, pp. 581-585, July/August 1990.

[27] N. Parekh and J. Price, "Corrosion characterization of metallization systems with XRF", VMIC conference, pp. 506, June 12-13, 1989.

[28] J. Curry, G. Fitzgibbon, Y. Guan, R. Muollo, G. Nelson, and A. Thomas, "New failure mechanisms in sputtered aluminum-silicon films", Proceedings of IEEE/IRPS, pp. 6-8, 1984.

[29] S. Mayumi, I. Murozono, H. Nanatsue, and Ueda, "Corrosion-induced contact failures in double-level Al-Si-Cu metallization", Journal of Electrochemical Society, Vol. 137, No. 6, pp. 1861-1867, June 1990.

[30] J.D. Lawrence and J.W. McPherson, "Corrosion susceptibility of Al-Cu and Al-Cu-Si films", Proceedings of IEEE/IRPS, pp. 102-106, 1991.

[31] K. Sakuma, S. Yagi, and K. Imai, "Study of a veil structure and a two-step corrosion suppression process in Al-Si-Cu etching", Extended Abstracts of the 1992 International Conference on Solid State Devices and Materials , Tsukuba, pp. 93-95, 1992.

[32] D. Weston, S.R. Wilson, and M. Kottke, "Microcorrosion of Al-Cu and Al-Cu-Si alloys: Interaction of metallization with subsequent aqueous photolithographic

processing", Journal of Vacuum Science and Technology A, Vol. 8, No. 3, pp. 2025-2032, May/June 1990.

[33] D.A. Danner, M. Dalvie, and D.W. Hess, "Plasma etching of aluminum - a comparison of chlorinated etchants", Journal of Electrochemical Society, Vol. 134, No. 3, pp. 669-673, March 1987.

[34] S. Somekh, "Introduction to ion and plasma etching", Journal of Vacuum Science and Technology , Vol. 13, No. 5, pp. 1003-1007, September/October 1976.

[35] S. Kanai, K. Nojiri, M. Nawata, "Microwave plasma etching system", Semiconductor International, pp 71-76, May 1992.

[36] L. Peters, "Plasma etch chemistry: the untold story", Semiconductor International, pp 66-70, May 1992.

[37] K. Gupta, "Contact etch", Internal report, LSI Logic Corporation, Milpitas, CA.

[38] G.J. van der Kolk, M.J. Verkerk, and W.A.M.C. Brankaert, "Effects of contamination on aluminum films", Semiconductor International, pp 224-228, May 1988.

[39] A. Metze, D.W. Ernie, and H.J. Oskam, "The energy distribution of ions bombarding electrode surfaces in rf plasma reactors", Journal of Applied Physics, Vol. 65. No. 3, pp. 993-998, 1 February 1989.

[40] S. Menezes, R. Haak, G. Hagen, and M. Kendig, "Photoelectrochemical characterization of corrosion inhibiting oxide films on aluminum and its alloys", Journal of Electrochemical Society, Vol. 136, No. 7, pp. 1884-1886, July 1989.

[41] G.S. Oehrlein, S.W. Robey, J.L. Lindstrom, K.K. Chan, M.A. Jaso, and G.J. Scilla, "Surface modifications of electronic materials induced by plasma etching", Journal of Electrochemical Society, Vol. 136, No. 7, pp. 2050-2057, July 1989.

[42] L.Y. Tsou, "Effect of photoresist on plasma etching", Journal of Electrochemical Society, Vol. 136, No. 8, pp. 2354-2356, August 1989.

[43] D.N.K. Wang, "Ion assisted plasma etching of aluminum and its alloys", Technical Report, Applied Materials Inc., pp. 1-5, May 1983.

[44] C.B. Shin and D.J. Economou, "Effect of transport and reaction on the shape evolution of cavities during wet chemical etching", Journal of Electrochemical Society, Vol. 136, No. 7, pp. 1997-2004, July 1989.

[45] B. Chapman and M. Nowak, "Troublesome aspects of aluminum plasma etching", Semiconductor International, pp. 139-152, November 1980.

[46] D.H.G. Choe, C. Knapp, and A. Jacob, "Productive RIE - II. Selective aluminum alloy etching", Solid State Technology, pp. 165-171, March 1985.

[47] R.H. Bruce and G.P. Malafsky, "High rate anisotropic aluminum etching", Journal of Electrochemical Society: Solid-State Science and Technology, Vol. 130, No. 6, pp. 1369-1372, June 1983.

[48] T.H. Daubenspeck and E.J. White, "Reactive ion etching of tungsten with chlorinated fluorocarbons", Journal of Electrochemical Society, Vol. 136, No. 10, pp. 2973-2979, October 1989.

[49] W. Zagozdzon-Wosik, "Defect generation and gettering during rapid thermal annealing", Journal of Electrochemical Society: Solid-State Science and Technology, Vol. 135, No. 8, pp. 2065-2069, August 1988.

[50] H.B. Bell, H.M. Anderson, and R.W. Light, "Reactive ion etching of aluminum/silicon in BBr_3/Cl_2 and BCl_3/Cl_2 mixtures", Journal of Electrochemical Society: Solid-State Science and Technology, Vol. 135, No. 5, pp. 1184-1191, May 1988.

[51] T.H. Fedynyshyn and G.W. Grynkewich, "The effect of metal masks on plasma etch rate of silicon", Journal of Electrochemical Society, Vol. 136, No. 6, pp. 1799-1804, June 1989.

[52] P-I. Lee, J. Cronin, and C. Kaanta, "Chemical vapor deposition of tungsten (CVD W) as submicron interconnection and via stud", Journal of Electrochemical Society, Vol. 136, No. 7, pp. 2108-2112, July 1989.

[53] S.B. Dolins, A. Srivastava, and B.F. Flinchbaugh, "Monitoring and diagnosis of plasma etch processes", IEEE Transactions on Semiconductor Manufacturing, Vol. 1, No. 1, pp. 23-27, February 1988.

[54] H. Shin and C. Hu, "Monitoring plasma-process induced damage in thin oxide", IEEE Transactions on Semiconductor Manufacturing, Vol. 6, No. 2, pp. 96-102, May 1993.

[55] K.J. Mclaughlin, T.F. Edgar, and I. Trachtenberg, "Real-time monitoring and control in plasma etching", IEEE Control Systems, pp 3-10, April 1991.

[56] S.P. Venkatesan, T.F. Edgar, and I. Trachtenberg, "On the dynamics of an isothermal radial-flow plasma etcher", Journal of Electrochemical Society, Vol. 136, No. 9, pp. 2532-2545, September 1989.

[57] L.E. Kline and M.J. Kushner, "Computer simulation of materials processing plasma discharges", Critical Reviews in Solid State and Material Sciences, Vol. 16, Issue 1, 1989.

[58] S. Noda, S. Nishikawa, and S. Ohno, "MOS gate etching using an advanced magnetron etching system", Japanese Journal of Applied Physics, Vol. 28. No. 11, pp. 2362-2367, November 1989.

[59] A. Nagata, H. Ichihashi, and Y. Kusunoki, "Downstream etching of Si and SiO_2 employing CF_4/O_2 or NF_3/O_2 at high temperature", Japanese Journal of Applied Physics, Vol. 28. No. 11, pp. 2368-2371, November 1989.

[60] J.A. Barkanic, D.M. Reynolds, R.J. Jaccodine, H.G. Stenger, J. Parks, and H. Vedage, "Plasma etching using NF_3: A review", Solid State Technology, pp. 109-115, April 1989.

[61] P.E. Riley and D.A. Hansen, "Study of etch rate characteristics of SF_6/He plasmas by response-surface methodology: Effects of interelectrode spacing", IEEE Transactions on Semiconductor Manufacturing, Vol. 2, No. 4, pp. 178-182, November 1989.

[62] P.E. Riley, T.E. Clark, E.F. Gleason, and M.M. Garver, "Implementation of tungsten metallization in multilevel interconnection technologies", IEEE

Transactions on Semiconductor Manufacturing, Vol. 3, No. 4, pp. 150-157, November 1990.

[63] R.L. Torrisi, P. Vasquez, O. Viscuso, and C. Magro, "surface characterization of the Al/Si-Ti/W metallization after plasma treatments", Journal of Electrochemical Society, Vol. 138, No. 4, pp. 1171-1174, April 1991.

[64] J.M. Parks and R.J. Jaccodine, "Plasma etching of tungsten polycide structures using NF_3-mixed halocarbon etchants", Journal of Electrochemical Society, Vol. 138, No. 9, pp. 2736-2714, September 1991.

[65] G.S. May, J. Huang, and C.J. Spanos, "Statistical experimental design in plasma etch modeling", IEEE Transactions on Semiconductor Manufacturing, Vol. 4, No. 2, pp. 83-98, May 1991.

[66] S-K. Park and D.J. Economou, "A mathematical model for etching of silicon using CF_4 in a radial flow plasma reactor", Journal of Electrochemical Society, Vol. 138, No. 5, pp. 1499-1508, May 1991.

[67] H. Hubner, "Calculations on deposition and redeposition in plasma etch processes", Journal of Electrochemical Society, Vol. 139, No. 11, pp. 3302-3309, November 1992.

[68] G.G. Barna, "Automatic problem detection and documentation in a plasma etch reactor", IEEE Transactions on Semiconductor Manufacturing, Vol. 5, No. 1, pp. 56-59, February 1992.

[69] S. Yin, F.T.S. Yu, and S. Wu, "Optical monitoring for plasma-etching depth process", IEEE Photonics Letters, Vol. 4, No. 8, pp. 894-896, August 1992.

[70] G.C.H. Zau and H.H. Sawin, "Effects of O_2 feed gas impurity on Cl_2 based plasma etching of polysilicon", Journal of Electrochemical Society, Vol. 139, No. 1, pp. 250-256, January 1992.

[71] E.S. Aydil and D.J. Economou, "Modeling of plasma etching reactors including wafer heating effects", Journal of Electrochemical Society, Vol. 140, No. 5, pp. 1471-1481, May 1993.

[72] C. Jerbic, "Wafer-to-wafer repeatability of ULVAC TiN etch rate and uniformity for a 25 wafer batch", Project report, LSI Logic Corporation, Milpitas, CA, May 1991.

[73] C. Jerbic, "Characterization of MRC TiN etch rate and uniformity using RSM in the LRC 4600 etcher", Project report, LSI Logic Corporation, Milpitas, CA, July 1991.

[74] C. Jerbic, "Characterization of ULVAC TiN etch rate and uniformity using a 3-variable full factorial experiment", Project report, LSI Logic Corporation, Milpitas, CA, July 1991.

[75] I. Suni, M. Blomberg, and J. Sarilathil, "Performance of titanium nitride diffusion barriers in aluminum-titanium metallization schemes for integrated circuits", Journal of Vacuum Science and Technology A, Vol. 3, No. 6, pp. 2233-2236, Nov/Dec. 1985.

[76] J. Stimmel, "Properties of dc magnetron reactively sputtered TiN", Journal of Vacuum Science and Technology B, Vol. 4, No. 6, pp. 1377-1382, Nov/Dec. 1986.

[77] M. Wittmer, "Properties and microelectronic applications of thin films of refractory metal nitrides", Journal of Vacuum Science and Technology A, Vol. 3, No. 4 , pp. 1797-1803.

[78] H.F. Winters, "The etching of W(111) with XeF_2", Journal of Vacuum Science and Technology A, Vol. 3, No. 3, pp. 700-704, May/Jun 1985.

[79] S.P. Muraka, "Refractory silicides for integrated circuits", Journal of Vacuum Science and Technology, Vol. 17 , No. 4, pp. 775-792, Jul/Aug 1980.

[80] A. Armigliato, M. Finetti, J. Garrido, S. Guerri, P. Ostoja, and A. Scorzoni, "Ion-implanted, electron-beam annealed TiN films as diffusion barriers for Al on Si shallow junctions", Journal of Vacuum Science and Technology A, Vol. 3, No. 6, pp. 2237-2241, Nov/Dec 1985.

[81] C.K. Hu, B. Canney, D.J. Pearson, and M.B. Small, "A process for improved Al(Cu) reactive ion etching", Journal of Vacuum Science and Technology A, Vol. 7, No. 3, pp. 682-685, May/Jun 1989.

[82] A.J. Purdes, "Aluminum plasma etch limitations", Journal of Vacuum Science and Technology A, Vol. 1, No. 2, pp. 712-715, Apr/Jun. 1983.

[83] H.F. Winters, "The role of chemisorption in plasma etching", Journal of Applied Physics, Vol. 49, No. 10, pp. 5165-5170, Oct. 1978.

[84] C.J. Mogab, A.C. Adams, and D.L. Flamm, "Plasma etching of Si and SiO_2 - The effect of oxygen additions to CF4 plasmas", Journal of Applied Physics, Vol. 49, No. 7, pp. 3796-3803, July 1978.

[85] F. Fracassi and J.W. Coburn, "Plasma-assisted etching of tungsten films: A quartz-crystal microbalance study", Journal of Applied Physics, Vol. 63, No. 5, pp. 1758-1761, Mar 1988.

[86] D.A. Danner and D.W. Hess, "Reaction of atomic and molecular chlorine with aluminum", Journal of Applied Physics, Vol. 59, No. 3, pp. 940-947, Feb 1986.

[87] J.W. Coburn, H.F. Winters, and T.J. Chuang, "Ion-surface interactions in plasma etching", Journal of Applied Physics, Vol. 48, No. 8, pp. 3532-3540, Aug. 1977.

[88] S.M. Sze, "VLSI Technology", pp 303-346, McGraw-Hill, 1983.

[89] T.P. Chow and A.J. Steckl, "Plasma Etching of Refractory Gates for VLSI Applications", Journal of Electrochemical Society, Vol. 131, No. 10, pp. 2325-2335, October 1984.

[90] C.Y. Ting and B.L. Crowder, "Electrcial Properties of Al/Ti Contact Metallurgy for VLSI Application", Journal of Electrochemical Society, Vol. 129, No. 11, pp 2590-2594, November 1982.

[91] C.J. Mogab and T.A. Shankoff, "Plasma Etching of Titanium for Application to the Patterning of Ti-Pd-Au Metallization", Journal of Electrochemical Society, Vol. 124, No. 11, pp. 1766-1771, November 1977.

[92] P. May and A.I. Spiers, "Dry Etching of Aluminum/TiW Layers for Multilevel Metallization in VLSI", Journal of Electrochemical Society, Vol. 135, No. 6, pp. 1592-1594, June 1988.

[93] K. Tokunaga, F.C. Redekar, D.A. Danner, and D.W. Hess, "Comparison of Aluminum Etch Rates in Carbon Tetrachloride and Boron Trichloride Plasmas", Journal of Electrochemical Society, Vol. 128, No. 4, pp. 851-855, April 1981.

[94] T. Honda and W.W. Brandt, "Mass Spectrometric Transient Study of DC Plasma Etching of Si in NF_3 and NF_3/O_2 Mixtures", Journal of Electrochemical Society, Vol. 131, No. 11, pp. 2667-2670, November 1984.

[95] V.M. Donnelly, D.L. Flamm, C.W. Tu, and D.E. Ibbotson, "Temperature Dependence of InP and GaAs Etching in a Chlorine Plasma", Journal of Electrochemical Society, Vol. 129, No. 11, pp. 2533-2537, November 1982.

[96] D.H. Bower, "Plasma Etching of Polysilicon Using CCl_4 and NF_3", Journal of Electrochemical Society, Vol. 129, No. 4, pp. 795-799, April 1982.

[97] M. Sato and H. Nakamura, "The Effects of Mixing N_2 in CCL_4 on Aluminum Reactive Ion Etching", Journal of Electrochemical Society, Vol. 129, No. 11, pp. 2522-2527, November 1982.

[98] S.E. Bernacki and B.B. Kosicki, "Controlled Film Formation during CCl_4 Plasma Etching", Journal of Electrochemical Society: Solid-State Science and Technology, Vol. 131, No. 8, pp. 1926-1931, August 1984.

[99] C.B. Zorowin and R.S. Horwath, "Control of Plasma Etch Profiles with Plasma Sheath Electric Field and RF Power Density", Journal of Electrochemical Society, Vol. 129, No. 11, pp. 2541-2547, November 1982.

[100] K. Tokunaga and D.W. Hess, "Aluminum Etching in Carbon Tetrachloride Plasmas", Journal of Electrochemical Society: Solid-State Science and Technology, Vol. 127, No. 4, pp. 928-932, April 1980.

[101] A.J. Learn, "Evolution and Current Status of Aluminum Metallization", Journal of Electrochemical Society: Solid-State Science and Technology, Vol. 123, No. 6, pp. 894-906, June 1976.

[102] M.M. Chen and Y.H. Lee, "Heating Effects in Reactive Etching of Nb and Nb_2O_5", Journal of Electrochemical Society: Solid-State Science and Technology, Vol. 131, No. 9, pp. 2118-2123, September 1984.

[103] B.E. Thompson and H.H. Sarwin, "Polysilicon Etching in SF_6 RF Discharges - Characteristics and Diagnostic Measurements", Journal of Electrochemical Society: Solid-State Science and Technology, Vol. 133, No. 9, pp. 1887-1895, September 1986.

[104] C. Cardinaud, A. Rhounna, G. Turban, and B. Grolleau, "Contamination of Silicon Surfaces Exposed to CHF_3 Plasmas - An XPS Study of the Film and the Film-Surface Interface", Journal of Electrochemical Society: Solid-State Science and Technology, Vol. 135, No 6, pp. 1472-1477, June 1988.

[105] P.E. Riley, "Development of a Highly Uniform Silicon Dioxide Etching Process Using Response-Surface Methodology", Journal of Electrochemical Society:

Solid-State Science and Technology, Vol. 133, No. 9, pp. 1971-1972, September 1986.

[106] R.W. Light, "Reactive Ion Etching of Aluminum/Silicon", Journal of Electrochemical Society: Solid-State Science and Technology, Vol. 130, No. 11, pp. 2225-2230, November 1983.

[107] A.L. Keaton and D.W. Hess, "Aluminum etching in boron tribromide plasmas", Journal of Vacuum Science and Technology A, Vol. 3, No. 3, pp. 962-966, May/June 1985.

[108] C. B. Zarowin, "Reaction between the RF dishcarge parameters and plasma etch rates, selectivity, and anisotropy", Journal of Vacuum Science and Technology A, Vol. 2, No. 4, pp. 1537-1549, October-December 1984.

[109] C.J. Dell'Oca, D.L. Pulfrey, and L. Young, " Gaseous Anodization - Anodic Oxide Films", Physics of Thin Films, Vol. 6, pp 1-77, 1971.

[110] R.W. Bower, "Characteristics of aluminum-titanium electrical contacts on silicon", Applied Physics Letters, Vol. 23, No. 2, pp 99-101, July 1973.

[111] T. Smith, "Chlorine adsorption on clean aluminum", Surface Science, Vol. 32, pp 527-542, 1972.

[112] K. Watanabe, T. Tanigaki, and S. Wakayama, "The properties of LPCVD SiO2 film deposited by SiH2Cl2 and N2O mixtures", Journal of Electrochemical Society: Solid-State Science and Technology, Vol. 128, No. 12, pp. 2630-2635, December 1981.

[113] W.L. Brien, T.N. Rhodin, L.C. Rathbun, "Chemically enhanced ion etching on refractory metal silicides", Journal of Vacuum Science and Technology A, Vol. 6, No. 3, pp. 1384-1387, May/June 1988.

[114] W.L. Brien, T.N. Rhodin, L.C. Rathbun, "Ion-induced chlorination of titanium leading to enhanced etching", Journal of Chemical Physics, Vol. 89, No. 8, pp 5264-5272, October 1988.

[115] W.L. Brien and T.N. Rhodin, "Investigations of the altered surface formed during the ion-assisted etching of titanium", Journal of Vacuum Science and Technology B, Vol. 7, No. 5, pp. 1244-1251, Sep/Oct 1989.

[116] K. Blumenstock and D. Stephani "Anisotropic reactive ion etching of titanium", Journal of Vacuum Science and Technology B, Vol. 7, No. 4, pp. 627-632, Jul/Aug 1989.

[117] J.D. Chinn, W. Phillips, I. Adesia, and E.D. Wolf, "Ion Beam Etching of Silicon, Refractory Metals, and Refractory Metal Silicides Using a Chemistry Assisted Technique", Journal of Electrochemical Society: Solid-State Science and Technology, Vol. 131, No. 2, pp. 375-380, February 1984.

[118] J-Y. park, I.R. Slagle, and D. Gutman, "Kinetics of the Reaction of Chlorine Atoms with Vinyl Bromide and Its Use for Measuring Chlorine ATom Concentrations", Journal of Physical Chemistry, Vol. 87, No. 10, pp 1812-1818, 1983.

[119] P.E. Riley, A.P. Turley, and W.J. Malkowski, "Development of a Multistep SiO_2 Plasma Etching Process in a Minibatch Reactor Using Response-Surface

Methodology", Journal of Electrochemical Society, Vol. 136, No. 4, pp. 1112-1119, April 1989.

[120] E. Gogolides and H.H. Sawin, "n+ Polysilicon Etching in CCl_4/He Discharges: Characterization and Modeling", Journal of Electrochemical Society, Vol. 136, No. 4, pp. 1147-1154, April 1989.

[121] P.E. Riley, V.D. Kulkarni, and S.H. Bishop, "Examination of fluorocarbon-based plasmas used in the selective and uniform etching of silicon dioxide by response-surface methodology: Effects of helium addition", Journal of Vacuum Science and Technology B, Vol. 7, No. 1, pp. 24-34, Jan/Feb1989.

[122] D.L. Smith and R.H. Bruce, "Si and Al Etching and product Detection in a Plasma Beam under Ultrahigh Vacuum",Journal of Electrochemical Society: Solid-State Science and Technology, Vol. 129, No. 9, pp. 2045-2051, September 1982.

[123] M.W. Jenkins, M.T. Mocella, K.D. Allen, and H.H. Sawin, "The Modeling of Plasma Etching Processes Using Response Surface Methodology", Solid State Technology, pp 175-182, April 1986.

[124] P.C. Karulkar and M.A. Wirzbicki, "Characterization of etching of silicon dioxide and photoresist in a flurocarbon plasma", Journal of Vacuum Science and Technology B, Vol. 6, No. 5, pp. 1595-1599, Sep/Oct 1988.

[125] P.E. Rilley and E.D. Castel, "Planarization of Dielectric Layers for Multilevel Metallization", IEEE Trans. on Semiconductor Manufacturing, Vol. 1, No. 4, pp 154-156, November 1988.

[126] C.J. Mogab, "The Loading Effect in Plasma Etching", Journal of Electrochemical Society: Solid-State Science and Technology, Vol. 124, No. 8, pp. 1262-1268, August 1977.

[127] C.C. Tong and D.W. Hess, "Tunsten Etching in CF_4 and SF_6 Discharges", Journal of Electrochemical Society: Solid-State Science and Technology, Vol. 131, No. 1, pp. 115-120, January 1984.

[128] J.L. Mauer and J.S. Logan, "Reactant Supply in reactive ion etching", Journal of Vacuum Science and Technology , Vol. 16, No. 2, pp. 404-406, Mar/Apr 1979.

[129] T. Enomoto, M. Denda, A. Yasuoka, and H. Nakata, "Loading Effect and Temperature Dependence of Etch Rate in CF_4 Plasma", Japanese Journal of Applied Physics, Vol. 18, No. 1, pp 155-163, January 1979.

[130] P.W. Bohn and R.C. Manz, " A Multiresponse Factorial Study of Reactor Parameters in Plasma Enhanced CVD Growth of Amorphous Silicon Nitride", Journal of Electrochemical Society: Solid-State Science and Technology, Vol. 132, No. 8, pp. 1981-1984, August 1985.

[131] T.E. Clark, "Characterization and optimization of low-pressure chemical vapor deposited tungsten silicide using screening and response surface experimental design", Journal of Vacuum Science and Technology B, Vol. 6, No. 6, pp. 1678-1687, Nov/Dec 1988.

[132] M.L. Barry, "Doped Oxides as Diffusion Sources", Journal of Electrochemical Society, Solid State Science, Vol. 117, No. 11, pp 1405-1410, Nov. 1970.

[133] "MRC Eclipse brochure", Materials Research Corporation, Santa Clara, CA.

[134] " Lam Rainbow 4600 Brochure", Lam Research Corporation, Fremont, CA.
[135] G.E.P. Box, W.G. Hunter, and J.S. Hunter, "Statistics for Experimenters", John Wiley &Sons, New York, 1978.
[136] RS1 software, BBN inc.
[137] JMP software, SAS Institute Inc.
[138] Richard Post, "Statistics for Experimenters", lecture notes, 1996.
[139] " Four-point probe - Automap system Model 280C brochure", Four Dimensions, Inc., Hayward, CA.

Appendix A

Etch rate calculation from sheet resistance measurements

The sheet resistance of the conductive Ti or TiN film is measured using four point probe technique. In this appendix, the steps involved in calculating the film thickness from the sheet resistance are shown.

Let ρ be the bulk resistivity of the conductive film and ρ_s be the sheet resistance. The following equation relates ρ and ρ_s.

$$\text{Sheet resistance } \rho_s = \rho/d \qquad \text{(i)}$$

where d is the film thickness.

Therefore,

$$\text{Film thickness } d = \rho/\rho_s \qquad \text{(ii)}$$

The film sheet resistance is measured before and after etch. Let ρ_{s1} be sheet resistance before etch and ρ_{s2} be the sheet resistance after etch. The etch rate of the film can be calculated from the equation (iii), knowing the etch time t.

$$\text{Etch rate ER} = (d_1-d_2)/t \qquad \text{(iii)}$$

where d_1 and d_2 are film thicknesses before and after etch, respectively. Expressing the etch rate in sheet resistance,

$$\text{Etch rate ER} = (\rho/\rho_{s1} - \rho/\rho_{s2})/t \qquad \text{(iv)}$$

$$\text{Etch rate ER} = \frac{\rho\,(1/\rho_{s1} - 1/\rho_{s2})}{t} \qquad \text{(v)}$$

Appendix B

Lotus 123 Program for calculation of etch rate from sheet resistance

The following is the Lotus 123 formula entered in the spread sheet to calculate the etch rate:

(60/D2) * (1/B7-1/C7) * (@IF(D1=1, 12800, @IF(D1=2, 800,

@IF(D1=3, 265, @IF(D1=4, 6507, @ERR)))))

If D1 = 1, then TiN, constant = 12800
If D1 = 2, then W (tungsten), constant = 800
If D1 = 3, then Al, constant = 265
If D1 = 4, then Ti, constant = 6507
If D1 is any other number, gives an Error message.

Cell D2 contains the etch time in seconds.
Cell B7 contains the sheet resistance before etch.
Cell C7 contains the sheet resistance after etch.
The result is multiplied by 60 in order to get the etch rate in Å/min.

Vita

The author was born on November 24, 1960 in Madurai, Tamil Nadu State, India. He received his Bachelor of Engineering in Electronics and Communications Engineering at P.S.G. College of Technology, Coimbatore, India in 1983. He received his Master of Technology in Electrical Engineering at Indian Institute of Technology, Madras, India in 1985 and received his Master of Science in Electrical Engineering at Virginia Polytechnic Institute and State University, Blacksburg, Virginia, USA in 1989.

In 1990, he joined LSI Logic corporation as a process engineer in semiconductor manufacturing facility. He worked on projects in photolithography, plasma etch and chemical vapor deposition areas. In 1996, he became a process development engineer at LSI Logic Research and Development Group. Currently he is working on electrical test development for submicron integrated circuits. His main areas of interests are plasma etch, chemical vapor deposition, hot carrier injection and life time tests on submicron transistors, characterization of chemical mechanical polishing, and electrical testing and analysis of mixed signal devices.

N. Muthukrishnan